



N°d'ordre NNT: 2018LYSET012

DOCTORAL THESIS OF THE UNIVERSITY OF LYON

prepared at

Ecole Nationale des Travaux Publics de l'Etat

Ecole Doctorale N° 162

Mécanique, Energétique, Génie Civil et Acoustique (MEGA)

Specialty: Civil Engineering

Publicly defended the 11th of December 2018 by:

Jean-Claude Carret

Linear viscoelastic characterization of bituminous mixtures from dynamic tests back analysis

Appendices

Before the committee composed of:

TOUSSAINT, Evelyne	Prof., Clermont Auvergne University	President
BHASIN, Amit	Ass. Prof., University of Texas	Reviewer
RYDEN, Nils	Ass. Prof., Lund University	Reviewer
WISTUBA, Michael	Prof., University of Braunschweig	Examiner
DI BENEDETTO, Hervé	Prof., University of Lyon	Advisor
SAUZEAT Cédric	Prof., University of Lyon	Co-advisor
GUDMARSSON, Anders	Dr., PEAB asphalt	Invited



N°d'ordre NNT : 2018LYSET012

THESE de DOCTORAT DE L'UNIVERSITE DE LYON
opérée au sein de
L'École Nationale des Travaux Publics de l'Etat

Ecole Doctorale N° 162
Mécanique, Energétique, Génie Civil et Acoustique (MEGA)

Spécialité/ discipline de doctorat : Génie Civil

Soutenue publiquement le 11/12/2018, par :
Jean-Claude Carret

**Caractérisation viscoélastique linéaire
des enrobés bitumineux par analyse
inverse d'essais dynamiques**

Annexes

Devant le jury composé de :

TOUSSAINT, Evelyne	Prof., Clermont Auvergne Université	Présidente
BHASIN, Amit	Prof. Ass., Université du Texas	Rapporteur
RYDEN, Nils	Prof. Ass., Université de Lund	Rapporteur
WISTUBA, Michael	Prof., Université de Braunschweig	Examineur
DI BENEDETTO, Hervé	Prof., Université de Lyon	Directeur de thèse
SAUZEAT Cédric	Prof., Université de Lyon	Co-directeur
GUDMARSSON, Anders	Dr., PEAB asphalte	Invité

TABLE OF CONTENTS

TABLE OF CONTENTS..... 3

LIST OF TABLES 4

LIST OF FIGURES 8

APPENDIX A - DETAILS ABOUT THE EXPERIMENTAL DEVICES 20

**APPENDIX B - DATA BASE OF 2S2P1D MODEL AND WLF EQUATION
CONSTANTS OBTAINED FROM CYCLIC TENSION-COMPRESSION TESTS
PERFORMED ON DIFFERENT BITUMINOUS MIXTURES 29**

**APPENDIX C - RESULTS OF THE PARAMETRIC ANALYSIS FOR THE
COMPLEX MODULUS AND COMPLEX POISSON’S RATIO..... 32**

**APPENDIX D - RESULTS OF THE PARAMETRIC ANALYSIS FOR THE
CONSTANTS OF THE 2S2P1D MODEL..... 35**

**APPENDIX E - RESULTS OF METHOD II FOR THE REFERENCE LVE
MATERIAL 68**

**APPENDIX F - RESULTS OF METHOD III FOR THE REFERENCE LVE
MATERIAL 76**

**APPENDIX G - RESULTS OF METHOD IV FOR THE REFERENCE LVE
MATERIAL 84**

**APPENDIX H - RESULTS OF METHOD V FOR THE REFERENCE LVE
MATERIAL 90**

**APPENDIX I - DETAILS OF THE MATERIALS TESTED IN THE
EXPERIMENTAL CAMPAIGNS..... 95**

APPENDIX J - RESULTS OF THE FSDYN EXPERIMENTAL CAMPAIGN . 102

APPENDIX K - RESULTS OF THE SM EXPERIMENTAL CAMPAIGN..... 126

**APPENDIX L - RESULTS OF THE MOGS EXPERIMENTAL CAMPAIGN
WITH THE 128**

**APPENDIX M - RESULTS OF THE MHRAPC EXPERIMENTAL CAMPAIGN
134**

APPENDIX N - RESULTS OF THE MAP EXPERIMENTAL CAMPAIGN..... 145

LIST OF TABLES

Table B.1. 2S2P1D model and WLF equation constants obtained from cyclic tension-compression tests performed on different bituminous mixtures.	30
Table C.1. Values of the RSD for the two first resonance frequencies and amplitudes for the flexural mode of the disc. The LVE property indicated in the left column varies while the other properties are set to their median values indicated in Table 4.4.	33
Table C.2. Values of the RSD for the two first resonance frequencies and amplitudes for the torsional mode of the straight beam. The LVE property indicated in the left column varies while the other properties are set to their median values indicated in Table 4.4.	34
Table E.1. Frequencies selected for the comparison of the values of the complex modulus at each temperature for the longitudinal mode of the cylinder.	72
Table E.2. Frequencies selected for the comparison of the values of the complex modulus at each temperature for the longitudinal and flexural modes of the cylinder.	72
Table E.3. Frequencies selected for the comparison of the values of the complex modulus at each temperature for the longitudinal mode of the straight beam.	72
Table E.4. Frequencies selected for the comparison of the values of the complex modulus at each temperature for the flexural mode of the disc.	72
Table F.1. Final values of the four constants E_0 , $\tau_{E15^\circ C}$, k and δ of the 2S2P1D model that are identified at each temperature in the first step of method III for the longitudinal and flexural modes of the cylinder.	77
Table F.2. Final values of the four constants E_0 , $\tau_{E15^\circ C}$, k and δ of the 2S2P1D model that are identified at each temperature in the first step of method III for the flexural mode of the disc.	77
Table F.3. Final values of the four constants E_0 , $\tau_{E15^\circ C}$, k and δ of the 2S2P1D model that are identified at each temperature in the first step of method III for the longitudinal mode of the straight beam.	77
Table G.1. First resonance frequency and values of $ E^*_{BC4} $ and φ_{E^*BC4} determined in the first step of method IV for the longitudinal mode of the cylinder.	85
Table G.2. First resonance frequency and values of $ E^*_{BC4} $ and φ_{E^*BC4} determined in the first step of method IV for the longitudinal and flexural modes of the cylinder.	85
Table G.3. First resonance frequency and values of $ E^*_{BC4} $ and φ_{E^*BC4} determined in the first step of method IV for the flexural mode of the disc.	85
Table G.4. First resonance frequency and values of $ E^*_{BC4} $ and φ_{E^*BC4} determined in the first step of method IV for the longitudinal mode of the straight beam.	85

Table H.1. Final values of the four constants E_0 , $\tau_{E15^\circ C}$, k and δ of the 2S2P1D model and of the Poisson's ratio ν that are identified at each temperature in the first step of the method V for the longitudinal mode of the cylinder.....	91
Table H.2. Final values of the four constants E_0 , $\tau_{E15^\circ C}$, k and δ of the 2S2P1D model and of the Poisson's ratio ν that are identified at each temperature in the first step of the method V for the longitudinal mode of the straight beam.	91
Table J.1. Values of the four constants E_0 , $\tau_{E15^\circ C}$, k and δ of the 2S2P1D model determined from dynamic tests at each temperature in the first step of method III for specimen ABD-D9.	104
Table J.2. Values of the four constants E_0 , $\tau_{E15^\circ C}$, k and δ of the 2S2P1D model determined from dynamic tests at each temperature in the first step of method III for specimen ABD-D10.	106
Table J.3. Values of the four constants E_0 , $\tau_{E15^\circ C}$, k and δ of the 2S2P1D model determined from dynamic tests at each temperature in the first step of method III for specimen GB5-D1.	108
Table J.4. Values of the four constants E_0 , $\tau_{E15^\circ C}$, k and δ of the 2S2P1D model determined from dynamic tests at each temperature in the first step of method III for specimen GB5-D3.	110
Table J.5. Values of the four constants E_0 , $\tau_{E15^\circ C}$, k and δ of the 2S2P1D model and of the Poisson's ratio ν determined from the 1 st round of dynamic tests at each temperature in the first step of method V for specimen GB5-C1.....	111
Table J.6. Values of the four constants E_0 , $\tau_{E15^\circ C}$, k and δ of the 2S2P1D model and of the Poisson's ratio ν determined from the 2 nd round of dynamic tests at each temperature in the first step of method V for specimen GB5-C1.....	113
Table J.7. Values of the four constants E_0 , $\tau_{E15^\circ C}$, k and δ of the 2S2P1D model and of the Poisson's ratio ν determined from the 1 st round of dynamic tests at each temperature in the first step of method V for specimen GB5-C2.....	115
Table J.8. Values of the four constants E_0 , $\tau_{E15^\circ C}$, k and δ of the 2S2P1D model and of the Poisson's ratio ν determined from the 2 nd round of dynamic tests at each temperature in the first step of method V for specimen GB5-C2.....	118
Table J.9. Values of the four constants E_0 , $\tau_{E15^\circ C}$, k and δ of the 2S2P1D model determined from dynamic tests at each temperature in the first step of method III for specimen GB5-B2.	123
Table J.10. Values of the four constants E_0 , $\tau_{E15^\circ C}$, k and δ of the 2S2P1D model determined from dynamic tests at each temperature in the first step of method III for specimen GB5-B4.	125
Table K.1. Values of the four constants E_0 , $\tau_{E15^\circ C}$, k and δ of the 2S2P1D model determined from dynamic tests at each temperature in the first step of method III for specimen ABS-P4.	127
Table L.1. First resonance frequency and values of $ E_{BC4}^* $ and φ_{E^*BC4} determined from dynamic tests at each temperature in the first step of method IV for specimen GB5-C3.	129

Table L.2. Values of the four constants E_0 , $\tau_{E15^\circ C}$, k and δ of the 2S2P1D model determined from dynamic tests at each temperature in the first step of method III for specimen GB5-C3.	130
Table L.3. First resonance frequency and values of $ E^*_{BC4} $ and φ_{E^*BC4} determined from dynamic tests at each temperature in the first step of method IV for specimen GB5-C3.	131
Table L.4. Values of the four constants E_0 , $\tau_{E15^\circ C}$, k and δ of the 2S2P1D model determined from dynamic tests at each temperature in the first step of method III for specimen GB5-C4.	132
Table M.1. First resonance frequency and values of $ E^*_{BC4} $ and φ_{E^*BC4} determined from dynamic tests at each temperature in the first step of method IV for specimen WF-4.	135
Table M.2. Values of the four constants E_0 , $\tau_{E15^\circ C}$, k and δ of the 2S2P1D model and of the Poisson's ratio ν determined from the 2 nd round of dynamic tests at each temperature in the first step of method V for specimen WF-4.	136
Table M.3. First resonance frequency and values of $ E^*_{BC4} $ and φ_{E^*BC4} determined from dynamic tests at each temperature in the first step of method IV for specimen WF-6.	139
Table M.4. Values of the four constants E_0 , $\tau_{E15^\circ C}$, k and δ of the 2S2P1D model and of the Poisson's ratio ν determined from the 2 nd round of dynamic tests at each temperature in the first step of method V for specimen WF-6.	140
Table M.5. First resonance frequency and values of $ E^*_{BC4} $ and φ_{E^*BC4} determined from dynamic tests at each temperature in the first step of method IV for specimen WF-8.	143
Table M.6. Values of the four constants E_0 , $\tau_{E15^\circ C}$, k and δ of the 2S2P1D model and of the Poisson's ratio ν determined from the 2 nd round of dynamic tests at each temperature in the first step of method V for specimen WF-8.	144
Table N.1. Values of the four constants E_0 , $\tau_{E15^\circ C}$, k and δ of the 2S2P1D model and of the Poisson's ratio ν determined from dynamic tests at each temperature in the first step of method V for specimen GB-L-1.	147
Table N.2. Values of the four constants E_0 , $\tau_{E15^\circ C}$, k and δ of the 2S2P1D model determined from dynamic tests at each temperature in the first step of method III for specimen GB-L-2.	150
Table N.3. Values of the four constants E_0 , $\tau_{E15^\circ C}$, k and δ of the 2S2P1D model determined from dynamic tests at each temperature in the first step of method III for specimen GB-L-3.	152
Table N.4. Values of the four constants E_0 , $\tau_{E15^\circ C}$, k and δ of the 2S2P1D model determined from dynamic tests at each temperature in the first step of method III for specimen GB-L-4.	154
Table N.5. Values of the four constants E_0 , $\tau_{E15^\circ C}$, k and δ of the 2S2P1D model determined from dynamic tests at each temperature in the first step of method III for specimen GB-L-5.	156
Table N.6. Values of the four constants E_0 , $\tau_{E15^\circ C}$, k and δ of the 2S2P1D model determined from dynamic tests at each temperature in the first step of method III for specimen GB'-L-1.	158

Table N.7. Values of the four constants E_0 , $\tau_{E15^\circ C}$, k and δ of the 2S2P1D model determined from dynamic tests at each temperature in the first step of method III for specimen GB'-L-2.	160
Table N.8. Values of the four constants E_0 , $\tau_{E15^\circ C}$, k and δ of the 2S2P1D model determined from dynamic tests at each temperature in the first step of method III for specimen GB'-L-3.	162
Table N.9. Values of the four constants E_0 , $\tau_{E15^\circ C}$, k and δ of the 2S2P1D model determined from dynamic tests at each temperature in the first step of method III for specimen GB-T-1.	164
Table N.10. Values of the four constants E_0 , $\tau_{E15^\circ C}$, k and δ of the 2S2P1D model determined from dynamic tests at each temperature in the first step of method III for specimen GB-T-2.	166
Table N.11. Values of the four constants E_0 , $\tau_{E15^\circ C}$, k and δ of the 2S2P1D model and of the Poisson's ratio ν determined from dynamic tests at each temperature in the first step of method V for specimen BB-L-1.	167
Table N.12. Values of the four constants E_0 , $\tau_{E15^\circ C}$, k and δ of the 2S2P1D model determined from dynamic tests at each temperature in the first step of method III for specimen BB-L-2.	169
Table N.13. Values of the four constants E_0 , $\tau_{E15^\circ C}$, k and δ of the 2S2P1D model determined from dynamic tests at each temperature in the first step of method III for specimen BB-T-1.	171
Table N.14. Values of the four constants E_0 , $\tau_{E15^\circ C}$, k and δ of the 2S2P1D model determined from dynamic tests at each temperature in the first step of method III for specimen BB-T-2.	173

LIST OF FIGURES

Figure C.1. Influence of the LVE properties on the FRFs of the flexural mode of the disc: (a) norm of the complex modulus; (b) phase angle of the complex modulus; (c) norm of the complex Poisson's ratio; (d) phase angle of the complex Poisson's ratio. The constants not listed in each figure have the median value given in Table 4.4.	33
Figure C.2. Influence of the LVE properties on the FRFs of the torsional mode of the straight beam: (a) norm of the complex modulus; (b) phase angle of the complex modulus; (c) norm of the complex Poisson's ratio; (d) phase angle of the complex Poisson's ratio. The constants not listed in each figure have the median value given in Table 4.4.	34
Figure D.1. RSD in function of temperature for each of the ten constants of the 2S2P1D model for the flexural mode of the disc: (a) 1 st resonance frequency; (b) 2 nd resonance frequency; (c) 3 rd resonance frequency; (d) 1 st resonance amplitude; (e) 2 nd resonance amplitude; (f) 3 rd resonance amplitude.....	36
Figure D.2. RSD in function of temperature for each of the ten constants of the 2S2P1D model for the torsional mode of the straight beam: (a) 1 st resonance frequency; (b) 2 nd resonance frequency; (c) 3 rd resonance frequency; (d) 1 st resonance amplitude; (e) 2 nd resonance amplitude; (f) 3 rd resonance amplitude.....	37
Figure D.3. Influence of constant E_0 of the 2S2P1D model on the FRFs of the longitudinal mode of the cylinder at: (a) -20°C; (b) 0°C; (c) 15°C; (d) 35°C; (e) 50°C. The constants not listed in each figure have the median value given in Table 4.6.	38
Figure D.4. Influence of constant $\tau_{E15^\circ C}$ of the 2S2P1D model on the FRFs of the longitudinal mode of the cylinder at: (a) -20°C; (b) 0°C; (c) 15°C; (d) 35°C; (e) 50°C. The constants not listed in each figure have the median value given in Table 4.6.	39
Figure D.5. Influence of constant k of the 2S2P1D model on the FRFs of the longitudinal mode of the cylinder at: (a) -20°C; (b) 0°C; (c) 15°C; (d) 35°C; (e) 50°C. The constants not listed in each figure have the median value given in Table 4.6.	40
Figure D.6. Influence of constant δ of the 2S2P1D model on the FRFs of the longitudinal mode of the cylinder at: (a) -20°C; (b) 0°C; (c) 15°C; (d) 35°C; (e) 50°C. The constants not listed in each figure have the median value given in Table 4.6.	41
Figure D.7. Influence of constant h of the 2S2P1D model on the FRFs of the longitudinal mode of the cylinder at: (a) -20°C; (b) 0°C; (c) 15°C; (d) 35°C; (e) 50°C. The constants not listed in each figure have the median value given in Table 4.6.	42
Figure D.8. Influence of constant β of the 2S2P1D model on the FRFs of the longitudinal mode of the cylinder at: (a) -20°C; (b) 0°C; (c) 15°C; (d) 35°C; (e) 50°C. The constants not listed in each figure have the median value given in Table 4.6.	43

Figure D.22. Influence of constant v_{00} of the 2S2P1D model on the FRFs of the flexural mode of the disc at: (a) -20°C ; (b) 0°C ; (c) 15°C ; (d) 35°C ; (e) 50°C . The constants not listed in each figure have the median value given in Table 4.6.	57
Figure D.23. Influence of constant E_0 of the 2S2P1D model on the FRFs of the torsional mode of the straight beam at: (a) -20°C ; (b) 0°C ; (c) 15°C ; (d) 35°C ; (e) 50°C . The constants not listed in each figure have the median value given in Table 4.6.	58
Figure D.24. Influence of constant $\tau_{E15^{\circ}\text{C}}$ of the 2S2P1D model on the FRFs of the torsional mode of the straight beam at: (a) -20°C ; (b) 0°C ; (c) 15°C ; (d) 35°C ; (e) 50°C . The constants not listed in each figure have the median value given in Table 4.6.	59
Figure D.25. Influence of constant k of the 2S2P1D model on the FRFs of the torsional mode of the straight beam at: (a) -20°C ; (b) 0°C ; (c) 15°C ; (d) 35°C ; (e) 50°C . The constants not listed in each figure have the median value given in Table 4.6.	60
Figure D.26. Influence of constant δ of the 2S2P1D model on the FRFs of the torsional mode of the straight beam at: (a) -20°C ; (b) 0°C ; (c) 15°C ; (d) 35°C ; (e) 50°C . The constants not listed in each figure have the median value given in Table 4.6.	61
Figure D.27. Influence of constant h of the 2S2P1D model on the FRFs of the torsional mode of the straight beam at: (a) -20°C ; (b) 0°C ; (c) 15°C ; (d) 35°C ; (e) 50°C . The constants not listed in each figure have the median value given in Table 4.6.	62
Figure D.28. Influence of constant β of the 2S2P1D model on the FRFs of the torsional mode of the straight beam at: (a) -20°C ; (b) 0°C ; (c) 15°C ; (d) 35°C ; (e) 50°C . The constants not listed in each figure have the median value given in Table 4.6.	63
Figure D.29. Influence of constant E_{00} of the 2S2P1D model on the FRFs of the torsional mode of the straight beam at: (a) -20°C ; (b) 0°C ; (c) 15°C ; (d) 35°C ; (e) 50°C . The constants not listed in each figure have the median value given in Table 4.6.	64
Figure D.30. Influence of constant v_0 of the 2S2P1D model on the FRFs of the torsional mode of the straight beam at: (a) -20°C ; (b) 0°C ; (c) 15°C ; (d) 35°C ; (e) 50°C . The constants not listed in each figure have the median value given in Table 4.6.	65
Figure D.31. Influence of constant $\tau_{v15^{\circ}\text{C}}$ of the 2S2P1D model on the FRFs of the torsional mode of the straight beam at: (a) -20°C ; (b) 0°C ; (c) 15°C ; (d) 35°C ; (e) 50°C . The constants not listed in each figure have the median value given in Table 4.6.	66
Figure D.32. Influence of constant v_{00} of the 2S2P1D model on the FRFs of the torsional mode of the straight beam at: (a) -20°C ; (b) 0°C ; (c) 15°C ; (d) 35°C ; (e) 50°C . The constants not listed in each figure have the median value given in Table 4.6.	67
Figure E.1. Comparison of the reference FRFs (noted Ref. FRF) with the global LVE FRFs (noted G.LVE.FRF) for method II. Values of the reference FRFs at the frequencies where the optimization is performed (noted Opt. Points) are also plotted. Results for the longitudinal and flexural modes of the cylinder at: (a) -20°C ; (b) 0°C ; (c) 15°C ; (d) 35°C ; (e) 50°C	69
Figure E.2. Comparison of the reference FRFs (noted Ref. FRF) with the global LVE FRFs (noted G.LVE.FRF) for method II. Values of the reference FRFs at the frequencies where the optimization is performed (noted Opt. Points) are also plotted. Results for the flexural mode of the disc at: (a) -20°C ; (b) 0°C ; (c) 15°C ; (d) 35°C ; (e) 50°C	70

Figure E.3. Comparison of the reference FRFs (noted Ref. FRF) with the global LVE FRFs (noted G.LVE.FRF) for method II. Values of the reference FRFs at the frequencies where the optimization is performed (noted Opt. Points) are also plotted. Results for the longitudinal mode of the straight beam at: (a) -20°C ; (b) 0°C ; (c) 15°C ; (d) 35°C ; (e) 50°C 71

Figure E.4. Comparison of the values of the complex modulus determined with method II ($E_{\text{Dyn}2}^*$) with the values of the complex modulus of the reference LVE material (E_{Ref}^*). (a) Cole-Cole plot; (b) and (c) master curves of the norm and of the phase angle of the complex modulus at 15°C . Results for the longitudinal and flexural modes of the cylinder. 73

Figure E.5. Comparison of the values of the complex modulus determined with method II ($E_{\text{Dyn}2}^*$) with the values of the complex modulus of the reference LVE material (E_{Ref}^*). (a) Cole-Cole plot; (b) and (c) master curves of the norm and of the phase angle of the complex modulus at 15°C . Results for the flexural mode of the disc. 74

Figure E.6. Comparison of the values of the complex modulus determined with method II ($E_{\text{Dyn}2}^*$) with the values of the complex modulus of the reference LVE material (E_{Ref}^*). (a) Cole-Cole plot; (b) and (c) master curves of the norm and of the phase angle of the complex modulus at 15°C . Results for the longitudinal mode of the straight beam. 75

Figure F.1. Comparison of the reference FRFs (noted Ref. FRF) with the FRFs after optimization (noted FRF A.O) and the global LVE FRFs (noted G.LVE FRF) for method III. Values of the reference FRFs at the frequencies where the optimization is performed (noted Opt. Points) are also plotted. Longitudinal and flexural modes of the cylinder at: (a) -20°C ; (b) 0°C ; (c) 15°C ; (d) 35°C ; (e) 50°C 78

Figure F.2. Comparison of the reference FRFs (noted Ref. FRF) with the FRFs after optimization (noted FRF A.O) and the global LVE FRFs (noted G.LVE FRF) for method III. Values of the reference FRFs at the frequencies where the optimization is performed (noted Opt. Points) are also plotted. Flexural mode of the disc at: (a) -20°C ; (b) 0°C ; (c) 15°C ; (d) 35°C ; (e) 50°C 79

Figure F.3. Comparison of the reference FRFs (noted Ref. FRF) with the FRFs after optimization (noted FRF A.O) and the global LVE FRFs (noted G.LVE FRF) for method III. Values of the reference FRFs at the frequencies where the optimization is performed (noted Opt. Points) are also plotted. Longitudinal mode of the straight beam at: (a) -20°C ; (b) 0°C ; (c) 15°C ; (d) 35°C ; (e) 50°C 80

Figure F.4. Comparison of the values of the complex modulus determined with method III ($E_{\text{BC}3}^*$ and $E_{\text{Dyn}3}^*$) with the values of the complex modulus of the reference LVE material (E_{Ref}^*). (a) Cole-Cole plot; (b) and (c) master curves of the norm and of the phase angle of the complex modulus at 15°C . Results for the longitudinal and flexural modes of the cylinder... 81

Figure F.5. Comparison of the values of the complex modulus determined with method III ($E_{\text{BC}3}^*$ and $E_{\text{Dyn}3}^*$) with the values of the complex modulus of the reference LVE material (E_{Ref}^*). (a) Cole-Cole plot; (b) and (c) master curves of the norm and of the phase angle of the complex modulus at 15°C . Results for the flexural mode of the disc. 82

Figure F.6. Comparison of the values of the complex modulus determined with methods III ($E_{\text{BC}3}^*$ and $E_{\text{Dyn}3}^*$) and IV ($E_{\text{BC}4}^*$ and $E_{\text{Dyn}4}^*$) with the values of the complex modulus of the reference LVE material (E_{Ref}^*). (a) Cole-Cole plot; (b) and (c) master curves of the norm and

of the phase angle of the complex modulus at 15°C. Results for the longitudinal mode of the straight beam.	83
Figure G.1. Comparison of the reference FRFs (noted Ref. FRF) with the FRFs after optimization (noted FRF A.O) for method IV. Values of the reference FRFs at the frequencies where the optimization is performed (noted Opt. Points) are also plotted. Longitudinal and flexural modes of the cylinder at: (a) -20°C; (b) 0°C; (c) 15°C; (d) 35°C; (e) 50°C.	86
Figure G.2. Comparison of the reference FRFs (noted Ref. FRF) with the FRFs after optimization (noted FRF A.O) for method IV. Values of the reference FRFs at the frequencies where the optimization is performed (noted Opt. Points) are also plotted. Flexural mode of the disc at: (a) -20°C; (b) 0°C; (c) 15°C; (d) 35°C; (e) 50°C.	87
Figure G.3. Comparison of the reference FRFs (noted Ref. FRF) with the FRFs after optimization (noted FRF A.O) and the global LVE FRFs (noted G.LVE FRF) for method IV. Values of the reference FRFs at the frequencies where the optimization is performed (noted Opt. Points) are also plotted. Longitudinal mode of the straight beam at: (a) -20°C; (b) 0°C; (c) 15°C; (d) 35°C; (e) 50°C.	88
Figure G.4. Comparison of the values of the complex modulus of the reference LVE material with the values of the complex modulus back-calculated at each temperature (step 1) and the values of the complex modulus simulating the global LVE behaviour (step 2) for the third and fourth methods. Longitudinal mode of the straight beam: (a) Cole-Cole plot; (b) and (c) master curves of the norm and of the phase angle of the complex modulus at 15°C.	89
Figure H.1. Comparison of the reference FRFs (noted Ref. FRF) with the FRFs after optimization (noted FRF A.O) for method V. Values of the reference FRFs at the frequencies where the optimization is performed (noted Opt. Points) are also plotted. Longitudinal mode of the straight beam at: (a) -20°C; (b) 0°C; (c) 15°C; (d) 35°C; (e) 50°C.	92
Figure H.2. Comparison of the values of the complex modulus determined with methods III (E_{BC3}^* and E_{Dyn3}^*) and V (E_{BC5}^* and E_{Dyn5}^*) with the values of the complex modulus of the reference LVE material (E_{Ref}^*). (a) Cole-Cole plot; (b) and (c) master curves of the norm and of the phase angle of the complex modulus at 15°C. Results for the longitudinal mode of the straight beam.	93
Figure H.3. Comparison of the values of the complex Poisson's ratio determined with methods V (real values v_{BC5} and v_{Dyn5}^*) with the values of the complex Poisson's ratio of the reference LVE material (v_{Ref}^*). (a) Cole-Cole plot; (b) and (c) master curves of the norm and of the phase angle of the complex modulus at 15°C. Results for the longitudinal mode of the straight beam.	94
Figure I.1. Grading curves of the original mixture (BBSG 0/10) and of the RAP aggregates incorporated in the WF material.	98
Figure I.2. In-laboratory fabrication process of the WF material from the RAP, the original mixture (BBSG 0/10) and the 160/220 bitumen.	98
Figure J.1 Comparison of the experimental FRFs (noted Exp. FRF) with the FRFs after optimization (noted FRF A.O) and the global LVE FRFs (noted G.LVE FRF) for specimen ABS-D9. Values of the experimental FRFs at the frequencies where the optimization is performed (noted Opt. Points) are also plotted. (a) T=-18.3°C; (b) -0.5°C; (c) 13.8°C; (d) 30.1°C; (e) 39.9°C.	103

Figure J.2 Values of the complex modulus determined from dynamic tests with method III (E_{BC3}^* and E_{Dyn3}^*). (a) Cole-Cole plot; (b) and (c) master curves of the norm and of the phase angle of the complex modulus at 15°C. Results for specimen ABS-D9.....	104
Figure J.3 Comparison of the experimental FRFs (noted Exp. FRF) with the FRFs after optimization (noted FRF A.O) and the global LVE FRFs (noted G.LVE FRF) for specimen ABS-D10. Values of the experimental FRFs at the frequencies where the optimization is performed (noted Opt. Points) are also plotted. (a) T=-18.8°C; (b) -0.7°C; (c) 15.2°C; (d) 29.2°C; (e) 39.9°C.....	105
Figure J.4 Values of the complex modulus determined from dynamic tests with method III (E_{BC3}^* and E_{Dyn3}^*). (a) Cole-Cole plot; (b) and (c) master curves of the norm and of the phase angle of the complex modulus at 15°C. Results for specimen ABS-D10.....	106
Figure J.5 Comparison of the experimental FRFs (noted Exp. FRF) with the FRFs after optimization (noted FRF A.O) and the global LVE FRFs (noted G.LVE FRF) for specimen GB5-D1. Values of the experimental FRFs at the frequencies where the optimization is performed (noted Opt. Points) are also plotted. (a) T=-20.6°C; (b) -0.3°C; (c) 14.7°C; (d) 34.9°C; (e) 49.7°C.....	107
Figure J.6 Values of the complex modulus determined from dynamic tests with method III (E_{BC3}^* and E_{Dyn3}^*). (a) Cole-Cole plot; (b) and (c) master curves of the norm and of the phase angle of the complex modulus at 15°C. Results for specimen GB5-D1.....	108
Figure J.7 Comparison of the experimental FRFs (noted Exp. FRF) with the FRFs after optimization (noted FRF A.O) for specimen GB5-D3. Values of the experimental FRFs at the frequencies where the optimization is performed (noted Opt. Points) are also plotted. (a) T=-20.5°C; (b) -0.2°C; (c) 15.1°C; (d) 34.9°C; (e) 49.9°C.....	109
Figure J.8 Values of the complex modulus determined from dynamic tests with method III (E_{BC3}^* and E_{Dyn3}^*). (a) Cole-Cole plot; (b) and (c) master curves of the norm and of the phase angle of the complex modulus at 15°C. Results for specimen GB5-D3.....	110
Figure J.9 Comparison of the values of the complex modulus determined from the 1 st round of dynamic tests with method V (E_{BC5}^* and E_{Dyn5}^*) with the values of the complex modulus determined from cyclic tests (E_{ExpTC}^* and E_{TC}^*). (a) Cole-Cole plot; (b) and (c) master curves of the norm and of the phase angle of the complex modulus at 15°C. Results for specimen GB5-C1.....	111
Figure J.10 Comparison of the values of the complex Poisson's ratio determined from the 1 st round of dynamic tests with method V (real values v_{BC5} and v_{Dyn5}^*) with the values of the complex Poisson's ratio determined from cyclic test (v_{ExpTC}^* and v_{TC}^*). (a) Cole-Cole plot; (b) and (c) master curves of the norm and of the phase angle of the complex Poisson's ratio at 15°C. Results for specimen GB5-C1.....	112
Figure J.11 Comparison of the experimental FRFs measured at the end of the project (noted Exp. FRF) with the FRFs after optimization (noted FRF A.O) and the global LVE FRFs (noted G.LVE FRF) for specimen GB5-C1. Values of the experimental FRFs at the frequencies where the optimization is performed (noted Opt. Points) are also plotted. (a) T=-20.8°C; (b) -0.2°C; (c) 14.9°C; (d) 34.1°C; (e) 48.7°C.....	113
Figure J.12 Comparison of the experimental FRFs measured at the beginning of the project (noted Exp. FRF) with the FRFs after optimization (noted FRF A.O) and the global LVE FRFs	

(noted G.LVE FRF) for specimen GB5-C2. Values of the experimental FRFs at the frequencies where the optimization is performed (noted Opt. Points) are also plotted. (a) $T=-20.1^{\circ}\text{C}$; (b) -0.7°C ; (c) 15.1°C ; (d) 34.8°C ; (e) 49.7°C 114

Figure J.13 Comparison of the values of the complex modulus determined from the 1st round of dynamic tests with method V (E_{BC5}^* and E_{Dyn5}^*) with the values of the complex modulus determined from cyclic tests (E_{ExpTC}^* and E_{TC}^*). (a) Cole-Cole plot; (b) and (c) master curves of the norm and of the phase angle of the complex modulus at 15°C . Results for specimen GB5-C2. 115

Figure J.14 Comparison of the values of the complex Poisson's ratio determined from the 1st round of dynamic tests with method V (real values v_{BC5} and v_{Dyn5}^*) with the values of the complex Poisson's ratio determined from cyclic test (v_{ExpTC}^* and v_{TC}^*). (a) Cole-Cole plot; (b) and (c) master curves of the norm and of the phase angle of the complex Poisson's ratio at 15°C . Results for specimen GB5-C2. 116

Figure J.15 Comparison of the experimental FRFs measured at the end of the project (noted Exp. FRF) with the FRFs after optimization (noted FRF A.O) and the global LVE FRFs (noted G.LVE FRF) for specimen GB5-C2. Values of the experimental FRFs at the frequencies where the optimization is performed (noted Opt. Points) are also plotted. (a) $T=-21.2^{\circ}\text{C}$; (b) -0.4°C ; (c) 15.1°C ; (d) 34.8°C ; (e) 48.9°C 117

Figure J.16 Comparison of the values of the complex modulus determined from the 2nd round of dynamic tests with method V (E_{BC5}^* and E_{Dyn5}^*) with the values of the complex modulus determined from cyclic tests (E_{ExpTC}^* and E_{TC}^*). (a) Cole-Cole plot; (b) and (c) master curves of the norm and of the phase angle of the complex modulus at 15°C . Results for specimen GB5-C2. 118

Figure J.17 Comparison of the values of the complex Poisson's ratio determined from the 2nd round of dynamic tests with method V (real values v_{BC5} and v_{Dyn5}^*) with the values of the complex Poisson's ratio determined from cyclic test (v_{ExpTC}^* and v_{TC}^*). (a) Cole-Cole plot; (b) and (c) master curves of the norm and of the phase angle of the complex Poisson's ratio at 15°C . Results for specimen GB5-C2. 119

Figure J.18 FRFs measured at the beginning (1st dynamic test) and at the end (2nd dynamic test) of the FSDyn project for the specimen GB5-C1: (a) -20°C ; (b) 0°C ; (c) 15°C ; (d) 35°C ; (e) 50°C 120

Figure J.19 FRFs measured at the beginning (1st dynamic test) and at the end (2nd dynamic test) of the FSDyn project for the specimen GB5-C1: (a) -20°C ; (b) 0°C ; (c) 15°C ; (d) 35°C ; (e) 50°C 121

Figure J.20 Comparison of the experimental FRFs (noted Exp. FRF) with the FRFs after optimization (noted FRF A.O) and the global LVE FRFs (noted G.LVE FRF) for specimen GB5-B2. Values of the experimental FRFs at the frequencies where the optimization is performed (noted Opt. Points) are also plotted. (a) $T=-20.2^{\circ}\text{C}$; (b) -0.5°C ; (c) 15.1°C ; (d) 34.9°C ; (e) 49.6°C 122

Figure J.21 Values of the complex modulus determined from dynamic tests with method III (E_{BC3}^* and E_{Dyn3}^*). (a) Cole-Cole plot; (b) and (c) master curves of the norm and of the phase angle of the complex modulus at 15°C . Results for specimen GB5-B2. 123

Figure J.22 Comparison of the experimental FRFs (noted Exp. FRF) with the FRFs after optimization (noted FRF A.O) and the global LVE FRFs (noted G.LVE FRF) for specimen GB5-B4. Values of the experimental FRFs at the frequencies where the optimization is performed (noted Opt. Points) are also plotted. (a) $T=-19.7^{\circ}\text{C}$; (b) -0.5°C ; (c) 15.4°C ; (d) 34.6°C ; (e) 49.3°C 124

Figure J.23 Values of the complex modulus determined from dynamic tests with method III (E_{BC3}^* and E_{Dyn3}^*). (a) Cole-Cole plot; (b) and (c) master curves of the norm and of the phase angle of the complex modulus at 15°C . Results for specimen GB5-B4. 125

Figure K.1 Comparison of the experimental FRFs (noted Exp. FRF) with the FRFs after optimization (noted FRF A.O) and the global LVE FRFs (noted G.LVE FRF) for specimen ABS-P4. Values of the experimental FRFs at the frequencies where the optimization is performed (noted Opt. Points) are also plotted. (a) $T=-20.8^{\circ}\text{C}$; (b) 0.2°C ; (c) 14.5°C ; (d) 29.2°C ; (e) 39.1°C 127

Figure L.1 Comparison of the experimental FRFs (noted Exp. FRF) with the FRFs after optimization (noted FRF A.O) and the global LVE FRFs (noted G.LVE FRF) obtained with method IV for specimen GB5-C3. (a) $T=-20.6^{\circ}\text{C}$; (b) 0°C ; (c) 14.5°C ; (d) 34°C ; (e) 48.5°C 129

Figure L.2 Comparison of the experimental FRFs (noted Exp. FRF) with the FRFs after optimization (noted FRF A.O) and the global LVE FRFs (noted G.LVE FRF) obtained with method III for specimen GB5-C3. Values of the experimental FRFs at the frequencies where the optimization is performed (noted Opt. Points) are also plotted. (a) $T=-20.6^{\circ}\text{C}$; (b) 0°C ; (c) 14.5°C ; (d) 34°C ; (e) 48.5°C 130

Figure L.3 Comparison of the experimental FRFs (noted Exp. FRF) with the FRFs after optimization (noted FRF A.O) and the global LVE FRFs (noted G.LVE FRF) obtained with method IV for specimen GB5-C4. (a) $T=-20.8^{\circ}\text{C}$; (b) -0.3°C ; (c) 14.4°C ; (d) 34°C ; (e) 49°C 131

Figure L.4 Comparison of the experimental FRFs (noted Exp. FRF) with the FRFs after optimization (noted FRF A.O) and the global LVE FRFs (noted G.LVE FRF) obtained with method III for specimen GB5-C4. Values of the experimental FRFs at the frequencies where the optimization is performed (noted Opt. Points) are also plotted. (a) $T=-20.8^{\circ}\text{C}$; (b) -0.3°C ; (c) 14.4°C ; (d) 34°C ; (e) 49°C 132

Figure L.5 Comparison of the values of the complex modulus determined from dynamic tests with method III (E_{BC3}^* and E_{Dyn3}^*) and method IV (E_{BC4}^* and E_{Dyn4}^*) with the values of the complex modulus determined from cyclic tests (E_{ExpTC}^* and E_{TC}^*). (a) Cole-Cole plot; (b) and (c) master curves of the norm and of the phase angle of the complex modulus at 15°C . Results for specimen GB5-C4..... 133

Figure M.1 Comparison of the experimental FRFs (noted Exp. FRF) with the FRFs after optimization (noted FRF A.O) and the global LVE FRFs (noted G.LVE FRF) obtained with method IV for specimen WF-4. (a) $T=-20.7^{\circ}\text{C}$; (b) -0.1°C ; (c) 15.3°C ; (d) 34.2°C ; (e) 48.5°C 135

Figure M.2 Comparison of the experimental FRFs (noted Exp. FRF) with the FRFs after optimization (noted FRF A.O) and the global LVE FRFs (noted G.LVE FRF) obtained with method V for specimen WF-4. Values of the experimental FRFs at the frequencies where the

optimization is performed (noted Opt. Points) are also plotted. (a) $T=-20.7^{\circ}\text{C}$; (b) -0.1°C ; (c) 15.3°C ; (d) 34.2°C ; (e) 48.5°C	136
Figure M.3 Comparison of the values of the complex modulus back-calculated from dynamic tests at each temperature with methods III (E_{BC3}^*), IV (E_{BC4}^*) and V (E_{BC5}^*). Results for specimen WF-4.....	137
Figure M.4 Comparison of the values of the complex modulus determined from dynamic tests with method IV (E_{BC4}^* and E_{Dyn4}^*) and method V (E_{BC5}^* and E_{Dyn5}^*) with the values of the complex modulus determined from cyclic tests (E_{ExpTC}^* and E_{TC}^*). (a) Cole-Cole plot; (b) and (c) master curves of the norm and of the phase angle of the complex modulus at 15°C . Results for specimen WF-4.....	137
Figure M.5 Comparison of the values of the complex Poisson's ratio determined from dynamic tests with method V (real values v_{BC5} and v_{Dyn5}^*) with the values of the complex Poisson's ratio determined from cyclic test (v_{ExpTC}^* and v_{TC}^*). (a) Cole-Cole plot; (b) and (c) master curves of the norm and of the phase angle of the complex Poisson's ratio at 15°C . Results for specimen WF-4.....	138
Figure M.6 Comparison of the experimental FRFs (noted Exp. FRF) with the FRFs after optimization (noted FRF A.O) and the global LVE FRFs (noted G.LVE FRF) obtained with method IV for specimen WF-6. (a) $T=-21.1^{\circ}\text{C}$; (b) -0.3°C ; (c) 14.9°C ; (d) 34.3°C ; (e) 48.8°C	139
Figure M.7 Comparison of the experimental FRFs (noted Exp. FRF) with the FRFs after optimization (noted FRF A.O) and the global LVE FRFs (noted G.LVE FRF) obtained with method V for specimen WF-6. Values of the experimental FRFs at the frequencies where the optimization is performed (noted Opt. Points) are also plotted. (a) $T=-21.1^{\circ}\text{C}$; (b) -0.3°C ; (c) 14.9°C ; (d) 34.3°C ; (e) 48.8°C	140
Figure M.8 Comparison of the values of the complex modulus back-calculated from dynamic tests at each temperature with methods III (E_{BC3}^*), IV (E_{BC4}^*) and V (E_{BC5}^*). Results for specimen WF-6.....	141
Figure M.9 Comparison of the values of the complex modulus determined from dynamic tests with method IV (E_{BC4}^* and E_{Dyn4}^*) and method V (E_{BC5}^* and E_{Dyn5}^*) with the values of the complex modulus determined from cyclic tests (E_{ExpTC}^* and E_{TC}^*). (a) Cole-Cole plot; (b) and (c) master curves of the norm and of the phase angle of the complex modulus at 15°C . Results for specimen WF-6.....	141
Figure M.10 Comparison of the values of the complex Poisson's ratio determined from dynamic tests with method V (real values v_{BC5} and v_{Dyn5}^*) with the values of the complex Poisson's ratio determined from cyclic test (v_{ExpTC}^* and v_{TC}^*). (a) Cole-Cole plot; (b) and (c) master curves of the norm and of the phase angle of the complex Poisson's ratio at 15°C . Results for specimen WF-6.....	142
Figure M.11 Comparison of the experimental FRFs (noted Exp. FRF) with the FRFs after optimization (noted FRF A.O) and the global LVE FRFs (noted G.LVE FRF) obtained with method IV for specimen WF-8. (a) $T=-21^{\circ}\text{C}$; (b) -0.3°C ; (c) 15°C ; (d) 34.2°C ; (e) 48.7°C .	143
Figure M.12 Comparison of the experimental FRFs (noted Exp. FRF) with the FRFs after optimization (noted FRF A.O) and the global LVE FRFs (noted G.LVE FRF) obtained with method V for specimen WF-8. Values of the experimental FRFs at the frequencies where the	

optimization is performed (noted Opt. Points) are also plotted. (a) T=-21°C; (b) -0.3°C; (c) 15°C; (d) 34.2°C; (e) 48.7°C..... 144

Figure N.1 Comparison of the experimental FRFs measured at the end of the project (noted Exp. FRF) with the FRFs after optimization (noted FRF A.O) and the global LVE FRFs (noted G.LVE FRF) for specimen GB-L-1. Values of the experimental FRFs at the frequencies where the optimization is performed (noted Opt. Points) are also plotted. (a) T=-20.8°C; (b) -0.5°C; (c) 15.5°C; (d) 34.3°C; (e) 48.8°C. 146

Figure N.2 Comparison of the values of the complex modulus determined from dynamic tests with method V (E_{BC5}^* and E_{Dyn5}^*) with the values of the complex modulus determined from cyclic tests (E_{ExpTC}^* and E_{TC}^*). (a) Cole-Cole plot; (b) and (c) master curves of the norm and of the phase angle of the complex modulus at 15°C. Results for specimen GB-L-1. 147

Figure N.3 Comparison of the values of the complex Poisson’s ratio determined from dynamic tests with method V (real values v_{BC5} and v_{Dyn5}^*) with the values of the complex Poisson’s ratio determined from cyclic test (v_{ExpTC}^* and v_{TC}^*). (a) Cole-Cole plot; (b) and (c) master curves of the norm and of the phase angle of the complex Poisson’s ratio at 15°C. Results for specimen GB-L-1. 148

Figure N.4 Comparison of the experimental FRFs (noted Exp. FRF) with the FRFs after optimization (noted FRF A.O) and the global LVE FRFs (noted G.LVE FRF) for specimen GB-L-2. Values of the experimental FRFs at the frequencies where the optimization is performed (noted Opt. Points) are also plotted. (a) T=-21°C; (b) -0.6°C; (c) 15.5 °C; (d) 34.3°C; (e) 49°C. 149

Figure N.5 Values of the complex modulus determined from dynamic tests with method III (E_{BC3}^* and E_{Dyn3}^*). (a) Cole-Cole plot; (b) and (c) master curves of the norm and of the phase angle of the complex modulus at 15°C. Results for specimen GB-L-2. 150

Figure N.6 Comparison of the experimental FRFs (noted Exp. FRF) with the FRFs after optimization (noted FRF A.O) and the global LVE FRFs (noted G.LVE FRF) for specimen GB-L-3. Values of the experimental FRFs at the frequencies where the optimization is performed (noted Opt. Points) are also plotted. (a) T=-21.7°C; (b) -0.8°C; (c) 14.5°C; (d) 34.3°C; (e) 49.3°C..... 151

Figure N.7 Values of the complex modulus determined from dynamic tests with method III (E_{BC3}^* and E_{Dyn3}^*). (a) Cole-Cole plot; (b) and (c) master curves of the norm and of the phase angle of the complex modulus at 15°C. Results for specimen GB-L-3. 152

Figure N.8 Comparison of the experimental FRFs (noted Exp. FRF) with the FRFs after optimization (noted FRF A.O) and the global LVE FRFs (noted G.LVE FRF) for specimen GB-L-4. Values of the experimental FRFs at the frequencies where the optimization is performed (noted Opt. Points) are also plotted. (a) T=-21.7°C; (b) -0.9°C; (c) 14.6°C; (d) 34.2°C; (e) 49.3°C..... 153

Figure N.9 Values of the complex modulus determined from dynamic tests with method III (E_{BC3}^* and E_{Dyn3}^*). (a) Cole-Cole plot; (b) and (c) master curves of the norm and of the phase angle of the complex modulus at 15°C. Results for specimen GB-L-4. 154


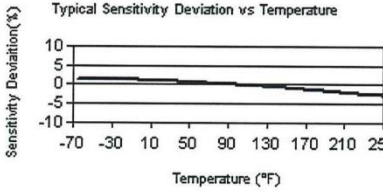

Figure N.10 Comparison of the experimental FRFs (noted Exp. FRF) with the FRFs after optimization (noted FRF A.O) and the global LVE FRFs (noted G.LVE FRF) for specimen GB-L-5. Values of the experimental FRFs at the frequencies where the optimization is performed

(noted Opt. Points) are also plotted. (a) $T=-21.5^{\circ}\text{C}$; (b) -0.8°C ; (c) 14.6°C ; (d) 34.3°C ; (e) 49.3°C	155
Figure N.11 Values of the complex modulus determined from dynamic tests with method III (E_{BC3}^* and E_{Dyn3}^*). (a) Cole-Cole plot; (b) and (c) master curves of the norm and of the phase angle of the complex modulus at 15°C . Results for specimen GB-L-5.	156
Figure N.12 Comparison of the experimental FRFs (noted Exp. FRF) with the FRFs after optimization (noted FRF A.O) and the global LVE FRFs (noted G.LVE FRF) for specimen GB'-L-1. Values of the experimental FRFs at the frequencies where the optimization is performed (noted Opt. Points) are also plotted. (a) $T=-21.7^{\circ}\text{C}$; (b) -0.9°C ; (c) 14.6°C ; (d) 34.3°C ; (e) 48.8°C	157
Figure N.13 Values of the complex modulus determined from dynamic tests with method III (E_{BC3}^* and E_{Dyn3}^*). (a) Cole-Cole plot; (b) and (c) master curves of the norm and of the phase angle of the complex modulus at 15°C . Results for specimen GB'-L-1.....	158
Figure N.14 Comparison of the experimental FRFs (noted Exp. FRF) with the FRFs after optimization (noted FRF A.O) and the global LVE FRFs (noted G.LVE FRF) for specimen GB'-L-2. Values of the experimental FRFs at the frequencies where the optimization is performed (noted Opt. Points) are also plotted. (a) $T=-21.3^{\circ}\text{C}$; (b) -0.7°C ; (c) 14.6°C ; (d) 34.2°C ; (e) 49.2°C	159
Figure N.15 Values of the complex modulus determined from dynamic tests with method III (E_{BC3}^* and E_{Dyn3}^*). (a) Cole-Cole plot; (b) and (c) master curves of the norm and of the phase angle of the complex modulus at 15°C . Results for specimen GB'-L-2.....	160
Figure N.16 Comparison of the experimental FRFs (noted Exp. FRF) with the FRFs after optimization (noted FRF A.O) and the global LVE FRFs (noted G.LVE FRF) for specimen GB'-L-3. Values of the experimental FRFs at the frequencies where the optimization is performed (noted Opt. Points) are also plotted. (a) $T=-21.5^{\circ}\text{C}$; (b) -0.8°C ; (c) 14.6°C ; (d) 34.3°C ; (e) 49.2°C	161
Figure N.17 Values of the complex modulus determined from dynamic tests with method III (E_{BC3}^* and E_{Dyn3}^*). (a) Cole-Cole plot; (b) and (c) master curves of the norm and of the phase angle of the complex modulus at 15°C . Results for specimen GB'-L-3.....	162
Figure N.18 Comparison of the experimental FRFs (noted Exp. FRF) with the FRFs after optimization (noted FRF A.O) and the global LVE FRFs (noted G.LVE FRF) for specimen GB-T-1. Values of the experimental FRFs at the frequencies where the optimization is performed (noted Opt. Points) are also plotted. (a) $T=-20.8^{\circ}\text{C}$; (b) -0.4°C ; (c) 15.4°C ; (d) 34.3°C ; (e) 48.8°C	163
Figure N.19 Values of the complex modulus determined from dynamic tests with method III (E_{BC3}^* and E_{Dyn3}^*). (a) Cole-Cole plot; (b) and (c) master curves of the norm and of the phase angle of the complex modulus at 15°C . Results for specimen GB-T-1.	164
Figure N.20 Comparison of the experimental FRFs (noted Exp. FRF) with the FRFs after optimization (noted FRF A.O) and the global LVE FRFs (noted G.LVE FRF) for specimen GB-T-2. Values of the experimental FRFs at the frequencies where the optimization is performed (noted Opt. Points) are also plotted. (a) $T=-21.1^{\circ}\text{C}$; (b) -0.5°C ; (c) 15.3°C ; (d) 34.3°C ; (e) 48.8°C	165

Figure N.21 Values of the complex modulus determined from dynamic tests with method III (E_{BC3}^* and E_{Dyn3}^*). (a) Cole-Cole plot; (b) and (c) master curves of the norm and of the phase angle of the complex modulus at 15°C. Results for specimen GB-T-2.	166
Figure N.22 Comparison of the experimental FRFs (noted Exp. FRF) with the FRFs after optimization (noted FRF A.O) and the global LVE FRFs (noted G.LVE FRF) for specimen BB-L-1. Values of the experimental FRFs at the frequencies where the optimization is performed (noted Opt. Points) are also plotted. (a) T=-20.9°C; (b) -0.4°C; (c) 15.1°C; (d) 29.4°C; (e) 43.9°C.....	167
Figure N.23 Comparison of the experimental FRFs (noted Exp. FRF) with the FRFs after optimization (noted FRF A.O) and the global LVE FRFs (noted G.LVE FRF) for specimen BB-L-2. Values of the experimental FRFs at the frequencies where the optimization is performed (noted Opt. Points) are also plotted. (a) T=-21.5°C; (b) -0.6°C; (c) 15.1°C; (d) 29.5°C; (e) 44.2°C.....	168
Figure N.24 Values of the complex modulus determined from dynamic tests with method III (E_{BC3}^* and E_{Dyn3}^*). (a) Cole-Cole plot; (b) and (c) master curves of the norm and of the phase angle of the complex modulus at 15°C. Results for specimen BB-L-2.	169
Figure N.25 Comparison of the experimental FRFs (noted Exp. FRF) with the FRFs after optimization (noted FRF A.O) and the global LVE FRFs (noted G.LVE FRF) for specimen BB-T-1. Values of the experimental FRFs at the frequencies where the optimization is performed (noted Opt. Points) are also plotted. (a) T=-21.1°C; (b) -0.4°C; (c) 15°C; (d) 29.4°C; (e) 44°C.	170
Figure N.26 Values of the complex modulus determined from dynamic tests with method III (E_{BC3}^* and E_{Dyn3}^*). (a) Cole-Cole plot; (b) and (c) master curves of the norm and of the phase angle of the complex modulus at 15°C. Results for specimen BB-T-1.	171
Figure N.27 Comparison of the experimental FRFs (noted Exp. FRF) with the FRFs after optimization (noted FRF A.O) and the global LVE FRFs (noted G.LVE FRF) for specimen BB-T-2. Values of the experimental FRFs at the frequencies where the optimization is performed (noted Opt. Points) are also plotted. (a) T=-21°C; (b) -0.4°C; (c) 15°C; (d) 29.4°C; (e) 43.9°C.	172
Figure N.28 Values of the complex modulus determined from dynamic tests with method III (E_{BC3}^* and E_{Dyn3}^*). (a) Cole-Cole plot; (b) and (c) master curves of the norm and of the phase angle of the complex modulus at 15°C. Results for specimen BB-T-2.	173

**APPENDIX A- DETAILS ABOUT THE
EXPERIMENTAL DEVICES**

TECHNICAL SPECIFICATIONS OF THE ACCELEROMETER

Model Number 353B15	ICP® ACCELEROMETER		Revision: M ECN #: 35369	
Performance	ENGLISH	SI	OPTIONAL VERSIONS	
Sensitivity(± 10 %)	10 mV/g	1.02 mV/(m/s ²)	Optional versions have identical specifications and accessories as listed for the standard model except where noted below. More than one option may be used.	
Measurement Range	± 500 g pk	± 4905 m/s ² pk	A - Adhesive Mount Supplied Accessory : Model 080A90 Quick Bonding Gel (1)	
Frequency Range(± 5 %)	1 to 10,000 Hz	1 to 10,000 Hz	B - Low bias electronics	
Frequency Range(± 10 %)	0.7 to 18,000 Hz	0.7 to 18,000 Hz	Output Bias Voltage 4.5 to 7.5 VDC 4.5 to 7.5 VDC	
Frequency Range(± 3 dB)	0.35 to 30,000 Hz	0.35 to 30,000 Hz	Excitation Voltage 12 to 30 VDC 12 to 30 VDC	
Resonant Frequency	≥ 70 kHz	≥ 70 kHz	Constant Current Excitation 1 to 20 mA 1 to 20 mA	
Broadband Resolution(1 to 10,000 Hz)	0.005 g rms	0.05 m/s ² rms [1]	Measurement Range ± 300 g pk ± 2943 m/s ² pk	
Non-Linearity	≤ 1 %	≤ 1 % [2]	J - Ground Isolated	
Transverse Sensitivity	≤ 5 %	≤ 5 % [3]	Frequency Range(± 5 %) 1 to 8000 Hz 1 to 8000 Hz	
Environmental			Frequency Range(± 10 %) 0.7 to 15,000 Hz 0.7 to 15,000 Hz	
Overload Limit(Shock)	± 10,000 g pk	± 98,100 m/s ² pk	Resonant Frequency ≥ 56 kHz ≥ 56 kHz	
Temperature Range(Operating)	-65 to +250 °F	-54 to +121 °C	Electrical Isolation(Base) ≥ 10 ⁹ ohm ≥ 10 ⁹ ohm	
Temperature Response	See Graph	See Graph [1]	Size - Hex x Height 0.37 in x 0.57 in 9.5 mm x 14.5 mm	
Base Strain Sensitivity	≤ 0.002 g/με	≤ 0.02 (m/s ²)/με [1]	Weight 0.11 oz 3.2 gm [1]	
Electrical			M - Metric Mount	
Excitation Voltage	20 to 30 VDC	20 to 30 VDC	Mounting Thread M3 x 0.50 Male M3 x 0.50 Male	
Constant Current Excitation	2 to 20 mA	2 to 20 mA	Supplied Accessory : Model M080A15 Adhesive Mounting Base (1) replaces Model 080A15	
Output Impedance	≤ 100 ohm	≤ 100 ohm	Q - Extended discharge time constant	
Output Bias Voltage	8 to 12 VDC	8 to 12 VDC	Frequency Range(± 5 %) 0.15 to 10,000 Hz 0.15 to 10,000 Hz	
Discharge Time Constant	0.5 to 2.0 sec	0.5 to 2.0 sec	Frequency Range(± 10 %) 0.1 to 18,000 Hz 0.1 to 18,000 Hz	
Settling Time(within 10% of bias)	<5 sec	<5 sec	Discharge Time Constant ≥ 5 sec ≥ 5 sec	
Spectral Noise(1 Hz)	2800 μg/√Hz	27,468 (μm/sec ²)/√Hz [1]	Settling Time(within 10% of bias) ≤ 45 sec ≤ 45 sec	
Spectral Noise(10 Hz)	700 μg/√Hz	6867 (μm/sec ²)/√Hz [1]	Supplied Accessory : Model ACS-4 Single axis, low frequency phase and amplitude response cal from 0.5 to 10 Hz (1)	
Spectral Noise(100 Hz)	180 μg/√Hz	1766 (μm/sec ²)/√Hz [1]	W - Water Resistant Cable	
Spectral Noise(1 kHz)	64 μg/√Hz	628 (μm/sec ²)/√Hz [1]	Electrical Connector Sealed Integral Cable Sealed Integral Cable	
Physical			Electrical Connection Position Side Side	
Sensing Element	Quartz	Quartz		
Sensing Geometry	Shear	Shear		
Housing Material	Titanium	Titanium		
Sealing	Welded Hermetic	Welded Hermetic		
Size (Hex x Height)	0.31 in x 0.43 in	7.9 mm x 10.9 mm [1]		
Weight	0.07 oz	2.0 gm		
Electrical Connector	5-44 Coaxial	5-44 Coaxial		
Electrical Connection Position	Side	Side		
Mounting Thread	5-40 Male	5-40 Male		
Mounting Torque	8 to 12 in-lb	90 to 135 N-cm		
<p>NOTES:</p> <p>[1] Typical. [2] Zero-based, least-squares, straight line method. [3] Transverse sensitivity is typically ≤ 3%. [4] See PCB Declaration of Conformance PS023 for details.</p>				
<p>SUPPLIED ACCESSORIES:</p> <p>Model 080A109 Petro Wax (1) Model 080A15 Adhesive Mounting Base (1) Model ACS-1 NIST traceable frequency response (10 Hz to upper 5% point). (1)</p>				
Entered: <i>49mu</i>	Engineer: <i>BAM</i>	Sales: <i>WDC</i>	Approved: <i>EB</i>	Spec Number:
Date: <i>3/24/11</i>	Date: <i>3/24/11</i>	Date: <i>3/24/11</i>	Date: <i>3/24/11</i>	353-2150-80
				
<p>All specifications are at room temperature unless otherwise specified. In the interest of constant product improvement, we reserve the right to change specifications without notice. ICP® is a registered trademark of PCB Group, Inc.</p>				
			Phone: 716-684-0001 Fax: 716-685-3886 E-Mail: vibration@pcb.com	
3425 Walden Avenue, Depew, NY 14043				

CALIBRATION CERTIFICATE OF THE ACCELEROMETER

~ Calibration Certificate ~
Per ISO 16063-21

Model Number: 353B15
 Serial Number: LW189420
 Description: ICP® Accelerometer
 Manufacturer: PCB Method: Back-to-Back Comparison AT401-3

Calibration Data

Sensitivity @ 100 Hz	10.43 mV/g (1.064 mV/m/s ²)	Output Bias	8.5 VDC
Discharge Time Constant	0.8 seconds	Transverse Sensitivity	0.6 %
		Resonant Frequency	73.7 kHz

Sensitivity Plot

Temperature: 73 °F (23 °C) Relative Humidity: 58 %

Data Points

Frequency (Hz)	Dev. (%)	Frequency (Hz)	Dev. (%)	Frequency (Hz)	Dev. (%)
10	-0.6	300	0.2	7000	2.3
15	-0.5	500	0.2	10000	2.8
30	-0.4	1000	0.3		
50	-0.2	3000	0.6		
REF. FREQ.	0.0	5000	1.1		

Mounting Surface: Tungsten Adapter w/Silicone Grease Fastener: 5-40 Male Fixture Orientation: Vertical
 Acceleration Level (pk): 10.0 g (98.1 m/s²)
 The acceleration level may be limited by shaker displacement at low frequencies. If the listed level cannot be obtained, the calibration system uses the following formula to set the vibration amplitude: Acceleration Level (g) = 0.008 x (freq)^{1.5} *The gravitational constant used for calculations by the calibration system is: 1 g = 9.80665 m/s²

Condition of Unit

As Found: n/a
 As Left: New Unit, In Tolerance

Notes

1. Calibration is NIST Traceable thru Project 683/283498 and PTB Traceable thru Project 10065.
2. This certificate shall not be reproduced, except in full, without written approval from PCB Piezotronics, Inc.
3. Calibration is performed in compliance with ISO 9001, ISO 10012-1, ANSI Z540.3 and ISO 17025.
4. See Manufacturer's Specification Sheet for a detailed listing of performance specifications.
5. Measurement uncertainty (95% confidence level with coverage factor of 2) for frequency ranges tested during calibration are as follows: 5-9 Hz; +/- 2.0%, 10-99 Hz; +/- 1.5%, 100-1999 Hz; +/- 1.0%, 2-10 kHz; +/- 2.5%.

Technician: Mary Warren *MW* Date: 6/10/2015

ACCREDITED
CALIBRATION CERT #1862.01
PAGE 1 of 1



PCB PIEZOTRONICS
VIBRATION DIVISION
3425 Walden Avenue Depew, NY 14043
TEL: 888-684-0013 FAX: 716-685-3886 www.pcb.com

CAL63-3516783734.221+0

ACS-1



TECHNICAL SPECIFICATIONS OF THE SIGNAL CONDITIONER

Model Number 482C15	FOUR-CHANNEL, ICP SENSOR SIGNAL CONDITIONER		Revision: J ECN #: 47052	
Performance	ENGLISH	SI	OPTIONAL VERSIONS	
Channels	4	4	Optional versions have identical specifications and accessories as listed for the standard model except where noted below. More than one option may be used.	
Sensor Input Type(s)	ICP®, Voltage	ICP®, Voltage		[2]
Voltage Gain(± 1 %)(at 500 Hz)	x1, x10, x100	x1, x10, x100		[2]
Output Range(Maximum)	± 10 V	± 10 V		
Low Frequency Response(-5 %)	<0.05 Hz	<0.05 Hz		[5][3]
High Frequency Response(-3 dB)(x100)	>50 kHz	>50 kHz		
High Frequency Response(-5 %)(x100)	>17 kHz	>17 kHz		
High Frequency Response(-5 %)(x1)	>100 kHz	>100 kHz		
High Frequency Response(-5 %)(x10)	>40 kHz	>40 kHz		
High Frequency Response(-3 dB)(x1,x10)	>100 kHz	>100 kHz		
Phase Response(at 1 kHz)	± 1 °	± 1 °		
Cross Talk(maximum)	-72 dB	-72 dB		
Fault/Bias Monitor/Meter(LED)	Open/Short/Overload	Open/Short/Overload		
Environmental				
Temperature Range(Operating)	+32 to +120 °F	0 to +50 °C		
Electrical				
Power Required(for supplied AC power adaptor)	AC Power	AC Power		
Power Required(direct input to unit)	DC Power	DC Power		
AC Power(47 to 63 Hz)	100 to 240 VAC	100 to 240 VAC		
AC Power	≤ 0.7 Amps	≤ 0.7 Amps		
DC Power	<0.25 Amps	<0.25 Amps		
DC Power	+32 to 38 VDC	+32 to 38 VDC		
Excitation Voltage(± 1 VDC)(To Sensor)	+26 VDC	+26 VDC		
DC Offset	<20 mV	<20 mV		
Constant Current Excitation(To Sensor)	0 to 20 mA	0 to 20 mA	[1]	
Overload Threshold(± 1.0 Vpk)	± 10/5 Vpk	± 10/5 Vpk	[2]	
Discharge Time Constant(0 to 50 %)	>7 sec	>7 sec	[3]	
Broadband Electrical Noise(1 to 10,000 Hz)(Gain x1)	5.6 µV rms	5.6 µV rms	[4]	
Spectral Noise(1 Hz)	0.67 µV/√Hz	0.67 µV/√Hz	[4]	
Spectral Noise(10 Hz)	0.10 µV/√Hz	0.10 µV/√Hz	[4]	
Spectral Noise(100 Hz)	0.06 µV/√Hz	0.06 µV/√Hz	[4]	
Spectral Noise(1 kHz)	0.06 µV/√Hz	0.06 µV/√Hz	[4]	
Spectral Noise(10 kHz)	0.05 µV/√Hz	0.05 µV/√Hz	[4]	
Broadband Electrical Noise(1 to 10,000 Hz)(Gain x10)	21 µV/rms	21 µV/rms	[4]	
Spectral Noise(1 Hz)	5.10 µV/√Hz	5.10 µV/√Hz	[4]	
Spectral Noise(10 Hz)	0.60 µV/√Hz	0.60 µV/√Hz	[4]	
Spectral Noise(100 Hz)	0.22 µV/√Hz	0.22 µV/√Hz	[4]	
Spectral Noise(1 kHz)	0.22 µV/√Hz	0.22 µV/√Hz	[4]	
Spectral Noise(10 kHz)	0.19 µV/√Hz	0.19 µV/√Hz	[4]	
Broadband Electrical Noise(1 to 10,000 Hz)(Gain x100)	165 µV/rms	165 µV/rms	[4]	
Spectral Noise(1 Hz)	57 µV/√Hz	57 µV/√Hz	[4]	
Spectral Noise(10 Hz)	5.2 µV/√Hz	5.2 µV/√Hz	[4]	
Spectral Noise(100 Hz)	1.7 µV/√Hz	1.7 µV/√Hz	[4]	
Spectral Noise(1 kHz)	1.8 µV/√Hz	1.8 µV/√Hz	[4]	
Spectral Noise(10 kHz)	1.4 µV/√Hz	1.4 µV/√Hz	[4]	
Physical				
Electrical Connector(ICP® Sensor Input)	BNC Jack	BNC Jack		
Electrical Connector(Output)	BNC Jack	BNC Jack		
Electrical Connector(DC Power Input)	5-socket DIN (female)	5-socket DIN (female)		
Size (Height x Width x Depth)	3.2 in x 8.0 in x 5.9 in	8.1 cm x 20 cm x 15 cm		
Weight	1.25 lb	567 gm		
 [6]				
All specifications are at room temperature unless otherwise specified. In the interest of constant product improvement, we reserve the right to change specifications without notice.				
ICP® is a registered trademark of PCB Group, Inc.				
NOTES: [1] User adjustable, factory set at 4 mA (± 0.5 mA). One control adjusts all channels. [2] Jumper selectable on internal circuit board. [3] Un-buffered output, read out device input impedance affects discharge time constant and low frequency response of unit. [4] Typical. [5] The low frequency tolerance is accurate within ±25% of the specified frequency. [6] See PCB Declaration of Conformance PS024 for details.				
SUPPLIED ACCESSORIES: Model 017AXX Power Cord (1) Model 488B04/NC Power Converter (1)				
Entered: LK	Engineer: CPH	Sales: ML	Approved: ECB	Spec Number:
Date: 7/18/2017	Date: 7/18/2017	Date: 7/18/2017	Date: 7/18/2017	38208
			Phone: 716-684-0001 Fax: 716-684-0987 E-Mail: info@pcb.com	
3425 Walden Avenue, Depew, NY 14043				

CALIBRATION CERTIFICATE OF THE SIGNAL CONDITIONER

~ Calibration Certificate ~

Model Number: 482C15 Customer: _____
 Serial Number: 1535 _____
 Description: 4 Channel Signal Conditioner P.O.: _____
 Manufacturer: PCB Method: Comparison Method (AT104-29)

Calibration Data

Temperature: 73 °F (23 °C) Humidity: 58%

Channel	Volts	Current (mA)	Gain X1	Gain X10	Gain X100
1	25.7	4.18	1.000	10.008	99.9
2	25.7	4.19	0.999	10.009	99.9
3	25.7	4.22	1.000	10.008	99.9
4	25.7	4.22	1.000	10.009	99.9

Condition of Unit

As Found: n/a
 As Left: New unit, in tolerance

Notes

1. Calibration is N.I.S.T. traceable through PCB control number QC-214.
2. This certificate shall not be reproduced, except in full, without written approval from PCB Piezotronics, Inc.
3. Calibration is performed in compliance with ISO 9001, ISO 10012-1, ANSI/NCSL Z540.3 and ISO 17025.
4. Measurement uncertainty (95% confidence level with a coverage factor of 2) for the sensitivity reading is +/- 0.2 %
5. See Manufacturer's Specification Sheet for a detailed listing of performance specifications.

Technician: CVega C.V. Date: 05/08/15
 Due Date: _____



TEL: 888-684-0013

3425 Walden Avenue
 Depew, New York 14043
 FAX: 716-685-3886

www.pcb.com

TECHNICAL SPECIFICATIONS OF THE IMPACT HAMMER

Model Number 086E80	ICP® IMPACT HAMMER			Revision: C ECN #: 44362
Performance	ENGLISH	SI		OPTIONAL VERSIONS Optional versions have identical specifications and accessories as listed for the standard model except where noted below. More than one option may be used.
Sensitivity(± 20 %)	100 mV/lbf	22.5 mV/N	[2]	
Measurement Range	50 lbf pk	222 N pk		NOTES: [1]Typical. [2]Steel tip with no extender mass. [3]With plastic handle attached. [4]With aluminum handle attached. [5]See PCB Declaration of Conformance PS136 for details.
Resonant Frequency	≥ 100 kHz	≥ 100 kHz		
Non-Linearity	≤ 1 %	≤ 1 %	[1]	
Electrical				SUPPLIED ACCESSORIES: Model 001A20 Case (1) Model 018G10 Miniature coaxial cable, vinyl insulation jacket, 10-ft, 5-44 to 10-32 coaxial plug (1) Model 080A109 Petro Wax (1) Model 084A13 Extender mass (1) Model 084A14 Plastic handle assembly (2) Model 084A17 Aluminum handle with 5-44 connector (1) Model 084A28 Vinyl impact cap, red (3) Model HCS-2 Calibration of Series 086 instrumented impact hammers (1)
Excitation Voltage	20 to 30 VDC	20 to 30 VDC		
Constant Current Excitation	2 to 20 mA	2 to 20 mA		
Output Impedance	<100 Ohm	<100 Ohm		
Output Bias Voltage	8 to 14 VDC	8 to 14 VDC		Entered: JM Engineer: NJF Sales: RWM Approved: NJF Spec Number:
Discharge Time Constant	≥ 100 sec	≥ 100 sec	[1]	
Physical				Date: 6/29/2015 Date: 6/29/2015 Date: 6/29/2015 Date: 6/29/2015 38869
Sensing Element	Quartz	Quartz		PCB PIEZOTRONICS™ 3425 Walden Avenue, Depew, NY 14043 Phone: 716-684-0001 Fax: 716-684-0987 E-Mail: info@pcb.com
Sealing	Epoxy	Epoxy		
Hammer Mass	0.17 oz	4.8 gm	[3]	
Head Diameter	0.25 in	6.3 mm		
Tip Diameter	0.10 in	2.5 mm		
Hammer Length	4.2 in	107 mm	[3]	
Electrical Connection Position	Side	Side		
Extender Mass Weight	0.044 oz	1.25 gm		
Electrical Connector	5-44 Coaxial	5-44 Coaxial	[4]	



All specifications are at room temperature unless otherwise specified.
In the interest of constant product improvement, we reserve the right to change specifications without notice.
ICP® is a registered trademark of PCB Group, Inc.

CALIBRATION CERTIFICATE OF THE IMPACT HAMMER

~Calibration Certificate~

Model No.: 086E80 Customer: _____
 Serial No.: 36616 _____
 Description: Impulse Force Hammer PO No.: _____
 Manufacturer: PCB Calibration Method: Impulse (AT-303-1)

Data

Output Bias: **10.2** Temperature: 74 °F 23 °C Relative Humidity: 54 %

HAMMER SENSITIVITY:

Tip	Steel	Vinyl	Vinyl
Hammer Configuration			
Extender	None	Steel	None
Hammer Sensitivity	mV/lb	105.1	79.94
	(mV/N)	23.64	17.97
		76.54	17.21

Above data is valid for all supplied tips.

Condition of Unit:

As Found N/A
 As Left New Unit, In Tolerance

Notes:

1. Calibration is NIST Traceable thru Project 683/283498 and PTB Traceable thru Project 10065.
2. This certificate may not be reproduced, except in full, without written approval from PCB Piezotronics, Inc..
3. Calibration is performed in compliance with ISO 10012-1, ANSI/NCSL Z540.3.
4. See Manufacturer's specification sheet for a detailed listing of performance specifications.
5. Measurement uncertainty (95% confidence level with a coverage factor of 2) is +/-3.8%.

Technician: Richard Gardner *RG*

Date: 5/29/2015



3425 Walden Avenue
 Depew, N.Y. 14043

TEL: 716-684-0001

FAX: 716-684-0987

www.pcb.com

Calibration Station: 13

TECHNICAL SPECIFICATIONS OF THE ARDUINO MICROCONTROLLER

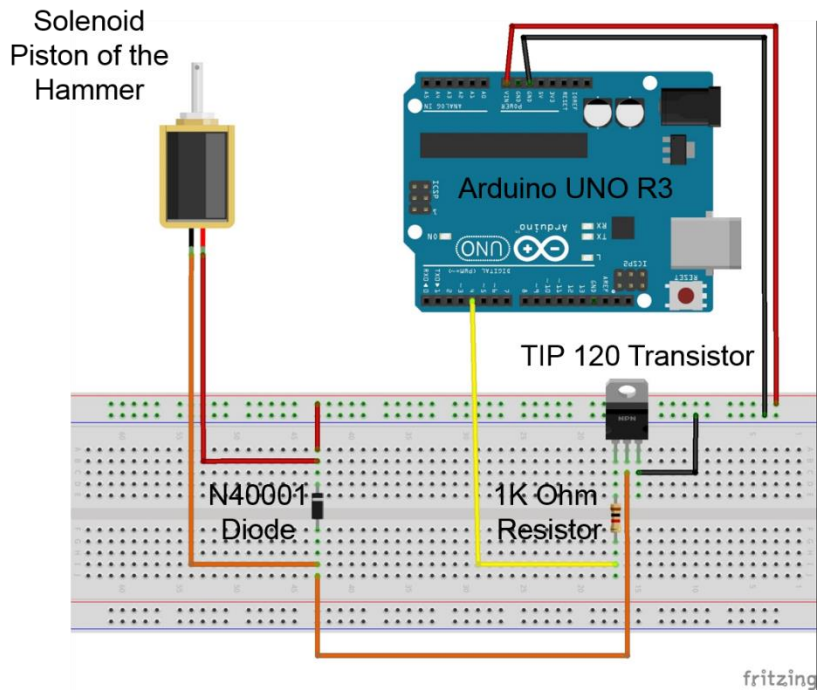


Microcontroller	ATmega328P
Operating Voltage	5V
Input Voltage (recommended)	7-12V
Input Voltage (limit)	6-20V
Digital I/O Pins	14 (of which 6 provide PWM output)
PWM Digital I/O Pins	6
Analog Input Pins	6
DC Current per I/O Pin	20 mA
DC Current for 3.3V Pin	50 mA
Flash Memory	32 KB (ATmega328P) of which 0.5 KB used by bootloader
SRAM	2 KB (ATmega328P)
EEPROM	1 KB (ATmega328P)
Clock Speed	16 MHz
LED_BUILTIN	13
Length	68.6 mm
Width	53.4 mm
Weight	25 g

CODE PROGRAMING THE ARDUINO MICROCONTROLLER

```
Essai
1 int solenoidPin = 13; //This is the output pin on the Arduino we are using
2
3 void setup() {
4   // put your setup code here, to run once:
5   pinMode(solenoidPin, OUTPUT); //Sets the pin as an output
6 }
7
8 void loop() {
9   // put your main code here, to run repeatedly:
10  // for loop increasing the value of variable i from 0 to 15 in steps of 1
11  for (int i=0; i <= 14; i++){
12    digitalWrite(solenoidPin, HIGH); //Switch Solenoid ON
13    delay(30); //Wait 30 Millisecond
14    digitalWrite(solenoidPin, LOW); //Switch Solenoid OFF
15    delay(1000); //Wait 1 Second
16  } // fin de la boucle for
17    delay(10000);
18 }
```

ELECTRONIC CIRCUIT CONTROLLING THE AUTOMATED IMPACT HAMMER



**APPENDIX B- DATA BASE OF 2S2P1D MODEL AND
WLF EQUATION CONSTANTS OBTAINED
FROM CYCLIC TENSION-COMPRESSION TESTS
PERFORMED ON DIFFERENT BITUMINOUS
MIXTURES**

APPENDIX B – DATA BASE OF 2S2P1D MODEL AND WLF EQUATION CONSTANTS OBTAINED FROM CYCLIC TENSION-COMPRESSION TESTS PERFORMED ON DIFFERENT BITUMINOUS MIXTURES

Table B.1. 2S2P1D model and WLF equation constants obtained from cyclic tension-compression tests performed on different bituminous mixtures.

Material	Specimen	2S2P1D model										WLF Equation at 15°C	
		E ₀₀ (MPa)	E ₀ (MPa)	v ₀	v ₀₀	δ	k	h	β	τ _{E15°C} (s)	τ _{v15°C} (s)	C ₁	C ₂
E1525-5.1-0	10	47	39 000	0.23	0.39	2.28	0.152	0.49	220	0.77	77.5	31.6	213.7
	1	47	40 000	0.24	0.39								
	2	47	39 400	0.21	0.44								
E1525-5.8-1.25	7	20	36 500	0.25	0.50	2.20				0.83	333.1	33.1	213.8
	12	20	36 500	0.24	0.47								
E3550-4.4-0	6	10	40 800	0.24	0.55	2.00				0.10	73.5		
	11	15	41 600	0.27	0.47								
E3550-4.4-1.25	1	11	40 800	0.26	0.47	1.95				0.14	54.5		
	4	11	41 100	0.26	0.54								
E3550-4.4-2.5	2	70	41 500	0.27	0.45	1.82				0.18	3.4		
	1	55	42 000	0.23	0.51								
E3550-5.1-0	1	19	38 800	0.26	0.50	2.0				0.09	57.4		
	2	25	38 700	0.26	0.50								
E3550-5.1-1.25	8	9	38 400	0.27	0.56	1.95	0.172	0.57	95	0.09	37.6	32.0	213.0
	12	10	39 300	0.25	0.58								
E3550-5.1-2.5	2	18	40 300	0.25	0.50	1.90				0.12	36.1		
	4	42	39 000	0.22	0.53								
E3550-5.8-0	4	20	37 700	0.27	0.51	2.00				0.04	25.4		
	12	18	36 700	0.27	0.60								
E3550-5.8-1.25	10	18	36 400	0.29	0.51	2.20				0.06	22.6		
	6	9	35 400	0.25	0.58								
E3550-5.8-2.5	1	9	37 600	0.23	0.49	2.00				0.07	43.5		
	4	12	38 600	0.24	0.63								
E3550M-5.1-1.25	4	20	38 900	0.22	0.48	2.40	0.142	0.45	3 000	0.04	20.5	33.1	215.2
	3	24	39 300	0.27	0.53								

APPENDIX B – DATA BASE OF 2S2P1D MODEL AND WLF EQUATION CONSTANTS OBTAINED FROM CYCLIC TENSION-COMPRESSION TESTS PERFORMED ON DIFFERENT BITUMINOUS MIXTURES

Material	Specimen	E ₀₀ (MPa)	E ₀ (MPa)	v ₀	v ₀₀	δ	k	h	β	τ _{E15°C} (s)	τ _{v15°C} (s)	C ₁	C ₂																																																																																																																																																																																																																																																																																																		
Ebip-5.1-1.25	9	43	40 600	0.25	0.52	2.05	0.166	0.55	1 000	0.09	50.3	33.8	209.0																																																																																																																																																																																																																																																																																																		
	2	17	40 000	0.35	0.52									Eort-5.1-1.25	3	17	40 000	0.30	0.61	1.79	0.178	0.53	9 000	0.002	0.2	32.0	215.4	9	21	39 300	0.30	0.42	M1	M1R1	180	42 000	0.19	0.49	2.00	0.230	0.50	400	0.04	-	27.1	187.4	M2	M2U2	12	30 900	0.21	0.38	2.30	0.170	0.55	150	0.20	-	17.8	132.8	A.0.15-25	-	13	37 200	0.22	0.48	2.50	0.165	0.51	680	2.90	19.0	41.6	249.9	A.0.35-50	-	14	36 000	0.35	0.35	2.25	0.179	0.56	200	0.21	1.5	30.9	196.0	A.20.35-50	-	16	37 250	0.47	0.47	2.40	0.173	0.54	300	0.30	10.0	31.7	198.8	A.40.35-50	-	18	38 450	-	-	2.54	0.168	0.51	480	2.10	-	32.0	196.1	A.60.35-50	-	20	38 750	0.14	0.38	2.63	0.162	0.51	900	7.00	40.0	35.5	219.7	A.0.70-100	-	13	38 600	0.20	0.51	2.15	0.179	0.54	300	0.018	0.1	36.9	237.0	A.20.70-100	-	21	39 250	0.21	0.50	2.15	0.173	0.53	500	0.045	1.0	36.6	238.4	A.60.70-100	-	17	39 500	0.20	0.47	2.62	0.162	0.50	1 400	2.00	15.0	38.8	239.9	A.100.RAP	-	23	39 100	-	-	2.26	0.153	0.48	500	16.50	-	59.0	376.3	HM	C5P2M1	50	36 200	0.12	0.35	2.10	0.165	0.51	100	0.15	0.48	27.6	192.8	C6P2M1	36 400	0.10	0.38	HM30	C2P2M2	70	37 500	0.14	0.38	2.10	0.165	0.51	100	0.15	0.22	27.0	190.8	C5P2M2	38 500	0.22	0.38	WME0.4	C2P2M3	30	35 200	0.12	0.35	2.10	0.165	0.51	100	0.15	0.24	28.0	196.2	C7P2M3	35 200	0.17	0.37	WM30E0.4	C2P2M4	40	34 500	0.12	0.32	2.10	0.165	0.51	100	0.15	0.15	26.7	195.8	C3P2M4	34 500	0.13	0.35	WM30B0.4	C3P2M5	35	34 900	0.11	0.41	2.10	0.165	0.51	100	0.15	0.12	26.9	193.0	C5P2M5	35 700	0.12	0.42	WM50E0.4	C2P2M6	50	35 200	0.18	0.38	2.10	0.165	0.51	100	0.15	0.14	27.2	195.9	C5P2M6	35 800	0.13	0.45	WM50B0.4	C2P2M7	40	35 200	0.15	0.38	2.10	0.165	0.51
Eort-5.1-1.25	3	17	40 000	0.30	0.61	1.79	0.178	0.53	9 000	0.002	0.2	32.0	215.4																																																																																																																																																																																																																																																																																																		
	9	21	39 300	0.30	0.42									M1	M1R1	180	42 000	0.19	0.49	2.00	0.230	0.50	400	0.04	-	27.1	187.4	M2	M2U2	12	30 900	0.21	0.38	2.30	0.170	0.55	150	0.20	-	17.8	132.8	A.0.15-25	-	13	37 200	0.22	0.48	2.50	0.165	0.51	680	2.90	19.0	41.6	249.9	A.0.35-50	-	14	36 000	0.35	0.35	2.25	0.179	0.56	200	0.21	1.5	30.9	196.0	A.20.35-50	-	16	37 250	0.47	0.47	2.40	0.173	0.54	300	0.30	10.0	31.7	198.8	A.40.35-50	-	18	38 450	-	-	2.54	0.168	0.51	480	2.10	-	32.0	196.1	A.60.35-50	-	20	38 750	0.14	0.38	2.63	0.162	0.51	900	7.00	40.0	35.5	219.7	A.0.70-100	-	13	38 600	0.20	0.51	2.15	0.179	0.54	300	0.018	0.1	36.9	237.0	A.20.70-100	-	21	39 250	0.21	0.50	2.15	0.173	0.53	500	0.045	1.0	36.6	238.4	A.60.70-100	-	17	39 500	0.20	0.47	2.62	0.162	0.50	1 400	2.00	15.0	38.8	239.9	A.100.RAP	-	23	39 100	-	-	2.26	0.153	0.48	500	16.50	-	59.0	376.3	HM	C5P2M1	50	36 200	0.12	0.35	2.10	0.165	0.51	100	0.15	0.48	27.6	192.8	C6P2M1	36 400	0.10	0.38	HM30	C2P2M2	70	37 500	0.14	0.38	2.10	0.165	0.51	100	0.15	0.22	27.0	190.8	C5P2M2	38 500	0.22	0.38	WME0.4	C2P2M3	30	35 200	0.12	0.35	2.10	0.165	0.51	100	0.15	0.24	28.0	196.2	C7P2M3	35 200	0.17	0.37	WM30E0.4	C2P2M4	40	34 500	0.12	0.32	2.10	0.165	0.51	100	0.15	0.15	26.7	195.8	C3P2M4	34 500	0.13	0.35	WM30B0.4	C3P2M5	35	34 900	0.11	0.41	2.10	0.165	0.51	100	0.15	0.12	26.9	193.0	C5P2M5	35 700	0.12	0.42	WM50E0.4	C2P2M6	50	35 200	0.18	0.38	2.10	0.165	0.51	100	0.15	0.14	27.2	195.9	C5P2M6	35 800	0.13	0.45	WM50B0.4	C2P2M7	40	35 200	0.15	0.38	2.10	0.165	0.51	100	0.15	0.12	27.4	195.9	C4P2M7	34 700	0.12	0.33										
M1	M1R1	180	42 000	0.19	0.49	2.00	0.230	0.50	400	0.04	-	27.1	187.4																																																																																																																																																																																																																																																																																																		
M2	M2U2	12	30 900	0.21	0.38	2.30	0.170	0.55	150	0.20	-	17.8	132.8																																																																																																																																																																																																																																																																																																		
A.0.15-25	-	13	37 200	0.22	0.48	2.50	0.165	0.51	680	2.90	19.0	41.6	249.9																																																																																																																																																																																																																																																																																																		
A.0.35-50	-	14	36 000	0.35	0.35	2.25	0.179	0.56	200	0.21	1.5	30.9	196.0																																																																																																																																																																																																																																																																																																		
A.20.35-50	-	16	37 250	0.47	0.47	2.40	0.173	0.54	300	0.30	10.0	31.7	198.8																																																																																																																																																																																																																																																																																																		
A.40.35-50	-	18	38 450	-	-	2.54	0.168	0.51	480	2.10	-	32.0	196.1																																																																																																																																																																																																																																																																																																		
A.60.35-50	-	20	38 750	0.14	0.38	2.63	0.162	0.51	900	7.00	40.0	35.5	219.7																																																																																																																																																																																																																																																																																																		
A.0.70-100	-	13	38 600	0.20	0.51	2.15	0.179	0.54	300	0.018	0.1	36.9	237.0																																																																																																																																																																																																																																																																																																		
A.20.70-100	-	21	39 250	0.21	0.50	2.15	0.173	0.53	500	0.045	1.0	36.6	238.4																																																																																																																																																																																																																																																																																																		
A.60.70-100	-	17	39 500	0.20	0.47	2.62	0.162	0.50	1 400	2.00	15.0	38.8	239.9																																																																																																																																																																																																																																																																																																		
A.100.RAP	-	23	39 100	-	-	2.26	0.153	0.48	500	16.50	-	59.0	376.3																																																																																																																																																																																																																																																																																																		
HM	C5P2M1	50	36 200	0.12	0.35	2.10	0.165	0.51	100	0.15	0.48	27.6	192.8																																																																																																																																																																																																																																																																																																		
	C6P2M1		36 400	0.10	0.38									HM30	C2P2M2	70	37 500	0.14	0.38	2.10	0.165	0.51	100	0.15	0.22	27.0	190.8	C5P2M2	38 500	0.22	0.38	WME0.4	C2P2M3	30	35 200	0.12	0.35	2.10	0.165	0.51	100	0.15	0.24	28.0	196.2	C7P2M3	35 200	0.17	0.37	WM30E0.4	C2P2M4	40	34 500	0.12	0.32	2.10	0.165	0.51	100	0.15	0.15	26.7	195.8	C3P2M4	34 500	0.13	0.35	WM30B0.4	C3P2M5	35	34 900	0.11	0.41	2.10	0.165	0.51	100	0.15	0.12	26.9	193.0	C5P2M5	35 700	0.12	0.42	WM50E0.4	C2P2M6	50	35 200	0.18	0.38	2.10	0.165	0.51	100	0.15	0.14	27.2	195.9	C5P2M6	35 800	0.13	0.45	WM50B0.4	C2P2M7	40	35 200	0.15	0.38	2.10	0.165	0.51	100	0.15	0.12	27.4	195.9	C4P2M7	34 700	0.12	0.33																																																																																																																																																																																						
HM30	C2P2M2	70	37 500	0.14	0.38	2.10	0.165	0.51	100	0.15	0.22	27.0	190.8																																																																																																																																																																																																																																																																																																		
	C5P2M2		38 500	0.22	0.38									WME0.4	C2P2M3	30	35 200	0.12	0.35	2.10	0.165	0.51	100	0.15	0.24	28.0	196.2	C7P2M3	35 200	0.17	0.37	WM30E0.4	C2P2M4	40	34 500	0.12	0.32	2.10	0.165	0.51	100	0.15	0.15	26.7	195.8	C3P2M4	34 500	0.13	0.35	WM30B0.4	C3P2M5	35	34 900	0.11	0.41	2.10	0.165	0.51	100	0.15	0.12	26.9	193.0	C5P2M5	35 700	0.12	0.42	WM50E0.4	C2P2M6	50	35 200	0.18	0.38	2.10	0.165	0.51	100	0.15	0.14	27.2	195.9	C5P2M6	35 800	0.13	0.45	WM50B0.4	C2P2M7	40	35 200	0.15	0.38	2.10	0.165	0.51	100	0.15	0.12	27.4	195.9	C4P2M7	34 700	0.12	0.33																																																																																																																																																																																																								
WME0.4	C2P2M3	30	35 200	0.12	0.35	2.10	0.165	0.51	100	0.15	0.24	28.0	196.2																																																																																																																																																																																																																																																																																																		
	C7P2M3		35 200	0.17	0.37									WM30E0.4	C2P2M4	40	34 500	0.12	0.32	2.10	0.165	0.51	100	0.15	0.15	26.7	195.8	C3P2M4	34 500	0.13	0.35	WM30B0.4	C3P2M5	35	34 900	0.11	0.41	2.10	0.165	0.51	100	0.15	0.12	26.9	193.0	C5P2M5	35 700	0.12	0.42	WM50E0.4	C2P2M6	50	35 200	0.18	0.38	2.10	0.165	0.51	100	0.15	0.14	27.2	195.9	C5P2M6	35 800	0.13	0.45	WM50B0.4	C2P2M7	40	35 200	0.15	0.38	2.10	0.165	0.51	100	0.15	0.12	27.4	195.9	C4P2M7	34 700	0.12	0.33																																																																																																																																																																																																																										
WM30E0.4	C2P2M4	40	34 500	0.12	0.32	2.10	0.165	0.51	100	0.15	0.15	26.7	195.8																																																																																																																																																																																																																																																																																																		
	C3P2M4		34 500	0.13	0.35									WM30B0.4	C3P2M5	35	34 900	0.11	0.41	2.10	0.165	0.51	100	0.15	0.12	26.9	193.0	C5P2M5	35 700	0.12	0.42	WM50E0.4	C2P2M6	50	35 200	0.18	0.38	2.10	0.165	0.51	100	0.15	0.14	27.2	195.9	C5P2M6	35 800	0.13	0.45	WM50B0.4	C2P2M7	40	35 200	0.15	0.38	2.10	0.165	0.51	100	0.15	0.12	27.4	195.9	C4P2M7	34 700	0.12	0.33																																																																																																																																																																																																																																												
WM30B0.4	C3P2M5	35	34 900	0.11	0.41	2.10	0.165	0.51	100	0.15	0.12	26.9	193.0																																																																																																																																																																																																																																																																																																		
	C5P2M5		35 700	0.12	0.42									WM50E0.4	C2P2M6	50	35 200	0.18	0.38	2.10	0.165	0.51	100	0.15	0.14	27.2	195.9	C5P2M6	35 800	0.13	0.45	WM50B0.4	C2P2M7	40	35 200	0.15	0.38	2.10	0.165	0.51	100	0.15	0.12	27.4	195.9	C4P2M7	34 700	0.12	0.33																																																																																																																																																																																																																																																														
WM50E0.4	C2P2M6	50	35 200	0.18	0.38	2.10	0.165	0.51	100	0.15	0.14	27.2	195.9																																																																																																																																																																																																																																																																																																		
	C5P2M6		35 800	0.13	0.45									WM50B0.4	C2P2M7	40	35 200	0.15	0.38	2.10	0.165	0.51	100	0.15	0.12	27.4	195.9	C4P2M7	34 700	0.12	0.33																																																																																																																																																																																																																																																																																
WM50B0.4	C2P2M7	40	35 200	0.15	0.38	2.10	0.165	0.51	100	0.15	0.12	27.4	195.9																																																																																																																																																																																																																																																																																																		
	C4P2M7		34 700	0.12	0.33																																																																																																																																																																																																																																																																																																										

**APPENDIX C- RESULTS OF THE PARAMETRIC
ANALYSIS FOR THE COMPLEX MODULUS AND
COMPLEX POISSON'S RATIO**

RESULTS FOR THE FLEXURAL MODE OF THE DISC

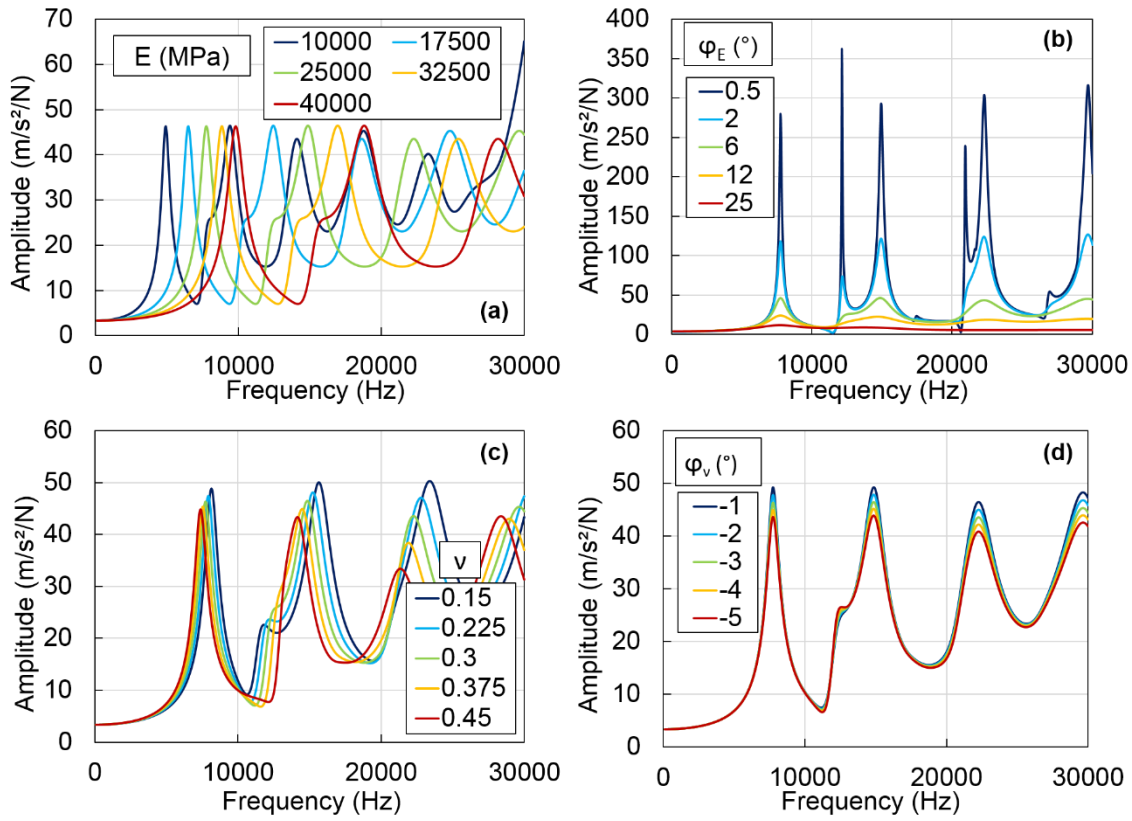


Figure C.1. Influence of the LVE properties on the FRFs of the flexural mode of the disc: (a) norm of the complex modulus; (b) phase angle of the complex modulus; (c) norm of the complex Poisson's ratio; (d) phase angle of the complex Poisson's ratio. The constants not listed in each figure have the median value given in Table 4.4.

Table C.1. Values of the RSD for the two first resonance frequencies and amplitudes for the flexural mode of the disc. The LVE property indicated in the left column varies while the other properties are set to their median values indicated in Table 4.4.

LVE property	RSD 1 st frequency (%)	RSD 1 st amplitude (%)	RSD 2 nd frequency (%)	RSD 2 nd amplitude (%)	RSD 3 rd frequency (%)	RSD 3 rd amplitude (%)
E	25.6	0.0	25.6	0.0	25.6	0.0
φ_E	0.2	115.4	3.7	119.0	-	-
ν	3.9	3.4	4.0	5.6	3.6	15.8
φ_ν	0.0	4.8	0.0	4.6	0.0	5.1

RESULTS FOR THE TORSIONAL MODE OF THE STRAIGHT BEAM

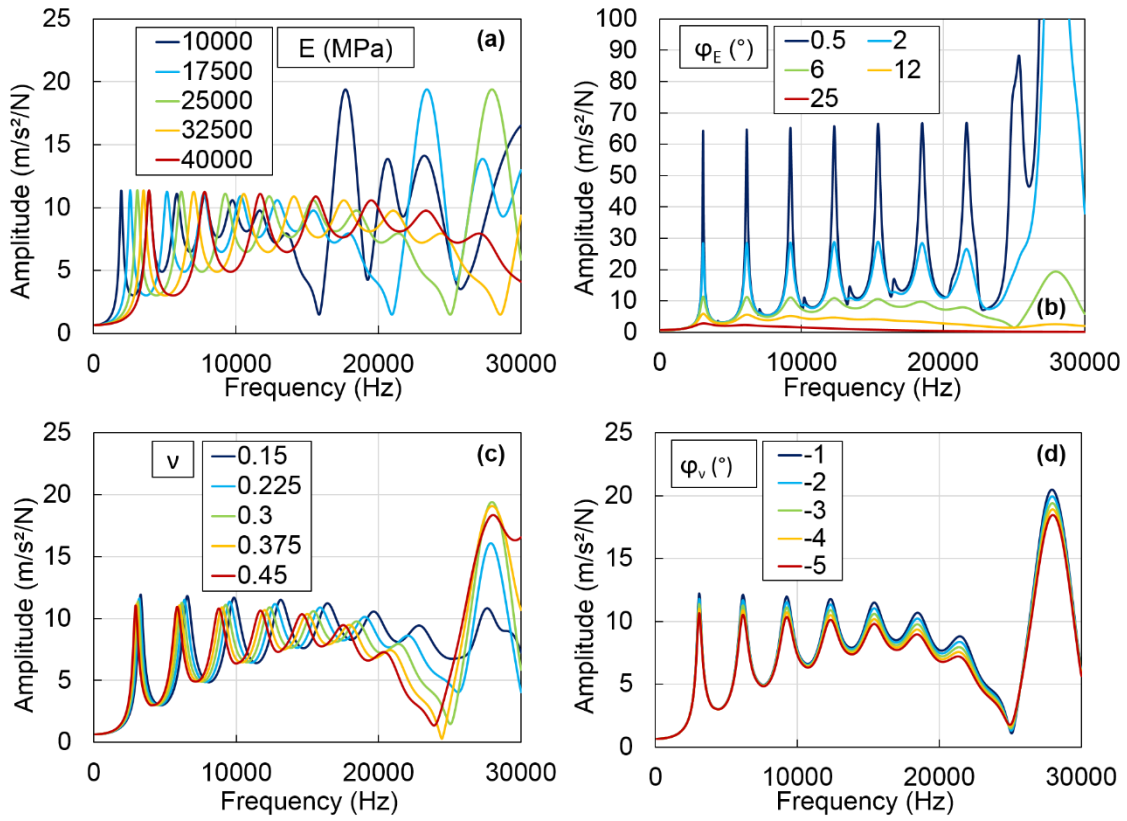


Figure C.2. Influence of the LVE properties on the FRFs of the torsional mode of the straight beam: (a) norm of the complex modulus; (b) phase angle of the complex modulus; (c) norm of the complex Poisson's ratio; (d) phase angle of the complex Poisson's ratio. The constants not listed in each figure have the median value given in Table 4.4.

Table C.2. Values of the RSD for the two first resonance frequencies and amplitudes for the torsional mode of the straight beam. The LVE property indicated in the left column varies while the other properties are set to their median values indicated in Table 4.4.

LVE property	RSD 1 st frequency (%)	RSD 1 st amplitude (%)	RSD 2 nd frequency (%)	RSD 2 nd amplitude (%)	RSD 3 rd frequency (%)	RSD 3 rd amplitude (%)
E	25.7	0.1	25.5	0.0	25.6	0.0
φ_E	0.6	112.3	1.1	114.2	-	-
ν	4.6	3.0	4.6	3.0	4.6	3.1
φ_ν	0.0	5.5	0.0	5.6	0.0	5.8

**APPENDIX D - RESULTS OF THE PARAMETRIC
ANALYSIS FOR THE CONSTANTS OF THE
2S2P1D MODEL**

RELATIVE STANDARD DEVIATION (RSD) RESULTS FOR THE FLEXURAL MODE OF THE DISC

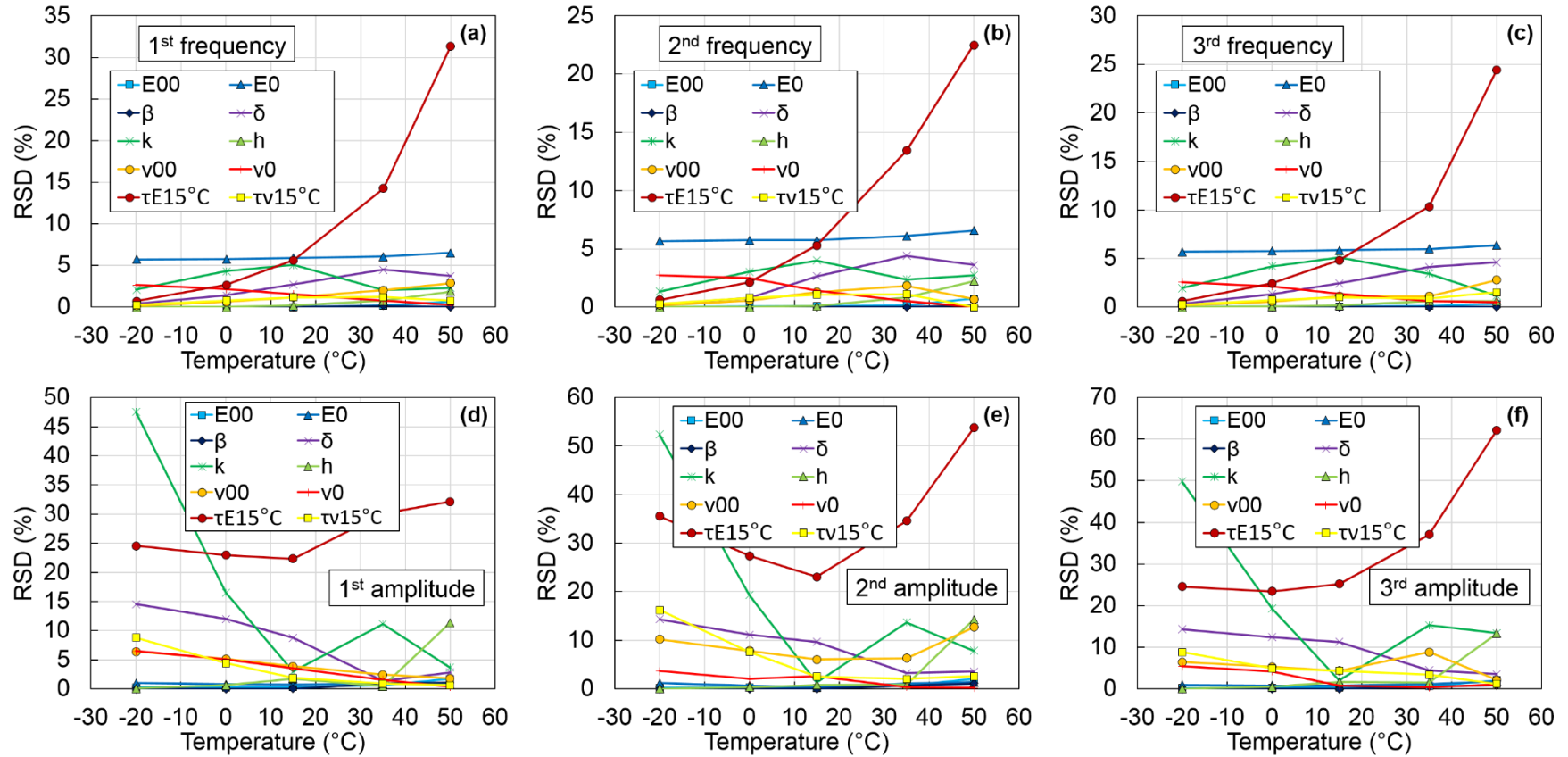


Figure D.1. RSD in function of temperature for each of the ten constants of the 2S2P1D model for the flexural mode of the disc: (a) 1st resonance frequency; (b) 2nd resonance frequency; (c) 3rd resonance frequency; (d) 1st resonance amplitude; (e) 2nd resonance amplitude; (f) 3rd resonance amplitude.

RELATIVE STANDARD DEVIATION (RSD) RESULTS FOR THE TORSIONAL MODE OF THE STRAIGHT BEAM

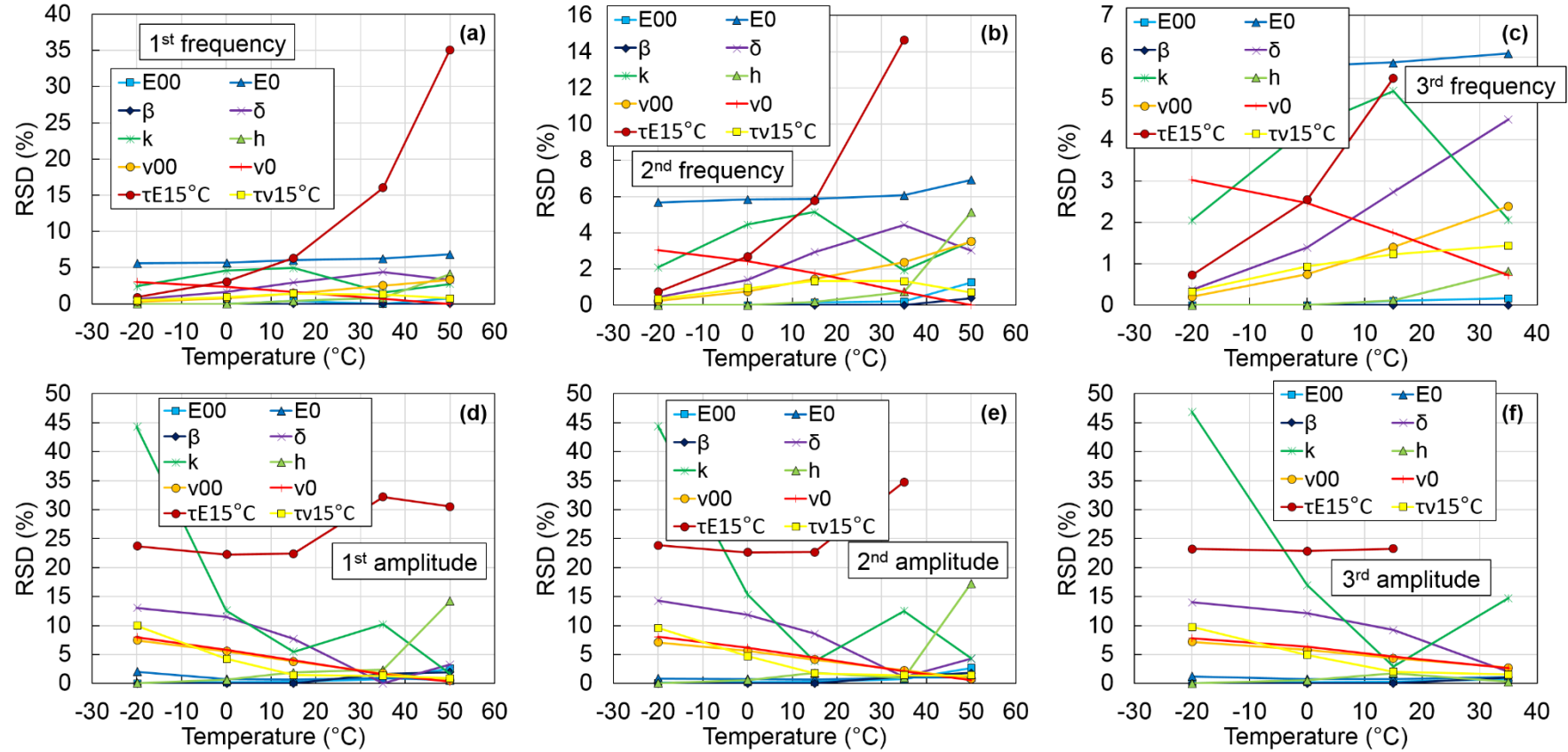


Figure D.2. RSD in function of temperature for each of the ten constants of the 2S2P1D model for the torsional mode of the straight beam: (a) 1st resonance frequency; (b) 2nd resonance frequency; (c) 3rd resonance frequency; (d) 1st resonance amplitude; (e) 2nd resonance amplitude; (f) 3rd resonance amplitude.

**FREQUENCY RESPONSE FUNCTIONS RESULTS FOR THE LONGITUDINAL
MODE OF THE CYLINDER**

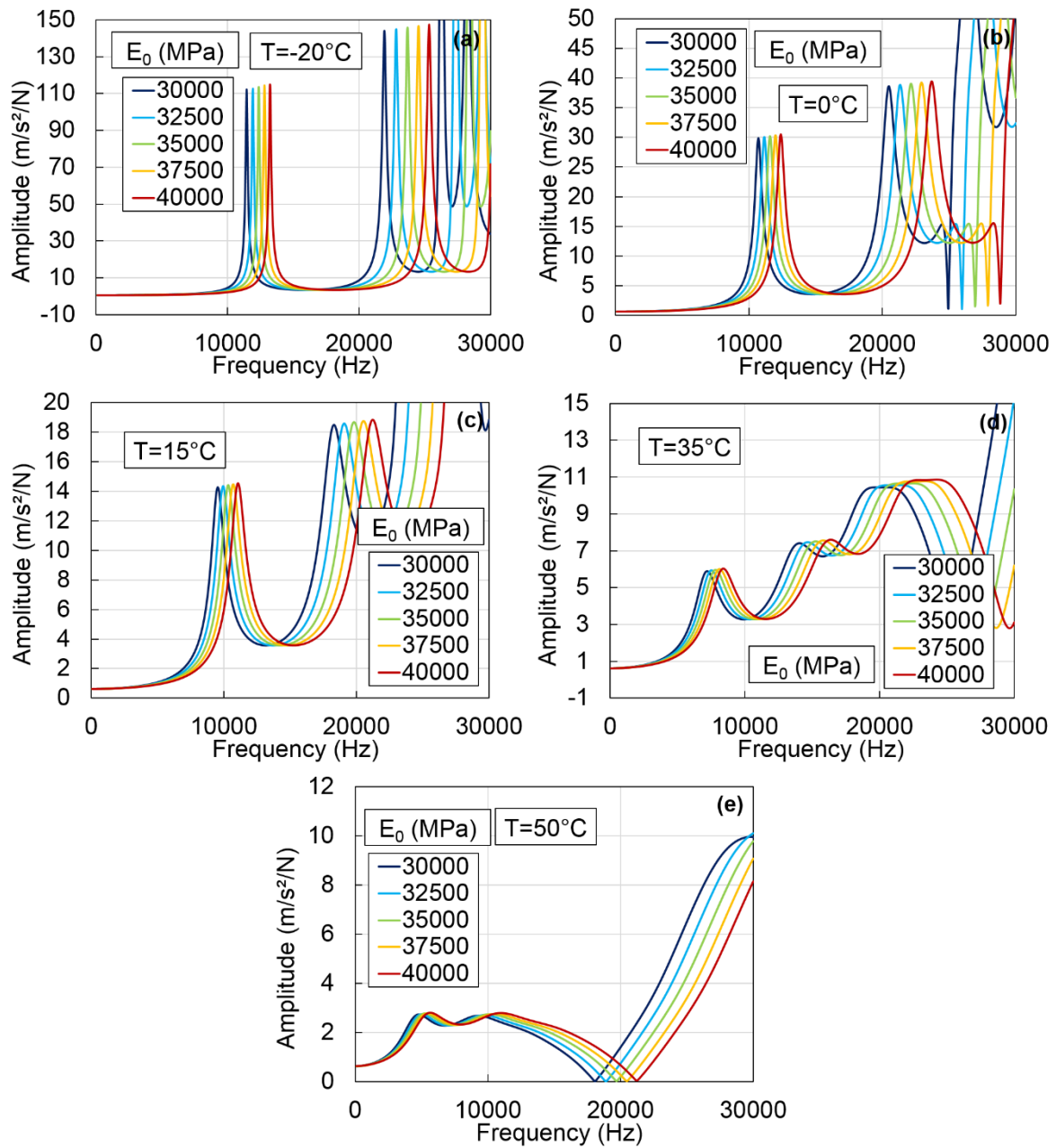


Figure D.3. Influence of constant E_0 of the 2S2P1D model on the FRFs of the longitudinal mode of the cylinder at: (a) -20°C ; (b) 0°C ; (c) 15°C ; (d) 35°C ; (e) 50°C . The constants not listed in each figure have the median value given in Table 4.6.

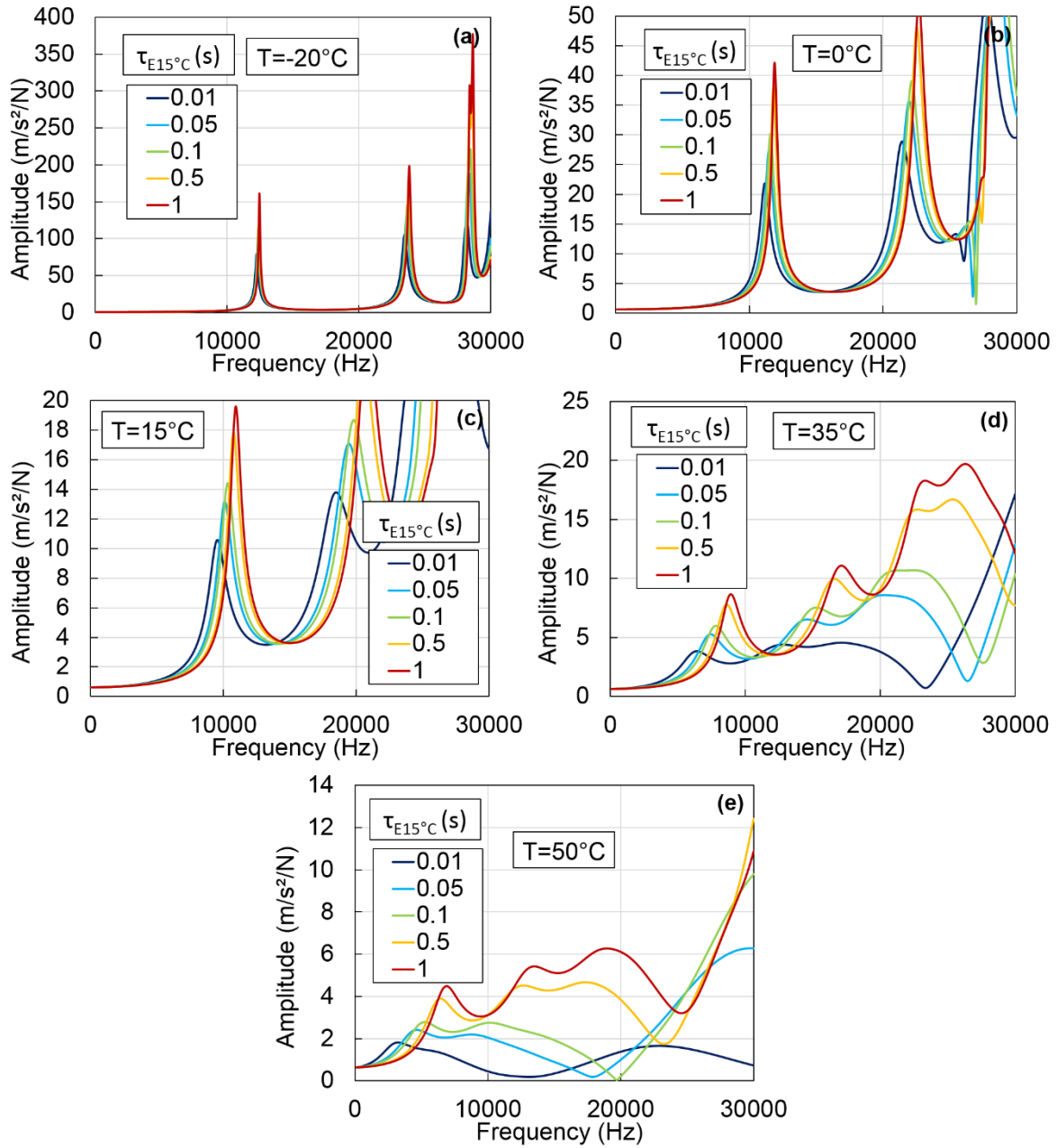


Figure D.4. Influence of constant $\tau_{E15^\circ C}$ of the 2S2P1D model on the FRFs of the longitudinal mode of the cylinder at: (a) -20°C ; (b) 0°C ; (c) 15°C ; (d) 35°C ; (e) 50°C . The constants not listed in each figure have the median value given in Table 4.6.

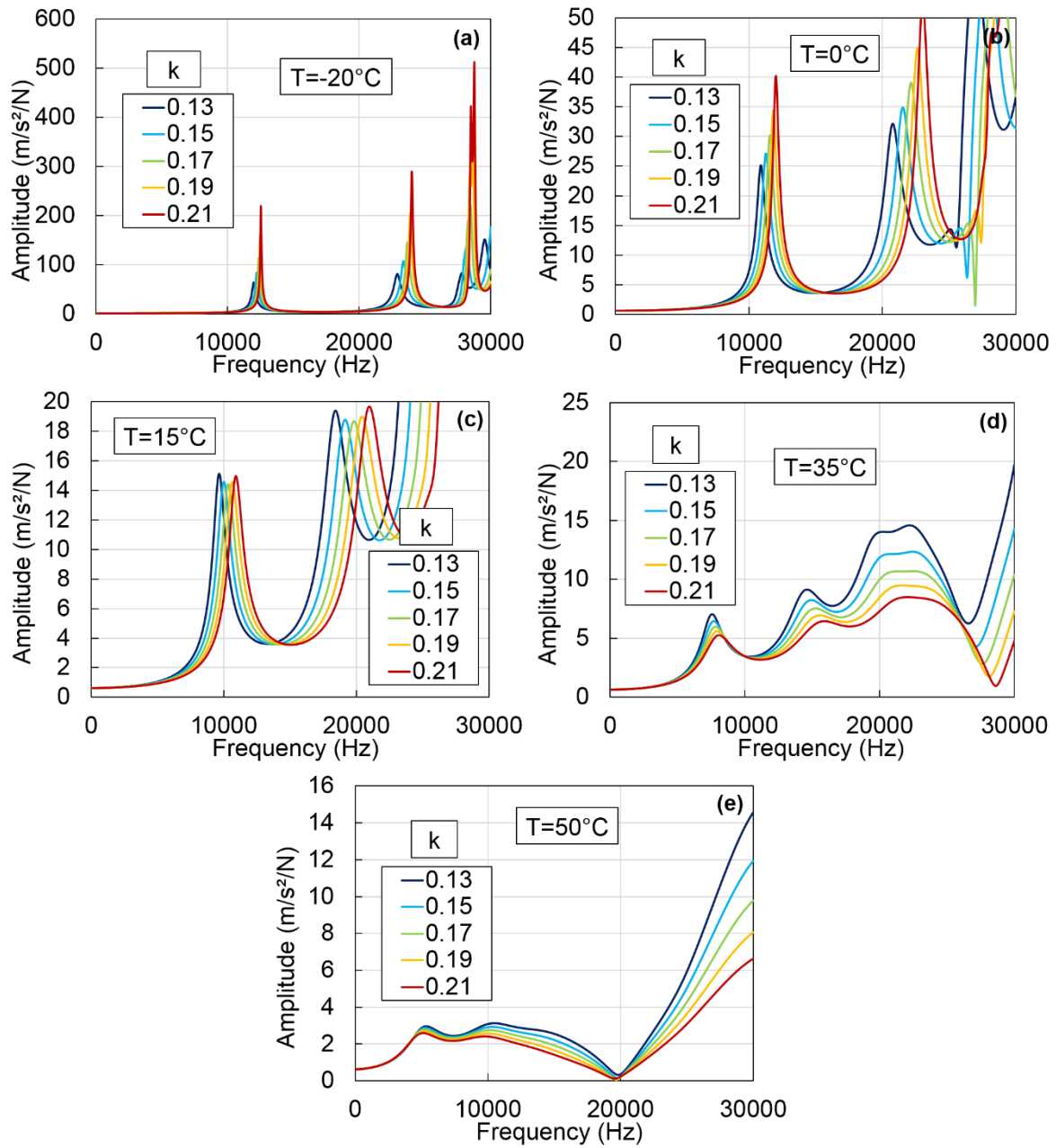


Figure D.5. Influence of constant k of the 2S2P1D model on the FRFs of the longitudinal mode of the cylinder at: (a) -20°C ; (b) 0°C ; (c) 15°C ; (d) 35°C ; (e) 50°C . The constants not listed in each figure have the median value given in Table 4.6.

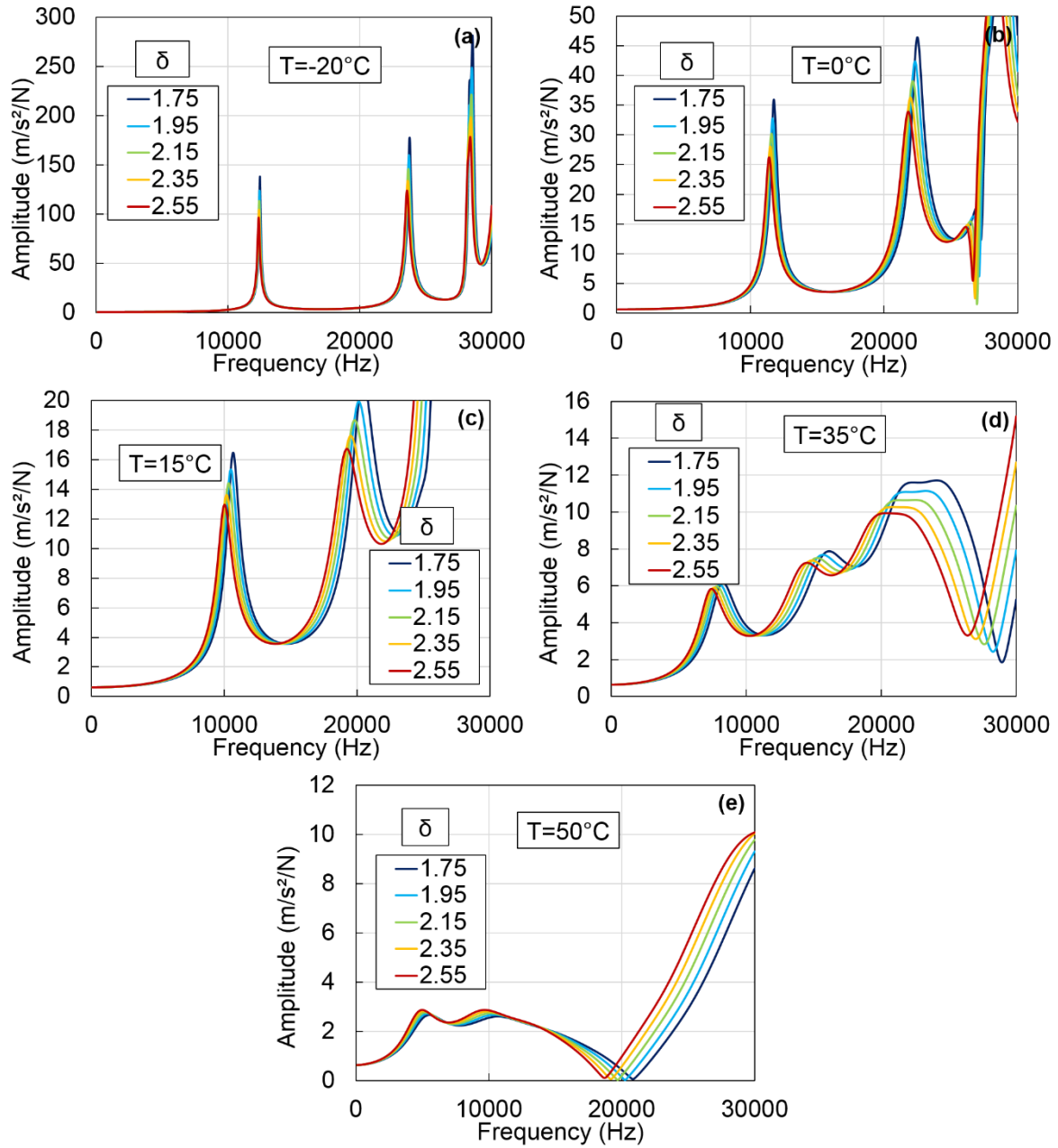


Figure D.6. Influence of constant δ of the 2S2P1D model on the FRFs of the longitudinal mode of the cylinder at: (a) -20°C; (b) 0°C; (c) 15°C; (d) 35°C; (e) 50°C. The constants not listed in each figure have the median value given in Table 4.6.

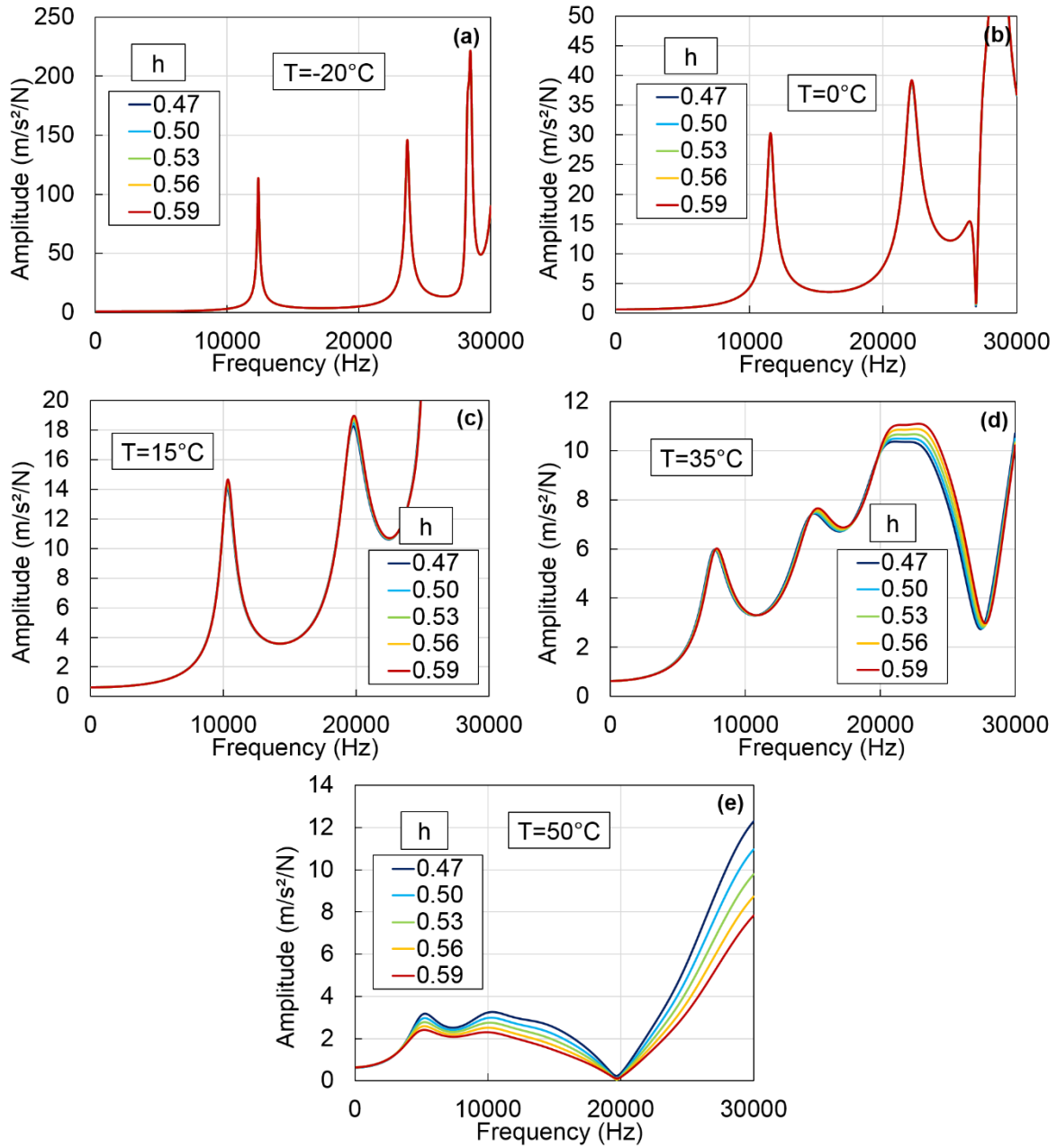


Figure D.7. Influence of constant h of the 2S2PID model on the FRFs of the longitudinal mode of the cylinder at: (a) -20°C ; (b) 0°C ; (c) 15°C ; (d) 35°C ; (e) 50°C . The constants not listed in each figure have the median value given in Table 4.6.

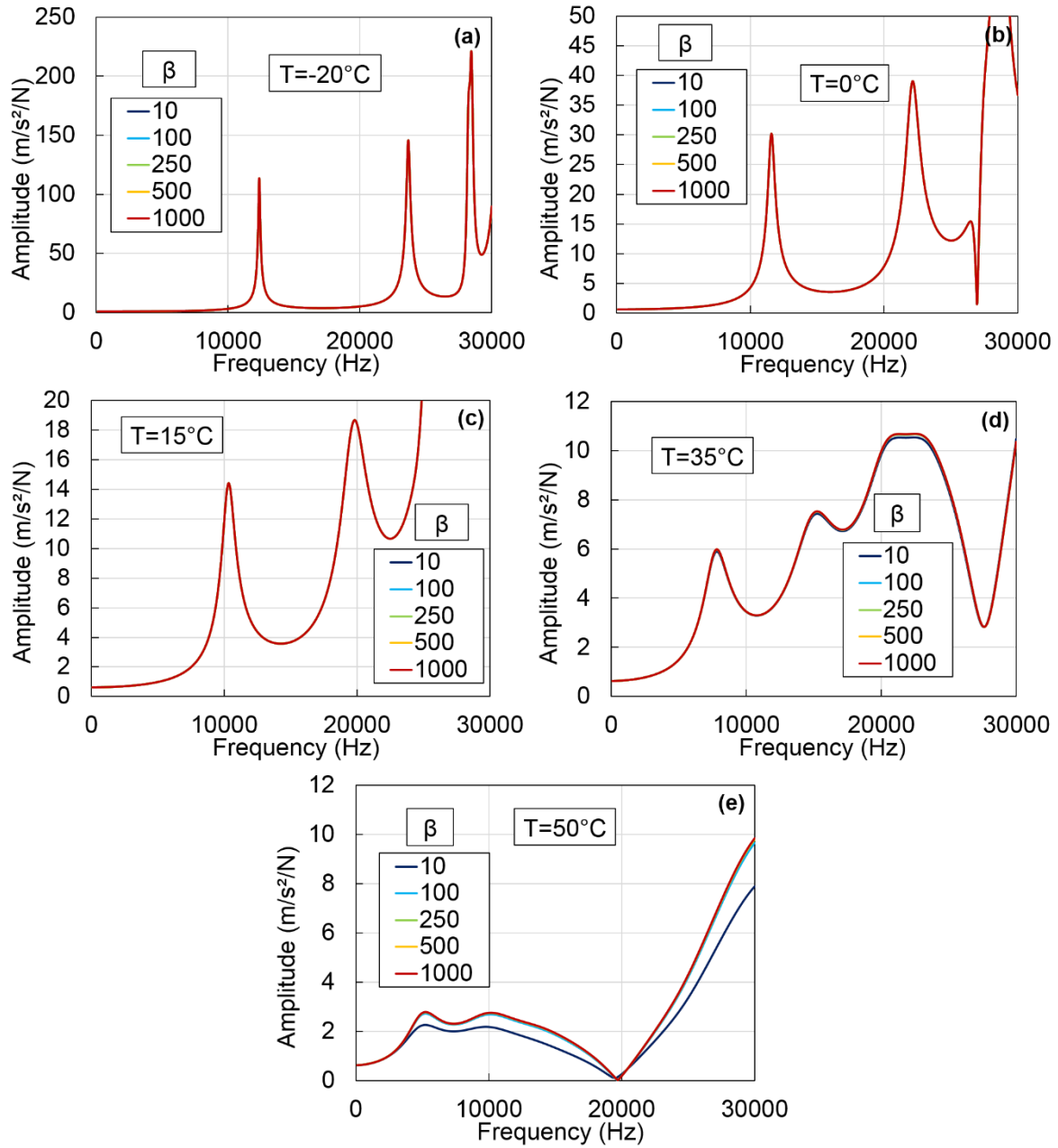


Figure D.8. Influence of constant β of the 2S2PID model on the FRFs of the longitudinal mode of the cylinder at: (a) -20°C ; (b) 0°C ; (c) 15°C ; (d) 35°C ; (e) 50°C . The constants not listed in each figure have the median value given in Table 4.6.

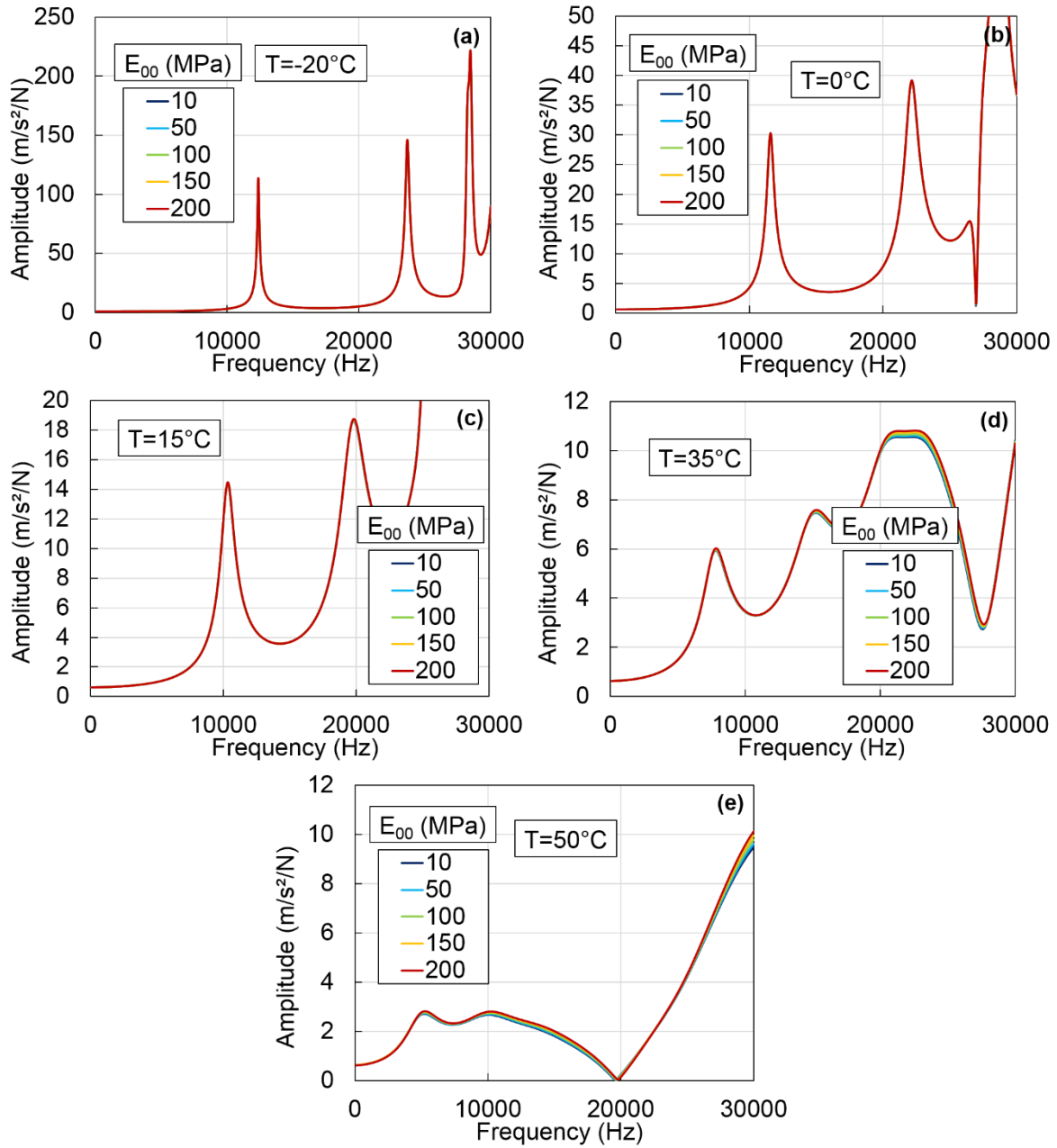


Figure D.9. Influence of constant E_{00} of the 2S2P1D model on the FRFs of the longitudinal mode of the cylinder at: (a) -20°C ; (b) 0°C ; (c) 15°C ; (d) 35°C ; (e) 50°C . The constants not listed in each figure have the median value given in Table 4.6.

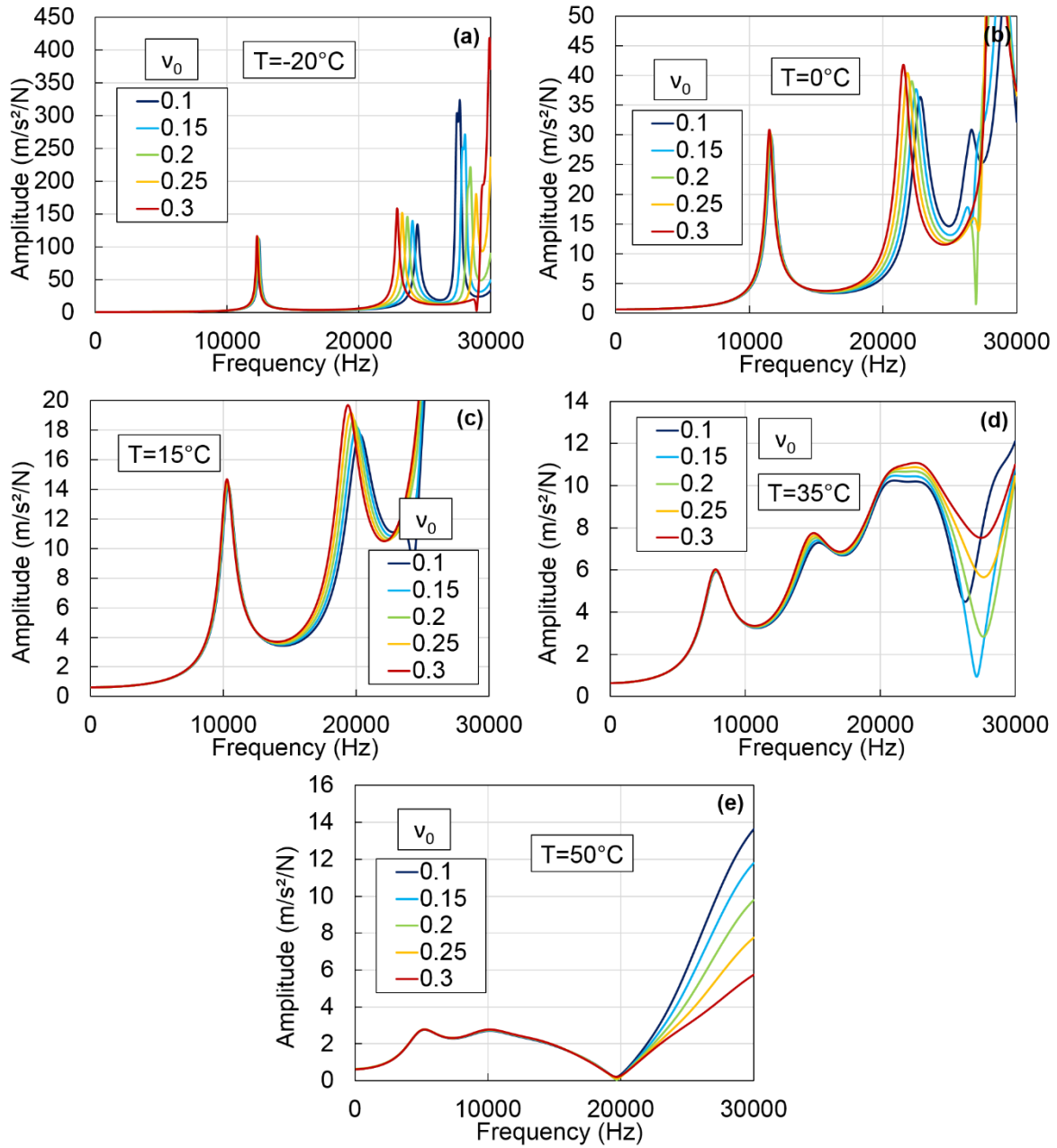


Figure D.10. Influence of constant v_0 of the 2S2P1D model on the FRFs of the longitudinal mode of the cylinder at: (a) -20°C ; (b) 0°C ; (c) 15°C ; (d) 35°C ; (e) 50°C . The constants not listed in each figure have the median value given in Table 4.6.

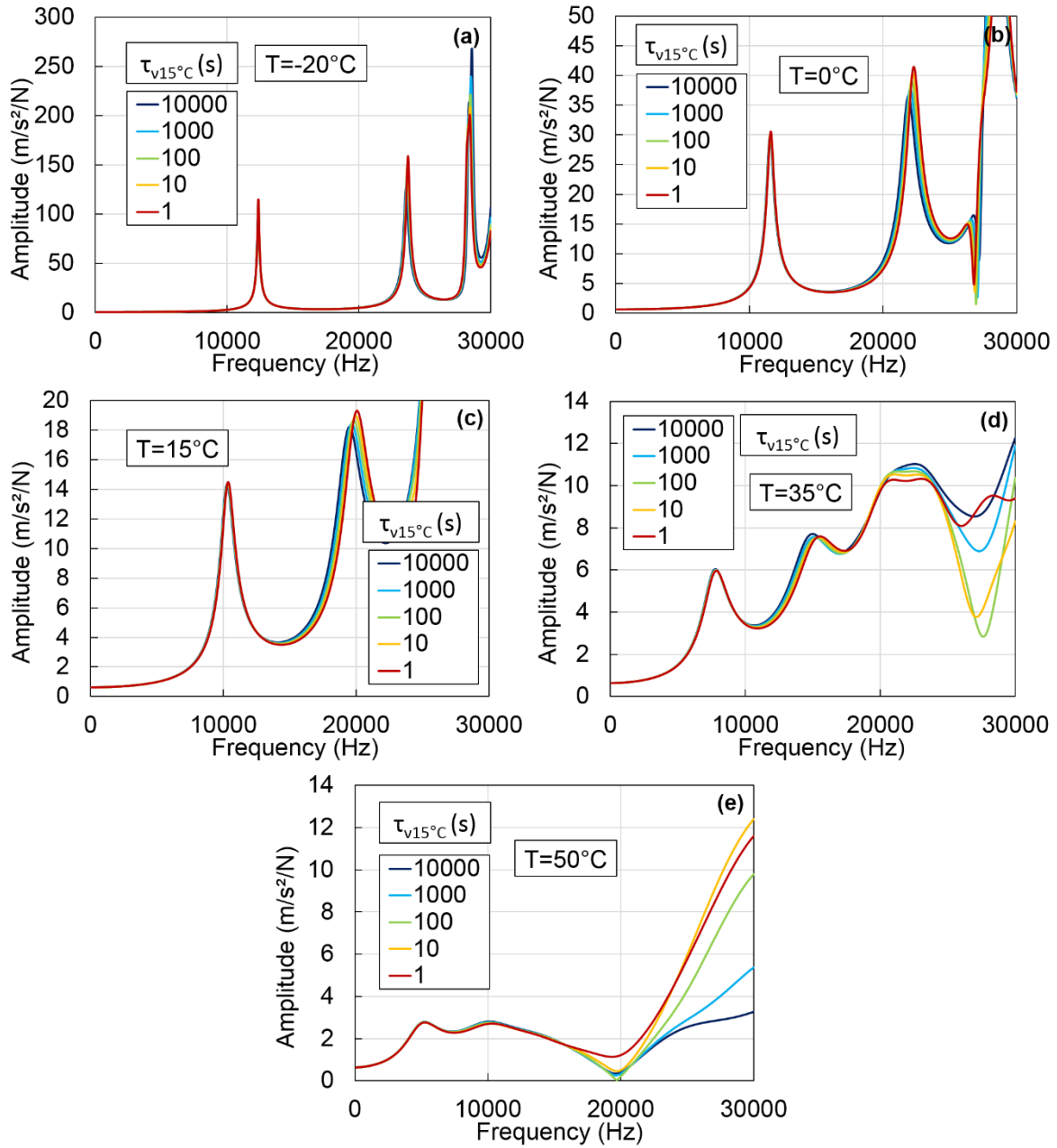


Figure D.11. Influence of constant $\tau_{v15^\circ C}$ of the 2S2PID model on the FRFs of the longitudinal mode of the cylinder at: (a) $-20^\circ C$; (b) $0^\circ C$; (c) $15^\circ C$; (d) $35^\circ C$; (e) $50^\circ C$. The constants not listed in each figure have the median value given in Table 4.6.

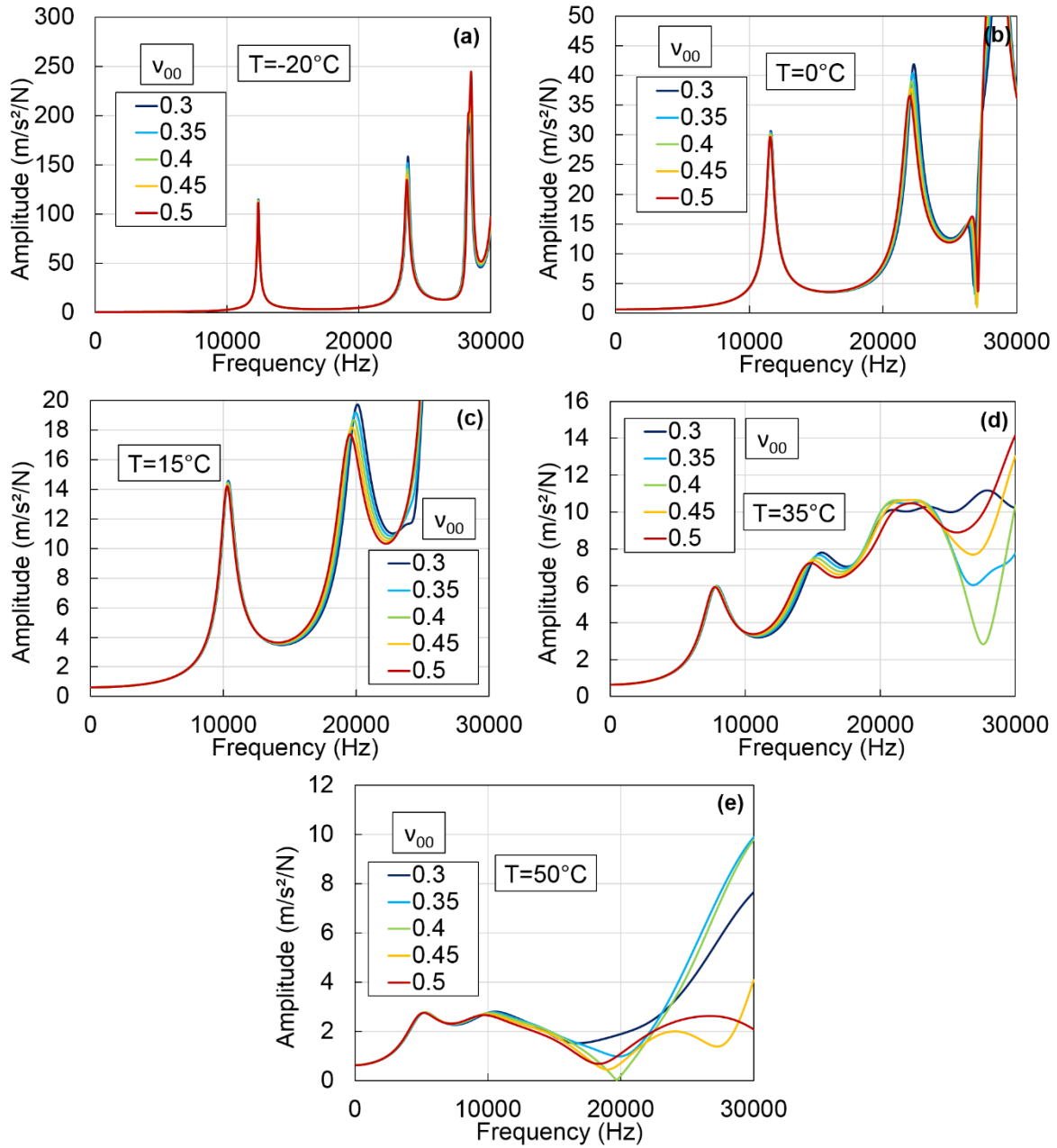


Figure D.12. Influence of constant v_{00} of the 2S2PID model on the FRFs of the longitudinal mode of the cylinder at: (a) -20°C ; (b) 0°C ; (c) 15°C ; (d) 35°C ; (e) 50°C . The constants not listed in each figure have the median value given in Table 4.6.

**FREQUENCY RESPONSE FUNCTIONS RESULTS FOR THE FLEXURAL MODE
OF THE DISC**

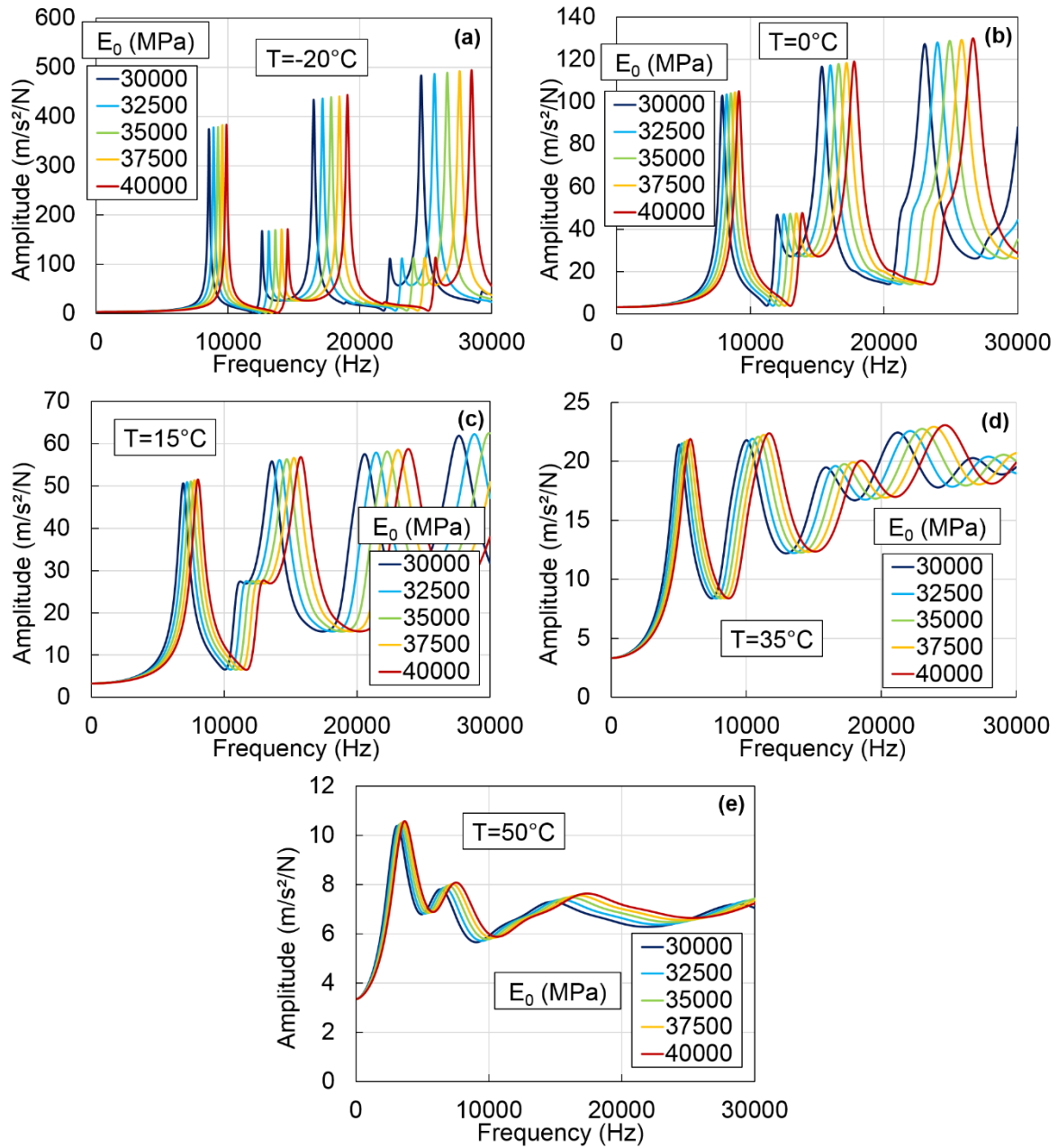


Figure D.13. Influence of constant E_0 of the 2S2P1D model on the FRFs of the flexural mode of the disc at: (a) -20°C ; (b) 0°C ; (c) 15°C ; (d) 35°C ; (e) 50°C . The constants not listed in each figure have the median value given in Table 4.6.

APPENDIX D - RESULTS OF THE PARAMETRIC ANALYSIS FOR THE
CONSTANTS OF THE 2S2P1D MODEL

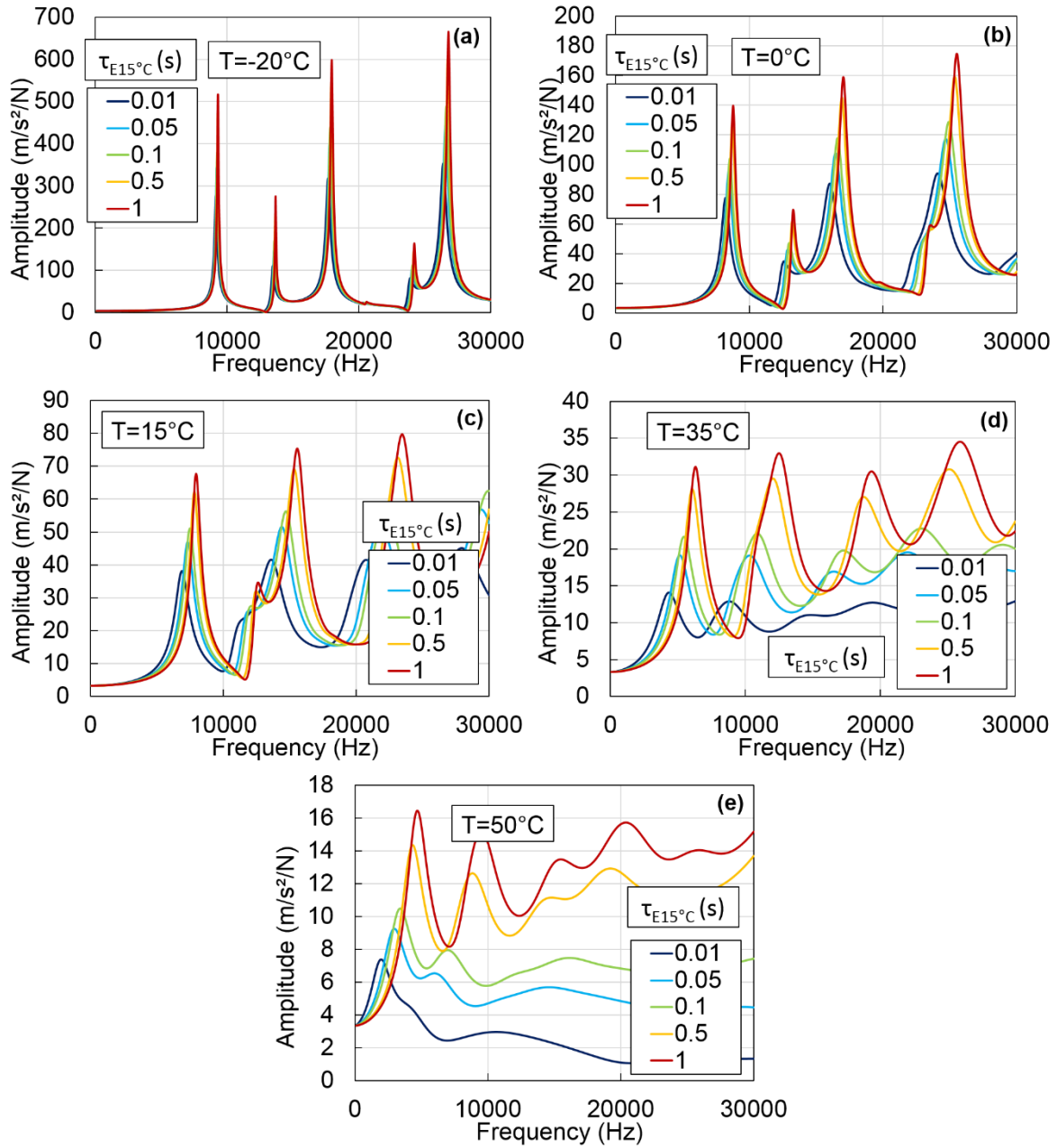


Figure D.14. Influence of constant $\tau_{E15^\circ C}$ of the 2S2P1D model on the FRFs of the flexural mode of the disc at: (a) -20°C; (b) 0°C; (c) 15°C; (d) 35°C; (e) 50°C. The constants not listed in each figure have the median value given in Table 4.6.

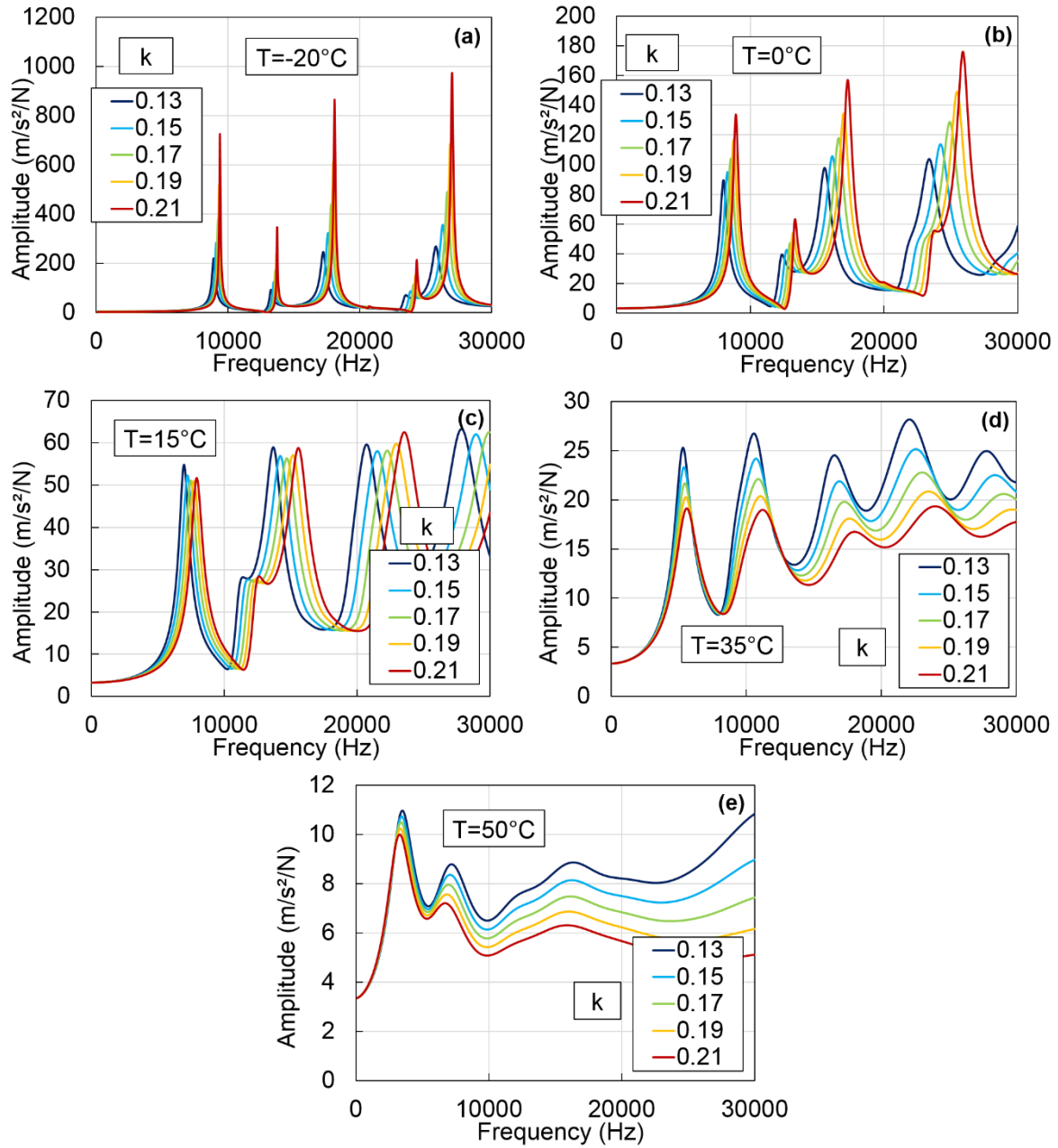


Figure D.15. Influence of constant k of the 2S2P1D model on the FRFs of the flexural mode of the disc at: (a) -20°C ; (b) 0°C ; (c) 15°C ; (d) 35°C ; (e) 50°C . The constants not listed in each figure have the median value given in Table 4.6.

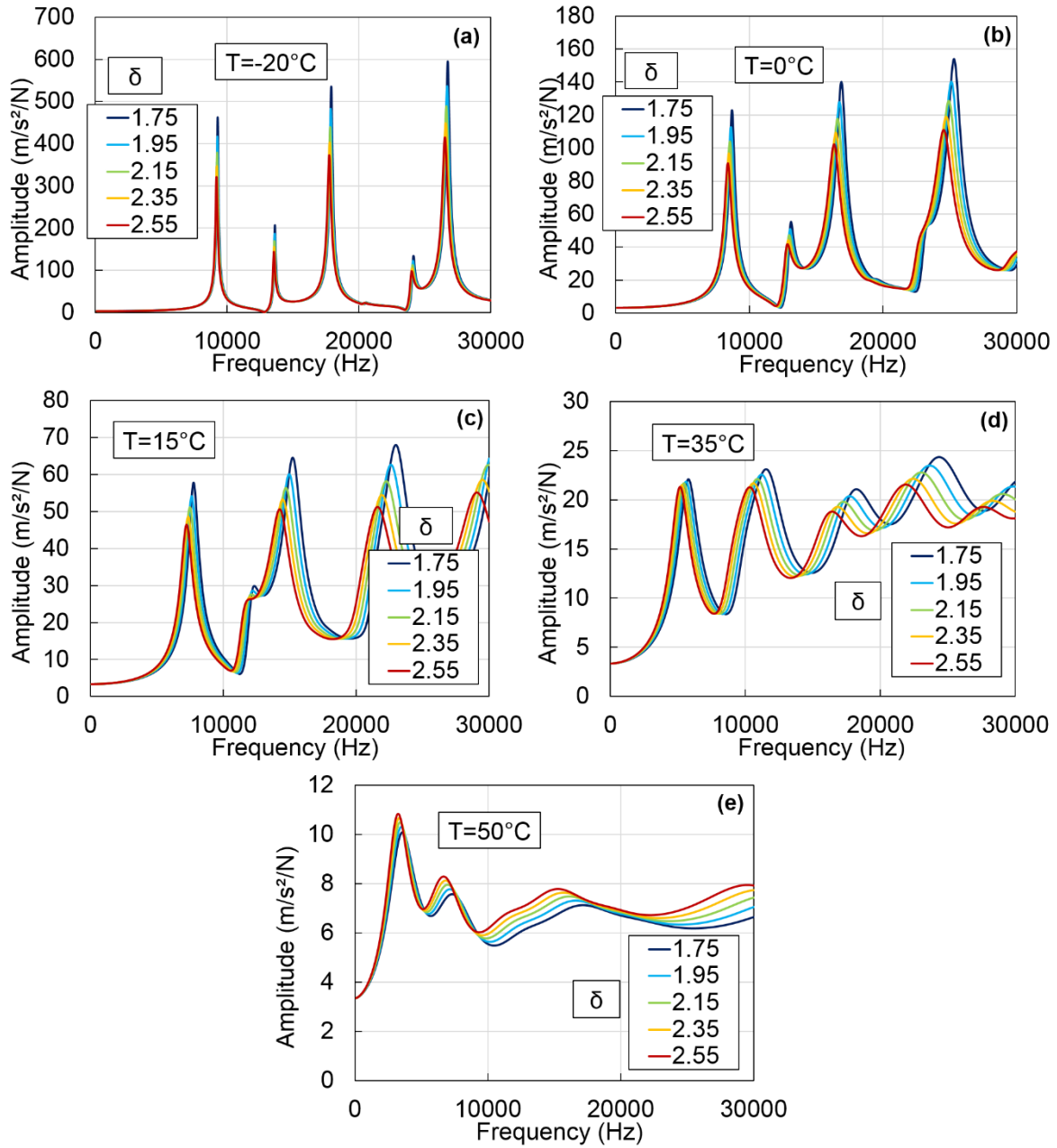


Figure D.16. Influence of constant δ of the 2S2P1D model on the FRFs of the flexural mode of the disc at: (a) -20°C; (b) 0°C; (c) 15°C; (d) 35°C; (e) 50°C. The constants not listed in each figure have the median value given in Table 4.6.

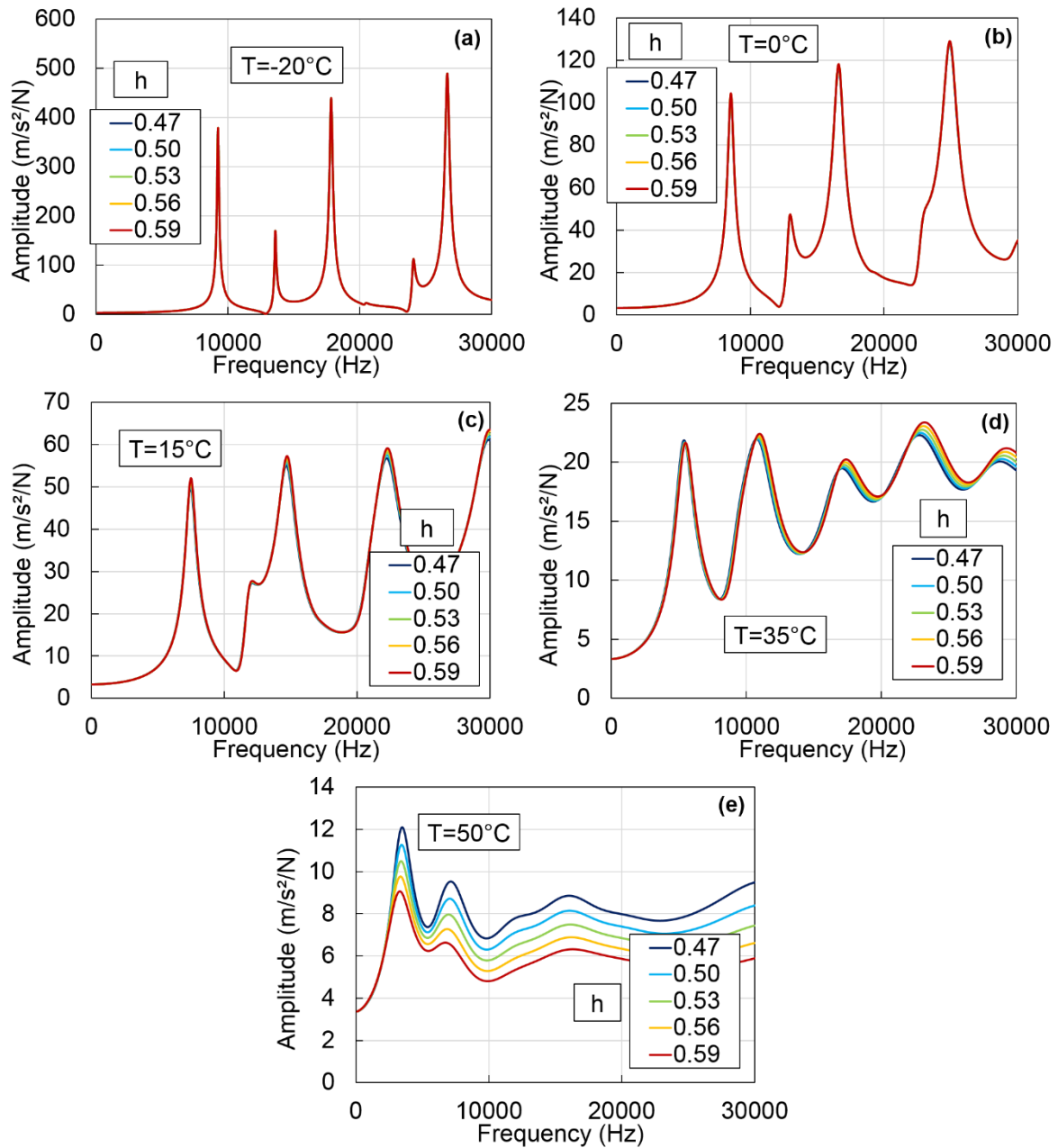


Figure D.17. Influence of constant h of the 2S2P1D model on the FRFs of the flexural mode of the disc at: (a) -20°C ; (b) 0°C ; (c) 15°C ; (d) 35°C ; (e) 50°C . The constants not listed in each figure have the median value given in Table 4.6.

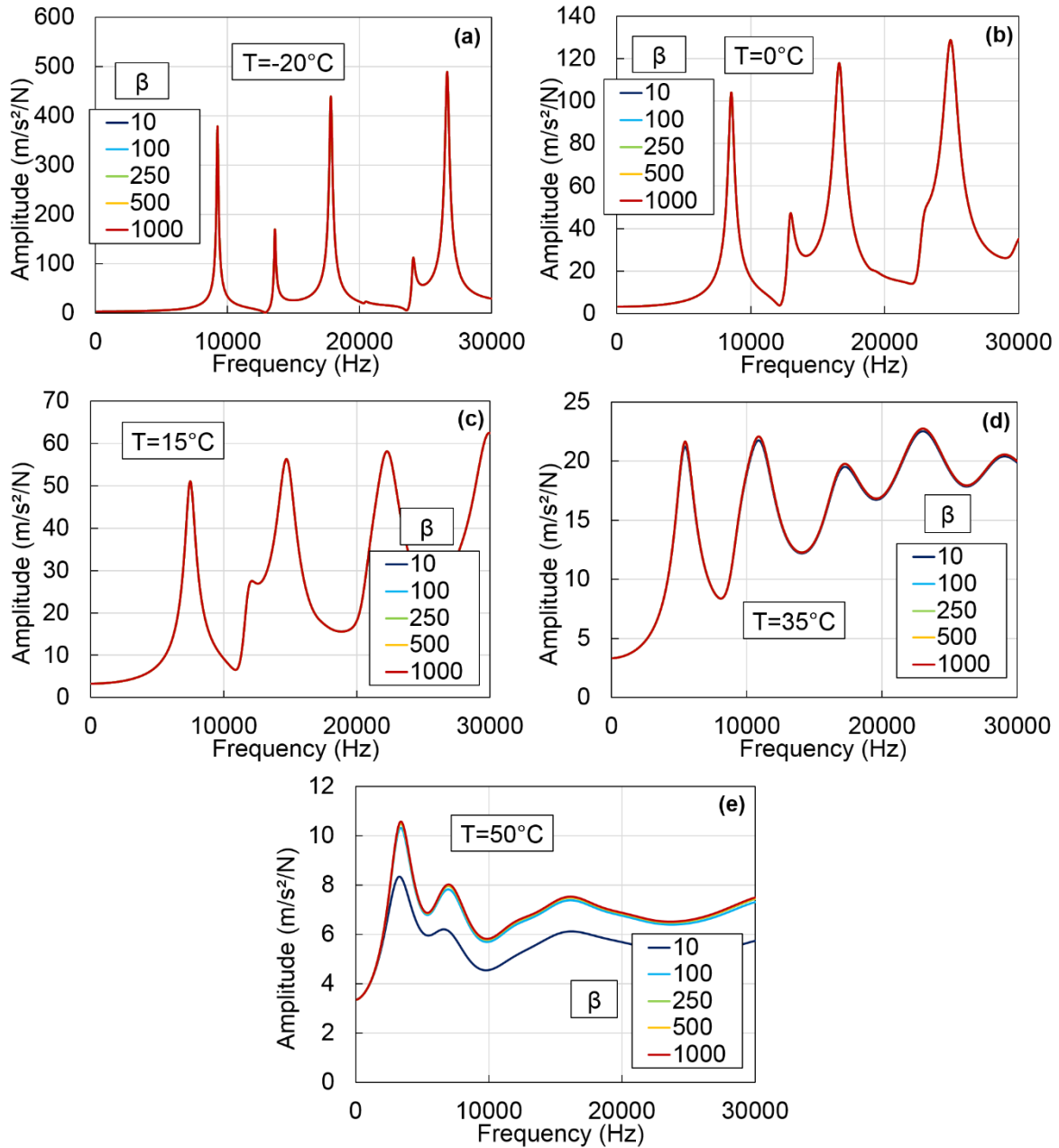


Figure D.18. Influence of constant β of the 2S2P1D model on the FRFs of the flexural mode of the disc at: (a) -20°C ; (b) 0°C ; (c) 15°C ; (d) 35°C ; (e) 50°C . The constants not listed in each figure have the median value given in Table 4.6.

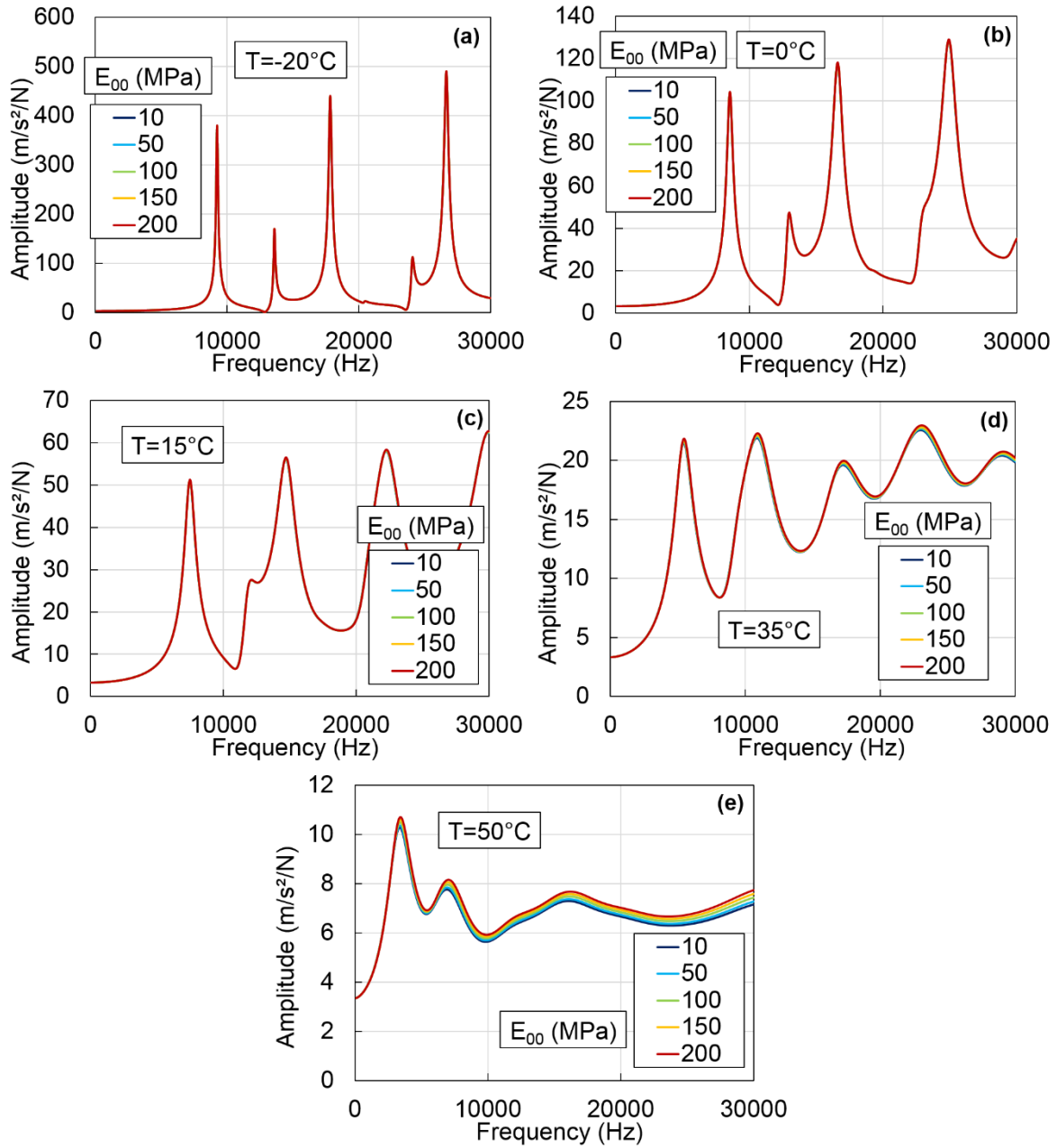


Figure D.19. Influence of constant E_{00} of the 2S2P1D model on the FRFs of the flexural mode of the disc at: (a) -20°C ; (b) 0°C ; (c) 15°C ; (d) 35°C ; (e) 50°C . The constants not listed in each figure have the median value given in Table 4.6.

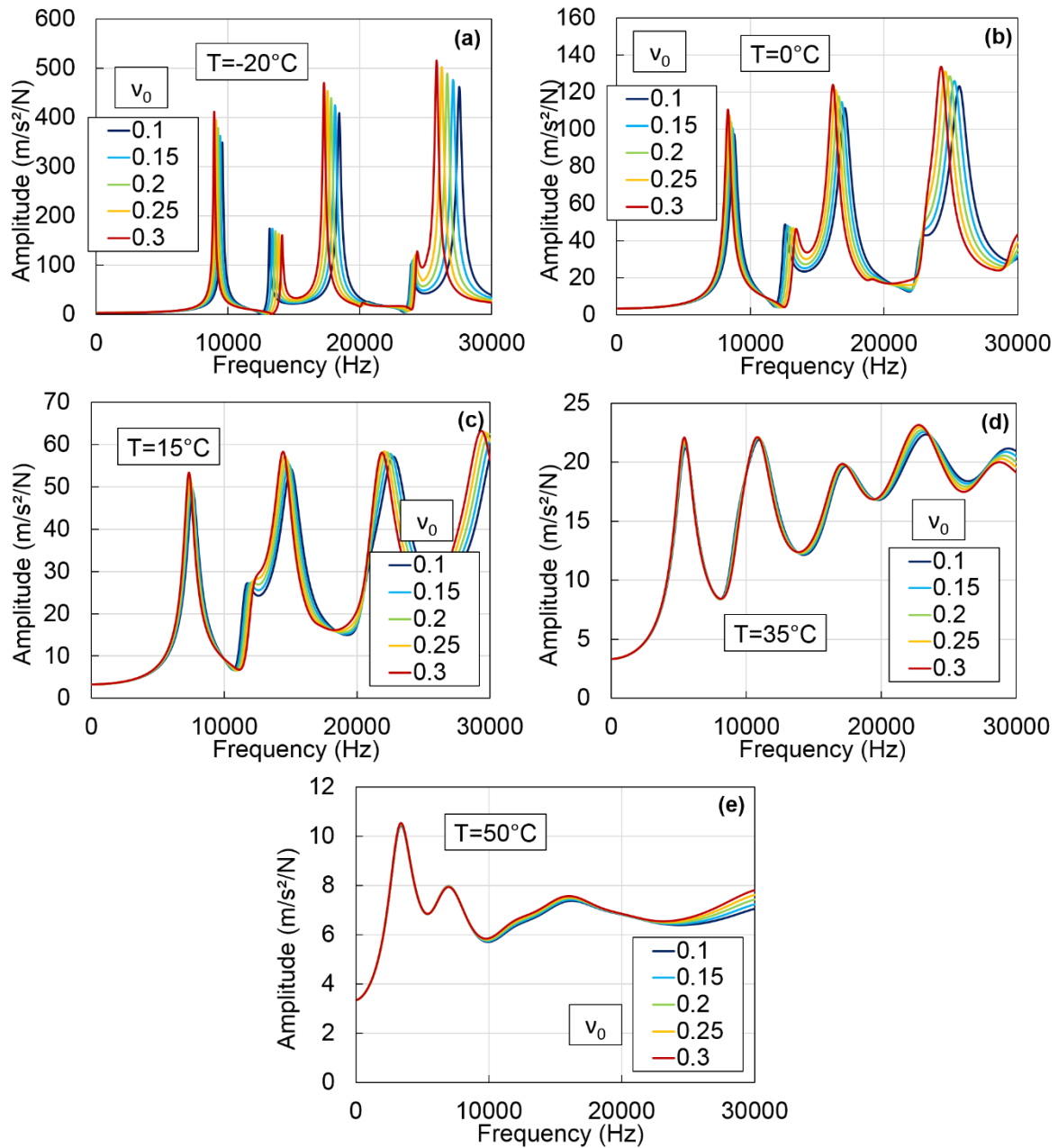


Figure D.20. Influence of constant v_0 of the 2S2P1D model on the FRFs of the flexural mode of the disc at: (a) -20°C ; (b) 0°C ; (c) 15°C ; (d) 35°C ; (e) 50°C . The constants not listed in each figure have the median value given in Table 4.6.

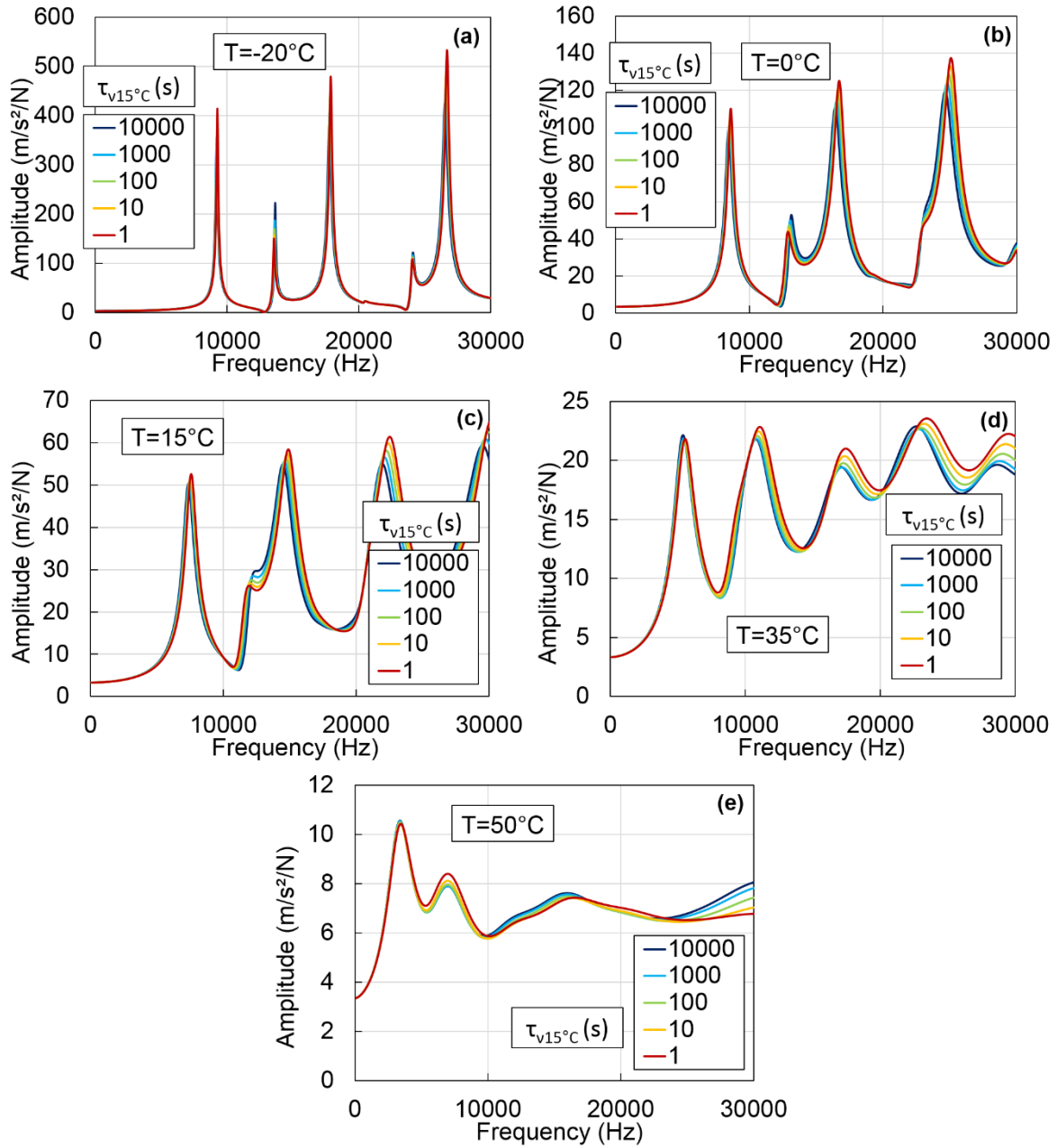


Figure D.21. Influence of constant $\tau_{v15^\circ\text{C}}$ of the 2S2P1D model on the FRFs of the flexural mode of the disc at: (a) -20°C ; (b) 0°C ; (c) 15°C ; (d) 35°C ; (e) 50°C . The constants not listed in each figure have the median value given in Table 4.6.

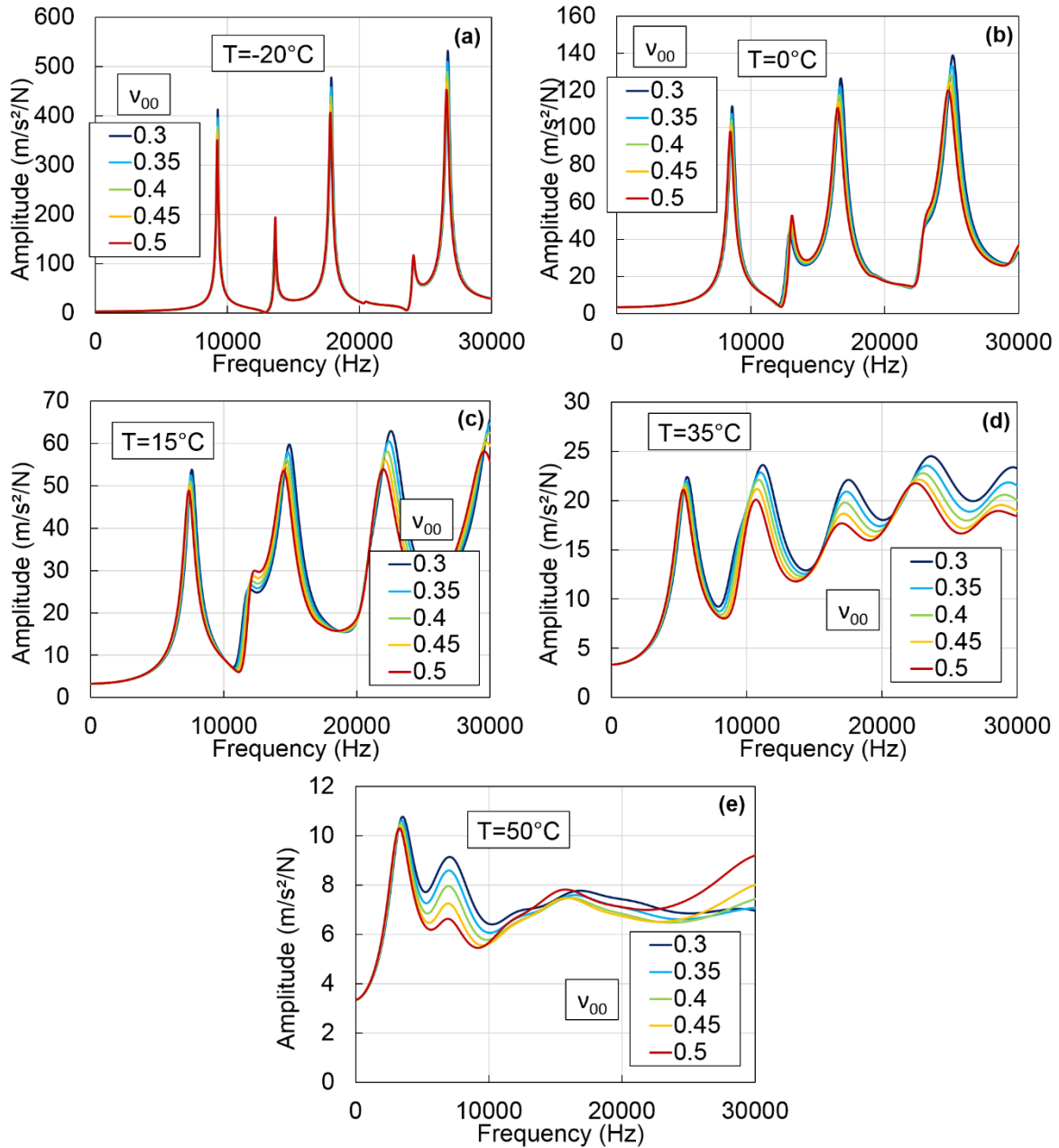


Figure D.22. Influence of constant v_{00} of the 2S2P1D model on the FRFs of the flexural mode of the disc at: (a) -20°C; (b) 0°C; (c) 15°C; (d) 35°C; (e) 50°C. The constants not listed in each figure have the median value given in Table 4.6.

**FREQUENCY RESPONSE FUNCTIONS RESULTS FOR THE TORSIONAL MODE
OF THE STRAIGHT BEAM**

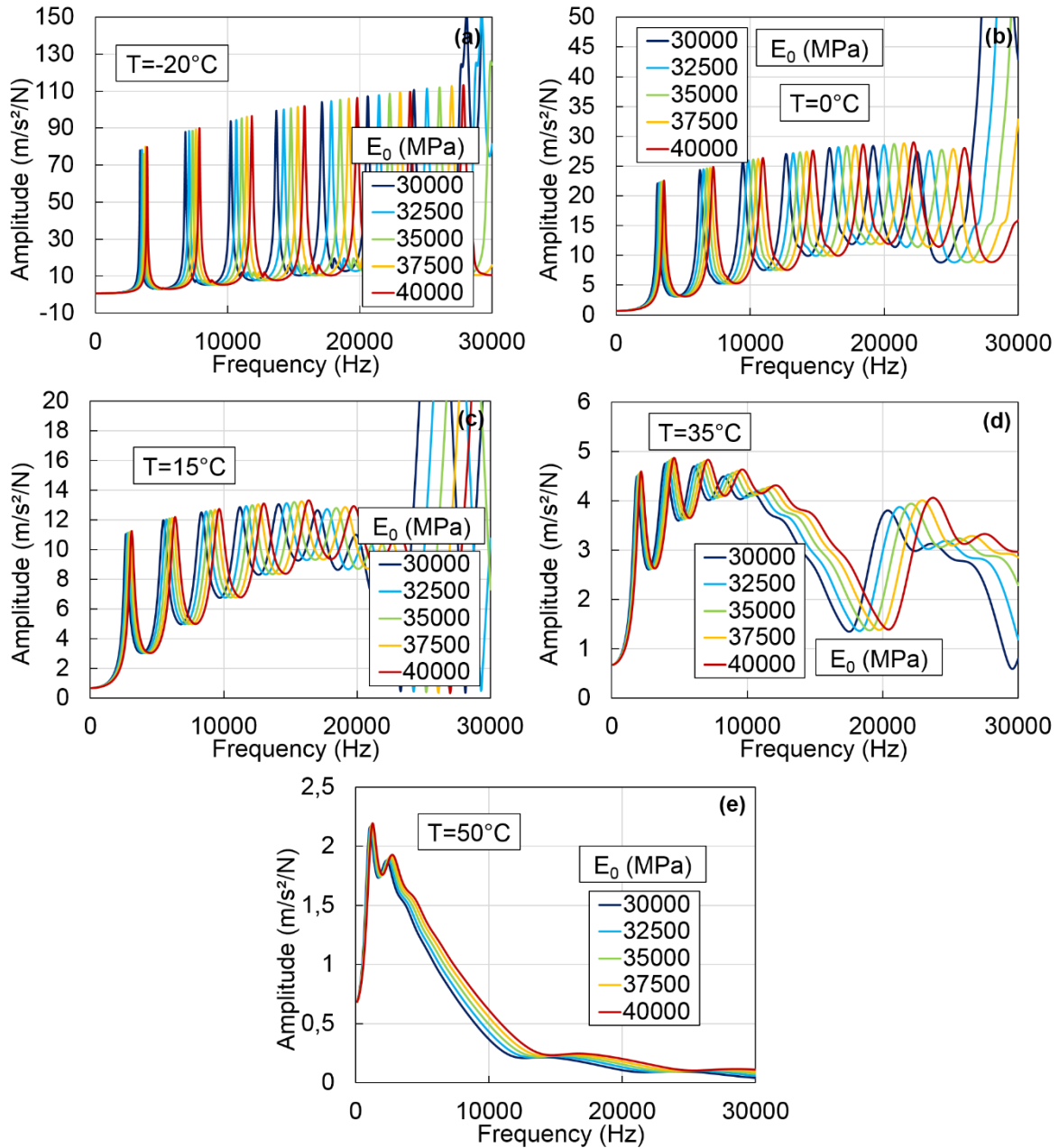


Figure D.23. Influence of constant E_0 of the 2S2P1D model on the FRFs of the torsional mode of the straight beam at: (a) -20°C ; (b) 0°C ; (c) 15°C ; (d) 35°C ; (e) 50°C . The constants not listed in each figure have the median value given in Table 4.6.

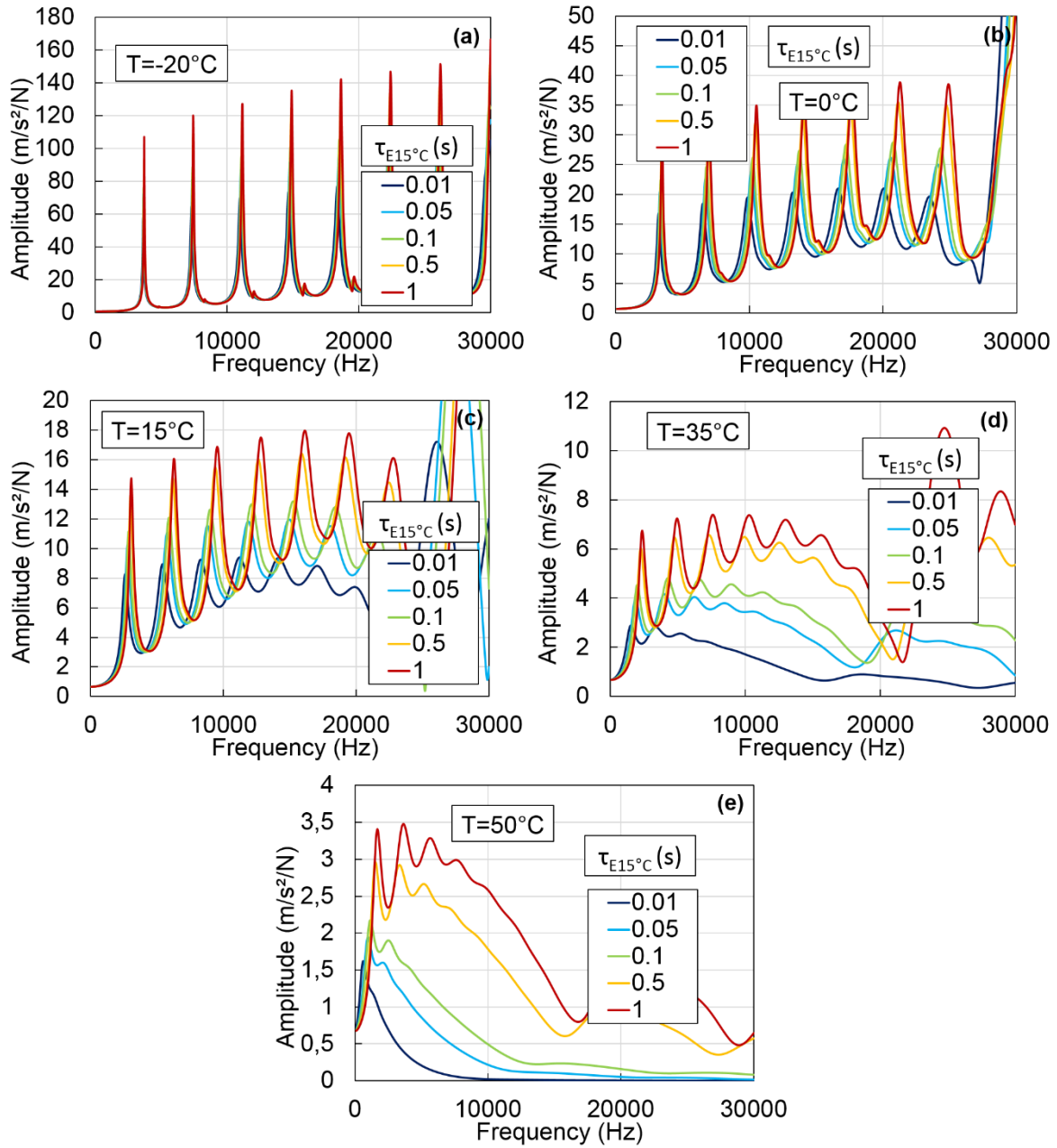


Figure D.24. Influence of constant $\tau_{E15^\circ C}$ of the 2S2P1D model on the FRFs of the torsional mode of the straight beam at: (a) $-20^\circ C$; (b) $0^\circ C$; (c) $15^\circ C$; (d) $35^\circ C$; (e) $50^\circ C$. The constants not listed in each figure have the median value given in Table 4.6.

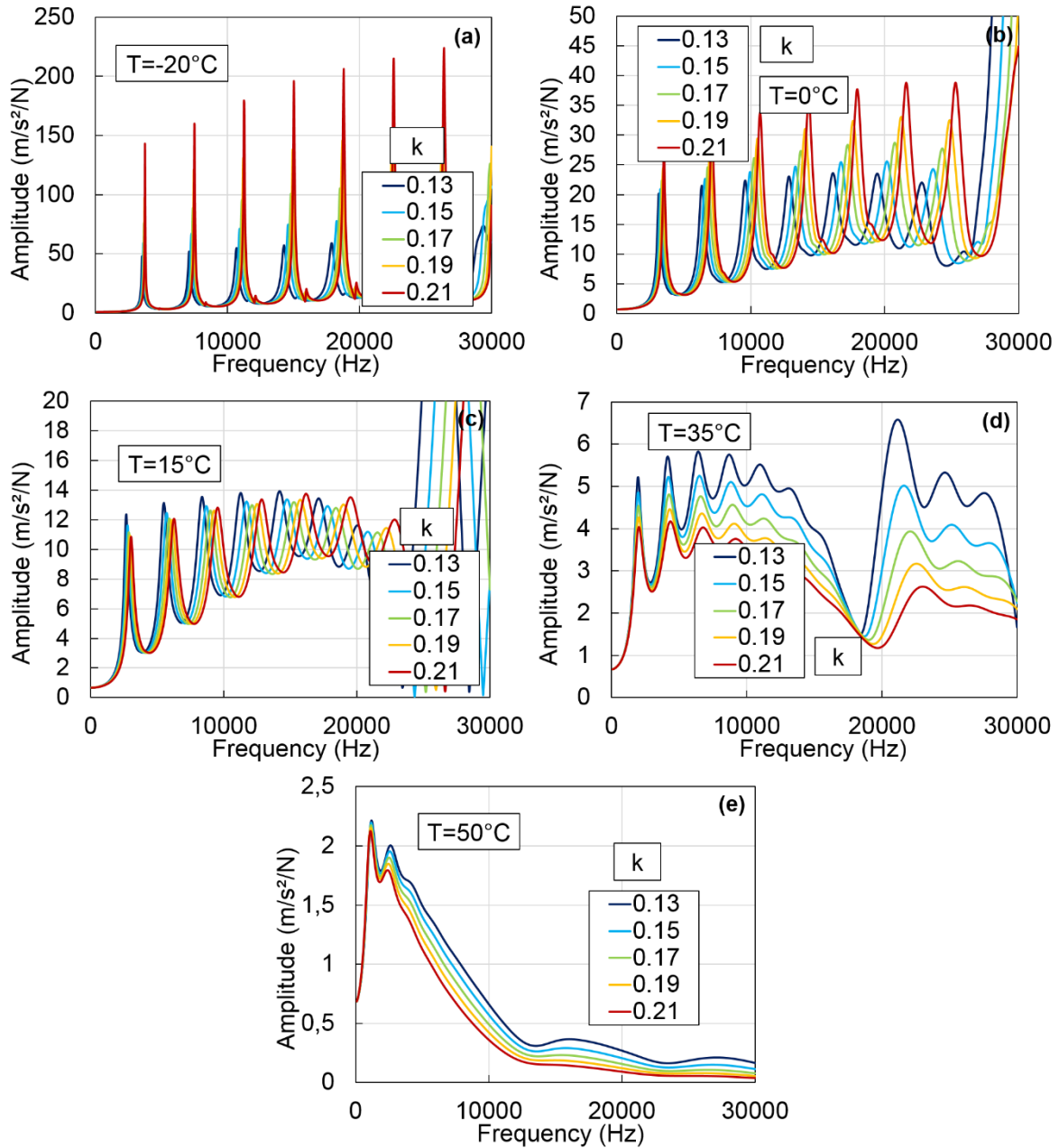


Figure D.25. Influence of constant k of the 2S2P1D model on the FRFs of the torsional mode of the straight beam at: (a) -20°C ; (b) 0°C ; (c) 15°C ; (d) 35°C ; (e) 50°C . The constants not listed in each figure have the median value given in Table 4.6.

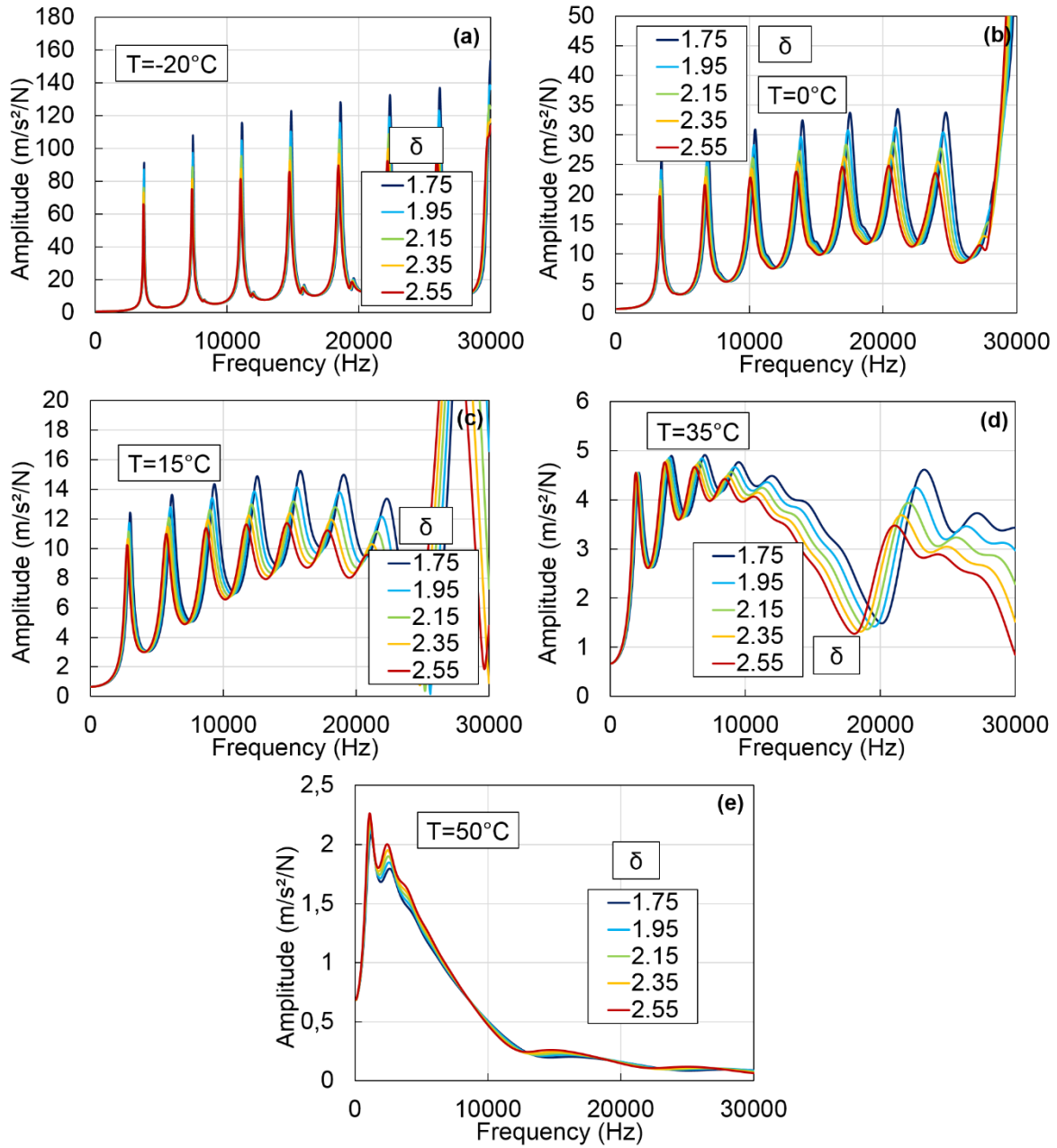


Figure D.26. Influence of constant δ of the 2S2PID model on the FRFs of the torsional mode of the straight beam at: (a) -20°C ; (b) 0°C ; (c) 15°C ; (d) 35°C ; (e) 50°C . The constants not listed in each figure have the median value given in Table 4.6.

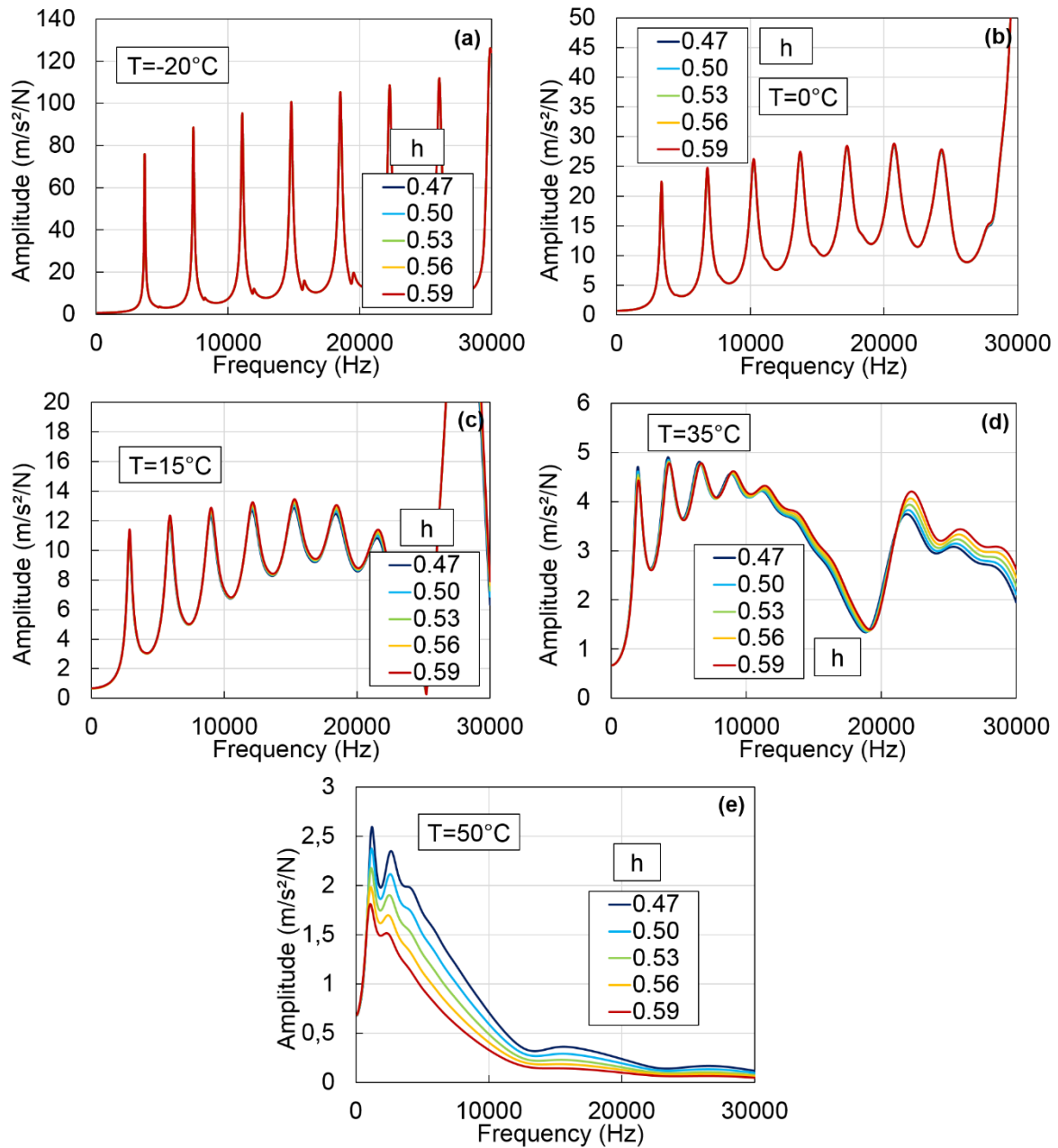


Figure D.27. Influence of constant h of the 2S2P1D model on the FRFs of the torsional mode of the straight beam at: (a) -20°C ; (b) 0°C ; (c) 15°C ; (d) 35°C ; (e) 50°C . The constants not listed in each figure have the median value given in Table 4.6.

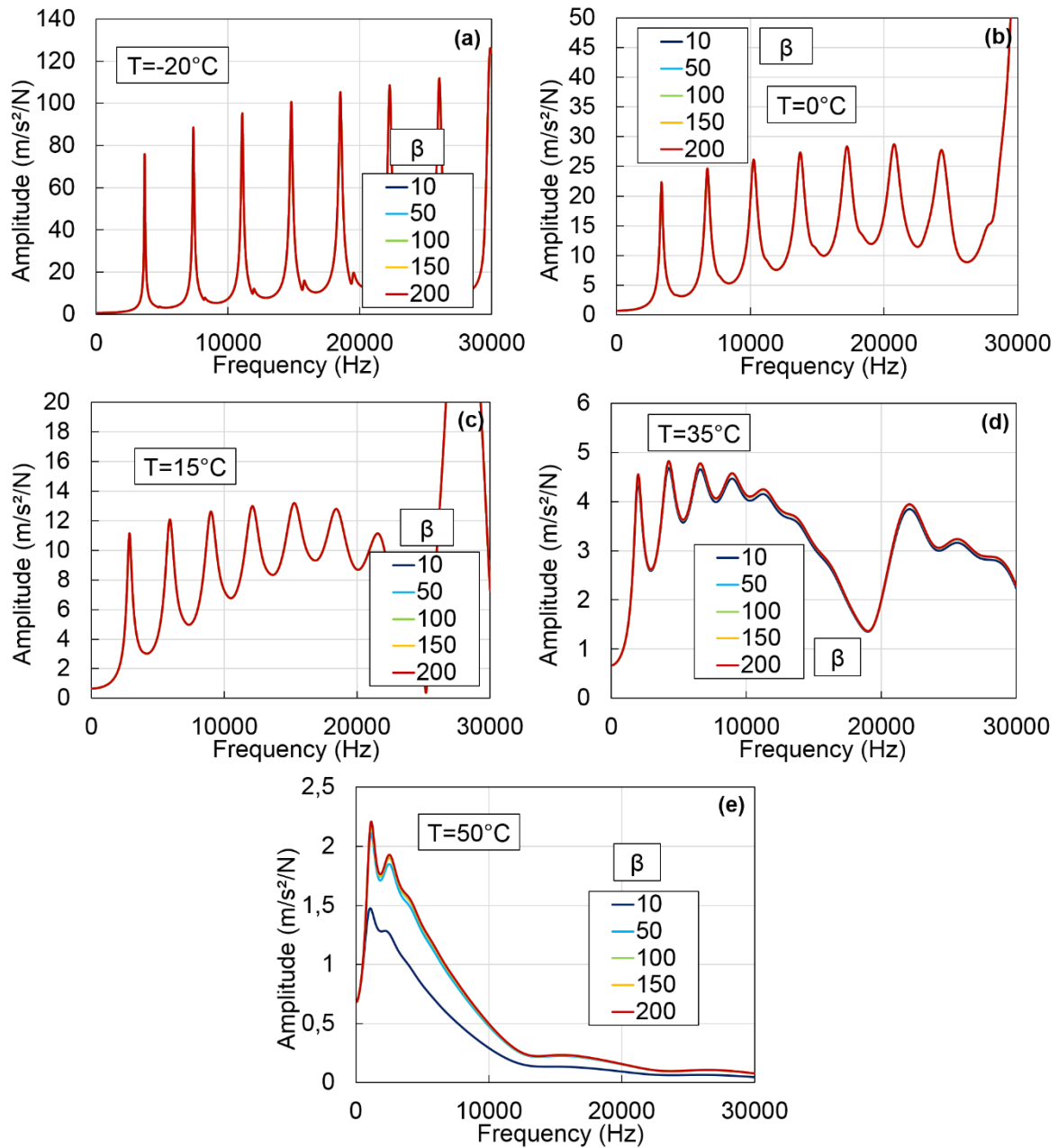


Figure D.28. Influence of constant β of the 2S2P1D model on the FRFs of the torsional mode of the straight beam at: (a) -20°C ; (b) 0°C ; (c) 15°C ; (d) 35°C ; (e) 50°C . The constants not listed in each figure have the median value given in Table 4.6.

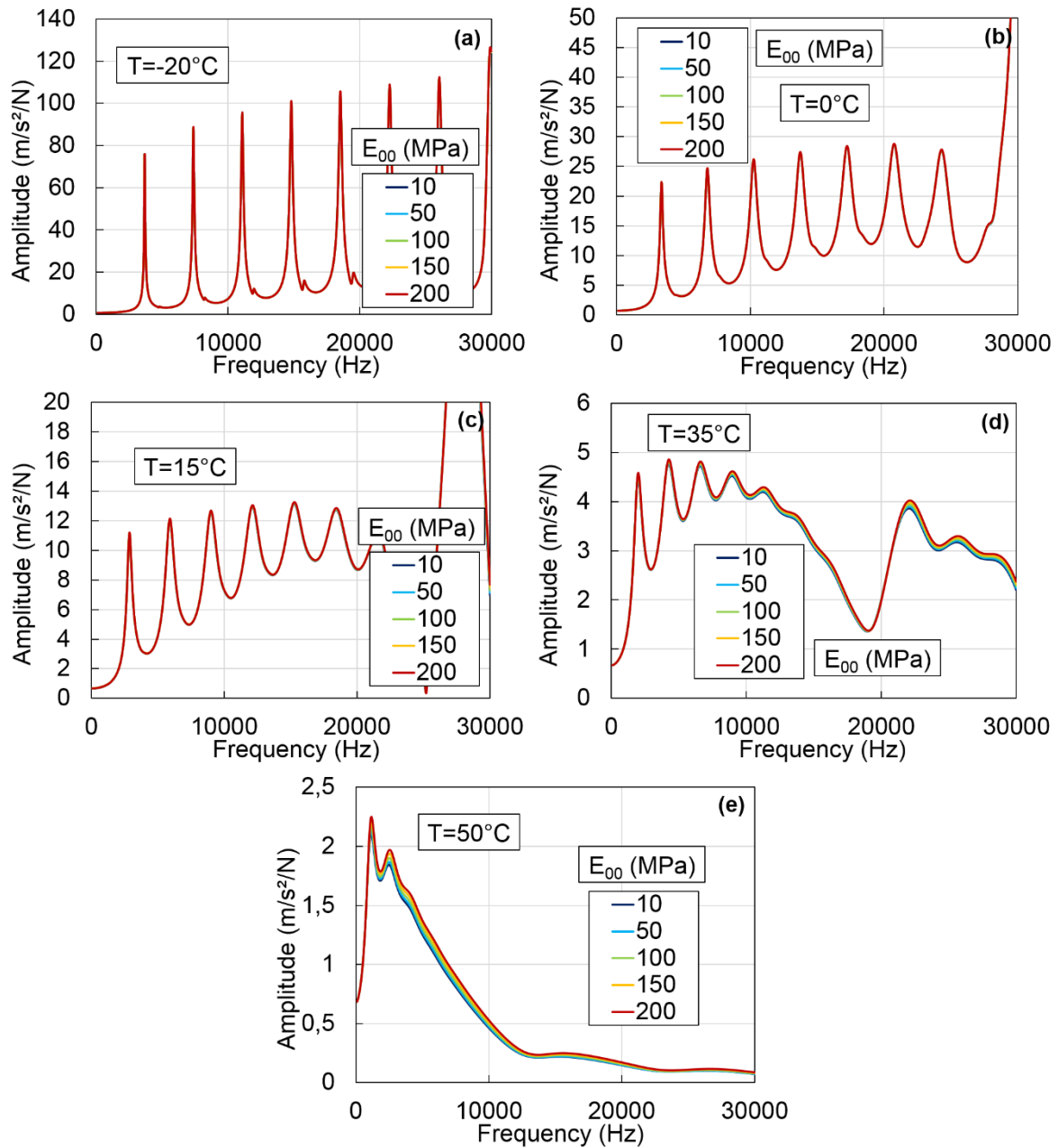


Figure D.29. Influence of constant E_{00} of the 2S2P1D model on the FRFs of the torsional mode of the straight beam at: (a) -20°C ; (b) 0°C ; (c) 15°C ; (d) 35°C ; (e) 50°C . The constants not listed in each figure have the median value given in Table 4.6.

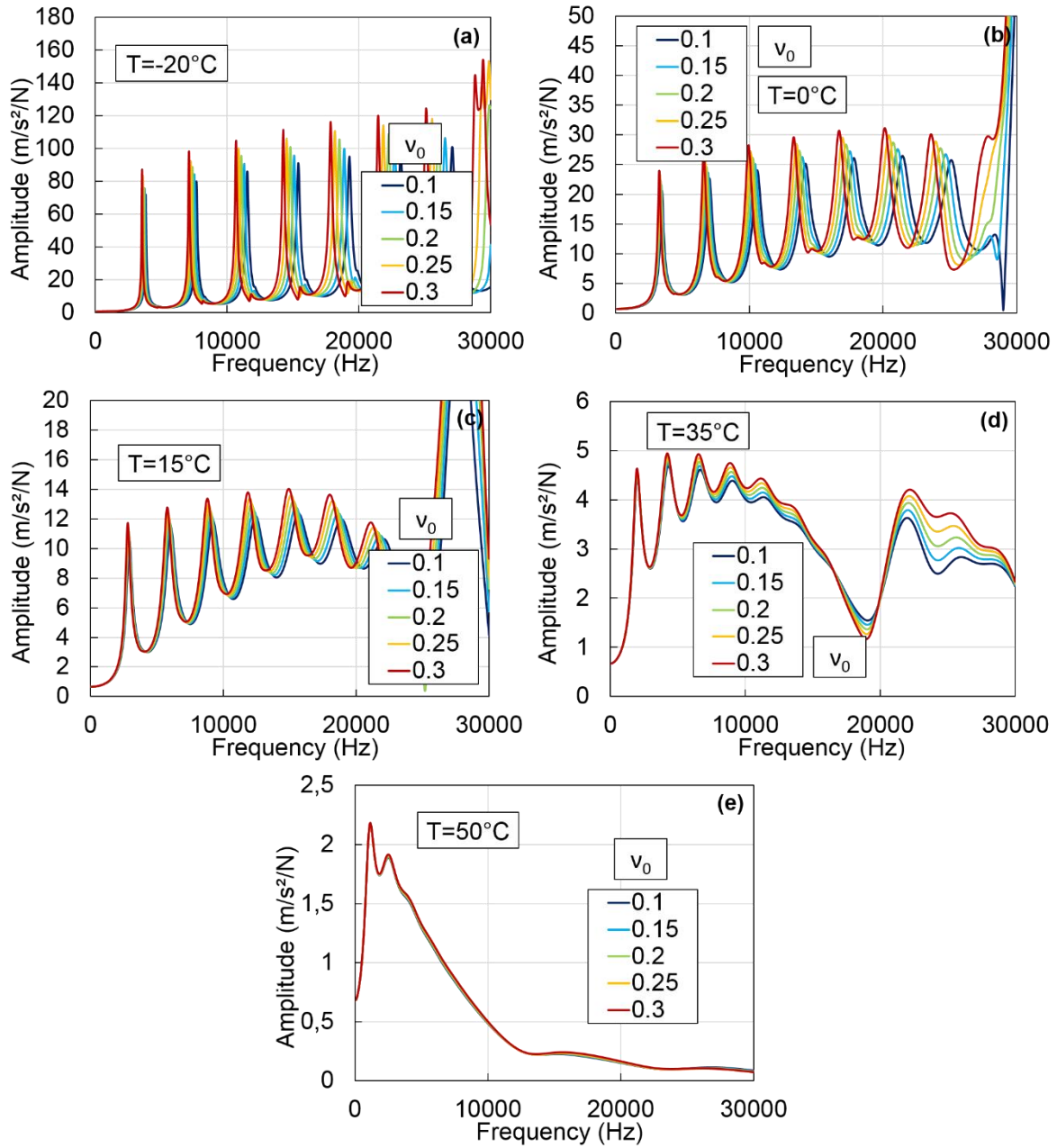


Figure D.30. Influence of constant v_0 of the 2S2P1D model on the FRFs of the torsional mode of the straight beam at: (a) -20°C ; (b) 0°C ; (c) 15°C ; (d) 35°C ; (e) 50°C . The constants not listed in each figure have the median value given in Table 4.6.

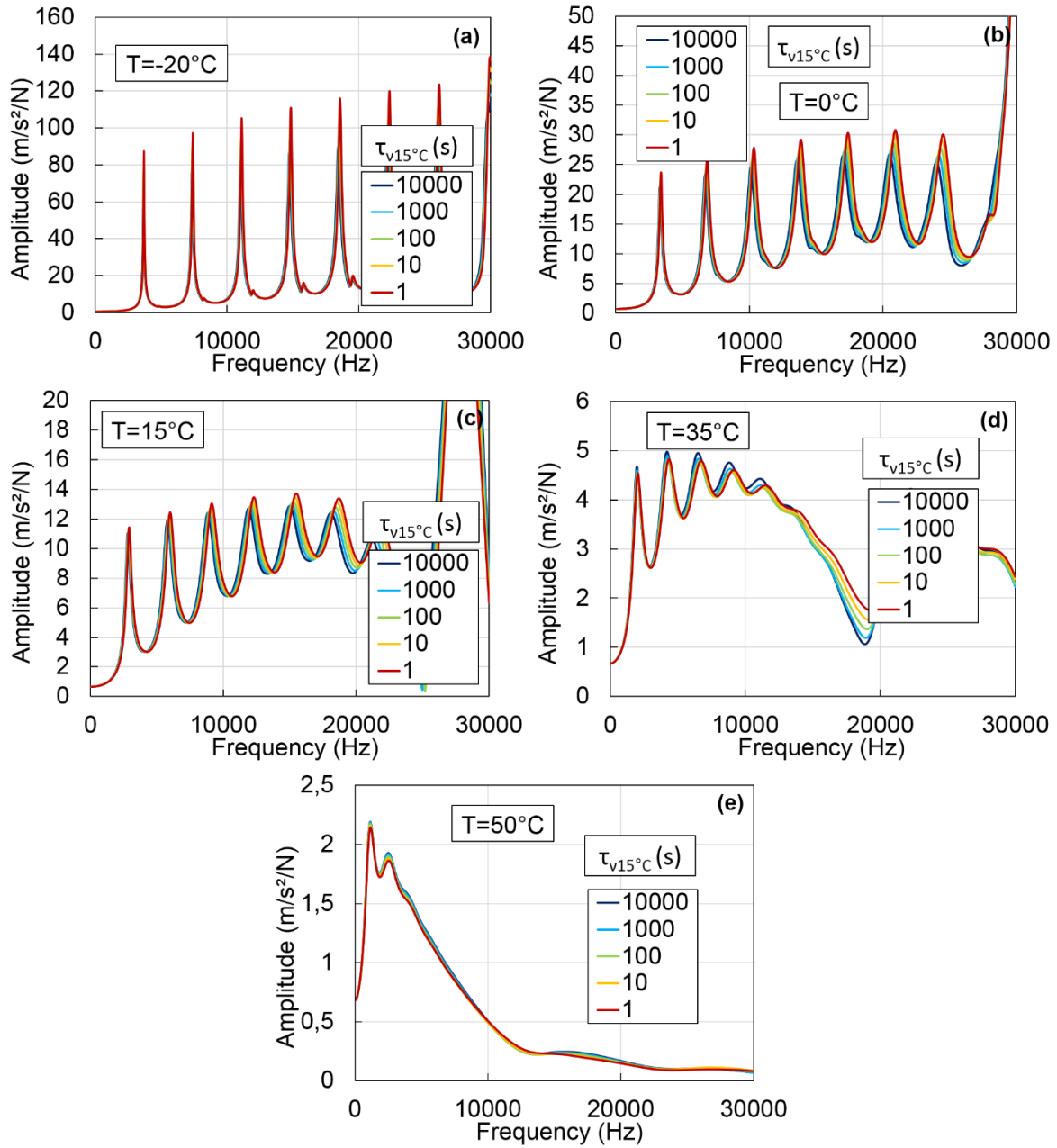


Figure D.31. Influence of constant $\tau_{v15^\circ\text{C}}$ of the 2S2P1D model on the FRFs of the torsional mode of the straight beam at: (a) -20°C ; (b) 0°C ; (c) 15°C ; (d) 35°C ; (e) 50°C . The constants not listed in each figure have the median value given in Table 4.6.

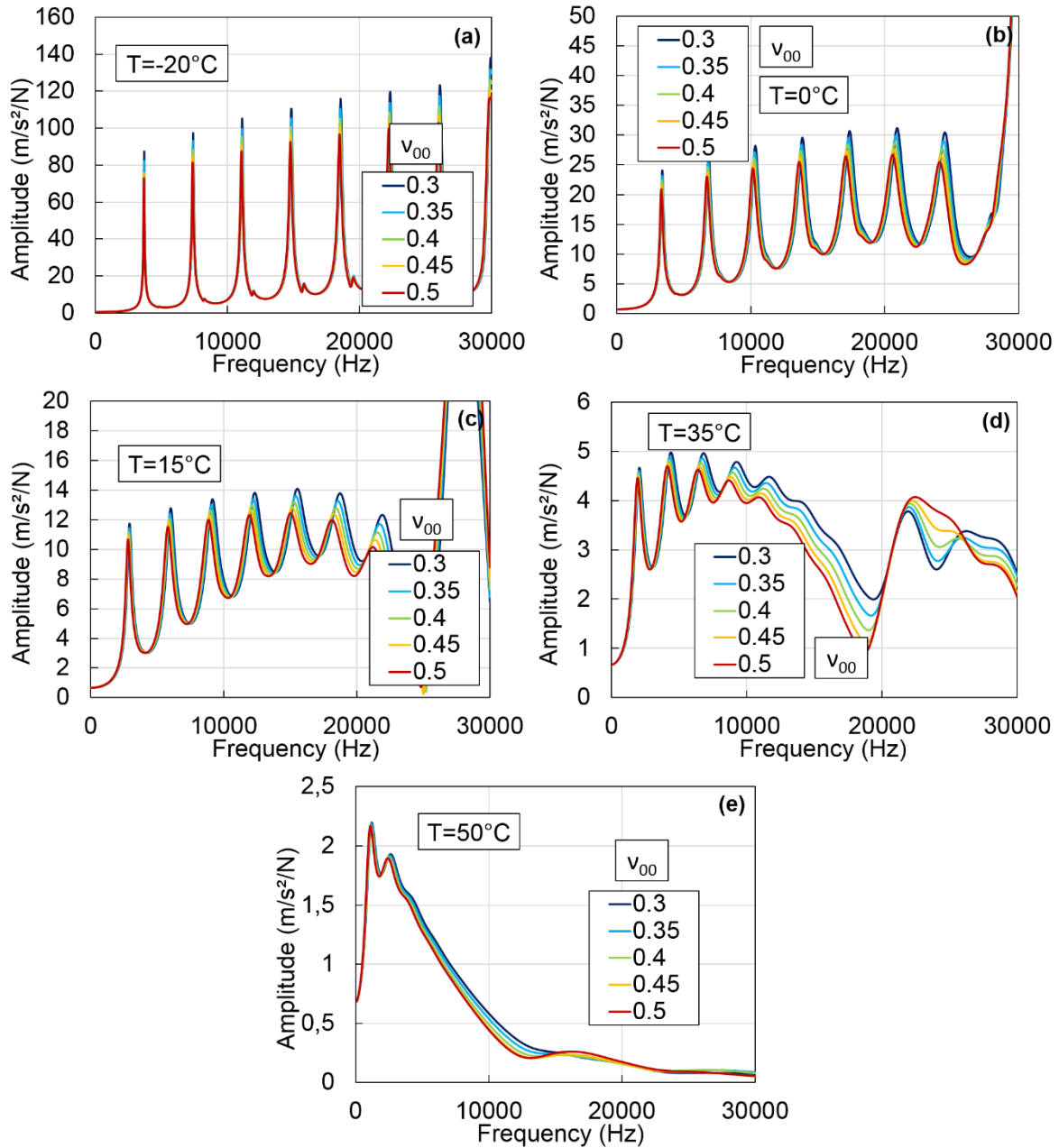


Figure D.32. Influence of constant v_{00} of the 2S2P1D model on the FRFs of the torsional mode of the straight beam at: (a) -20°C ; (b) 0°C ; (c) 15°C ; (d) 35°C ; (e) 50°C . The constants not listed in each figure have the median value given in Table 4.6.

**APPENDIX E - RESULTS OF METHOD II FOR THE
REFERENCE LVE MATERIAL**

FREQUENCY RESPONSE FUNCTIONS RESULTS

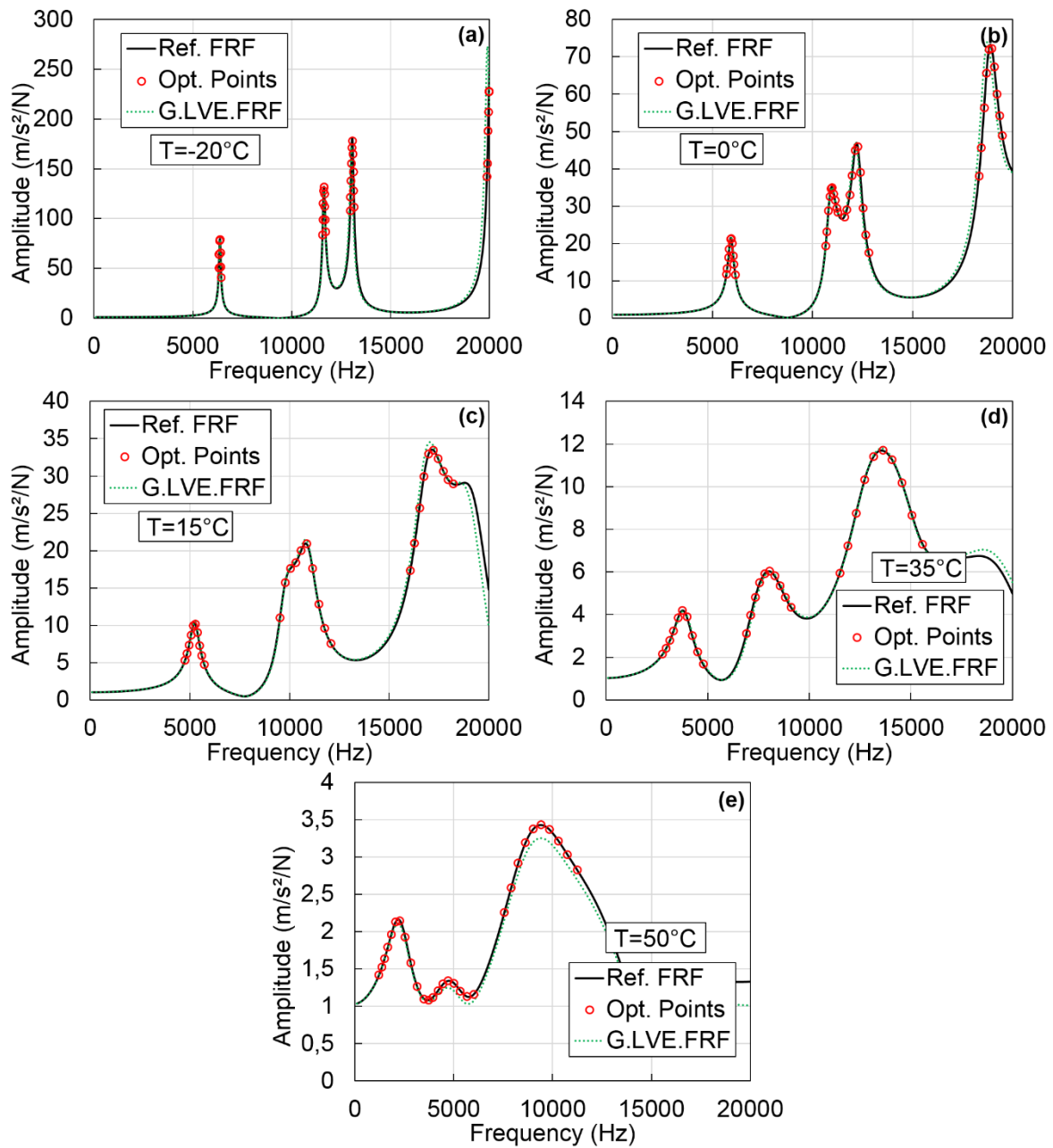


Figure E.1. Comparison of the reference FRFs (noted Ref. FRF) with the global LVE FRFs (noted G.LVE.FRF) for method II. Values of the reference FRFs at the frequencies where the optimization is performed (noted Opt. Points) are also plotted. Results for the longitudinal and flexural modes of the cylinder at: (a) -20°C; (b) 0°C; (c) 15°C; (d) 35°C; (e) 50°C.

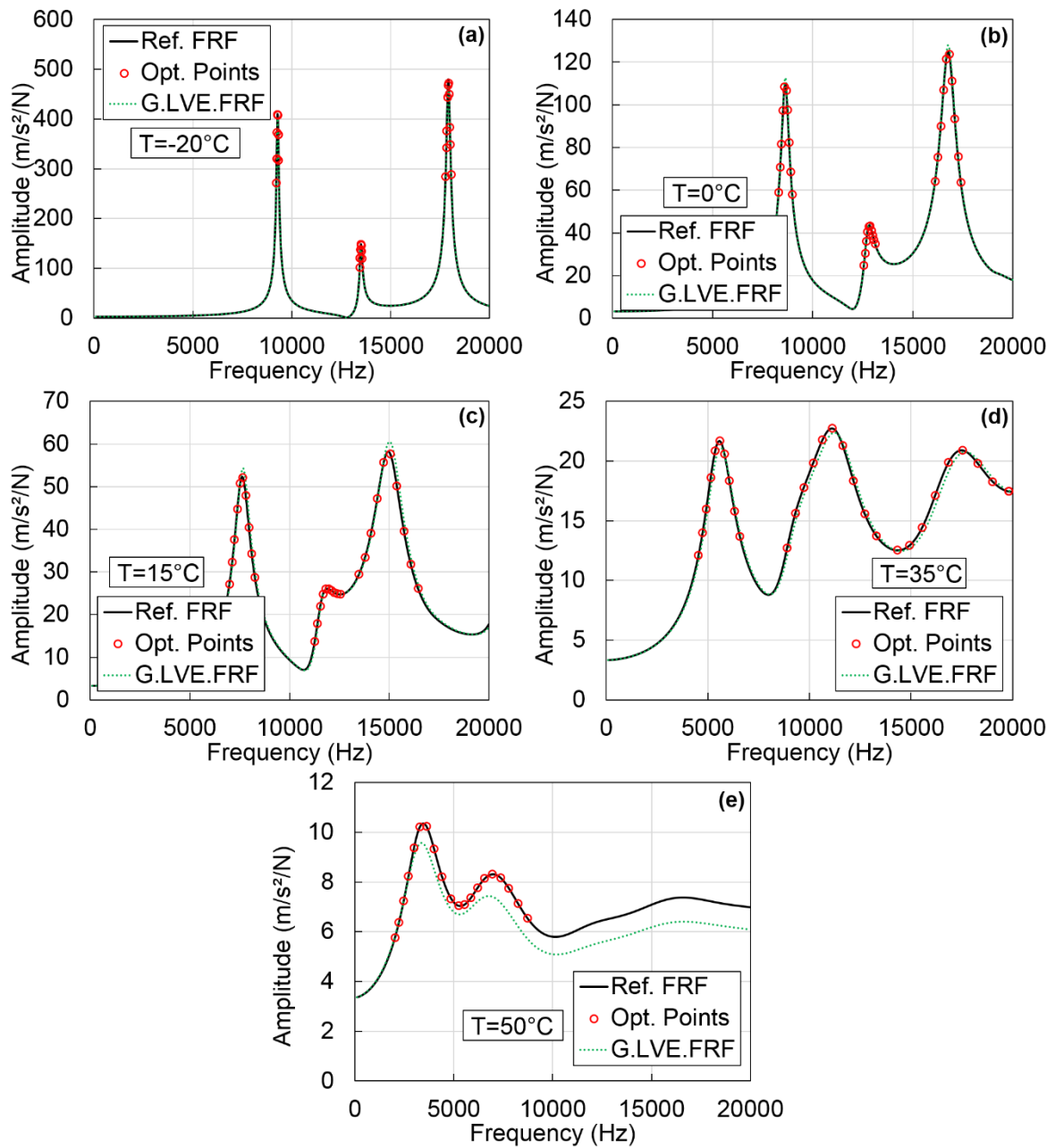


Figure E.2. Comparison of the reference FRFs (noted Ref. FRF) with the global LVE FRFs (noted G.LVE.FRF) for method II. Values of the reference FRFs at the frequencies where the optimization is performed (noted Opt. Points) are also plotted. Results for the flexural mode of the disc at: (a) -20°C ; (b) 0°C ; (c) 15°C ; (d) 35°C ; (e) 50°C .

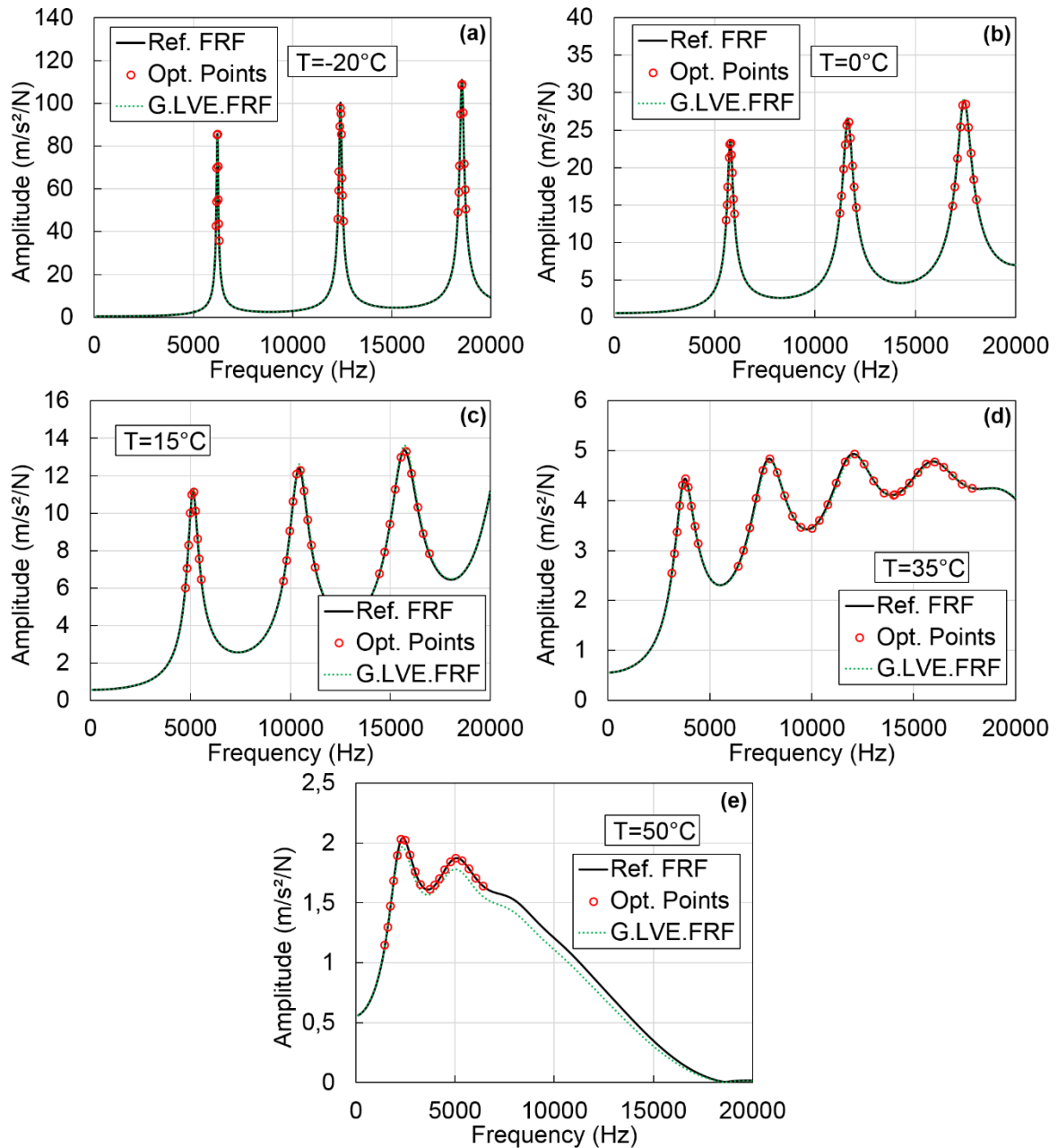


Figure E.3. Comparison of the reference FRFs (noted Ref. FRF) with the global LVE FRFs (noted G.LVE.FRF) for method II. Values of the reference FRFs at the frequencies where the optimization is performed (noted Opt. Points) are also plotted. Results for the longitudinal mode of the straight beam at: (a) -20°C ; (b) 0°C ; (c) 15°C ; (d) 35°C ; (e) 50°C .

FREQUENCY USED FOR THE COMPARISON OF THE VALUES OF THE COMPLEX MODULUS

Table E.1. Frequencies selected for the comparison of the values of the complex modulus at each temperature for the longitudinal mode of the cylinder.

Temperature (°C)	Frequencies (Hz)					
-20	10 000	12 000	14 000	16 000	18 000	20 000
0	10 000	12 000	14 000	16 000	18 000	20 000
15	8 000	10 000	12 000	14 000	16 000	18 000
35	6 000	8 000	10 000	12 000	14 000	16 000
50	4 000	6 000	8 000	10 000	12 000	14 000

Table E.2. Frequencies selected for the comparison of the values of the complex modulus at each temperature for the longitudinal and flexural modes of the cylinder.

Temperature (°C)	Frequencies (Hz)					
-20	10 000	12 000	14 000	16 000	18 000	20 000
0	10 000	12 000	14 000	16 000	18 000	20 000
15	8 000	10 000	12 000	14 000	16 000	18 000
35	6 000	8 000	10 000	12 000	14 000	16 000
50	4 000	6 000	8 000	10 000	12 000	14 000

Table E.3. Frequencies selected for the comparison of the values of the complex modulus at each temperature for the longitudinal mode of the straight beam.

Temperature (°C)	Frequencies (Hz)					
-20	10 000	12 000	14 000	16 000	18 000	20 000
0	10 000	12 000	14 000	16 000	18 000	20 000
15	8 000	10 000	12 000	14 000	16 000	18 000
35	6 000	8 000	10 000	12 000	14 000	16 000
50	4 000	6 000	8 000	10 000	12 000	14 000

Table E.4. Frequencies selected for the comparison of the values of the complex modulus at each temperature for the flexural mode of the disc.

Temperature (°C)	Frequencies (Hz)					
-20	10 000	12 000	14 000	16 000	18 000	20 000
0	10 000	12 000	14 000	16 000	18 000	20 000
15	8 000	10 000	12 000	14 000	16 000	18 000
35	6 000	8 000	10 000	12 000	14 000	16 000
50	4 000	6 000	8 000	10 000	12 000	14 000

COMPLEX MODULUS RESULTS

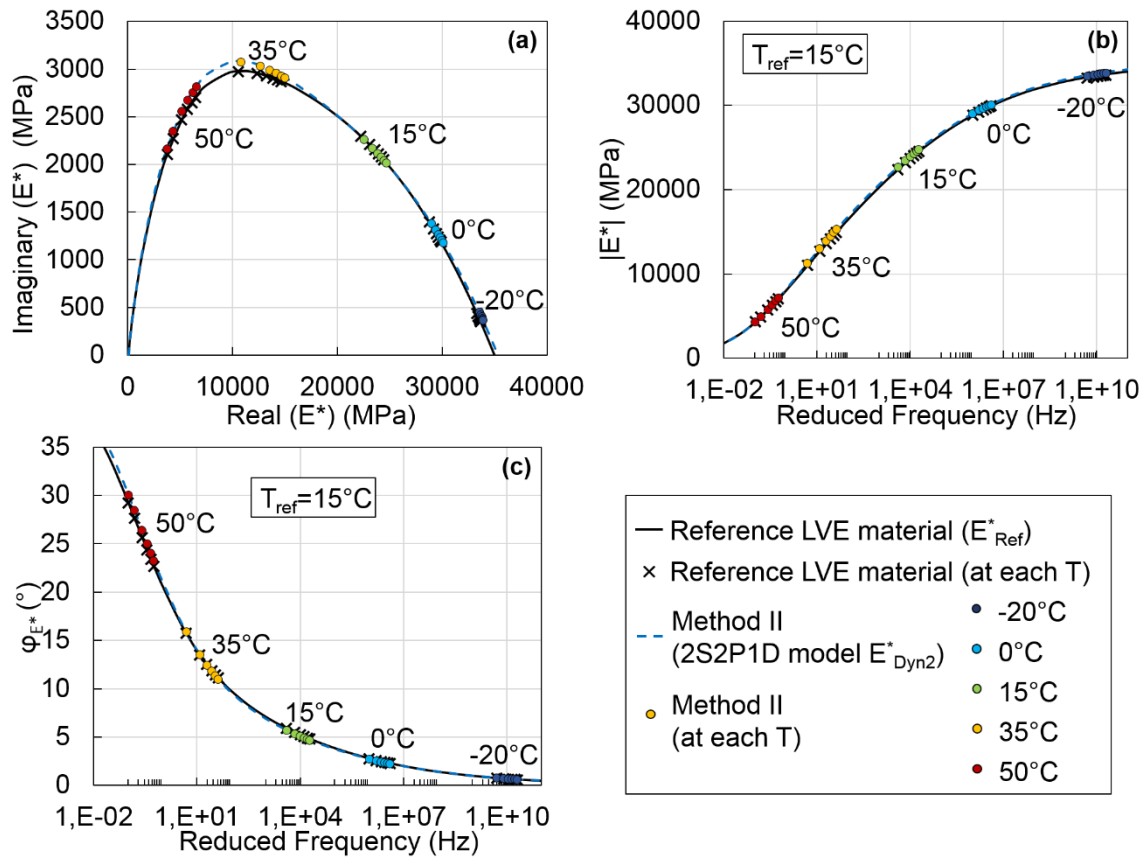


Figure E.4. Comparison of the values of the complex modulus determined with method II (E^*_{Dyn2}) with the values of the complex modulus of the reference LVE material (E^*_{Ref}). (a) Cole-Cole plot; (b) and (c) master curves of the norm and of the phase angle of the complex modulus at 15°C. Results for the longitudinal and flexural modes of the cylinder.

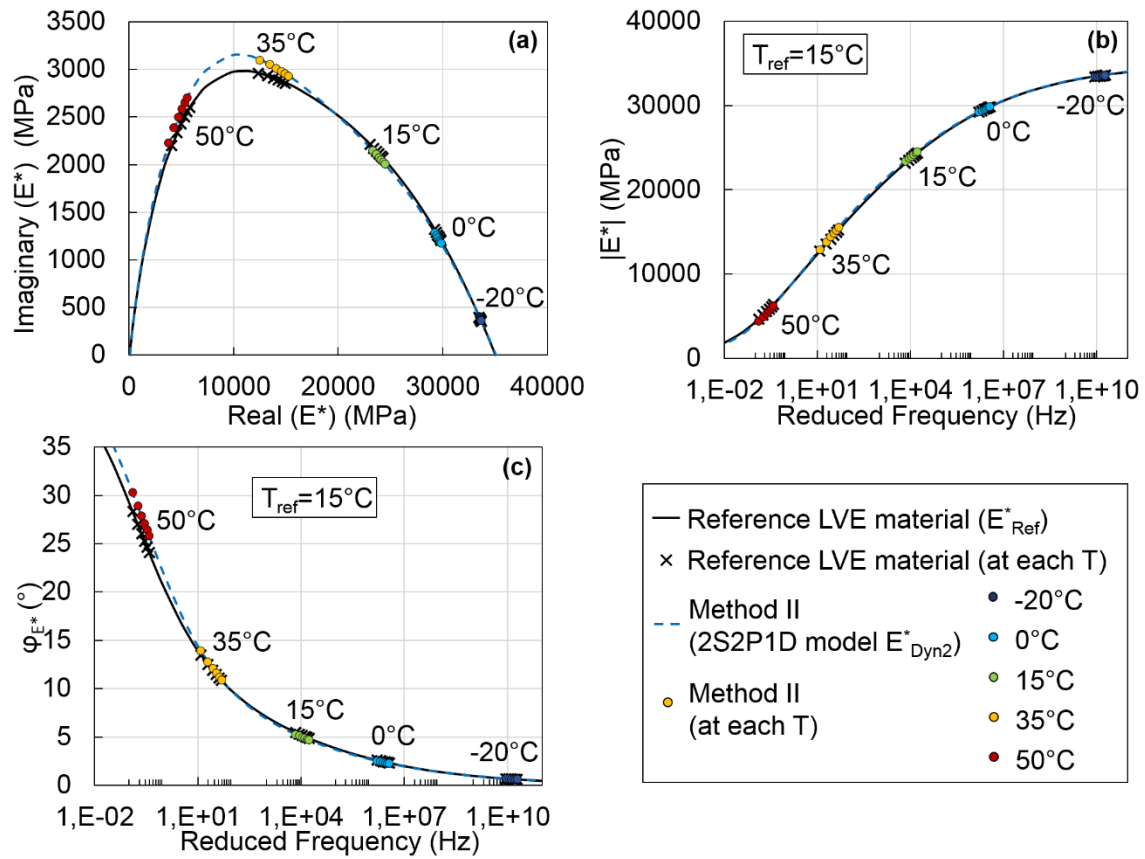


Figure E.5. Comparison of the values of the complex modulus determined with method II (E_{Dyn2}^*) with the values of the complex modulus of the reference LVE material (E_{Ref}^*). (a) Cole-Cole plot; (b) and (c) master curves of the norm and of the phase angle of the complex modulus at $15^\circ C$. Results for the flexural mode of the disc.

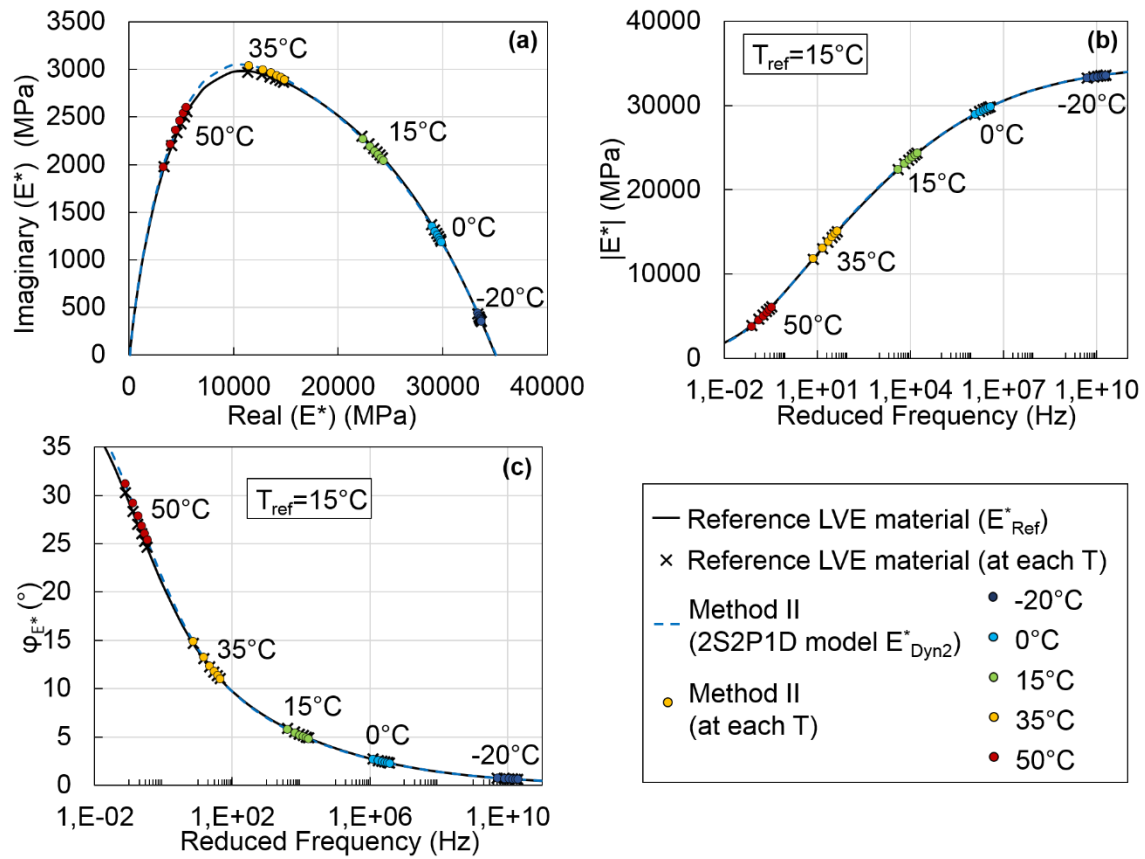


Figure E.6. Comparison of the values of the complex modulus determined with method II (E^*_{Dyn2}) with the values of the complex modulus of the reference LVE material (E^*_{Ref}). (a) Cole-Cole plot; (b) and (c) master curves of the norm and of the phase angle of the complex modulus at 15°C . Results for the longitudinal mode of the straight beam.

**APPENDIX F - RESULTS OF METHOD III FOR THE
REFERENCE LVE MATERIAL**

FINAL VALUES OF THE CONSTANTS OPTIMIZED AT EACH TEMPERATURE

Table F.1. Final values of the four constants E_0 , $\tau_{E15^\circ\text{C}}$, k and δ of the 2S2PID model that are identified at each temperature in the first step of method III for the longitudinal and flexural modes of the cylinder.

Temperature ($^\circ\text{C}$)	E_0 (MPa)	$\tau_{E15^\circ\text{C}}$ (s)	k	δ
-20	35 100	0.600	0.154	2.20
0	36 773	0.875	0.137	2.35
15	33 604	0.164	0.187	2.44
35	33 076	0.153	0.186	2.34
50	31 610	0.123	0.182	1.96

Table F.2. Final values of the four constants E_0 , $\tau_{E15^\circ\text{C}}$, k and δ of the 2S2PID model that are identified at each temperature in the first step of method III for the flexural mode of the disc.

Temperature ($^\circ\text{C}$)	E_0 (MPa)	$\tau_{E15^\circ\text{C}}$ (s)	k	δ
-20	35 396	6.820	0.136	2.21
0	36 874	1.430	0.135	2.50
15	33 156	0.063	0.189	1.95
35	31 265	0.128	0.189	1.93
50	33 409	0.090	0.140	1.95

Table F.3. Final values of the four constants E_0 , $\tau_{E15^\circ\text{C}}$, k and δ of the 2S2PID model that are identified at each temperature in the first step of method III for the longitudinal mode of the straight beam.

Temperature ($^\circ\text{C}$)	E_0 (MPa)	$\tau_{E15^\circ\text{C}}$ (s)	k	δ
-20	35 402	4.526	0.136	2.09
0	34 302	0.078	0.189	2.38
15	39 351	0.141	0.140	2.39
35	33 069	0.176	0.189	2.37
50	32 959	0.092	0.140	1.94

FREQUENCY RESPONSE FUNCTIONS RESULTS

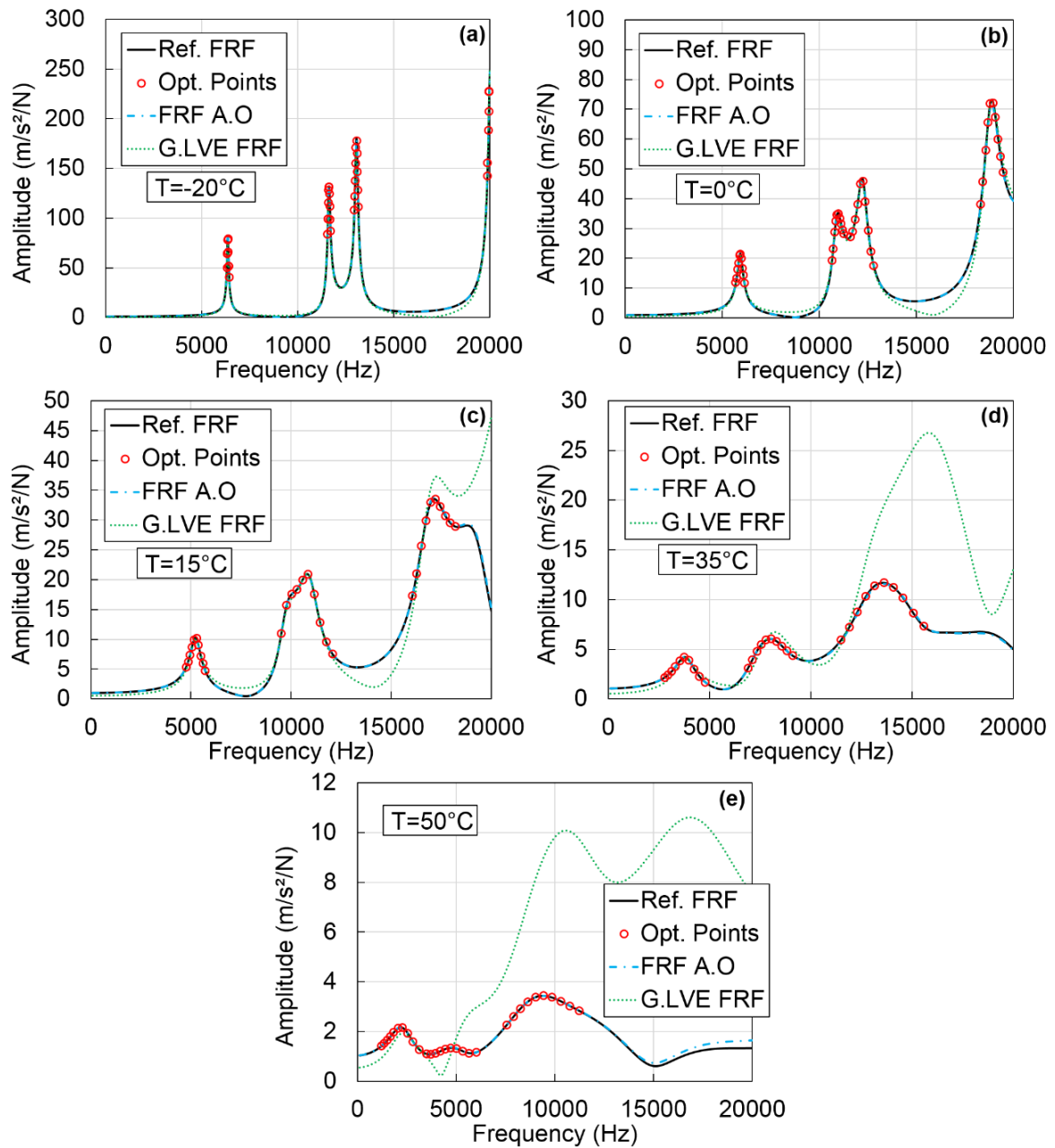


Figure F.1. Comparison of the reference FRFs (noted Ref. FRF) with the FRFs after optimization (noted FRF A.O) and the global LVE FRFs (noted G.LVE FRF) for method III. Values of the reference FRFs at the frequencies where the optimization is performed (noted Opt. Points) are also plotted. Longitudinal and flexural modes of the cylinder at: (a) -20°C ; (b) 0°C ; (c) 15°C ; (d) 35°C ; (e) 50°C .

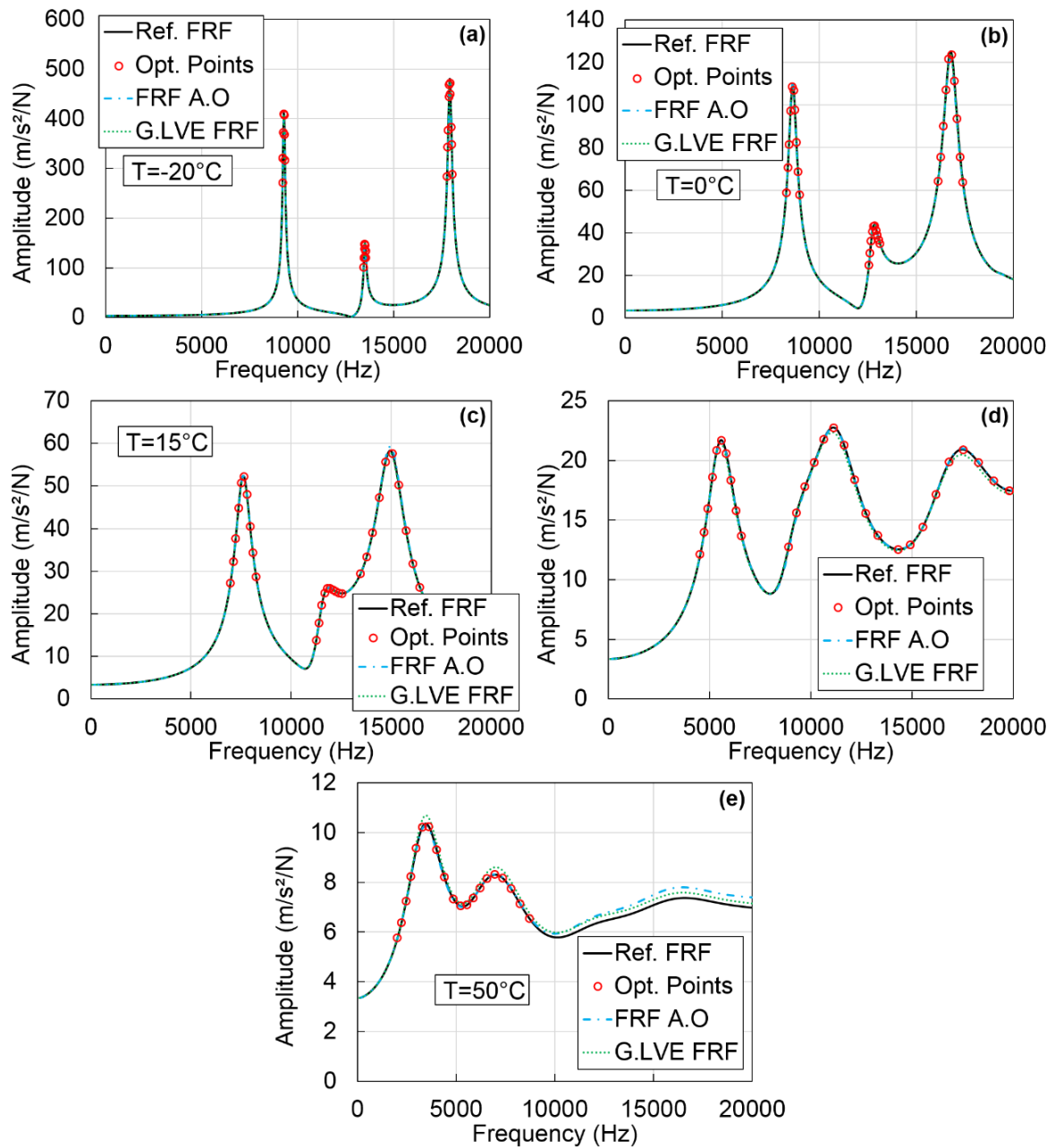


Figure F.2. Comparison of the reference FRFs (noted Ref. FRF) with the FRFs after optimization (noted FRF A.O) and the global LVE FRFs (noted G.LVE FRF) for method III. Values of the reference FRFs at the frequencies where the optimization is performed (noted Opt. Points) are also plotted. Flexural mode of the disc at: (a) -20°C; (b) 0°C; (c) 15°C; (d) 35°C; (e) 50°C.

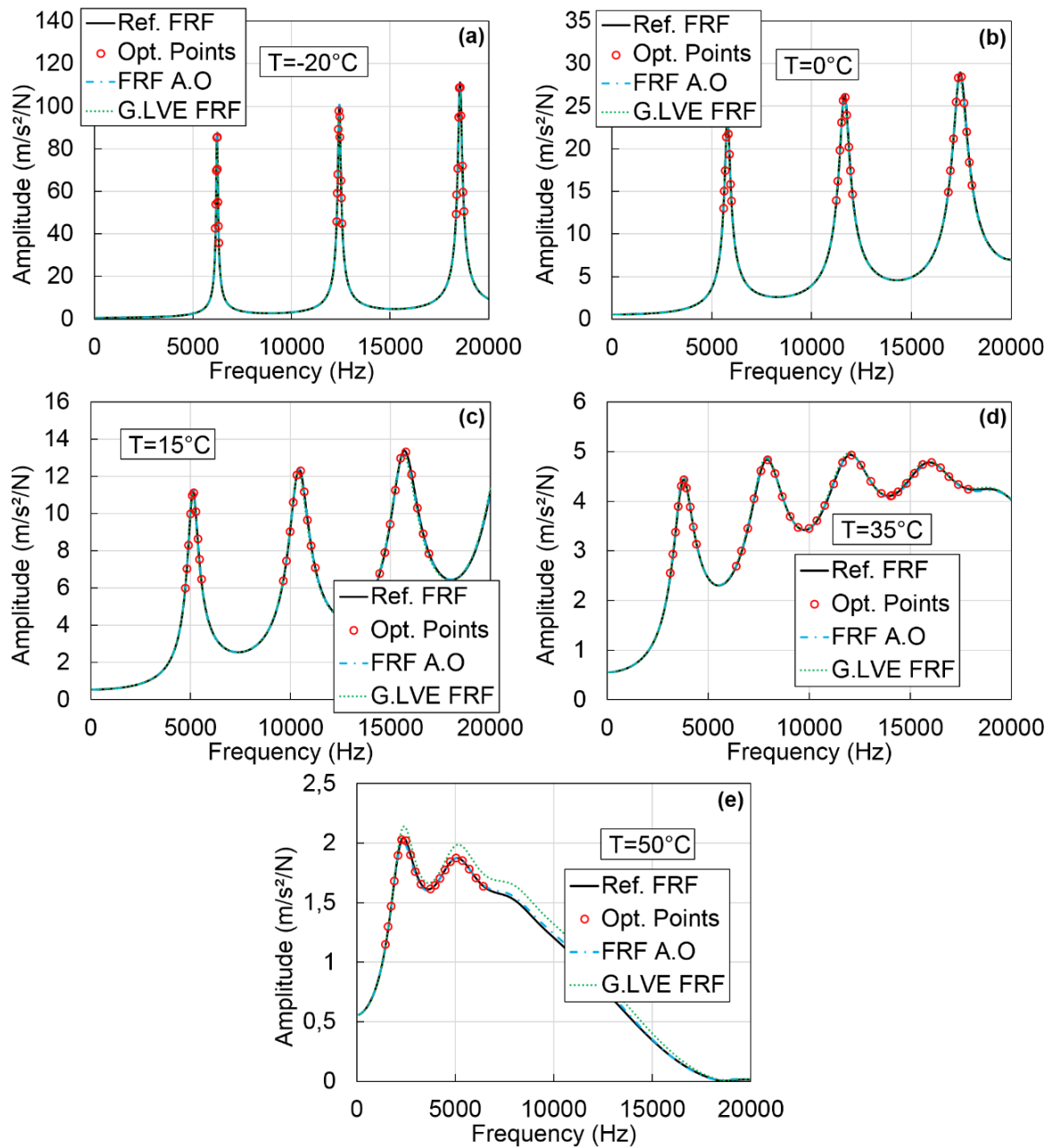


Figure F.3. Comparison of the reference FRFs (noted Ref. FRF) with the FRFs after optimization (noted FRF A.O.) and the global LVE FRFs (noted G.LVE FRF) for method III. Values of the reference FRFs at the frequencies where the optimization is performed (noted Opt. Points) are also plotted. Longitudinal mode of the straight beam at: (a) -20°C; (b) 0°C; (c) 15°C; (d) 35°C; (e) 50°C.

COMPLEX MODULUS RESULTS

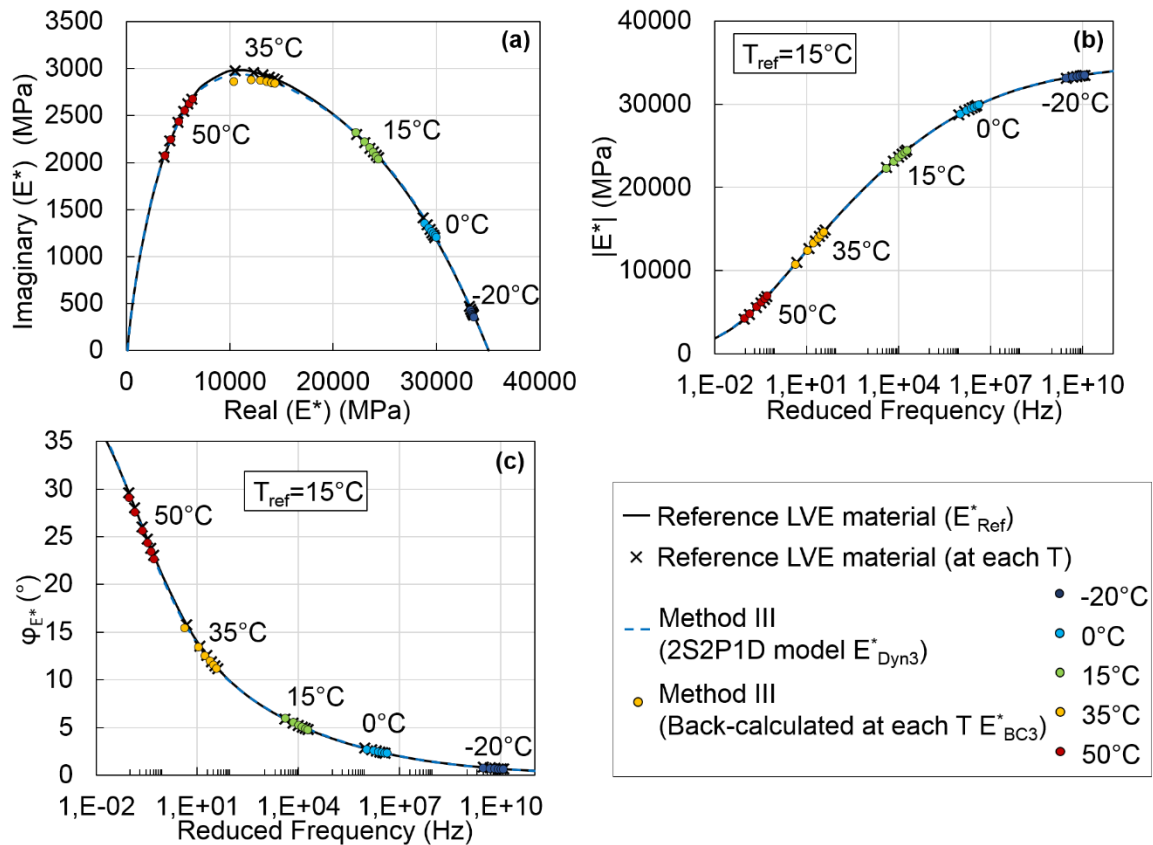


Figure F.4. Comparison of the values of the complex modulus determined with method III (E^*_{BC3} and E^*_{Dyn3}) with the values of the complex modulus of the reference LVE material (E^*_{Ref}). (a) Cole-Cole plot; (b) and (c) master curves of the norm and of the phase angle of the complex modulus at 15°C. Results for the longitudinal and flexural modes of the cylinder.

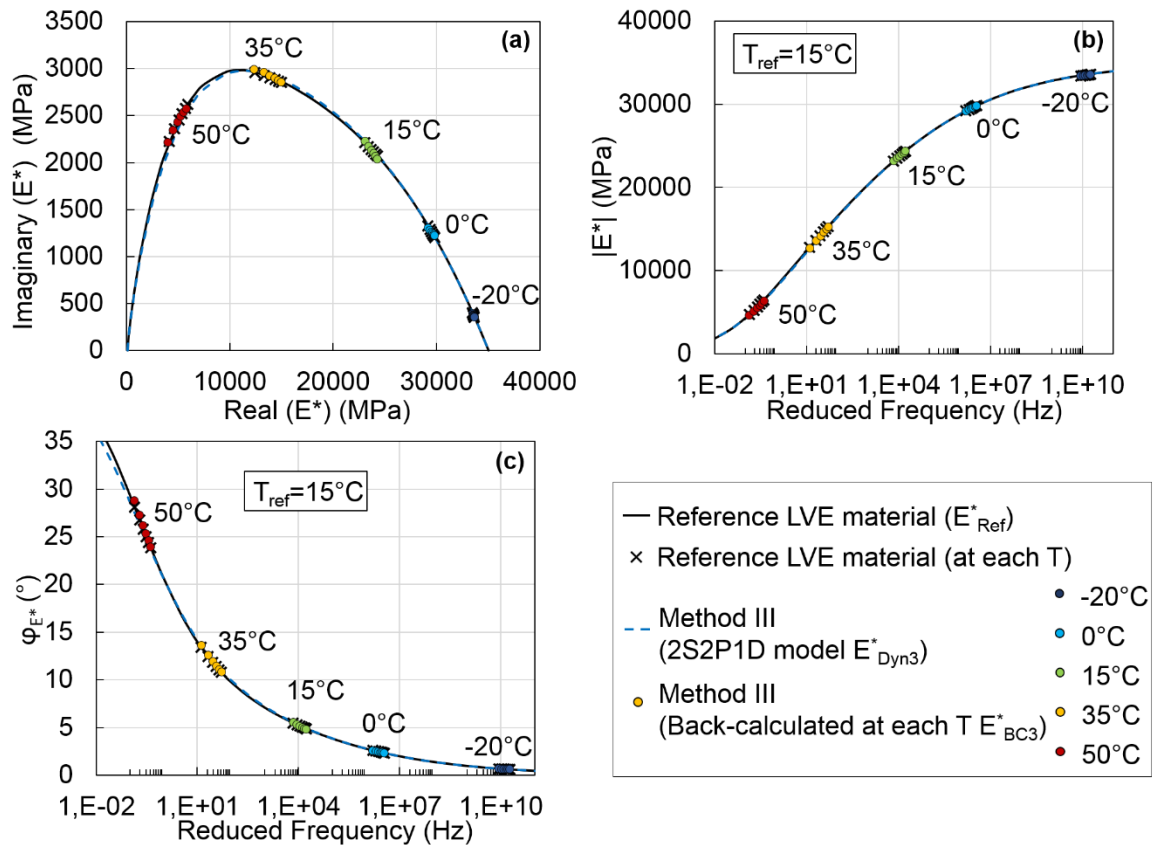


Figure F.5. Comparison of the values of the complex modulus determined with method III (E_{BC3}^* and E_{Dyn3}^*) with the values of the complex modulus of the reference LVE material (E_{Ref}^*). (a) Cole-Cole plot; (b) and (c) master curves of the norm and of the phase angle of the complex modulus at 15°C. Results for the flexural mode of the disc.

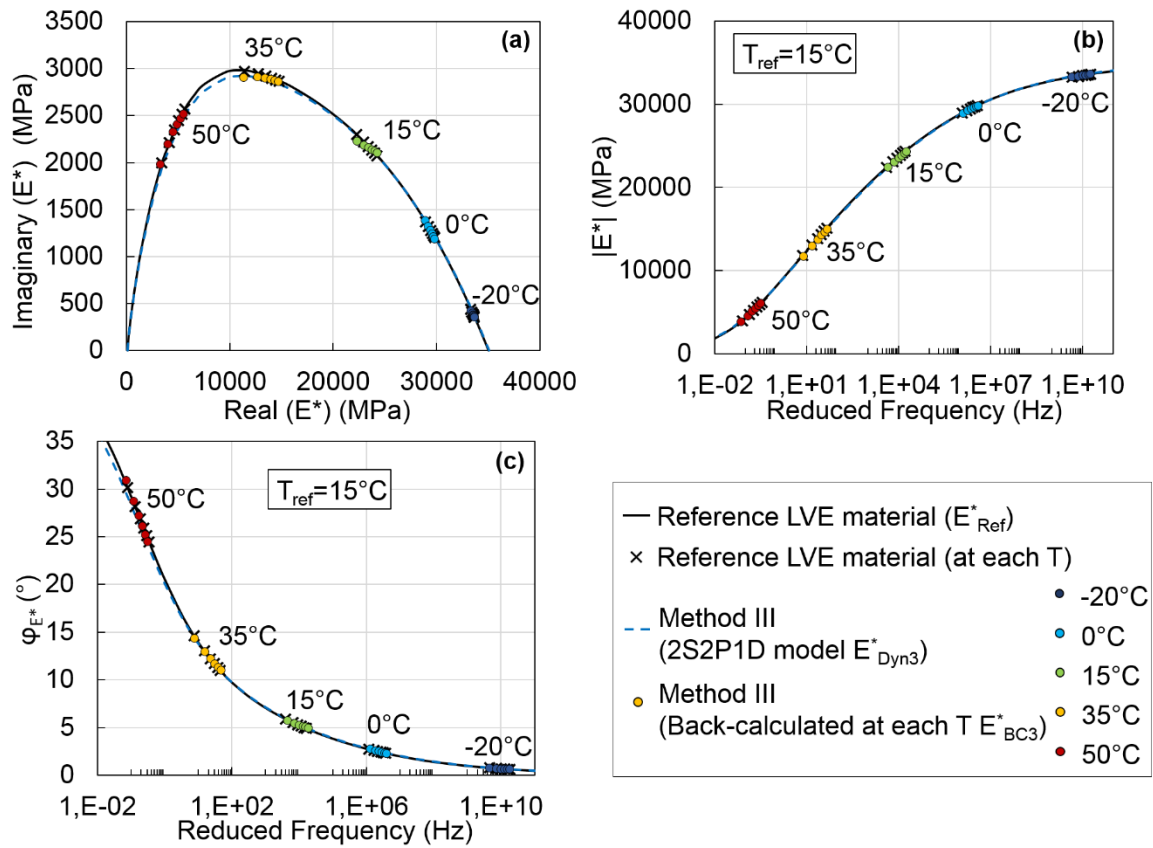


Figure F.6. Comparison of the values of the complex modulus determined with methods III (E^*_{BC3} and E^*_{Dyn3}) and IV (E^*_{BC4} and E^*_{Dyn4}) with the values of the complex modulus of the reference LVE material (E^*_{Ref}). (a) Cole-Cole plot; (b) and (c) master curves of the norm and of the phase angle of the complex modulus at 15°C. Results for the longitudinal mode of the straight beam.

**APPENDIX G - RESULTS OF METHOD IV FOR
THE REFERENCE LVE MATERIAL**

FINAL VALUES OF THE CONSTANTS OPTIMIZED AT EACH TEMPERATURE

*Table G.1. First resonance frequency and values of $|E^*_{BC4}|$ and φ_{E^*BC4} determined in the first step of method IV for the longitudinal mode of the cylinder.*

Temperature (°C)	1 st resonance frequency (Hz)	$ E^*_{BC4} $ (MPa)	φ_{E^*BC4} (°)
-20	11 620	33 900	0.68
0	10 880	29 750	2.6
15	9 740	23 800	5.4
35	7 360	13 500	12.7
50	4 880	5 720	25.9

*Table G.2. First resonance frequency and values of $|E^*_{BC4}|$ and φ_{E^*BC4} determined in the first step of method IV for the longitudinal and flexural modes of the cylinder.*

Temperature (°C)	1 st resonance frequency (Hz)	$ E^*_{BC4} $ (MPa)	φ_{E^*BC4} (°)
-20	6 380	33 700	0.72
0	5 940	29 150	2.7
15	5 280	22 750	5.7
35	3 760	11 800	13.8
50	2 280	3 950	26.0

*Table G.3. First resonance frequency and values of $|E^*_{BC4}|$ and φ_{E^*BC4} determined in the first step of method IV for the flexural mode of the disc.*

Temperature (°C)	1 st resonance frequency (Hz)	$ E^*_{BC4} $ (MPa)	φ_{E^*BC4} (°)
-20	9 280	35 960	0.74
0	8 600	31 050	2.8
15	7 660	24 250	5.8
35	5 580	13 000	13.9
50	3 620	5 000	28.0

*Table G.4. First resonance frequency and values of $|E^*_{BC4}|$ and φ_{E^*BC4} determined in the first step of method IV for the longitudinal mode of the straight beam.*

Temperature (°C)	1 st resonance frequency (Hz)	$ E^*_{BC4} $ (MPa)	φ_{E^*BC4} (°)
-20	6 220	33 460	0.74
0	5 800	29 000	2.8
15	5 160	22 800	5.7
35	3 800	12 300	14.1
50	2 280	4 550	28.6

FREQUENCY RESPONSE FUNCTIONS RESULTS

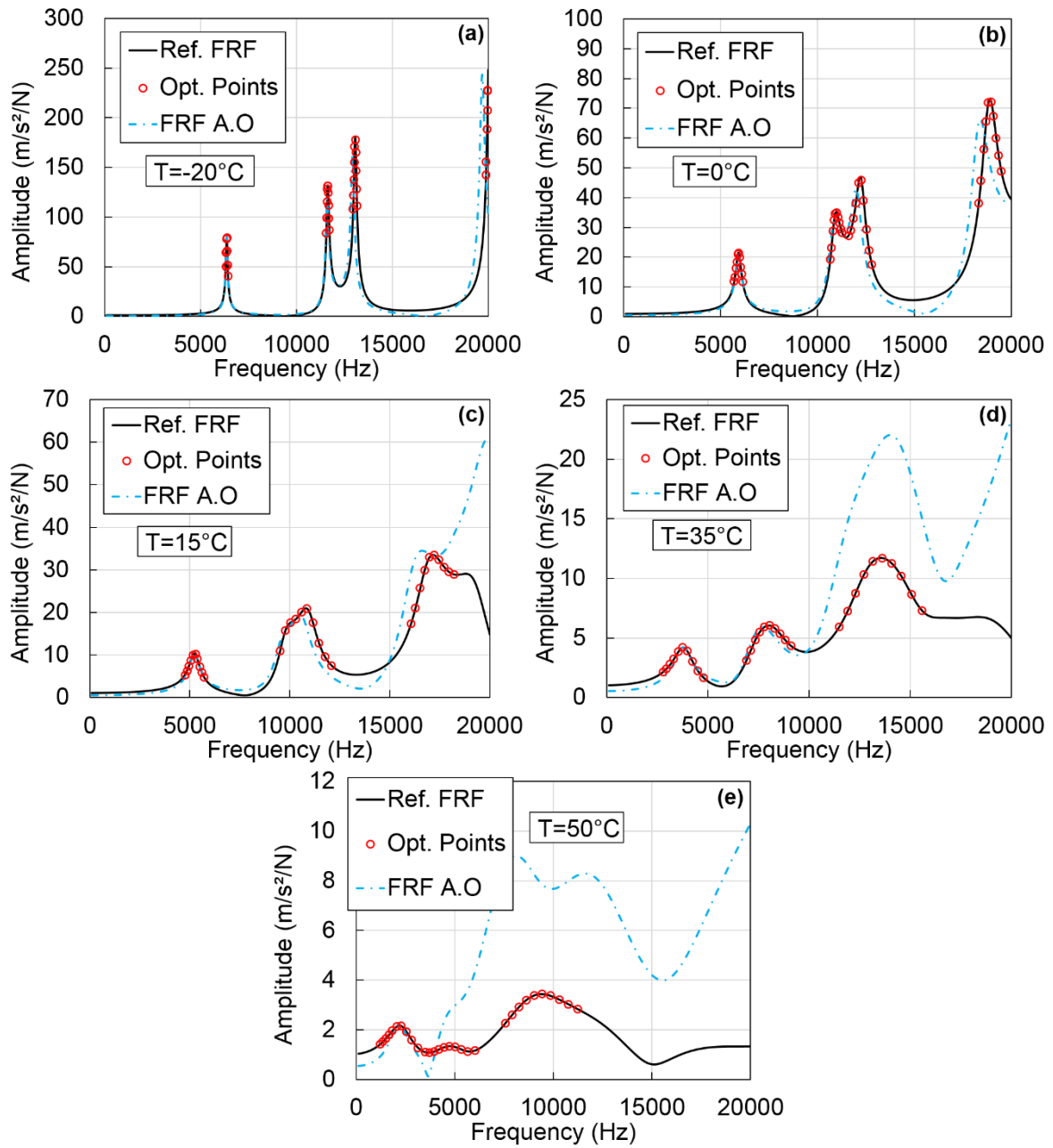


Figure G.1. Comparison of the reference FRFs (noted Ref. FRF) with the FRFs after optimization (noted FRF A.O) for method IV. Values of the reference FRFs at the frequencies where the optimization is performed (noted Opt. Points) are also plotted. Longitudinal and flexural modes of the cylinder at: (a) -20°C; (b) 0°C; (c) 15°C; (d) 35°C; (e) 50°C.

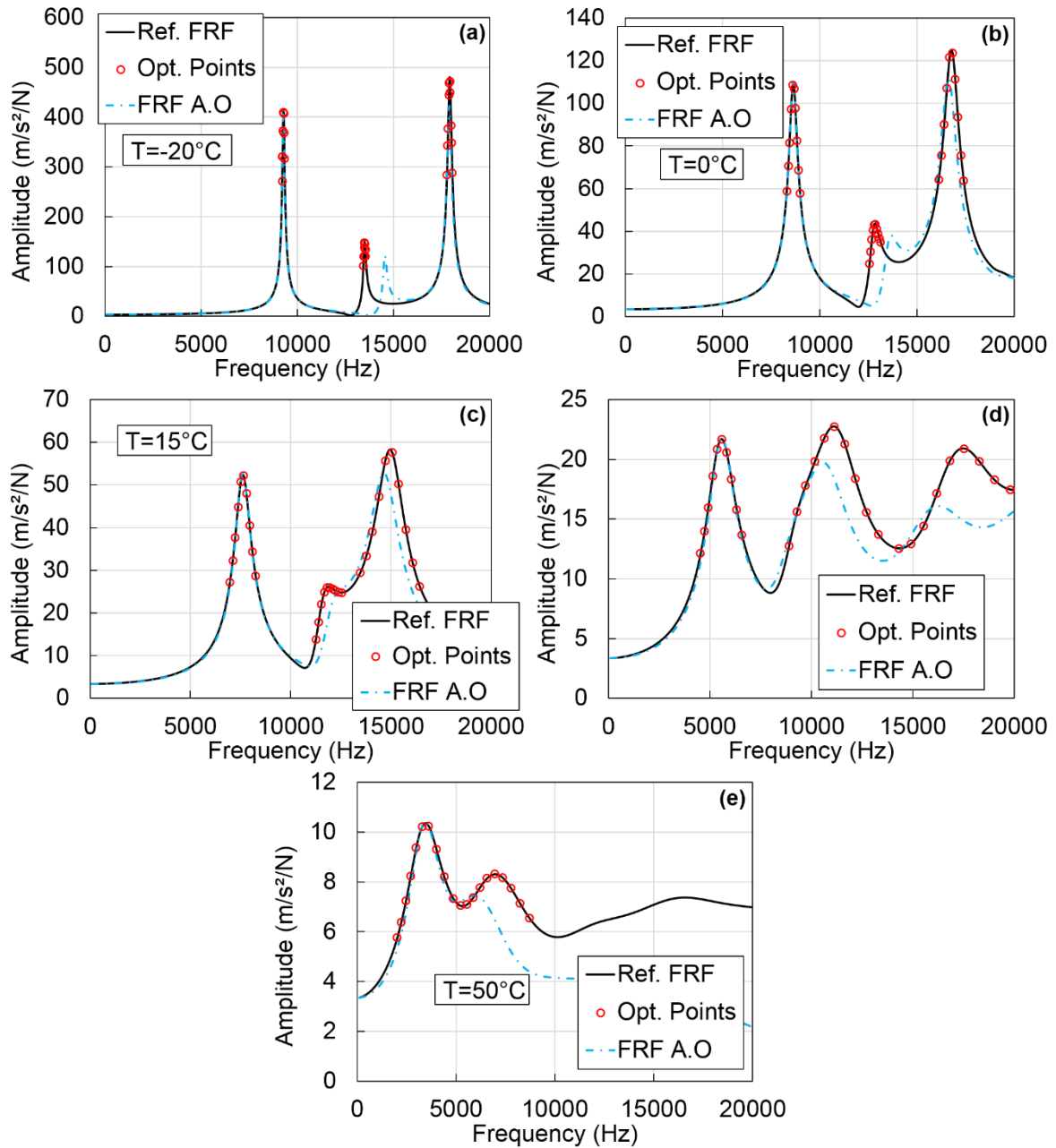


Figure G.2. Comparison of the reference FRFs (noted Ref. FRF) with the FRFs after optimization (noted FRF A.O) for method IV. Values of the reference FRFs at the frequencies where the optimization is performed (noted Opt. Points) are also plotted. Flexural mode of the disc at: (a) -20°C ; (b) 0°C ; (c) 15°C ; (d) 35°C ; (e) 50°C .

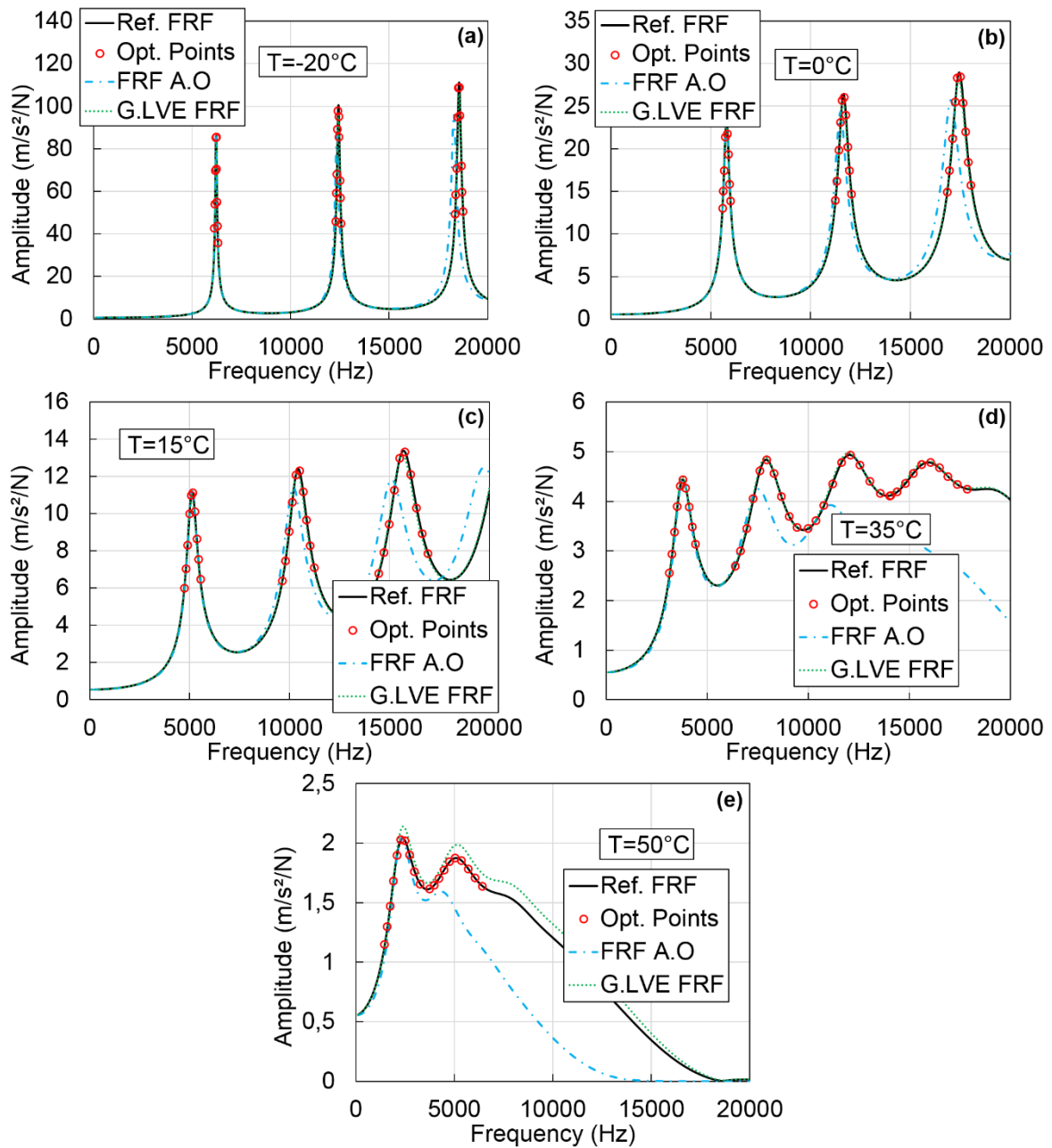


Figure G.3. Comparison of the reference FRFs (noted Ref. FRF) with the FRFs after optimization (noted FRF A.O) and the global LVE FRFs (noted G.LVE FRF) for method IV. Values of the reference FRFs at the frequencies where the optimization is performed (noted Opt. Points) are also plotted. Longitudinal mode of the straight beam at: (a) -20°C ; (b) 0°C ; (c) 15°C ; (d) 35°C ; (e) 50°C .

COMPLEX MODULUS RESULTS

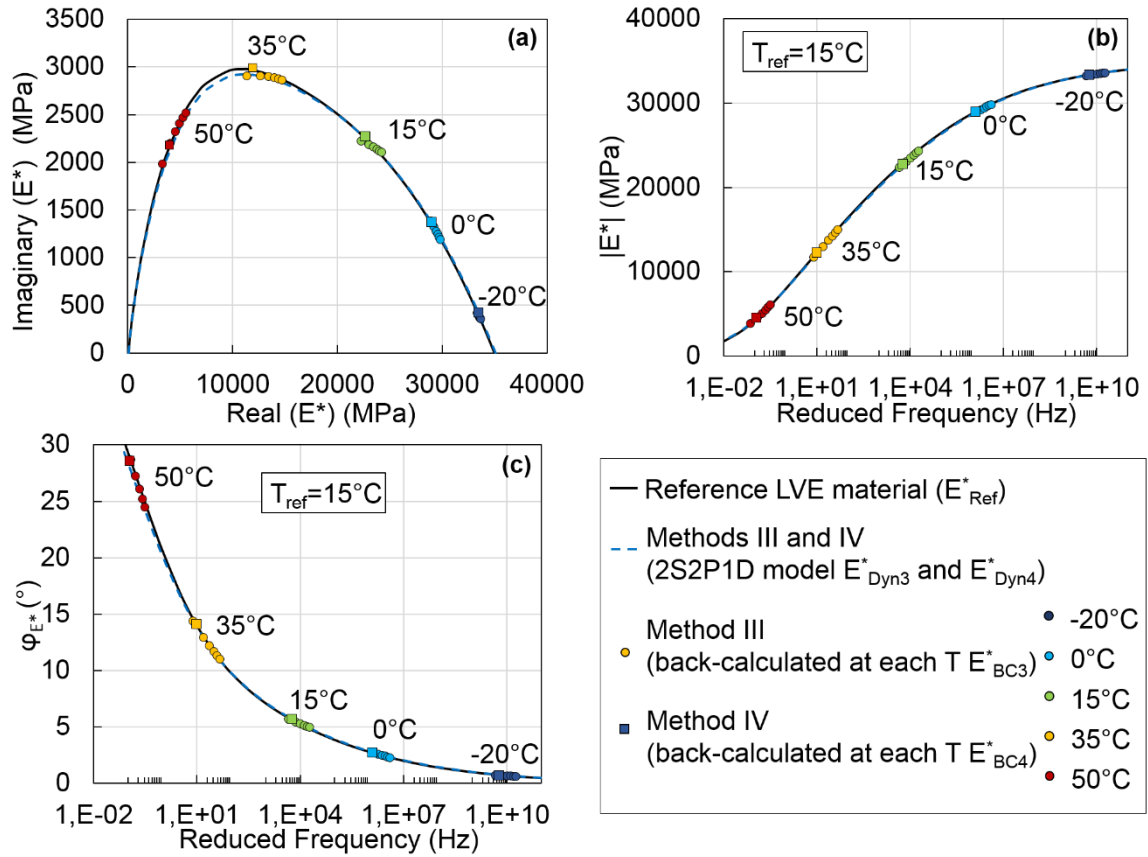


Figure G.4. Comparison of the values of the complex modulus of the reference LVE material with the values of the complex modulus back-calculated at each temperature (step 1) and the values of the complex modulus simulating the global LVE behaviour (step 2) for the third and fourth methods. Longitudinal mode of the straight beam: (a) Cole-Cole plot; (b) and (c) master curves of the norm and of the phase angle of the complex modulus at 15°C.

**APPENDIX H - RESULTS OF METHOD V FOR
THE REFERENCE LVE MATERIAL**

FINAL VALUES OF THE CONSTANTS OPTIMIZED AT EACH TEMPERATURE

Table H.1. Final values of the four constants E_0 , $\tau_{E15^\circ\text{C}}$, k and δ of the 2S2P1D model and of the Poisson's ratio ν that are identified at each temperature in the first step of the method V for the longitudinal mode of the cylinder.

Temperature (°C)	E_0 (MPa)	$\tau_{E15^\circ\text{C}}$ (s)	k	δ	ν
-20	35 171	0.342	0.153	1.95	0.195
0	36 351	0.124	0.144	1.89	0.213
15	33 728	0.187	0.188	2.54	0.247
35	38 505	0.108	0.171	2.60	0.311
50	39 102	0.101	0.200	2.54	0.363

Table H.2. Final values of the four constants E_0 , $\tau_{E15^\circ\text{C}}$, k and δ of the 2S2P1D model and of the Poisson's ratio ν that are identified at each temperature in the first step of the method V for the longitudinal mode of the straight beam.

Temperature (°C)	E_0 (MPa)	$\tau_{E15^\circ\text{C}}$ (s)	k	δ	ν
-20	35 313	2.337	0.144	2.25	0.195
0	34 334	0.077	0.190	2.42	0.213
15	39 418	0.132	0.141	2.41	0.241
35	40 493	0.068	0.152	2.43	0.308
50	32 531	0.103	0.149	1.95	0.366

FREQUENCY RESPONSE FUNCTIONS RESULTS

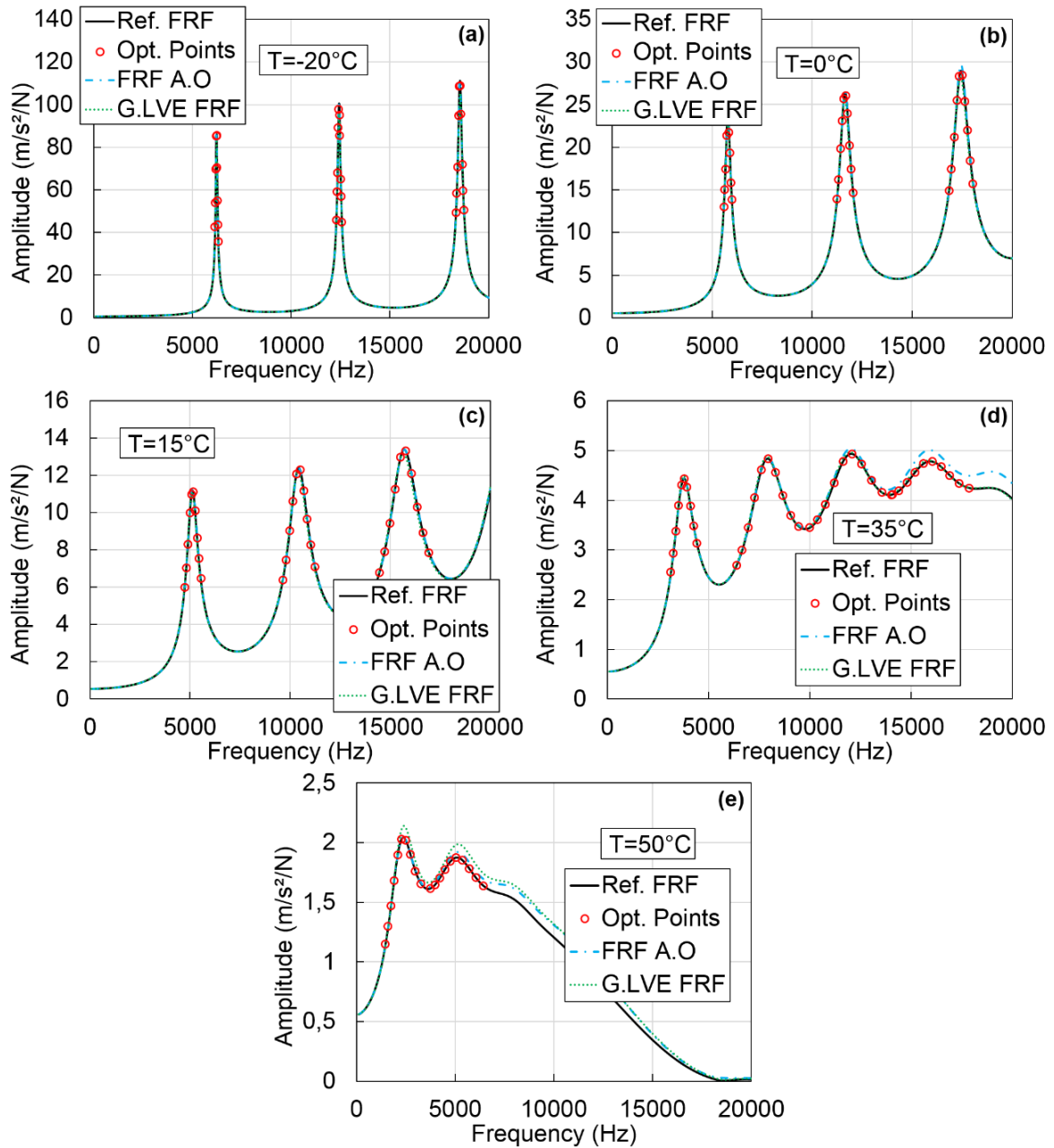


Figure H.1. Comparison of the reference FRFs (noted Ref. FRF) with the FRFs after optimization (noted FRF A.O) for method V. Values of the reference FRFs at the frequencies where the optimization is performed (noted Opt. Points) are also plotted. Longitudinal mode of the straight beam at: (a) -20°C ; (b) 0°C ; (c) 15°C ; (d) 35°C ; (e) 50°C .

COMPLEX MODULUS RESULTS

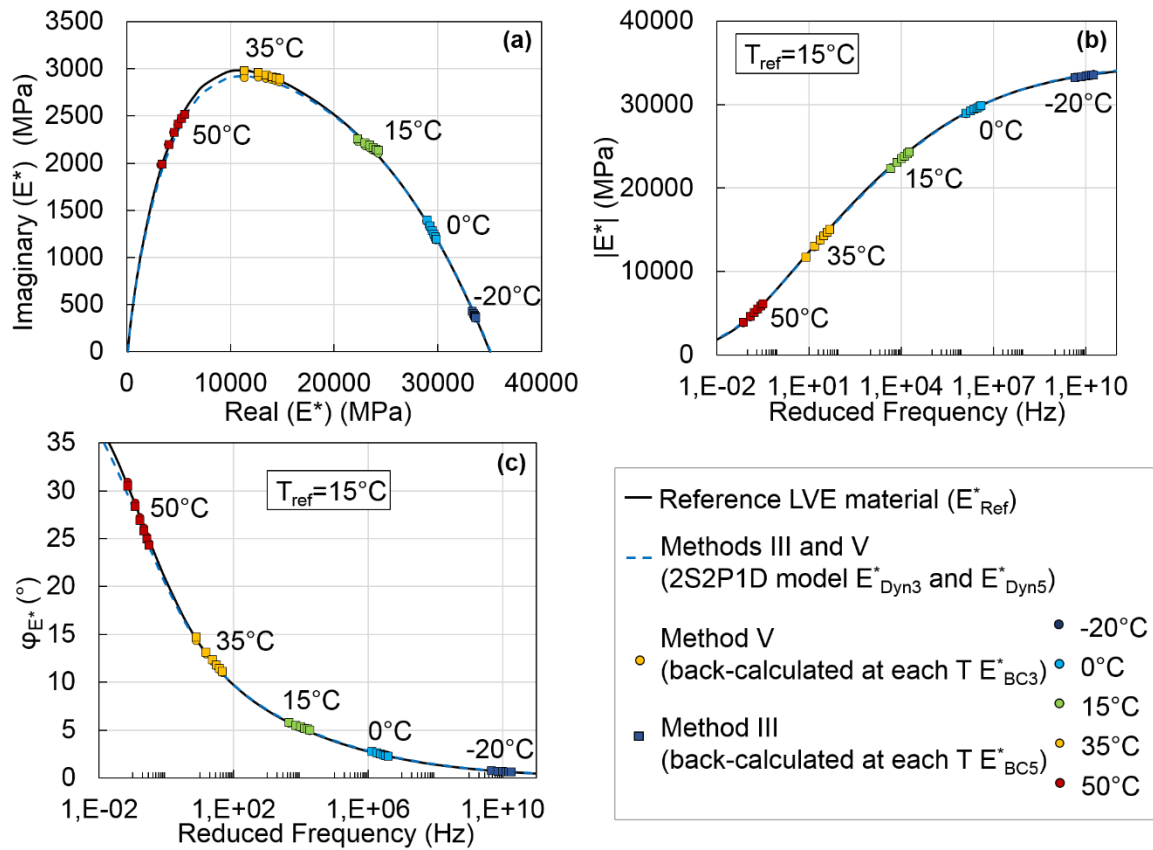


Figure H.2. Comparison of the values of the complex modulus determined with methods III (E_{BC3}^* and E_{Dyn3}^*) and V (E_{BC5}^* and E_{Dyn5}^*) with the values of the complex modulus of the reference LVE material (E_{Ref}^*). (a) Cole-Cole plot; (b) and (c) master curves of the norm and of the phase angle of the complex modulus at 15°C. Results for the longitudinal mode of the straight beam.

COMPLEX POISSON'S RATIO RESULTS

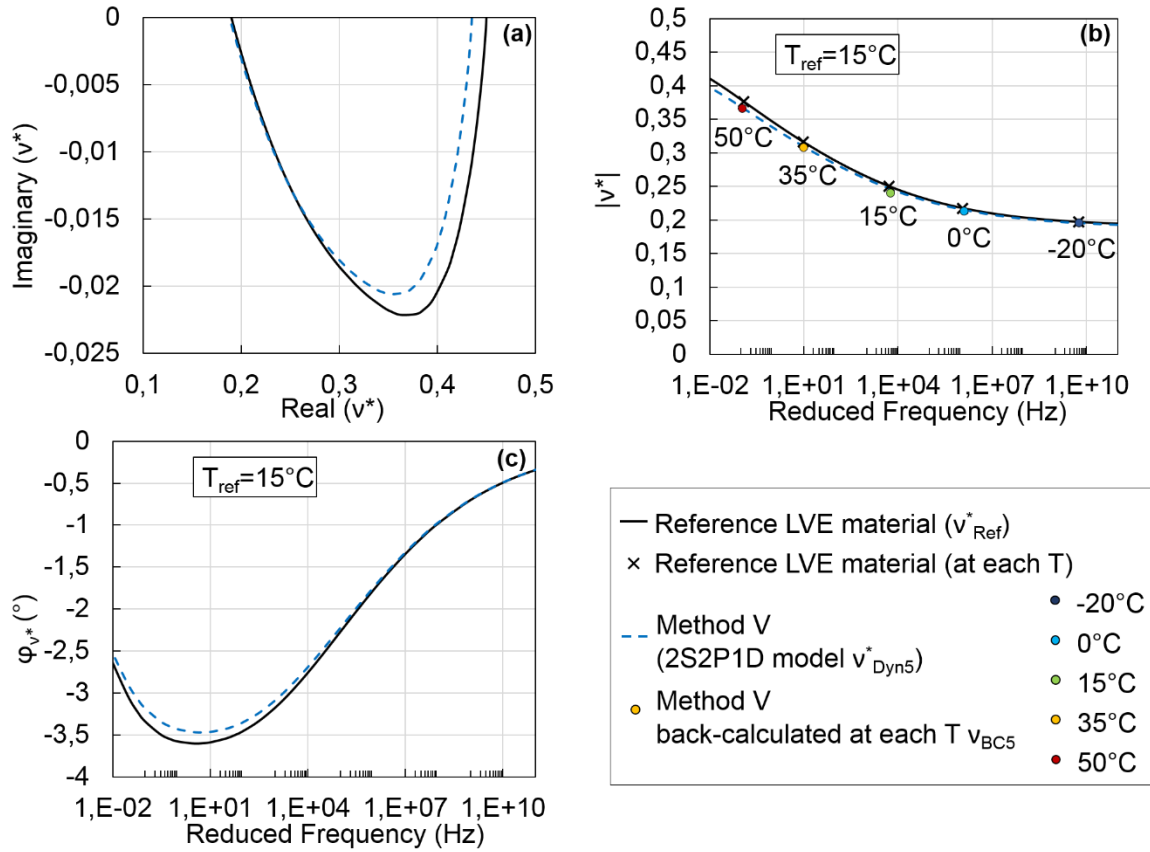


Figure H.3. Comparison of the values of the complex Poisson's ratio determined with methods V (real values v_{BC5} and v_{Dyn5}^*) with the values of the complex Poisson's ratio of the reference LVE material (v_{Ref}^*). (a) Cole-Cole plot; (b) and (c) master curves of the norm and of the phase angle of the complex modulus at 15°C . Results for the longitudinal mode of the straight beam.

**APPENDIX I - DETAILS OF THE MATERIALS
TESTED IN THE EXPERIMENTAL CAMPAIGNS**

DETAILS AND GRADING CURVE OF THE SWEDISH BASE COURSE MIXTURE (ABS MATERIAL)

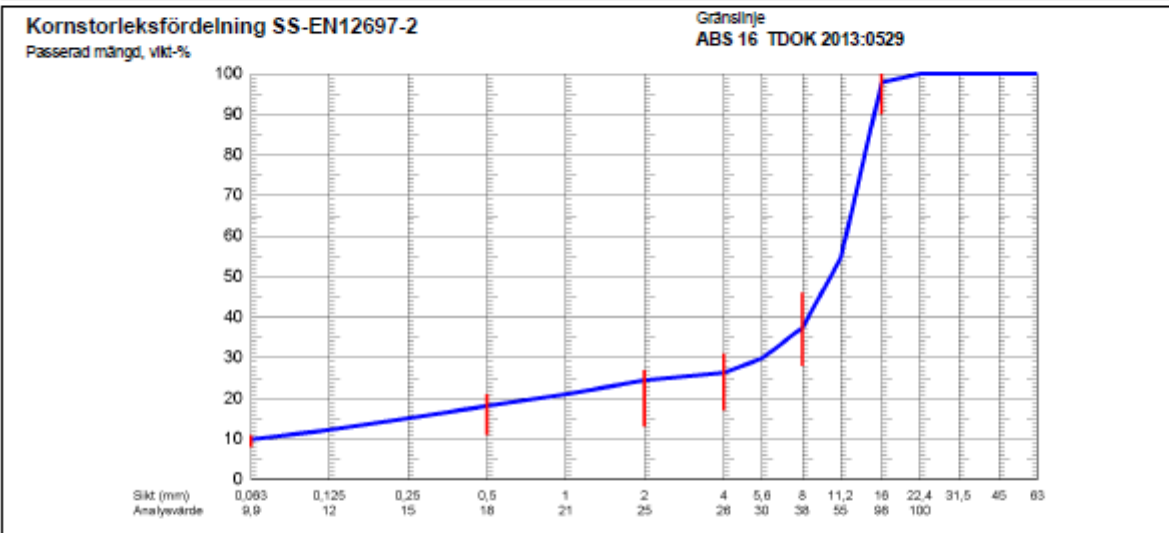


RAPPORT
utfärdat av ackrediterat provningslaboratorium
TEST REPORT issued by an Accredited Testing Laboratory
Provnr **170917**

LEVERANSKONTROLL Beläggingsmassa

Sidan 1 av 1

Beställare PEAB Asfalt AB	Provtagningsdatum 2017-06-14	Analys start 2017-06-15
Ångkraftv. 8A 721 30 Västerås	Ankomstdatum 2017-06-15	Analys slut 2017-06-15
Produkt ABS 16 70/100	Referens nr	Id-nummer
Leverantör Peab Asfalt AB, Västberga	Provtagningsplats Kl. 23:35	
Entreprenör PEAB Asfalt AB	Provtagare	
Objekt Stockholm ytterstad	Märkning Bergslagsvägen	



Sikt (mm)	0,063	0,5	2	4	5,6	8	11,2	16	22,4	31,5	Bindem.halt
Arbetsrecept 616 - 6	9,5	16	20	24		37		95			6,1
Analysvärde	9,9	18	25	26		38		96			6,1
Avvikelse	0,4	2	5	2		1		3			0,0

Provresultat	Medel-värde	Recept +/-	Notering
SS-EN 12697-1/ SS-EN 12697-2 Lösligt bindemedelshalt (%)	6,1	6,1	Ort och datum Stockholm 2017-06-15 <i>Åsa Wahlberg</i> Åsa Wahlberg Digitalt utfärdad signatur
Massans temperatur vid tillverkning (°C)	164		

Provresultatet avser endast till laboratoriet inkommet prov.
(E) = Enkelprov (EA) = Ej ackrediterad metod. Denna rapport får endast återges i sin helhet.
Kundbilaga finns på <http://www.peabasfalt.se/produkter-och-tjanster/provnings-tjanster-asfalt/>

PEAB Asfalt AB Väglaboratoriet Västberga Box 42202 126 17 Stockholm	Besöksadress Drivhjuls v.11, Hägersten Styrelsens säte Båstad	Telefon nr 0733-848344 Telefax nr 08-709 78 49	Org.nr 556098-8122 VAT nr 556098812201	E-post för.ettermann@peabasfalt.se Internet adress www.peabasfalt.se
--	--	---	---	---

DETAILS AND GRADING CURVE OF THE MATERIAL WITH AN OPTIMIZED GRANULAR SKELETON (GB5 MATERIAL)

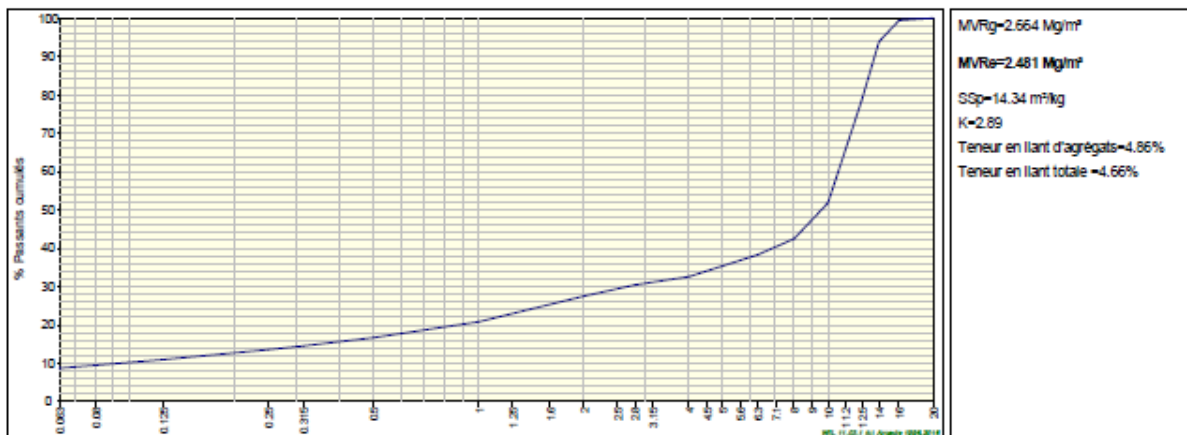
EIFPAGE RECOMPOSITION ENROBE Page 1/1

Branch Infrastructures - Laboratoire Central
5 rue du Dauphiné - CS 74305 - 69944 Colson - France

Produit : GB5 0/14 LA GARUSTIERE/BEUCAIRE - 30% Agrégats **Client :** STR Eiffage Route MEDITERRANEE
Type : Grave bitume **4, rue de Copenhague BP 70027**
Origine : Laboratoire **13741 VITROLLES Cedex**
Nom commercial : GB5
Granularité : 0/14
Désignation : EB 14 assise Biprène 41
Code : Code : EN o17-095

Dossier LA_CO-17-0113 : GB5 0/14 LA GARUSTIERE / BEUCAIRE - 30% Agrégats - Biprène 41
Demandeur : Philippe LAGARDE

Produit	Producteur	Nature	% intérieur
Gravillon 10/14 (pr n° LA_CO B7040308)	Carrière La Garustière	Calcaire	53.00
Sable 0/2 (pr n° LA_CO B7040309)	Carrière GSM Beaucaire	Silico-calcaire	10.00
Filler (pr n° LA_CO B6080206)	Carrière Châteauneuf-lès-Martigues	Calcaire	3.80
Agrégat d'enrobé 0/10 (pr n° LA_CO B7040310)	Poste BITUMIX	Concassé	30.00
Biprène 41 (pr n° LA_CO B6031408)	Usine ALE - Collonges	Bitume modifié	3.20



Constituants granulométriques																	
	0.063	0.125	0.25	0.315	0.5	1	2	2.8	4	5	6.3	8	10	12.5	14	16	20
Gravillon 10/14 CA_GARUST	1.7	2	3	3	3	3	3	3	3	3	3	4	16	62	89	99	100
Sable 0/2 CA_GSMBEAU	14.0	20	30	33	42	59	91	100	100	100	100	100	100	100	100	100	100
Filler CA_CLMARTI	83.0	94	98	99	100	100	100	100	100	100	100	100	100	100	100	100	100
Agrégat d'enrobé 0/10 PO_BITUMIX	9.9	13	17	19	22	30	41	48	55	64	74	86	95	99	100	100	100

Reconstitution granulométrique																	
Tamis	0.063	0.125	0.25	0.315	0.5	1	2	2.8	4	5	6.3	8	10	12.5	14	16	20
% Passants	8.7	11	14	14	17	21	27	30	33	35	38	42	52	79	94	99	100

Observations
Analyses granulométriques fournies par le demandeur

L'adjoint, Franck DESVIGNES

 DESVIGNES Franck
2017.05.22
14:18:16 +02'00'

GRADING CURVE AND FABRICATION PROCESS OF THE MATERIAL WITH HIGH RECLAIMED ASPHALT CONTENT (WF MATERIAL)

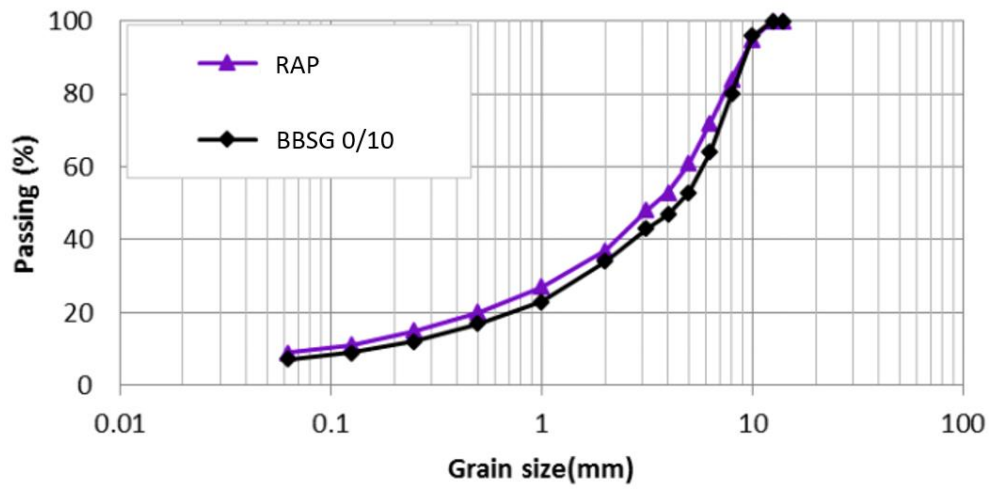


Figure I.1. Grading curves of the original mixture (BBSG 0/10) and of the RAP aggregates incorporated in the WF material.

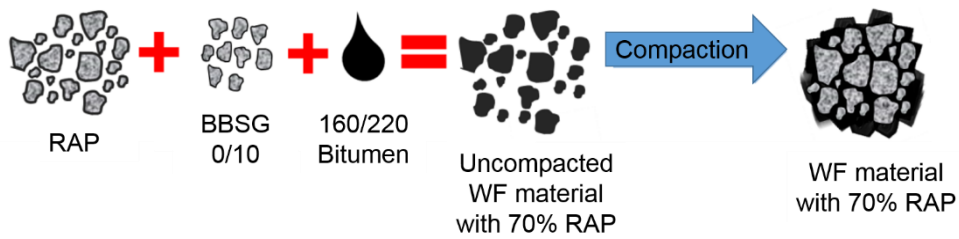


Figure I.2. In-laboratory fabrication process of the WF material from the RAP, the original mixture (BBSG 0/10) and the 160/220 bitumen.

DETAILS AND GRADING CURVE OF THE MATERIALS FROM AIRPORT PAVEMENT (GB AND BB MATERIALS)

Société Parisienne de Matériaux Enrobés

Laboratoire
7 route de l'île saint Julien
94388 Bonneuil / Marne cedex
☎ 01.43.39.24.48
☎ 01.43.99.05.12

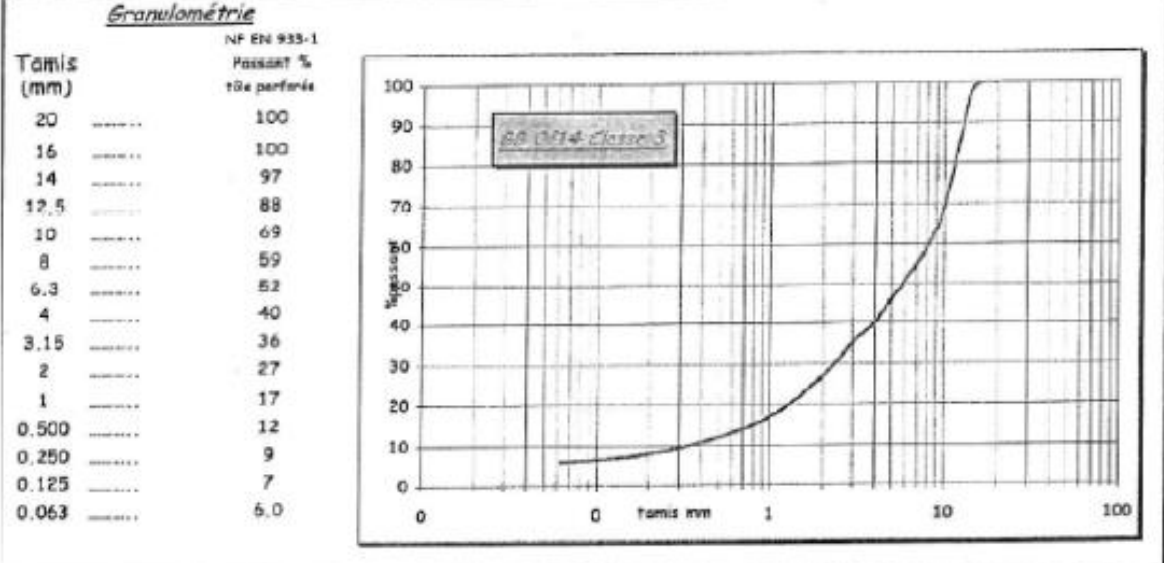
Centrale S.P.M.E Bonneuil
7 route de l'île saint Julien
94388 Bonneuil / Marne cedex
☎ 01.43.39.24.48
☎ 01.43.99.05.12

Fiche produit

Grave Bitume 0/14 Classe 3

GB 0/14 Classe 3 *Code : A064* *Norme : NF P 98-138*

Catégorie des Granulats	C III a		Composition Granulaire		
Massa Volumique Réelle des granulats	2.696		10/14	Calcaire dur CCM Wallers	35.0%
Module de Richesse de l'enrobé	2.9	> 2.8	6/10	Calcaire dur CCM Wallers	15.0%
Massa Volumique réelle de l'enrobé	2.512		4/6	Calcaire dur CCM Wallers	11.0%
Conformément à la circulaire ministérielle du 03/10/2006 SPME, se réserve le droit, sous réserve de disponibilité, d'incorporer 10% d'agrégats d'enrobés dans ce produit. Les caractéristiques techniques du produit sont maintenues.			0/4	Calcaire dur CCM Wallers	39.0%
			Bitume 35/50		4.50 PCE 4.31%



Recommandations d'utilisation selon la norme NF P 98-138

Domaine d'utilisation : → Couche de base ou de fondation

Application d'une couche d'accrochage : → 250g au moins de bitume résiduel au m².

Épaisseur moyenne d'utilisation : → 8 à 14 cm

Quantité : → Environ 24 kg au m² par centimètre d'épaisseur.

Température de fabrication : → 165 °C (+/- 10 °C)

Température minimale d'application : → 130 °C

Caractéristiques mécaniques au éco

APPENDIX I – DETAILS OF THE MATERIALS TESTED IN THE EXPERIMENTAL CAMPAIGNS

Grave Bitume 0/14 Classe 3

GB 0/14 Classe 3 Code : **A064**

Caractéristiques DURIEZ (NF P 98-251-1)

M. V. R de l'enrobé :	2.512	Résistance à sec R (Mpa)	9.5
M. V. A hydrostatique :	2.318	Résistance avec Invers. r (Mpa)	7.5
% Compacité :	92.3	Rapport r/R	0.79 ±0.70
% de vides :	7.7	% eau absorbée	3.2

Caractéristiques P.C.G (NF P 98-252)

Nombre de girations	5	15	25	40	60	100	120	200
% de vides moyen	21.5	16.5	14.1	12.0	10.2	8.0	7.3	5.4

Résultats	Spécifications
% de vides à 10 girations :	18.4%
% de vides à 100 girations :	8.0%
% de vides à 200 girations :	5.4%

Pente K :	4.27
% vides à C1 :	27.8%
Coef. cor. :	1.000
Régression à :	

Essai d'orniérage (NF P 98-253-1)

Nombre de cycles	Profondeur d'ornière en %	Spécifications
100	1.4	
300	1.7	
1000	2.3	
3000	2.8	
10000	3.5	< 10%
30000		

Epaisseur 100mm	% vides art essai	T°C essai	Nb jours avt. Essai
Moyenne	9.5%	50	

A = 2.31 (ornière à 1000 cycles)
b = 0.180 (pente de la droite)

Module de rigidité (NF EN 12697-26)

Appareillage d'essai	Pots vibrants	Spécifications
MV moyens des éprouvettes (kg/m ³) NF EN 12697-6/24	3 278	
Teneur moyenne des vides (%) NF EN 12697-6	9.6	
Température (°C)	15	
Fréquence (Hz)	10	
Déformation epsilon (µD)	50	
Module de rigidité E* (Mpa)	10 520	> 9000 Mpa

Date de l'étude de la présente formulation : Juillet 2007 par le Laboratoire SCRS IdF N

Document rédigé par
Bernard FILLEUL

Validé par le directeur d'exploitation
Jean-Denis PIERRE




APPENDIX I – DETAILS OF THE MATERIALS TESTED IN THE EXPERIMENTAL CAMPAIGNS

ENROBES 77
 Les Courceaux
 Montereau sur le Jard
 77950 MAINCY
 Tél. : 01.64.38.85.01
 Fax : 01.64.38.81.23

FICHE PRODUIT
BBA 0/10 - D (4/6)
Classe 3

Béton Bitumineux Aéronautique
BBA 0/10 - D classe 3
 Selon NF P 98-131 (nov. 1999)
 Date étude : mai 2006
 Laboratoire : CST - Eurobés 2

Bitume pur 35/50

Couches de surface
Roulement

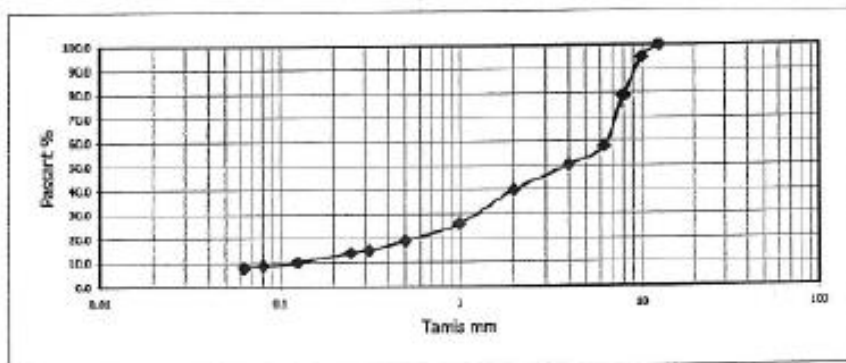
Couche d'accrochage (norme)
>= 250 g / m² bit. résiduel

<i>Epaisseur (norme)</i>	<i>Minimum</i>	<i>Moyenne</i>
	3	4 à 5 cm

Formulation			Granulats : Diorite bleue - BIIa	
6/10	La Noubleau	50%	Caractéristiques de l'enrobé	
2/4	La Noubleau	10%	MVRg : 2.839	S : 13.938
0/2	La Noubleau	38.5%	MVR : 2.590	a : 0.933
Fines d'apport			1.5%	Bitume pur 35/50 : 5.80 ppe
			K = 3.68	Spécification >= 3.40

Courbe granulométrique du mélange - NF EN 933-1

Tamis (mm)	0.06	0.08	0.13	0.25	0.32	0.50	1	2	4	6.3	8	10	12.5				
Passants %	7.9	8.6	10	14	15	19	26	40	50	58	79	95	100				



Essai Duriez - LCPC à 18°C (NF P.98-251-1)						Spécif.
MVA hydro : 2.40		V% : 7.3	Rc air (Mpa) : 11.1	Rc eau (Mpa) : 10.3	r/R : 0.93	>= 0.80

Essai de compactage à la PCG (NF P.98-252)											
K	Girations	V1	V10	V25	V40	V60	V80	V100	V120	V150	V200
3.82	% vides	22.0	13.5	9.8	7.8	6.2	5.1	4.4	3.8	3.1	2.3
Spécifications		>=9		5-9							

Orniéage (NF P.98-253-1)			Spécifications		
Epaisseur dalle	mm	50	50		
Température	°C	60	60		
Vides	%	7.7	7.9	4 à 7	
Ornière	%	7.0	7.1	<= 7.5	
Nombre cycles		10000			

**APPENDIX J- RESULTS OF THE FSDYN
EXPERIMENTAL CAMPAIGN**

SPECIMEN ABS-D9

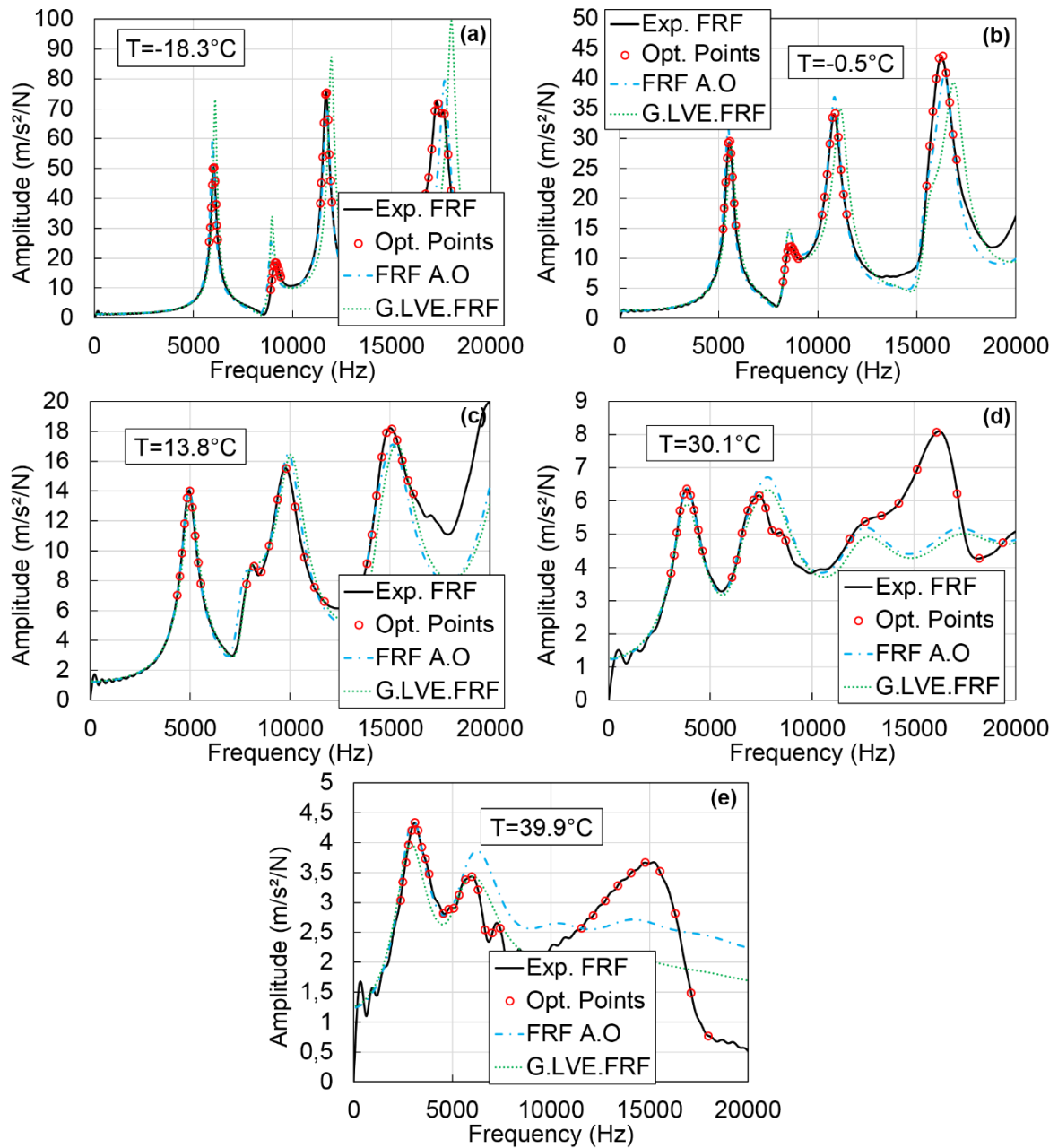


Figure J.1 Comparison of the experimental FRFs (noted Exp. FRF) with the FRFs after optimization (noted FRF A.O.) and the global LVE FRFs (noted G.LVE FRF) for specimen ABS-D9. Values of the experimental FRFs at the frequencies where the optimization is performed (noted Opt. Points) are also plotted. (a) $T = -18.3^{\circ}\text{C}$; (b) -0.5°C ; (c) 13.8°C ; (d) 30.1°C ; (e) 39.9°C .

Table J.1. Values of the four constants E_0 , $\tau_{E15^\circ\text{C}}$, k and δ of the 2S2P1D model determined from dynamic tests at each temperature in the first step of method III for specimen ABD-D9.

Temperature ($^\circ\text{C}$)	E_0 (MPa)	$\tau_{E15^\circ\text{C}}$ (s)	k	δ
-18.3	48 047	3.5E-05	0.106	1.12
-0.5	48 047	2.9E-04	0.106	1.12
13.8	41 763	1.1E-02	0.195	2.06
30.1	48 863	1.4E-02	0.193	1.98
39.9	49 942	2.4E-02	0.175	1.80

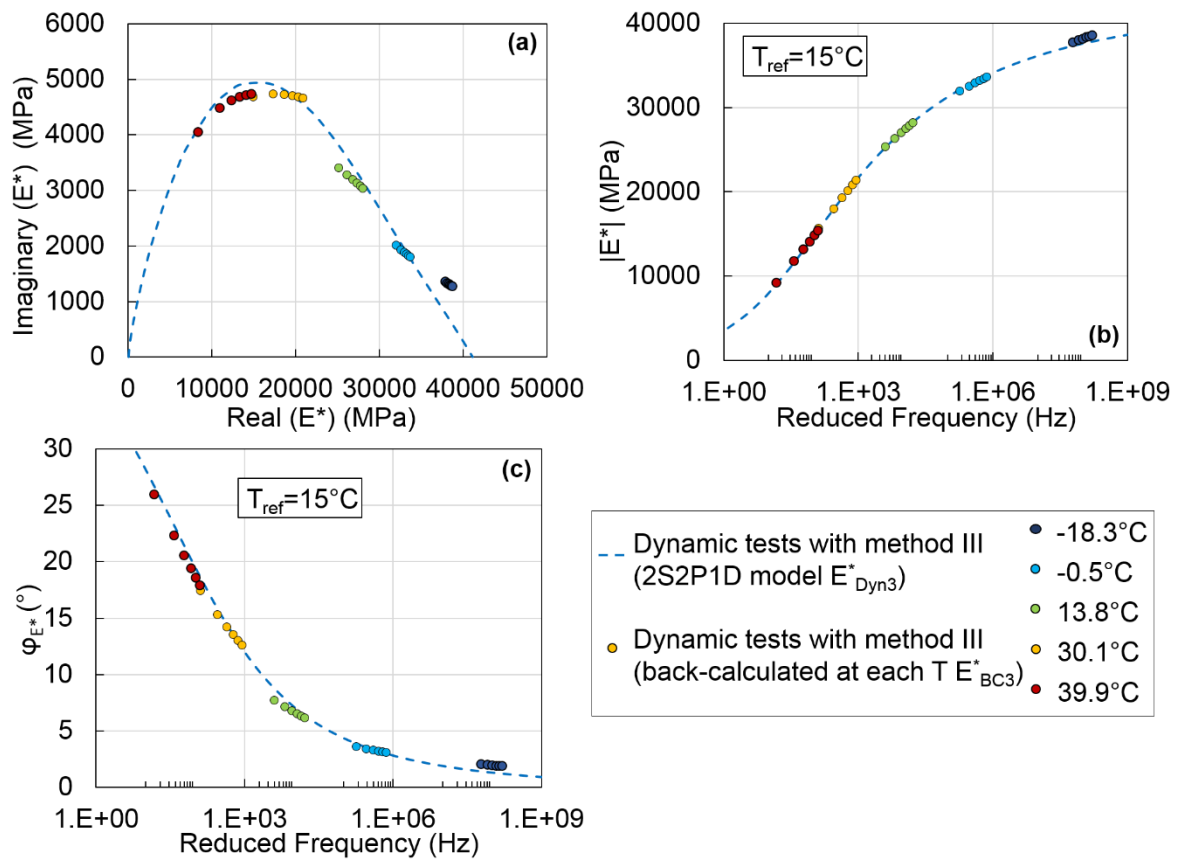


Figure J.2 Values of the complex modulus determined from dynamic tests with method III ($E_{\text{BC}3}^*$ and $E_{\text{Dyn}3}^*$). (a) Cole-Cole plot; (b) and (c) master curves of the norm and of the phase angle of the complex modulus at 15°C. Results for specimen ABS-D9.

SPECIMEN ABS-D10

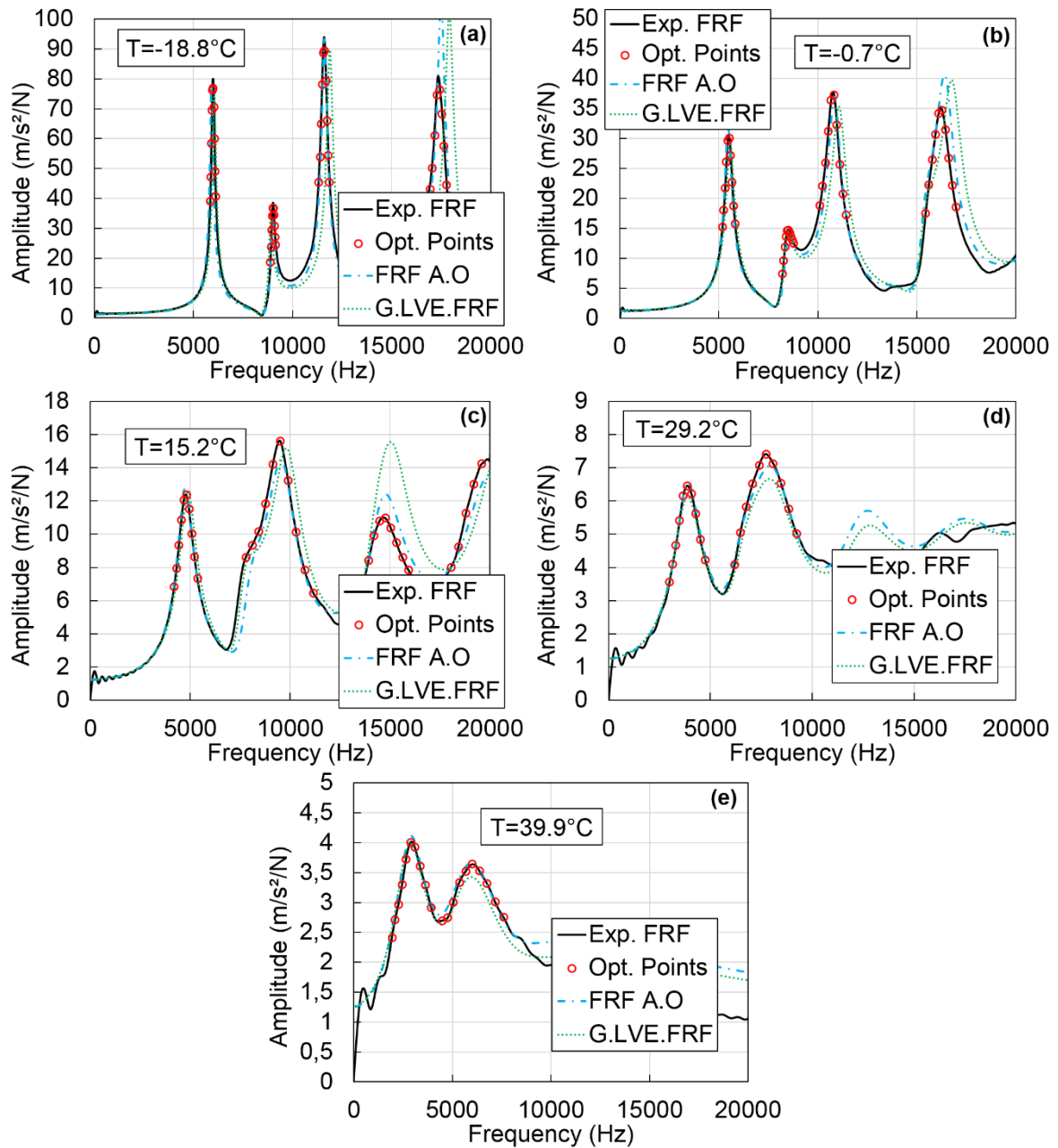


Figure J.3 Comparison of the experimental FRFs (noted Exp. FRF) with the FRFs after optimization (noted FRF A.O) and the global LVE FRFs (noted G.LVE FRF) for specimen ABS-D10. Values of the experimental FRFs at the frequencies where the optimization is performed (noted Opt. Points) are also plotted. (a) $T = -18.8^{\circ}\text{C}$; (b) -0.7°C ; (c) 15.2°C ; (d) 29.2°C ; (e) 39.9°C .

Table J.2. Values of the four constants E_0 , $\tau_{E15^\circ\text{C}}$, k and δ of the 2S2P1D model determined from dynamic tests at each temperature in the first step of method III for specimen ABD-D10.

Temperature ($^\circ\text{C}$)	E_0 (MPa)	$\tau_{E15^\circ\text{C}}$ (s)	k	δ
-18.8	40 620	3.5E-03	0.168	2.17
-0.7	41 609	2.2E-02	0.161	2.18
15.2	49 995	2.9E-03	0.159	1.81
29.2	47 904	1.1E-02	0.188	1.88
39.9	49 709	2.0E-02	0.193	1.82

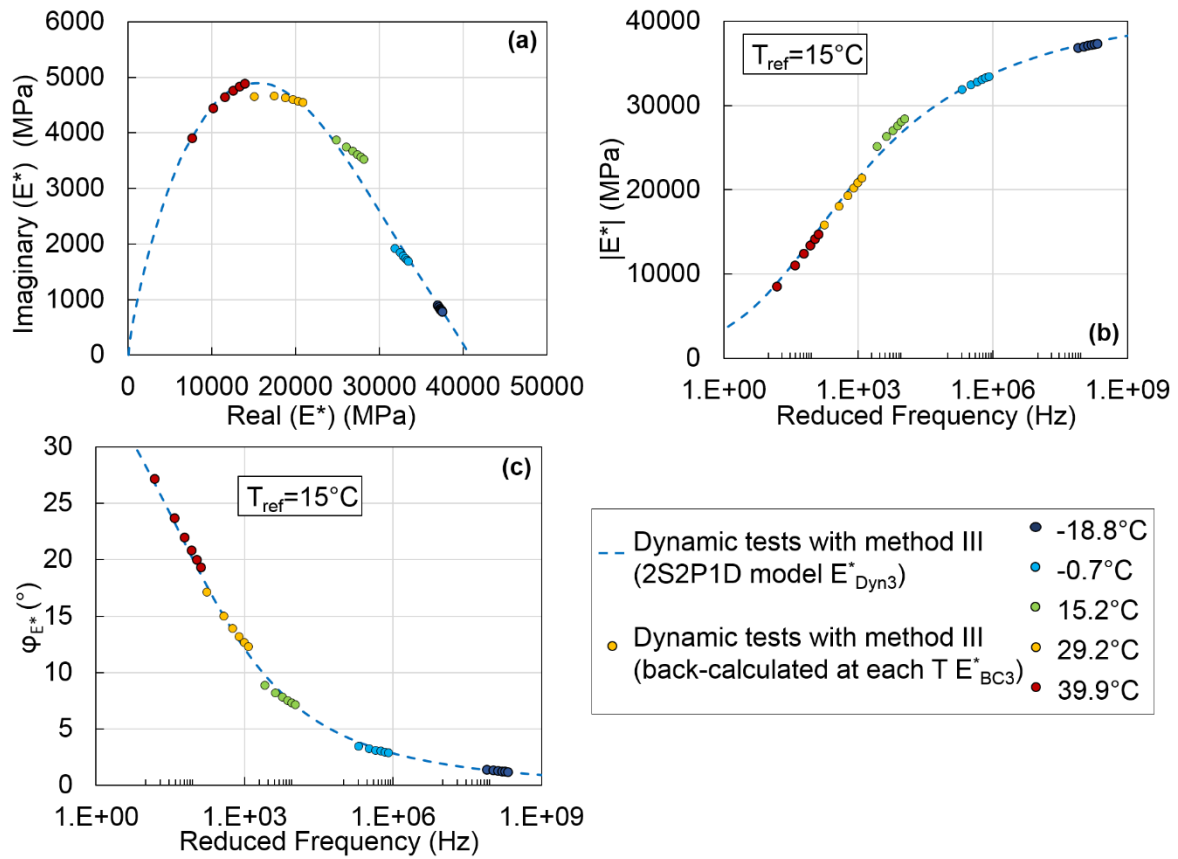


Figure J.4 Values of the complex modulus determined from dynamic tests with method III (E_{BC3}^* and E_{Dyn3}^*). (a) Cole-Cole plot; (b) and (c) master curves of the norm and of the phase angle of the complex modulus at 15°C . Results for specimen ABS-D10.

SPECIMEN GB5-D1

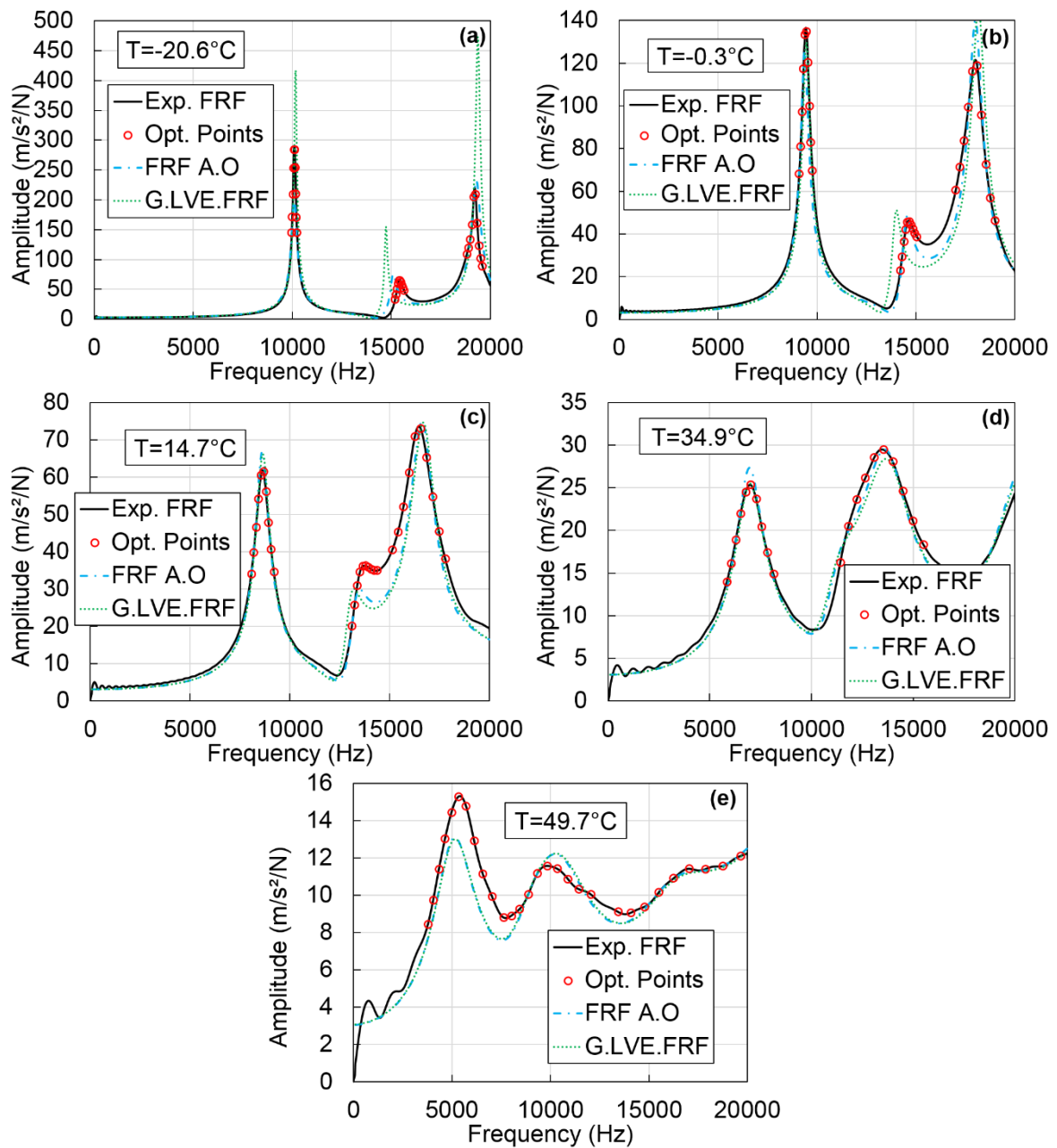


Figure J.5 Comparison of the experimental FRFs (noted Exp. FRF) with the FRFs after optimization (noted FRF A.O.) and the global LVE FRFs (noted G.LVE FRF) for specimen GB5-D1. Values of the experimental FRFs at the frequencies where the optimization is performed (noted Opt. Points) are also plotted. (a) $T = -20.6^{\circ}\text{C}$; (b) -0.3°C ; (c) 14.7°C ; (d) 34.9°C ; (e) 49.7°C .

Table J.3. Values of the four constants E_0 , $\tau_{E15^\circ\text{C}}$, k and δ of the 2S2P1D model determined from dynamic tests at each temperature in the first step of method III for specimen GB5-D1.

Temperature ($^\circ\text{C}$)	E_0 (MPa)	$\tau_{E15^\circ\text{C}}$ (s)	k	δ
-20.6	39 198	3.0E-01	0.146	2.38
-0.3	37 650	2.9E+00	0.146	2.15
14.7	37 404	4.8E-01	0.166	1.98
34.9	40 406	4.8E-01	0.162	2.10
49.7	43 962	4.1E-01	0.167	2.17

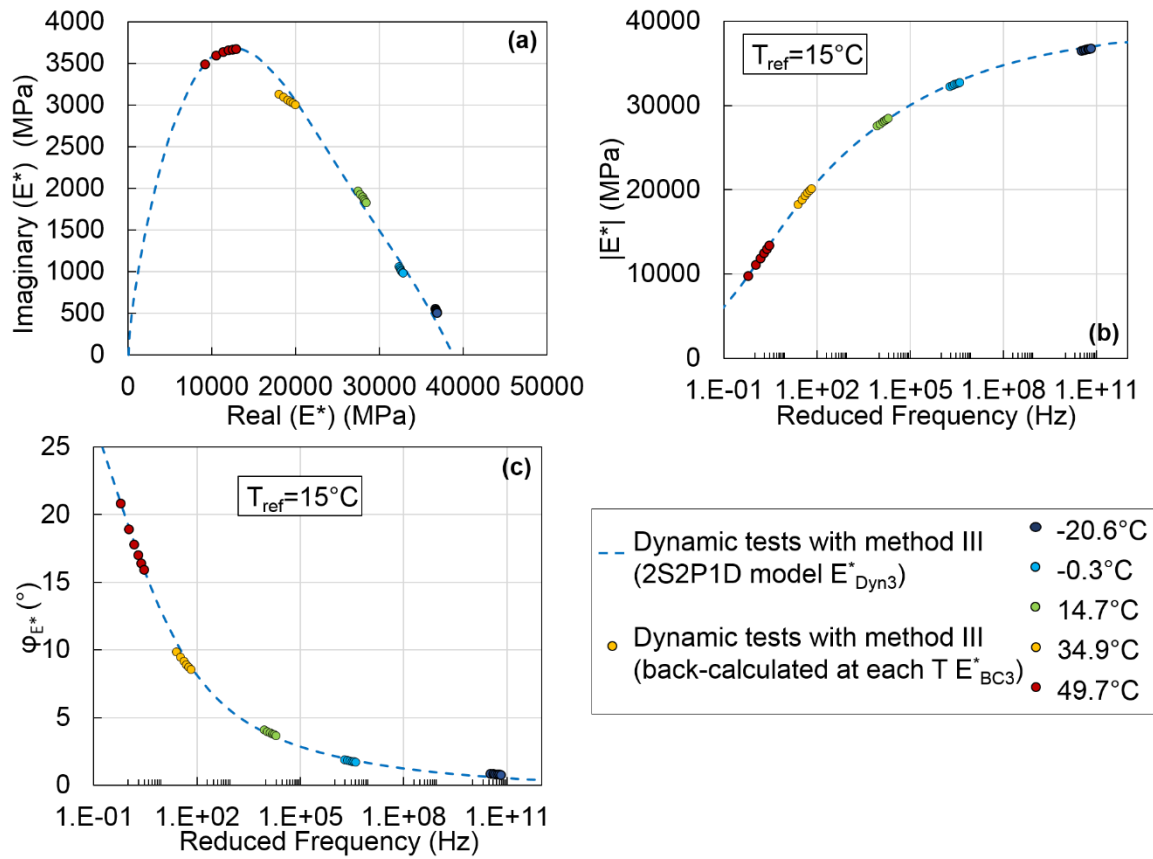


Figure J.6 Values of the complex modulus determined from dynamic tests with method III (E^*_{BC3} and E^*_{Dyn3}). (a) Cole-Cole plot; (b) and (c) master curves of the norm and of the phase angle of the complex modulus at 15°C . Results for specimen GB5-D1.

SPECIMEN GB5-D3

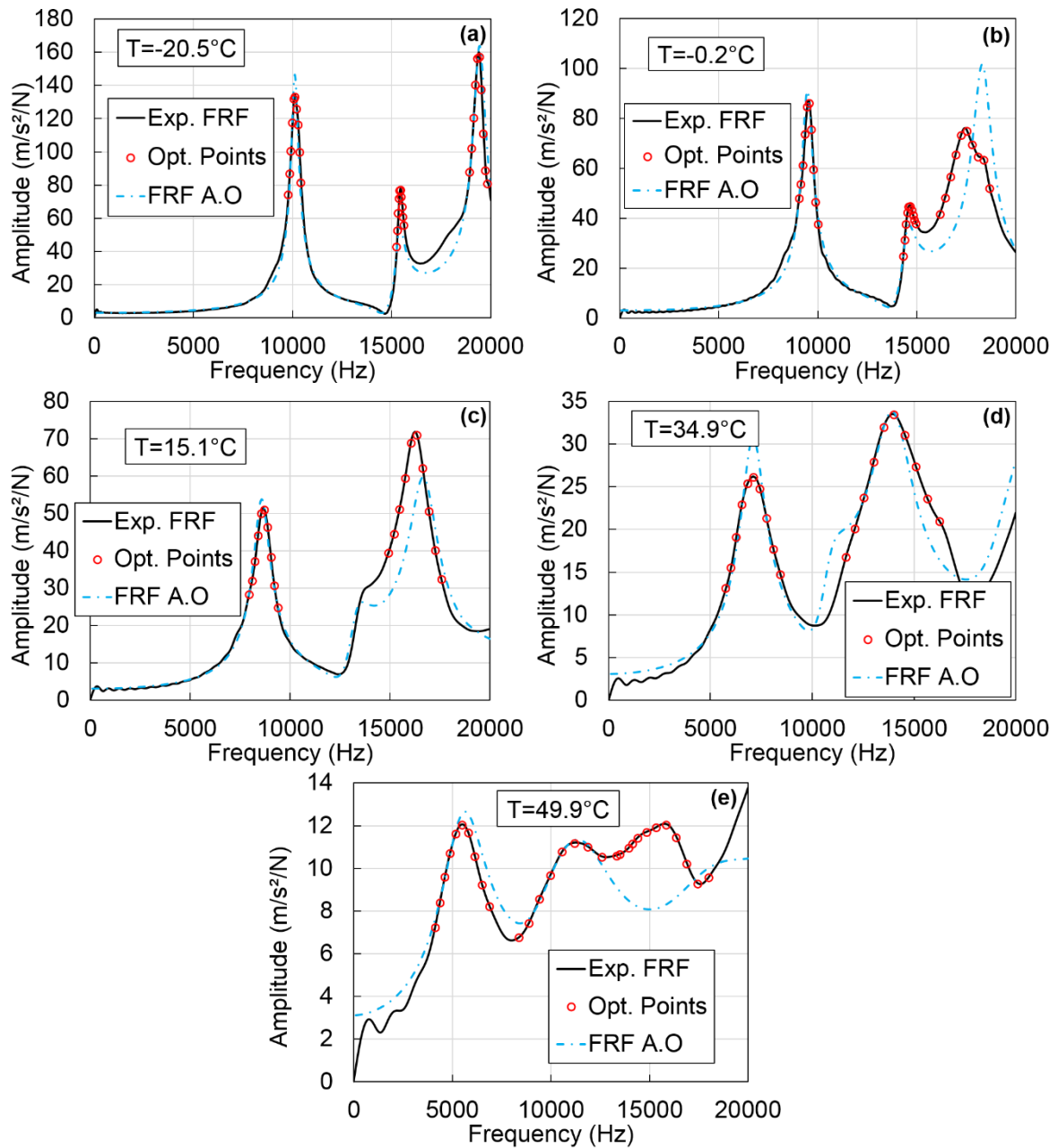


Figure J.7 Comparison of the experimental FRFs (noted Exp. FRF) with the FRFs after optimization (noted FRF A.O.) for specimen GB5-D3. Values of the experimental FRFs at the frequencies where the optimization is performed (noted Opt. Points) are also plotted. (a) $T = -20.5^{\circ}\text{C}$; (b) -0.2°C ; (c) 15.1°C ; (d) 34.9°C ; (e) 49.9°C .

Table J.4. Values of the four constants E_0 , $\tau_{E15^\circ\text{C}}$, k and δ of the 2S2PID model determined from dynamic tests at each temperature in the first step of method III for specimen GB5-D3.

Temperature ($^\circ\text{C}$)	E_0 (MPa)	$\tau_{E15^\circ\text{C}}$ (s)	k	δ
-20.5	46 259	3.0E-03	0.126	2.32
-0.2	44 306	8.8E-02	0.150	2.23
15.1	42 253	1.9E-01	0.164	2.17
34.9	42 506	2.0E+00	0.171	2.28
49.9	49 996	4.1E-01	0.185	1.81

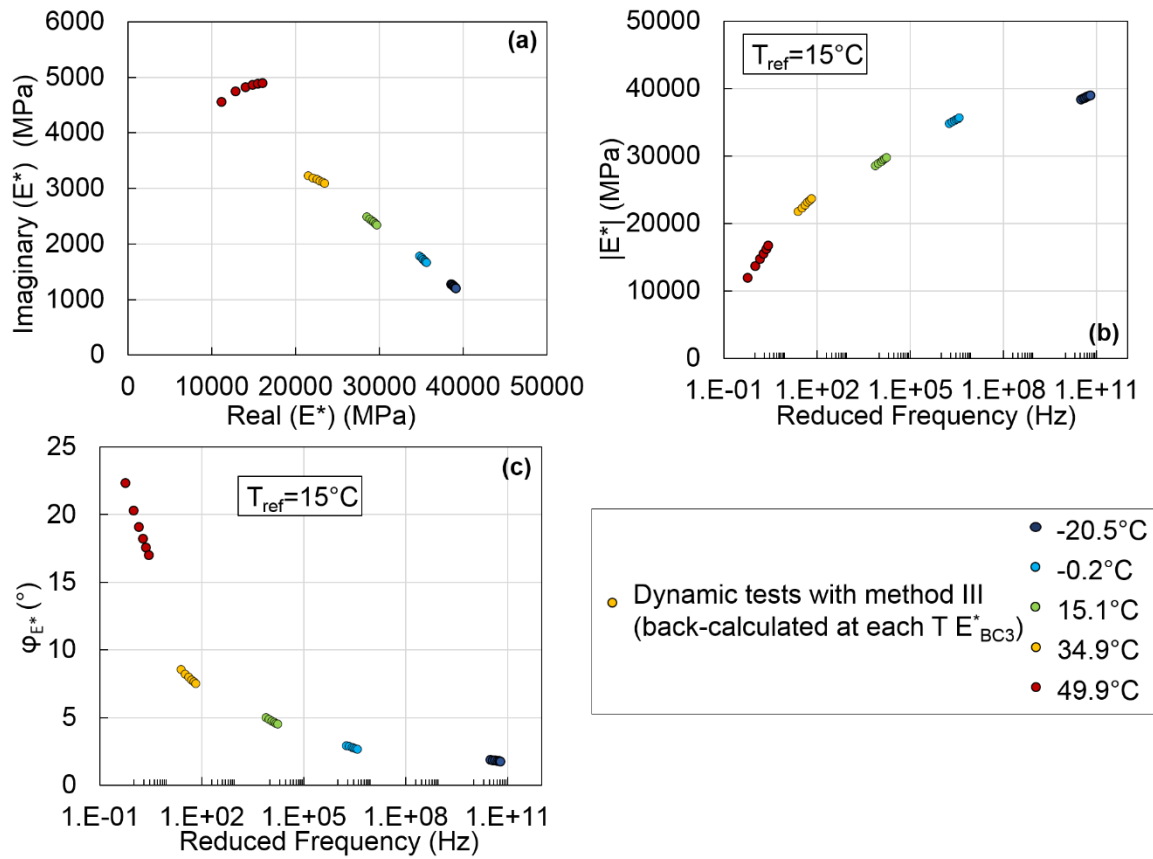


Figure J.8 Values of the complex modulus determined from dynamic tests with method III (E_{BC3}^* and E_{Dyn3}^*). (a) Cole-Cole plot; (b) and (c) master curves of the norm and of the phase angle of the complex modulus at 15°C . Results for specimen GB5-D3.

SPECIMEN GB5-C1 (1st ROUND OF DYNAMIC TESTS)

Table J.5. Values of the four constants E_0 , $\tau_{E15^\circ C}$, k and δ of the 2S2P1D model and of the Poisson's ratio ν determined from the 1st round of dynamic tests at each temperature in the first step of method V for specimen GB5-C1.

Temperature (°C)	E_0 (MPa)	$\tau_{E15^\circ C}$ (s)	k	δ	ν
-20.3	43 216	2.9E-01	0.163	2.24	0.330
-0.2	42 485	1.7E+00	0.146	1.85	0.339
14.8	39 651	7.3E-01	0.182	2.15	0.325
35.2	48 726	6.1E-01	0.159	2.52	0.496
49.4	49 992	4.0E-01	0.128	1.95	0.460

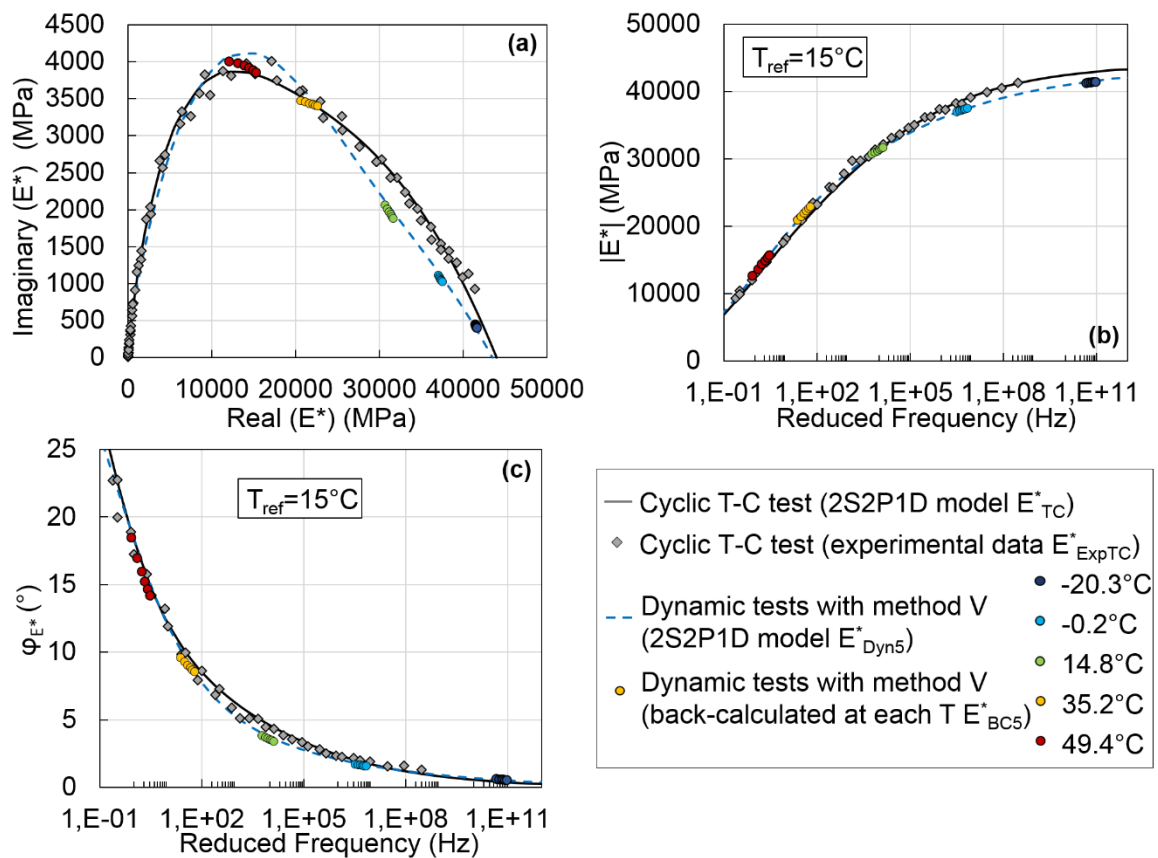


Figure J.9 Comparison of the values of the complex modulus determined from the 1st round of dynamic tests with method V (E_{BC5}^* and E_{Dyn5}^*) with the values of the complex modulus determined from cyclic tests (E_{ExpTC}^* and E_{TC}^*). (a) Cole-Cole plot; (b) and (c) master curves of the norm and of the phase angle of the complex modulus at 15°C. Results for specimen GB5-C1.

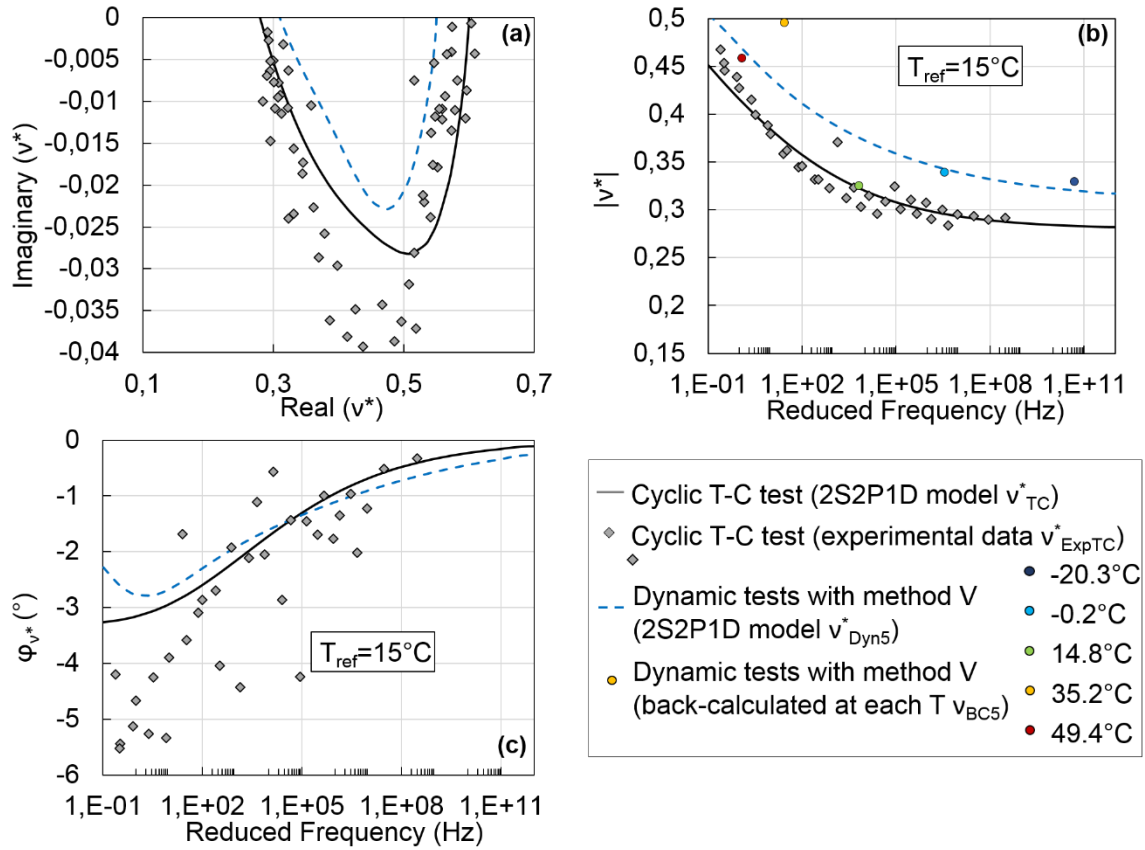


Figure J.10 Comparison of the values of the complex Poisson's ratio determined from the 1st round of dynamic tests with method V (real values v_{BC5} and v^*_{Dyn5}) with the values of the complex Poisson's ratio determined from cyclic test (v^*_{ExpTC} and v^*_{TC}). (a) Cole-Cole plot; (b) and (c) master curves of the norm and of the phase angle of the complex Poisson's ratio at 15°C . Results for specimen GB5-C1.

SPECIMEN GB5-C1 (2nd ROUND OF DYNAMIC TESTS)

Table J.6. Values of the four constants E_0 , $\tau_{E15^\circ C}$, k and δ of the 2S2PID model and of the Poisson's ratio ν determined from the 2nd round of dynamic tests at each temperature in the first step of method V for specimen GB5-C1.

Temperature (°C)	E_0 (MPa)	$\tau_{E15^\circ C}$ (s)	k	δ	ν
-20.8	44 306	4.1E-01	0.155	1.95	0.330
-0.2	41 920	2.2E+00	0.168	2.24	0.327
14.9	43 139	4.5E-01	0.154	1.85	0.336
34.1	43 812	2.1E-01	0.165	1.68	0.425
48.7	47 335	8.1E-01	0.205	2.55	0.490

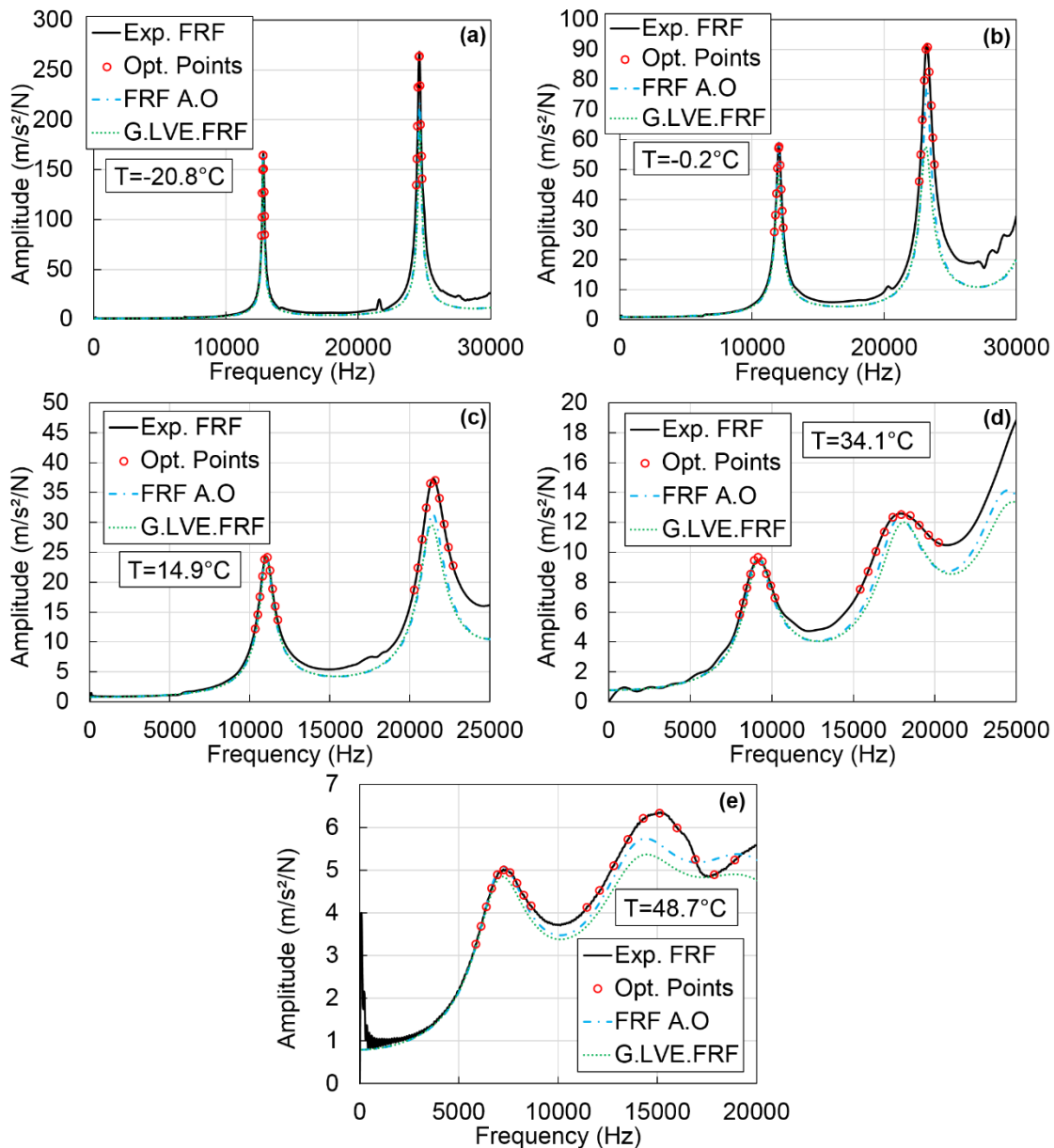


Figure J.11 Comparison of the experimental FRFs measured at the end of the project (noted Exp. FRF) with the FRFs after optimization (noted FRF A.O) and the global LVE FRFs (noted G.LVE FRF) for specimen GB5-C1. Values of the experimental FRFs at the frequencies where the optimization is performed (noted Opt. Points) are also plotted. (a) $T=-20.8^\circ C$; (b) $-0.2^\circ C$; (c) $14.9^\circ C$; (d) $34.1^\circ C$; (e) $48.7^\circ C$.

SPECIMEN GB5-C2 (1st ROUND OF DYNAMIC TESTS)

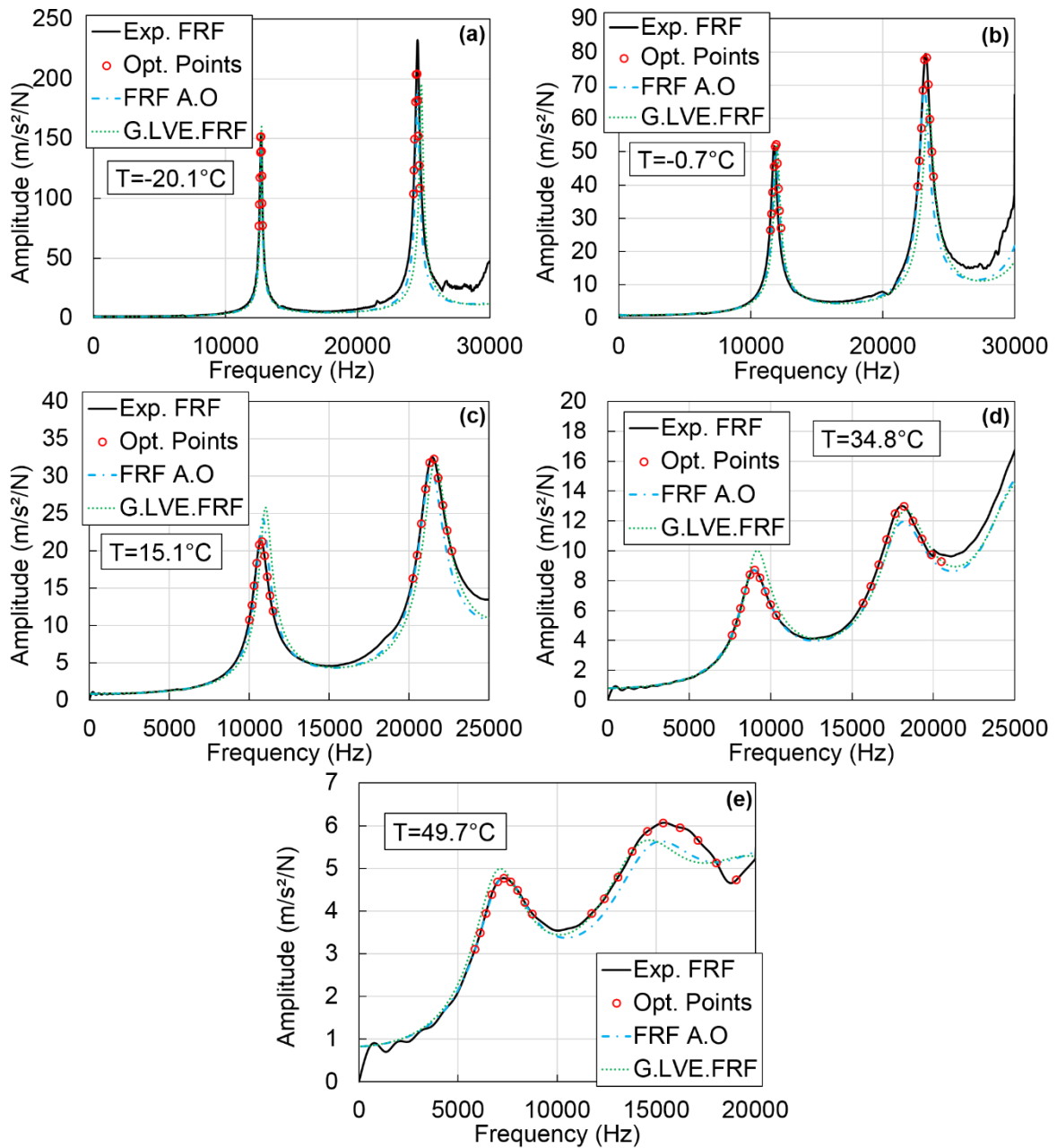


Figure J.12 Comparison of the experimental FRFs measured at the beginning of the project (noted Exp. FRF) with the FRFs after optimization (noted FRF A.O) and the global LVE FRFs (noted G.LVE FRF) for specimen GB5-C2. Values of the experimental FRFs at the frequencies where the optimization is performed (noted Opt. Points) are also plotted. (a) T=-20.1°C; (b) -0.7°C; (c) 15.1°C; (d) 34.8°C; (e) 49.7°C.

Table J.7. Values of the four constants E_0 , $\tau_{E15^\circ\text{C}}$, k and δ of the 2S2P1D model and of the Poisson's ratio ν determined from the 1st round of dynamic tests at each temperature in the first step of method V for specimen GB5-C2.

Temperature ($^\circ\text{C}$)	E_0 (MPa)	$\tau_{E15^\circ\text{C}}$ (s)	k	δ	ν
-20.1	40 535	8.3E-01	0.153	2.40	0.283
-0.7	38 520	3.0E-01	0.176	2.15	0.280
15.1	39 967	5.5E-01	0.149	2.04	0.257
34.8	35 779	6.4E-02	0.137	0.89	0.255
49.7	49 069	3.0E-01	0.157	1.97	0.294

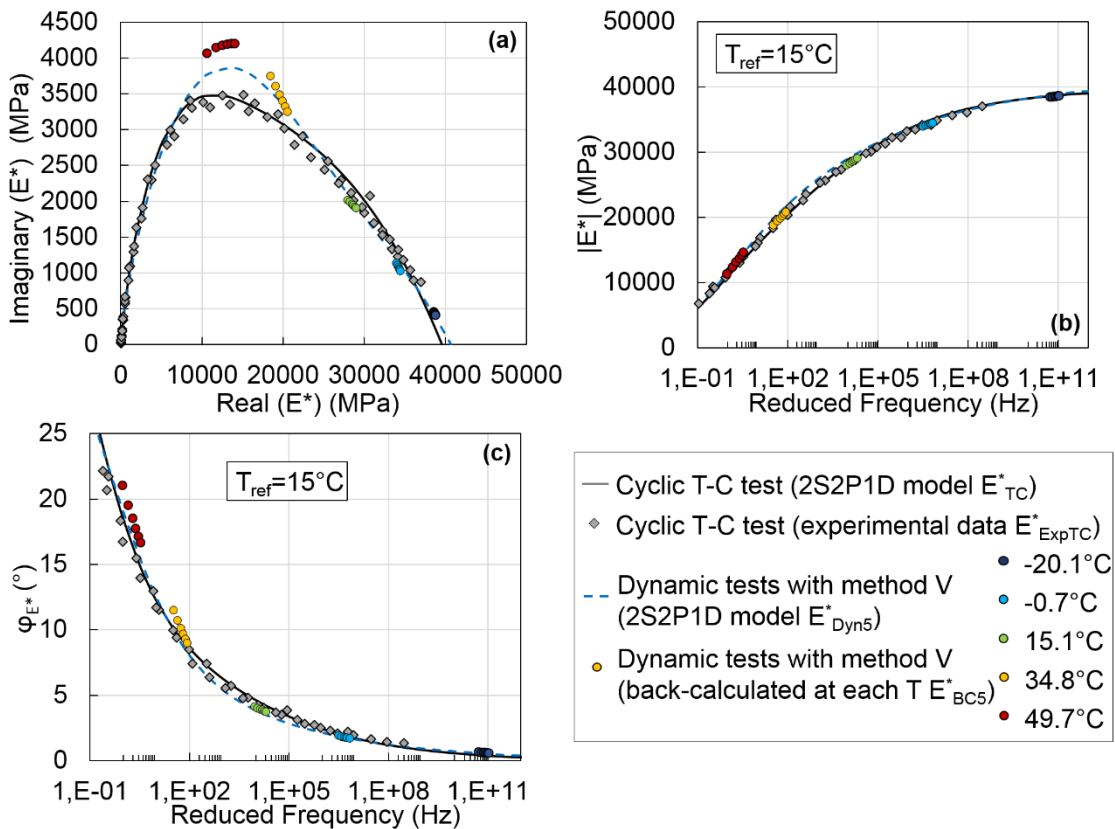


Figure J.13 Comparison of the values of the complex modulus determined from the 1st round of dynamic tests with method V (E_{BC5}^* and E_{Dyn5}^*) with the values of the complex modulus determined from cyclic tests (E_{ExpTC}^* and E_{TC}^*). (a) Cole-Cole plot; (b) and (c) master curves of the norm and of the phase angle of the complex modulus at 15 $^\circ\text{C}$. Results for specimen GB5-C2.

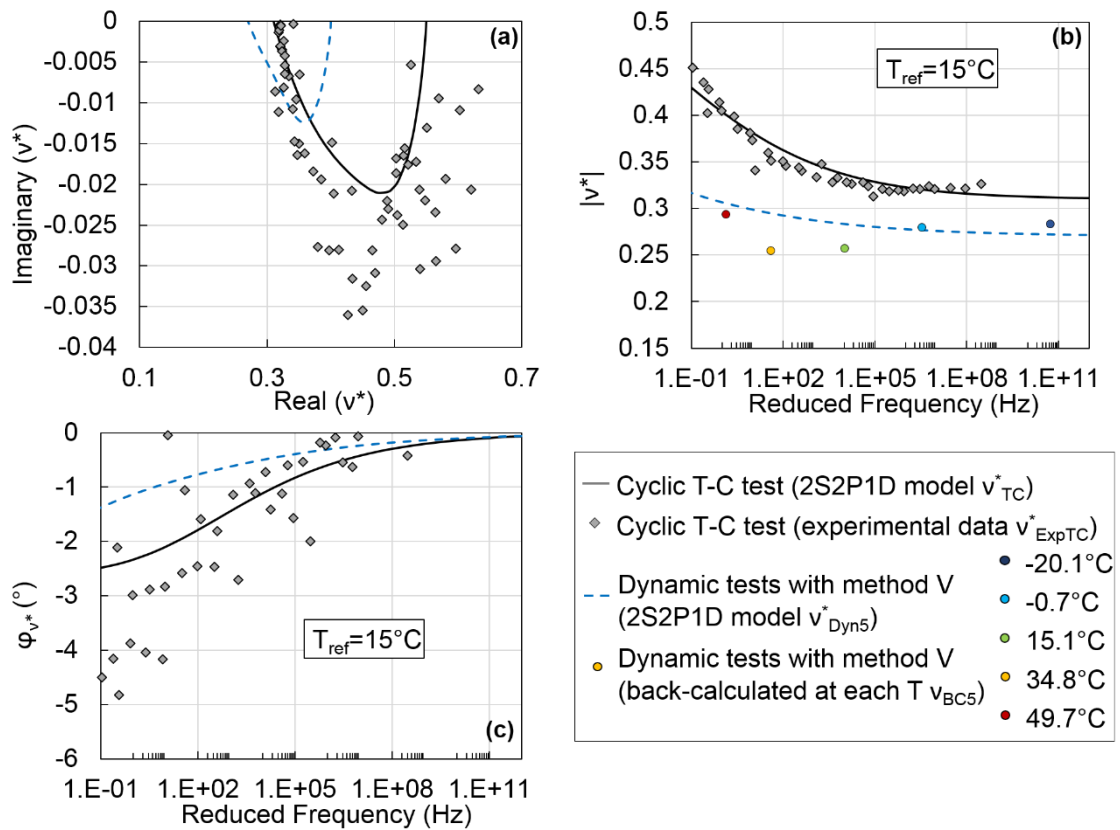


Figure J.14 Comparison of the values of the complex Poisson's ratio determined from the 1st round of dynamic tests with method V (real values v_{BC5} and v^*_{Dyn5}) with the values of the complex Poisson's ratio determined from cyclic test (v^*_{ExpTC} and v^*_{TC}). (a) Cole-Cole plot; (b) and (c) master curves of the norm and of the phase angle of the complex Poisson's ratio at 15°C . Results for specimen GB5-C2.

SPECIMEN GB5-C2 (2nd ROUND OF DYNAMIC TESTS)

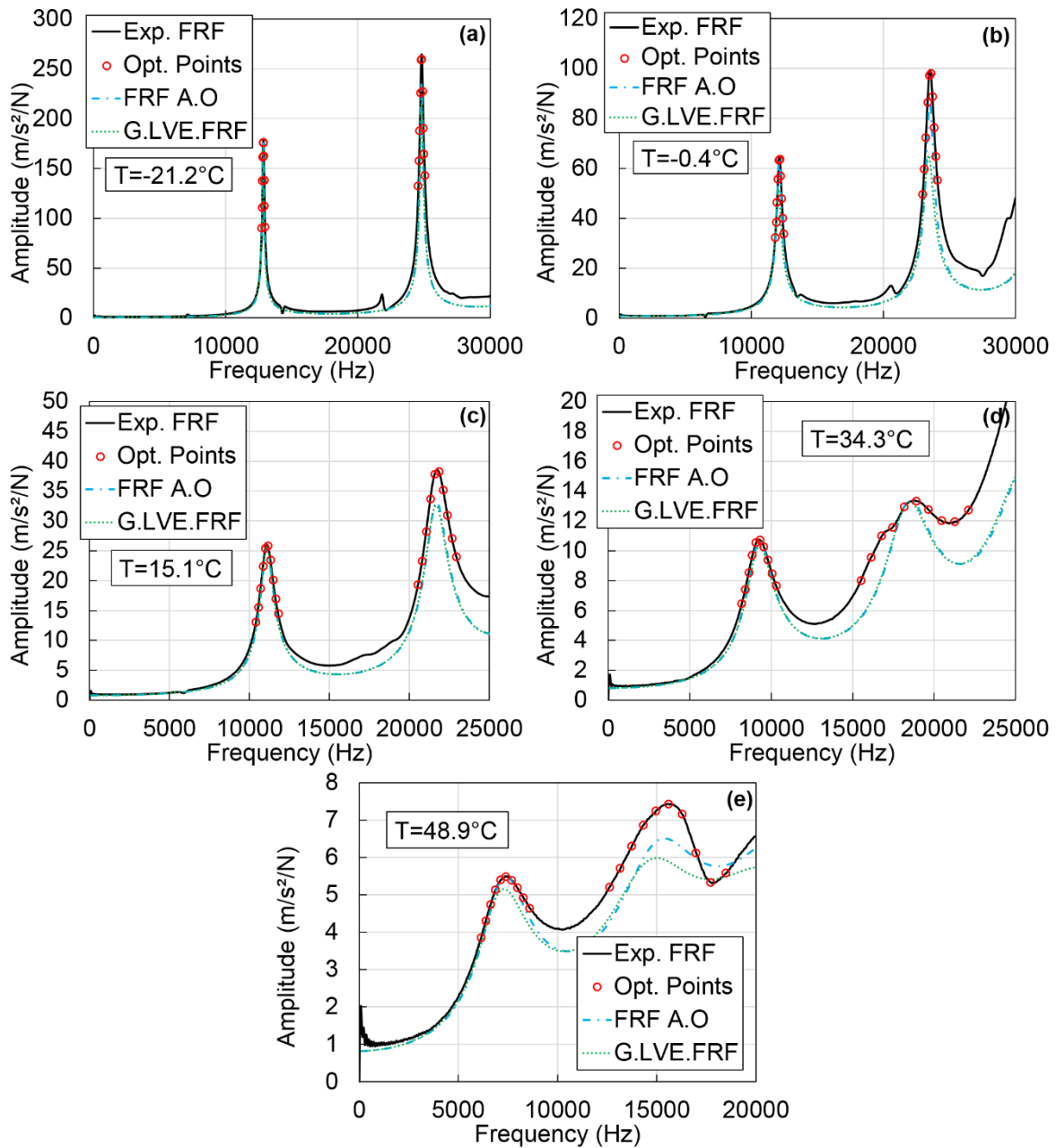


Figure J.15 Comparison of the experimental FRFs measured at the end of the project (noted Exp. FRF) with the FRFs after optimization (noted FRF A.O) and the global LVE FRFs (noted G.LVE FRF) for specimen GB5-C2. Values of the experimental FRFs at the frequencies where the optimization is performed (noted Opt. Points) are also plotted. (a) T=-21.2°C; (b) -0.4°C; (c) 15.1°C; (d) 34.8°C; (e) 48.9°C.

Table J.8. Values of the four constants E_0 , $\tau_{E15^\circ\text{C}}$, k and δ of the 2S2P1D model and of the Poisson's ratio ν determined from the 2nd round of dynamic tests at each temperature in the first step of method V for specimen GB5-C2.

Temperature (°C)	E_0 (MPa)	$\tau_{E15^\circ\text{C}}$ (s)	k	δ	ν
-21.2	40 891	1.2E-01	0.177	2.39	0.282
-0.4	38 431	4.8E-01	0.201	2.34	0.283
15.1	39 093	7.0E-01	0.171	2.08	0.289
34.3	45 300	6.0E-01	0.162	2.46	0.295
48.9	47 511	5.6E-01	0.171	2.43	0.240

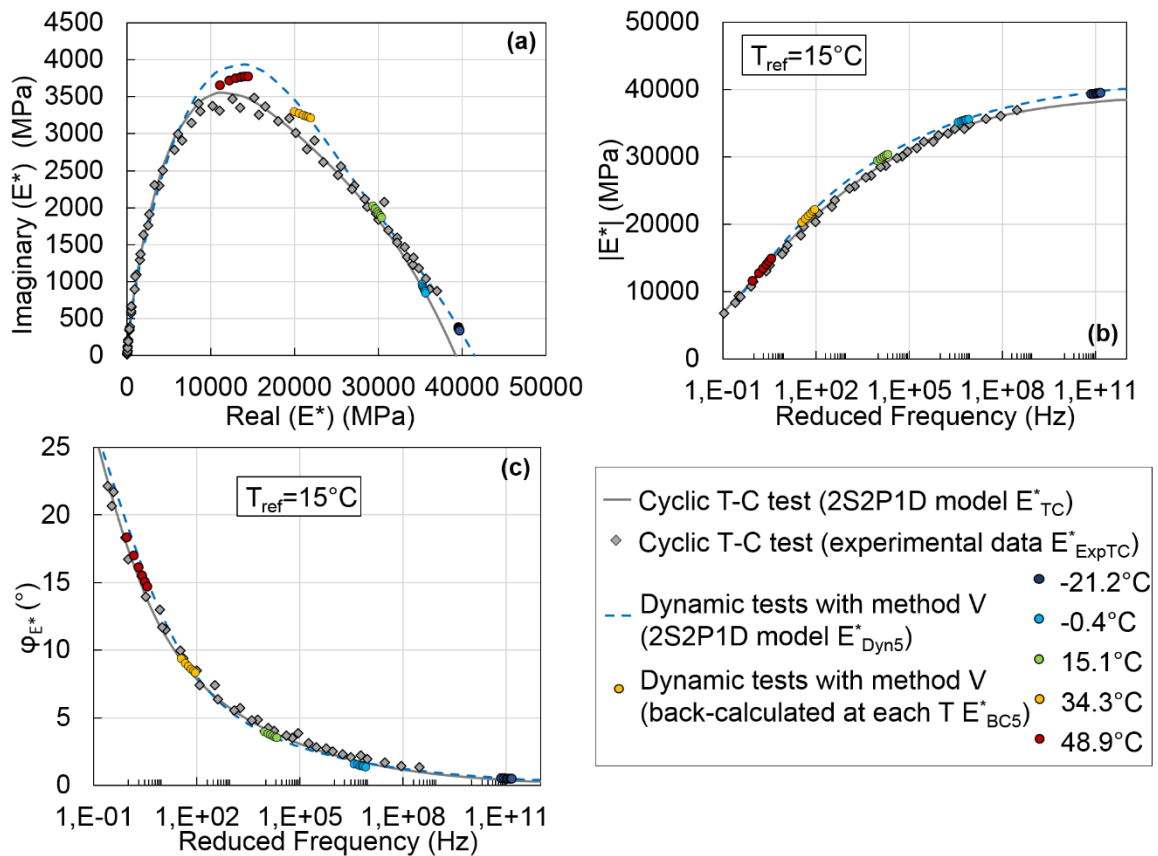


Figure J.16 Comparison of the values of the complex modulus determined from the 2nd round of dynamic tests with method V (E^*_{BC5} and E^*_{Dyn5}) with the values of the complex modulus determined from cyclic tests (E^*_{ExpTC} and E^*_{TC}). (a) Cole-Cole plot; (b) and (c) master curves of the norm and of the phase angle of the complex modulus at 15°C. Results for specimen GB5-C2.

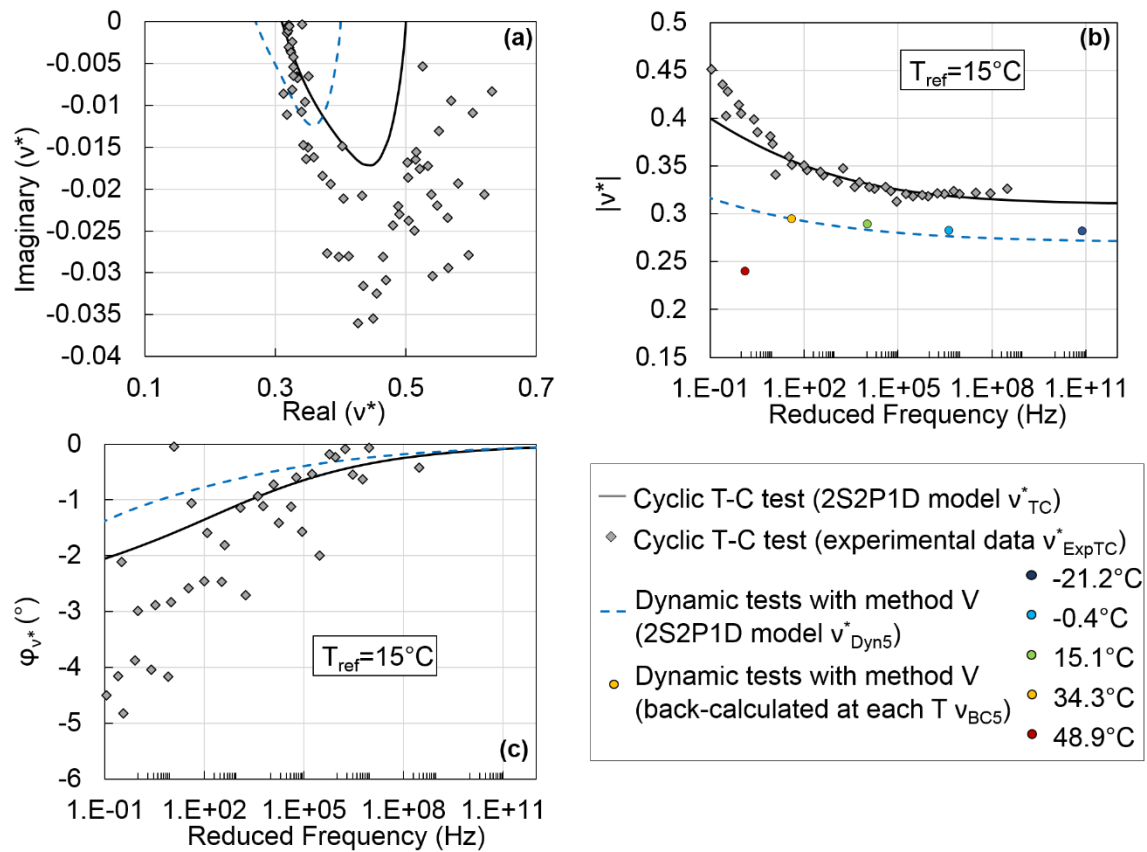


Figure J.17 Comparison of the values of the complex Poisson's ratio determined from the 2nd round of dynamic tests with method V (real values v_{BC5}^* and v_{Dyn5}^*) with the values of the complex Poisson's ratio determined from cyclic test (v_{ExpTC}^* and v_{TC}^*). (a) Cole-Cole plot; (b) and (c) master curves of the norm and of the phase angle of the complex Poisson's ratio at 15°C. Results for specimen GB5-C2.

COMPARISON OF THE FRFS MEASURED AT THE BEGINNING AND AT THE END OF THE FSDYN PROJECT FOR SPECIMENS GB5-C1 AND GB5-C2

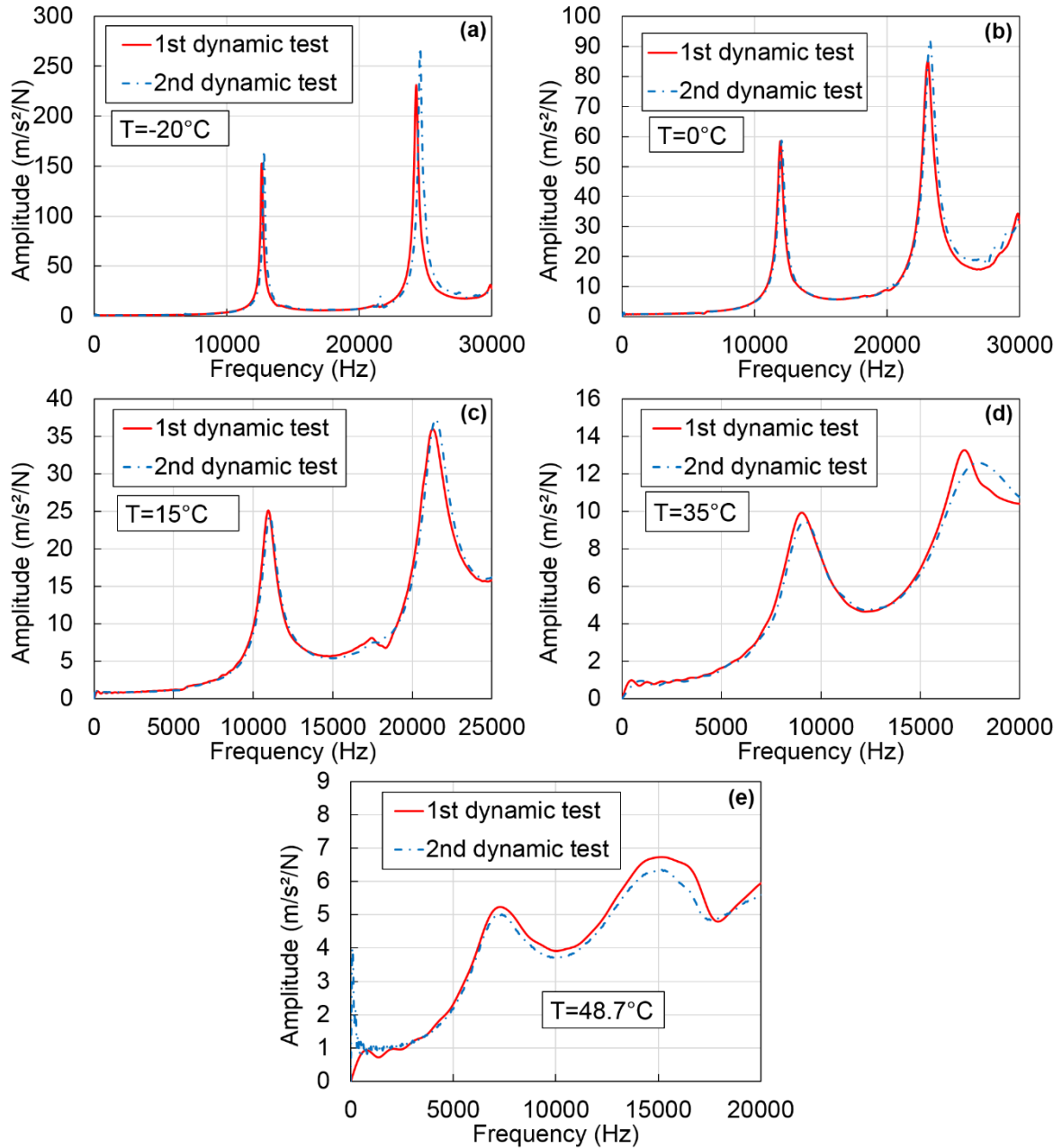


Figure J.18 FRFs measured at the beginning (1st dynamic test) and at the end (2nd dynamic test) of the FSDyn project for the specimen GB5-C1: (a) $-20^\circ C$; (b) $0^\circ C$; (c) $15^\circ C$; (d) $35^\circ C$; (e) $50^\circ C$.

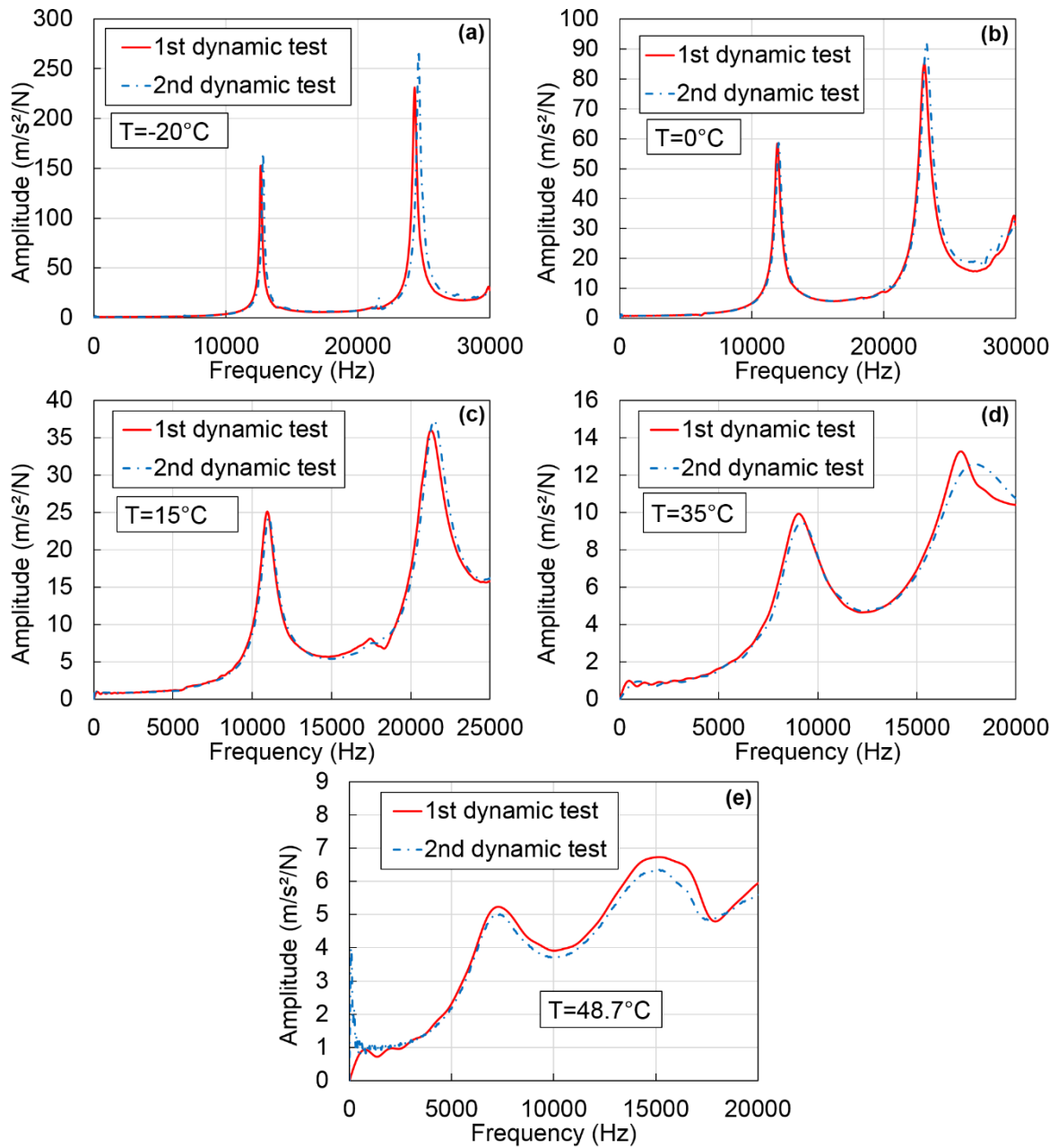


Figure J.19 FRFs measured at the beginning (1st dynamic test) and at the end (2nd dynamic test) of the FSDyn project for the specimen GB5-C1: (a) -20°C; (b) 0°C; (c) 15°C; (d) 35°C; (e) 50°C.

SPECIMEN GB5-B2

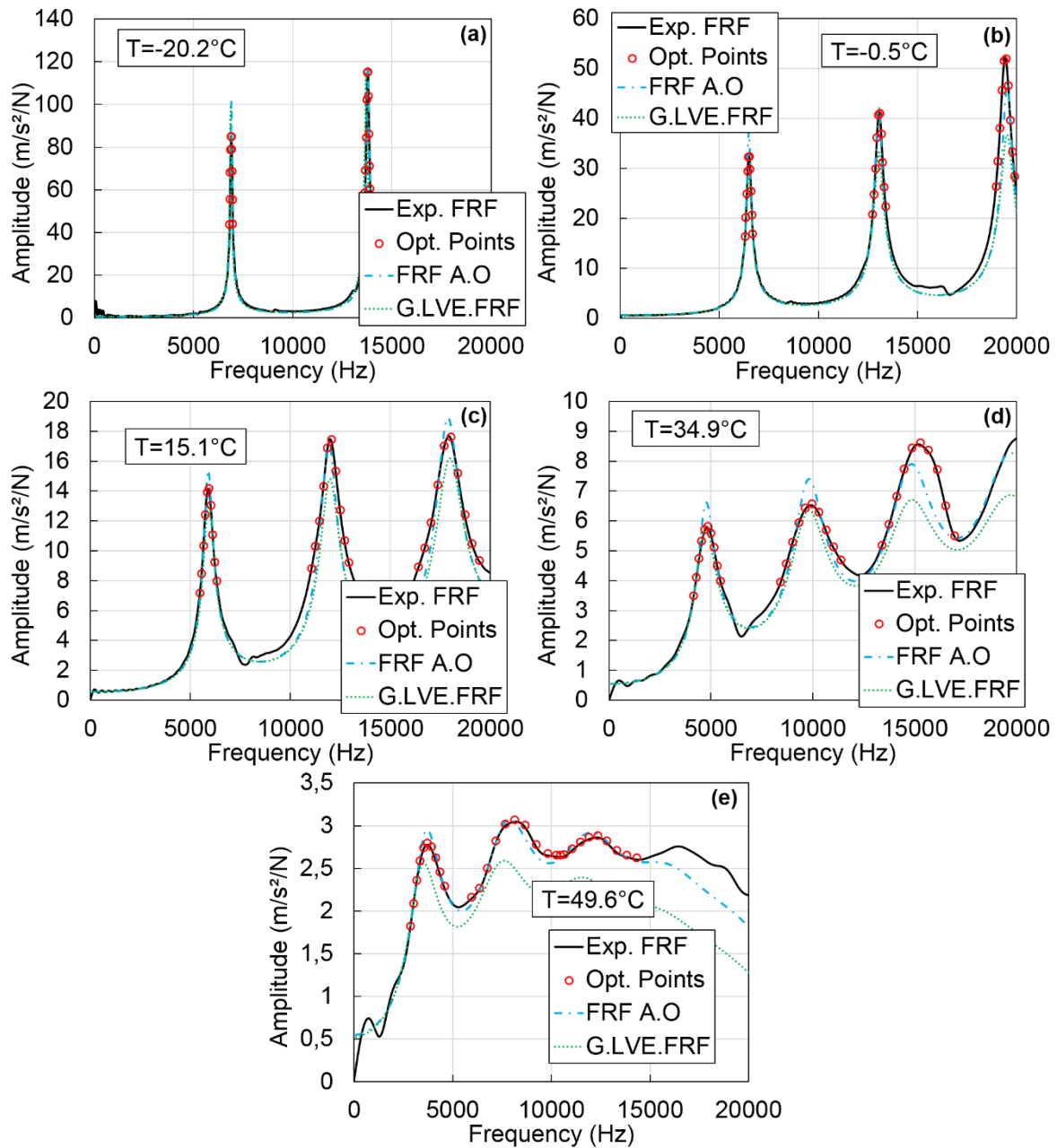


Figure J.20 Comparison of the experimental FRFs (noted *Exp. FRF*) with the FRFs after optimization (noted *FRF A.O.*) and the global LVE FRFs (noted *G.LVE FRF*) for specimen GB5-B2. Values of the experimental FRFs at the frequencies where the optimization is performed (noted *Opt. Points*) are also plotted. (a) $T = -20.2^{\circ}\text{C}$; (b) -0.5°C ; (c) 15.1°C ; (d) 34.9°C ; (e) 49.6°C .

Table J.9. Values of the four constants E_0 , $\tau_{E15^\circ C}$, k and δ of the 2S2P1D model determined from dynamic tests at each temperature in the first step of method III for specimen GB5-B2.

Temperature ($^\circ\text{C}$)	E_0 (MPa)	$\tau_{E15^\circ C}$ (s)	k	δ
-20.2	42 986	2.7E-01	0.165	2.38
-0.5	44 046	4.9E+00	0.121	1.77
15.1	41 397	5.0E-01	0.176	2.10
34.9	45 732	3.2E-01	0.178	2.13
49.6	48 196	5.1E-01	0.185	2.02

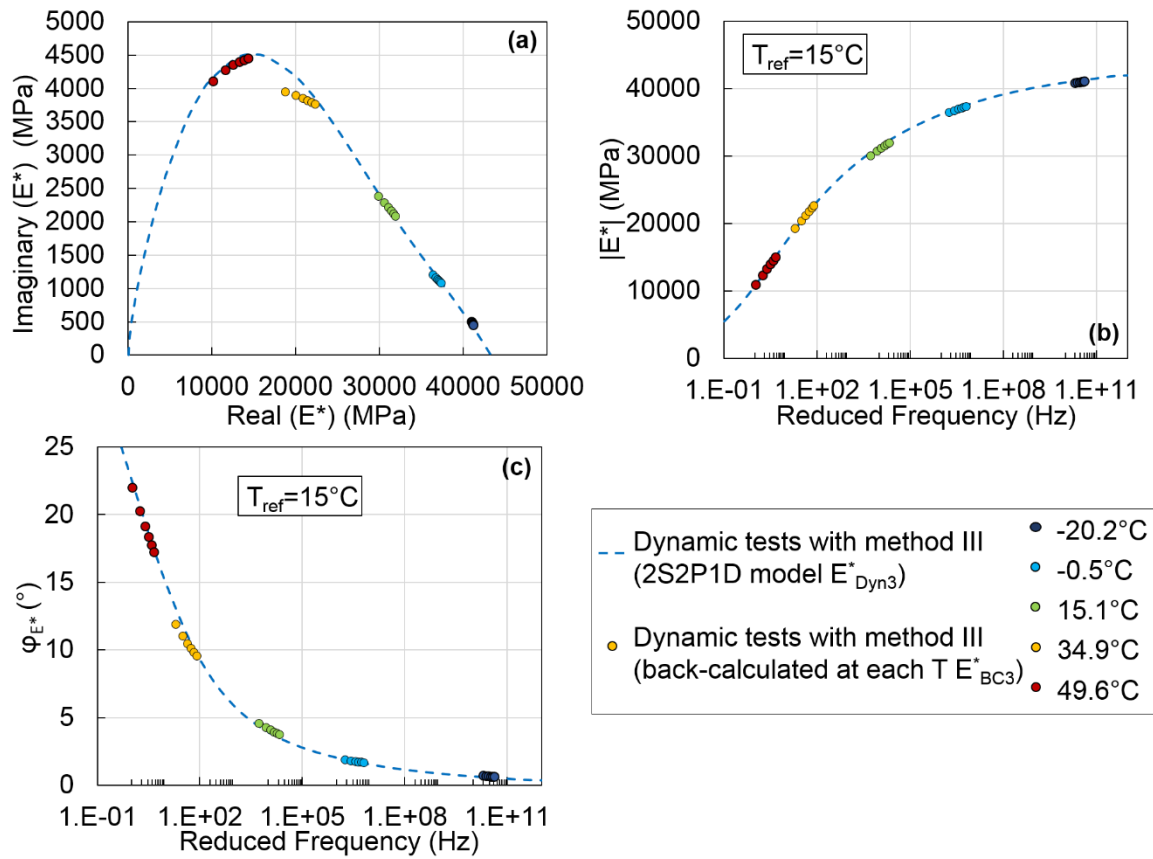


Figure J.21 Values of the complex modulus determined from dynamic tests with method III (E_{BC3}^* and E_{Dyn3}^*). (a) Cole-Cole plot; (b) and (c) master curves of the norm and of the phase angle of the complex modulus at 15°C . Results for specimen GB5-B2.

SPECIMEN GB5-B4

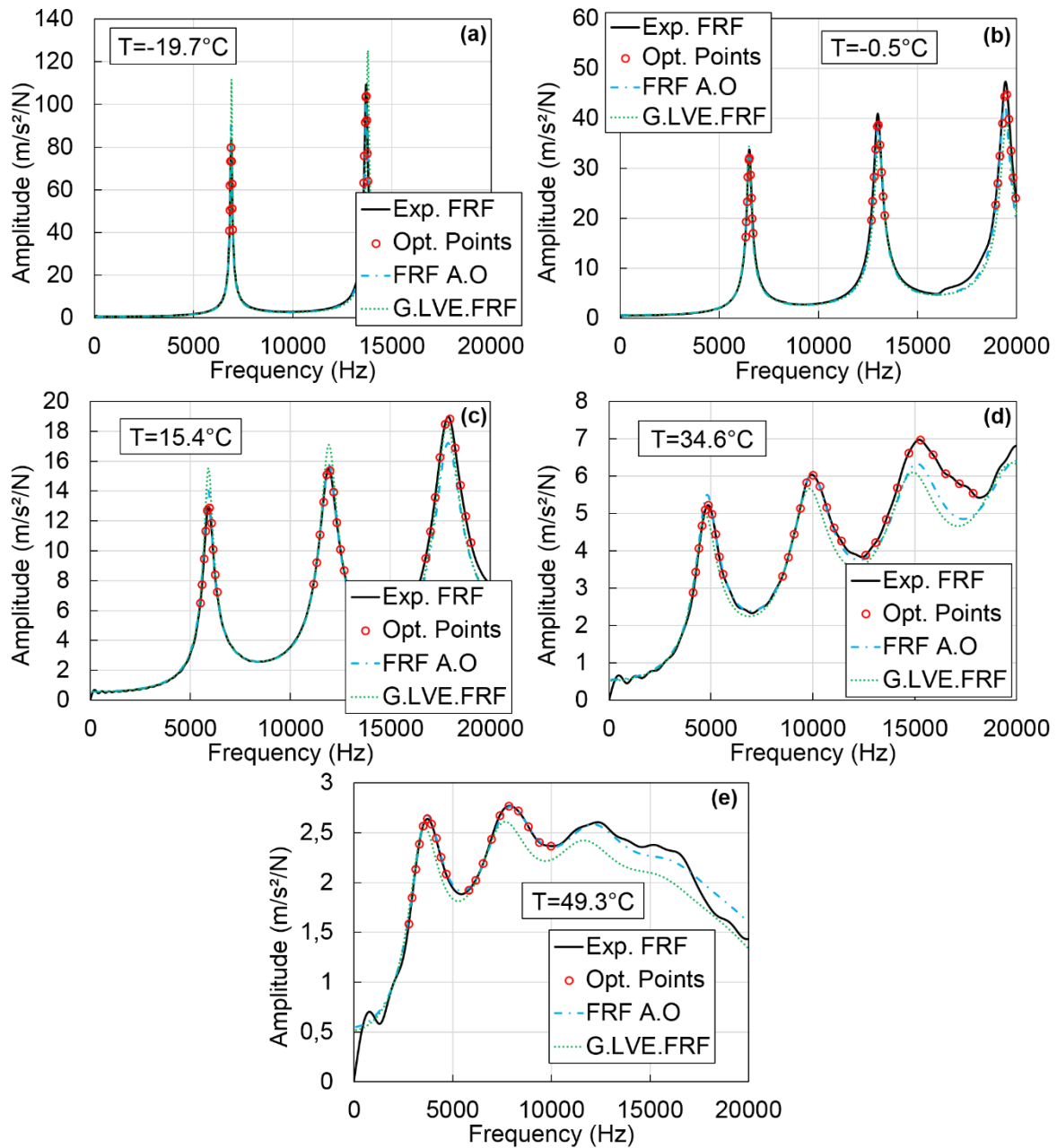


Figure J.22 Comparison of the experimental FRFs (noted Exp. FRF) with the FRFs after optimization (noted FRF A.O.) and the global LVE FRFs (noted G.LVE FRF) for specimen GB5-B4. Values of the experimental FRFs at the frequencies where the optimization is performed (noted Opt. Points) are also plotted. (a) $T = -19.7^{\circ}\text{C}$; (b) -0.5°C ; (c) 15.4°C ; (d) 34.6°C ; (e) 49.3°C .

Table J.10. Values of the four constants E_0 , $\tau_{E15^\circ C}$, k and δ of the 2S2P1D model determined from dynamic tests at each temperature in the first step of method III for specimen GB5-B4.

Temperature ($^\circ\text{C}$)	E_0 (MPa)	$\tau_{E15^\circ\text{C}}$ (s)	k	δ
-19.7	42 770	2.8E-01	0.169	2.52
-0.5	41 967	1.1E+00	0.161	2.15
15.4	41 623	4.5E-01	0.180	2.21
34.6	46 557	2.8E-01	0.185	2.15
49.3	49 282	2.9E-01	0.161	1.74

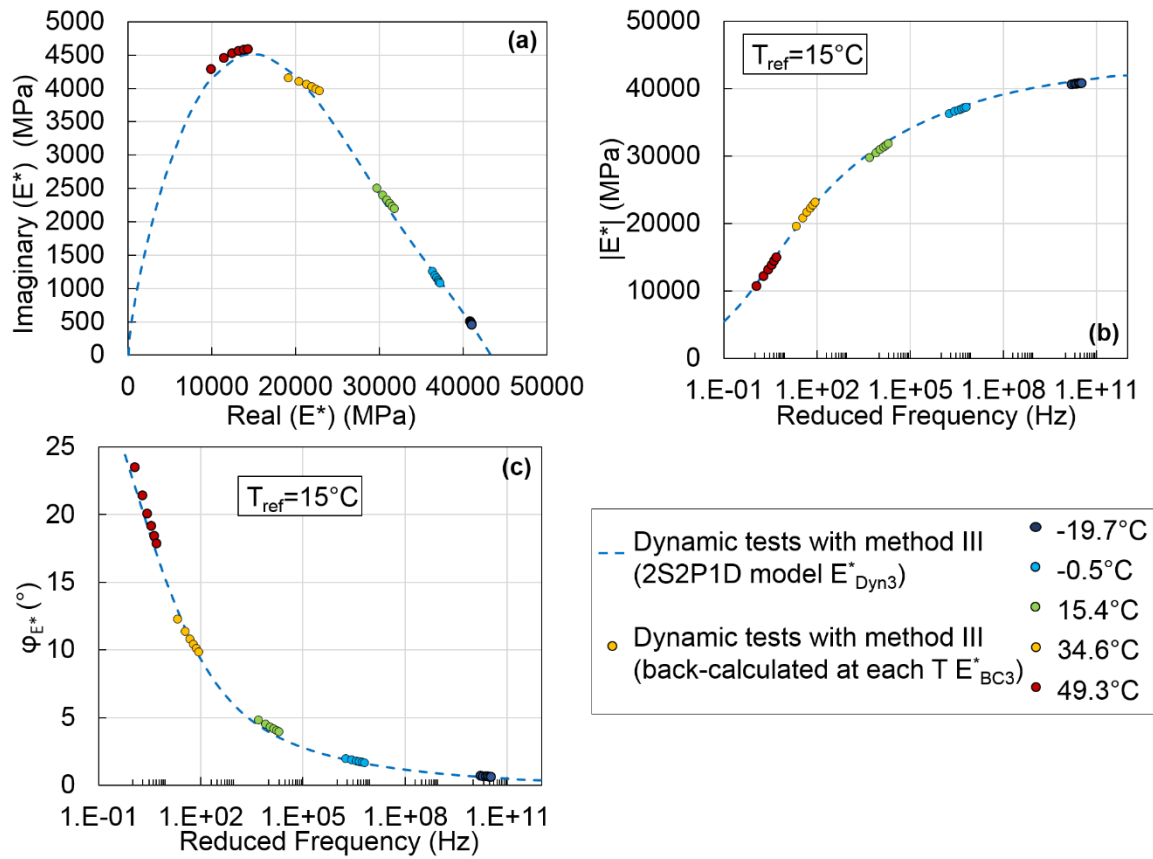


Figure J.23 Values of the complex modulus determined from dynamic tests with method III (E_{BC3}^* and E_{Dyn3}^*). (a) Cole-Cole plot; (b) and (c) master curves of the norm and of the phase angle of the complex modulus at 15°C. Results for specimen GB5-B4.

**APPENDIX K - RESULTS OF THE SM
EXPERIMENTAL CAMPAIGN**

Table K.1. Values of the four constants E_0 , $\tau_{E15^\circ\text{C}}$, k and δ of the 2S2P1D model determined from dynamic tests at each temperature in the first step of method III for specimen ABS-P4.

Temperature ($^\circ\text{C}$)	E_0 (MPa)	$\tau_{E15^\circ\text{C}}$ (s)	k	δ
-20.8	42 362	6.3E-02	0.169	2.09
0.2	43 229	5.3E-02	0.164	2.29
14.5	44 929	2.8E-03	0.177	1.77
29.2	48 859	7.9E-03	0.229	2.58
39.1	46 506	7.2E-03	0.230	1.42

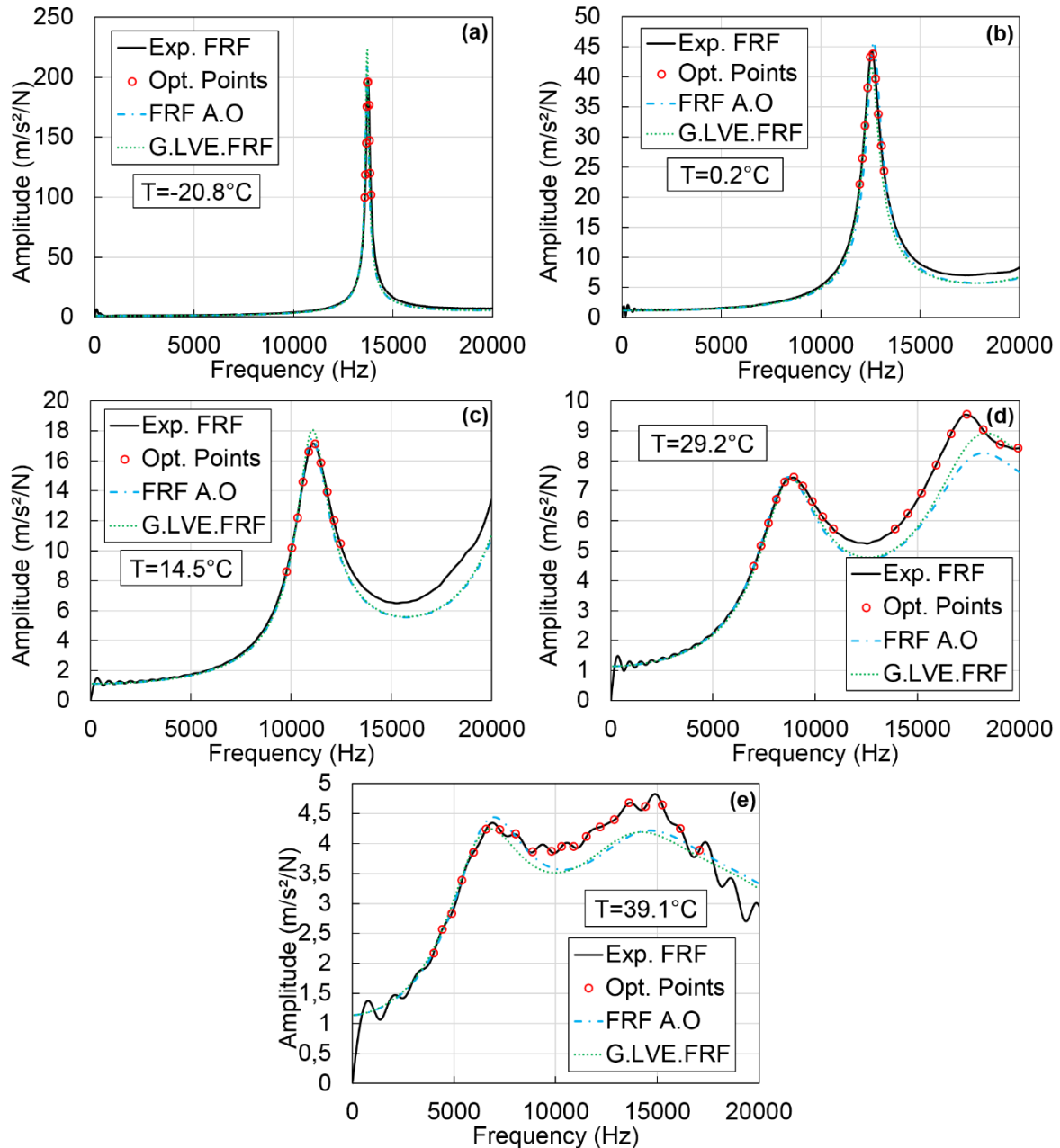


Figure K.1 Comparison of the experimental FRFs (noted *Exp. FRF*) with the FRFs after optimization (noted *FRF A.O.*) and the global LVE FRFs (noted *G.LVE FRF*) for specimen ABS-P4. Values of the experimental FRFs at the frequencies where the optimization is performed (noted *Opt. Points*) are also plotted. (a) $T=-20.8^\circ\text{C}$; (b) 0.2°C ; (c) 14.5°C ; (d) 29.2°C ; (e) 39.1°C .

**APPENDIX L - RESULTS OF THE MOGS
EXPERIMENTAL CAMPAIGN WITH THE**

SPECIMEN GB5-C3

Table L.1. First resonance frequency and values of $|E^*_{BC4}|$ and $\varphi_{E^*_{BC4}}$ determined from dynamic tests at each temperature in the first step of method IV for specimen GB5-C3.

Temperature (°C)	1 st resonance frequency (Hz)	$ E^*_{BC4} $ (MPa)	$\varphi_{E^*_{BC4}}$ (°)
-20.6	12 994	37 870	0.59
0	12 244	33 500	1.7
14.5	11 277	28 250	3.9
34	9 296	19 050	10.2
48.5	7 113	11 200	19.3

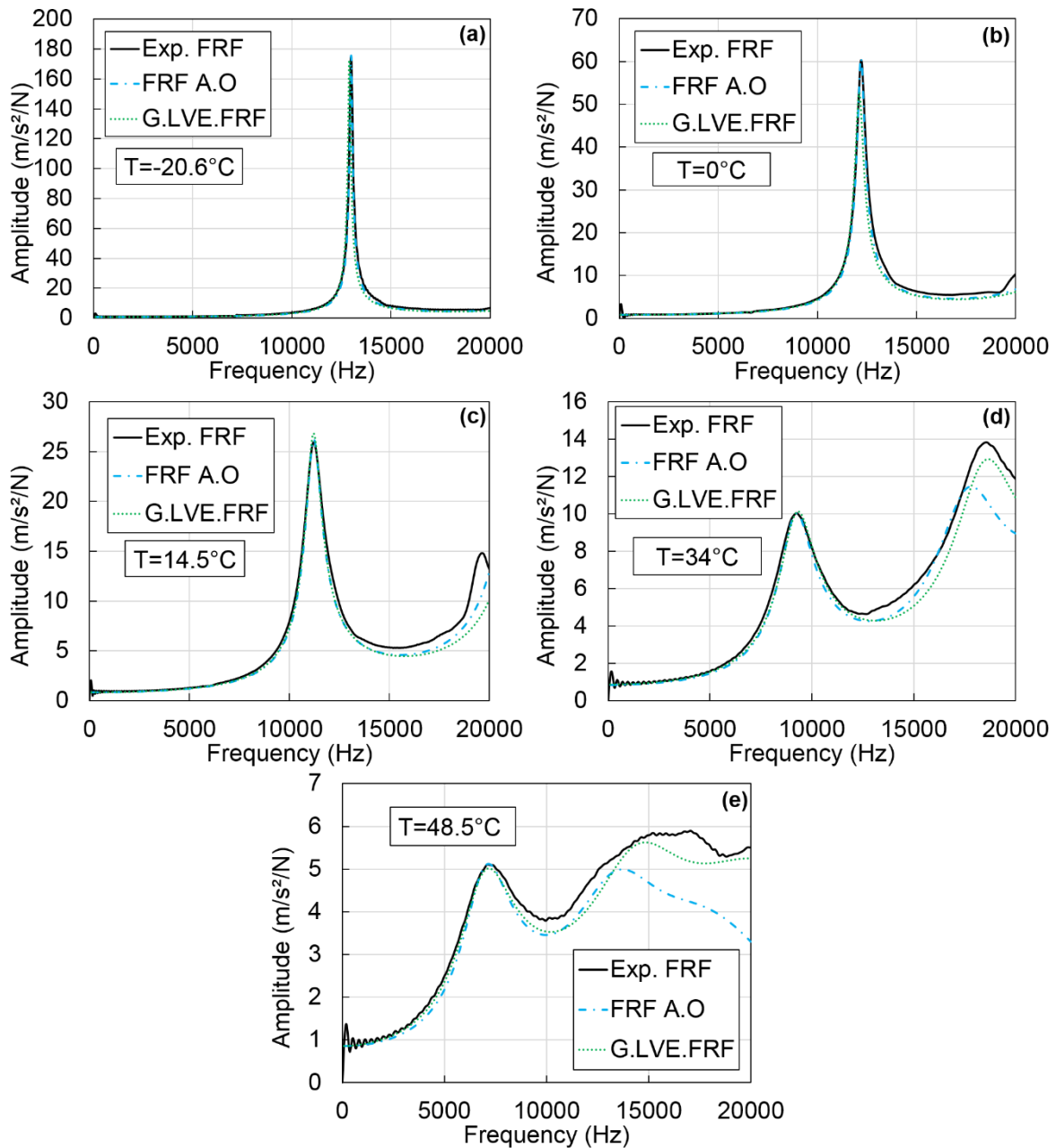


Figure L.1 Comparison of the experimental FRFs (noted Exp. FRF) with the FRFs after optimization (noted FRF A.O) and the global LVE FRFs (noted G.LVE.FRF) obtained with method IV for specimen GB5-C3. (a) $T=-20.6^{\circ}\text{C}$; (b) 0°C ; (c) 14.5°C ; (d) 34°C ; (e) 48.5°C .

Table L.2. Values of the four constants E_0 , $\tau_{E15^\circ\text{C}}$, k and δ of the 2S2P1D model determined from dynamic tests at each temperature in the first step of method III for specimen GB5-C3.

Temperature ($^\circ\text{C}$)	E_0 (MPa)	$\tau_{E15^\circ\text{C}}$ (s)	k	δ
-20.6	38 781	2.8E-01	0.163	1.91
0	37 452	3.1E+00	0.152	1.98
14.5	40 936	2.4E+00	0.131	2.30
34	42 223	2.2E-01	0.157	2.06
48.5	39 521	4.3E-01	0.189	2.07

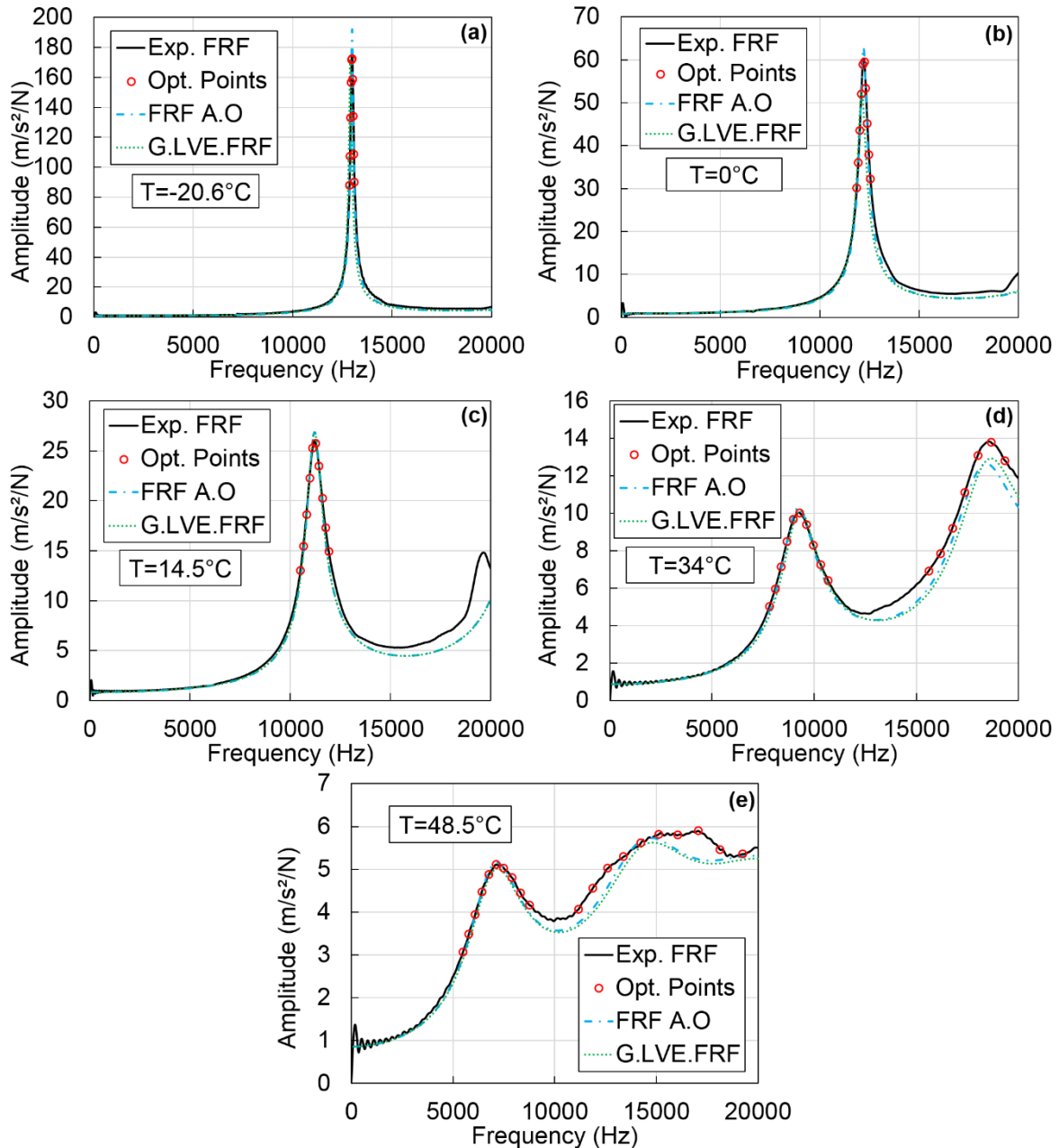


Figure L.2 Comparison of the experimental FRFs (noted *Exp. FRF*) with the FRFs after optimization (noted *FRF A.O.*) and the global LVE FRFs (noted *G.LVE FRF*) obtained with method III for specimen GB5-C3. Values of the experimental FRFs at the frequencies where the optimization is performed (noted *Opt. Points*) are also plotted. (a) $T = -20.6^\circ\text{C}$; (b) 0°C ; (c) 14.5°C ; (d) 34°C ; (e) 48.5°C .

SPECIMEN GB5-C4

Table L.3. First resonance frequency and values of $|E^*_{BC4}|$ and $\varphi_{E^*_{BC4}}$ determined from dynamic tests at each temperature in the first step of method IV for specimen GB5-C3.

Temperature (°C)	1 st resonance frequency (Hz)	$ E^*_{BC4} $ (MPa)	$\varphi_{E^*_{BC4}}$ (°)
-20.8	13 200	39 040	0.57
-0.3	12 462	34 700	1.6
14.4	11 531	29 500	3.7
34	9 635	20 300	9.5
49	7 622	12 600	18.6

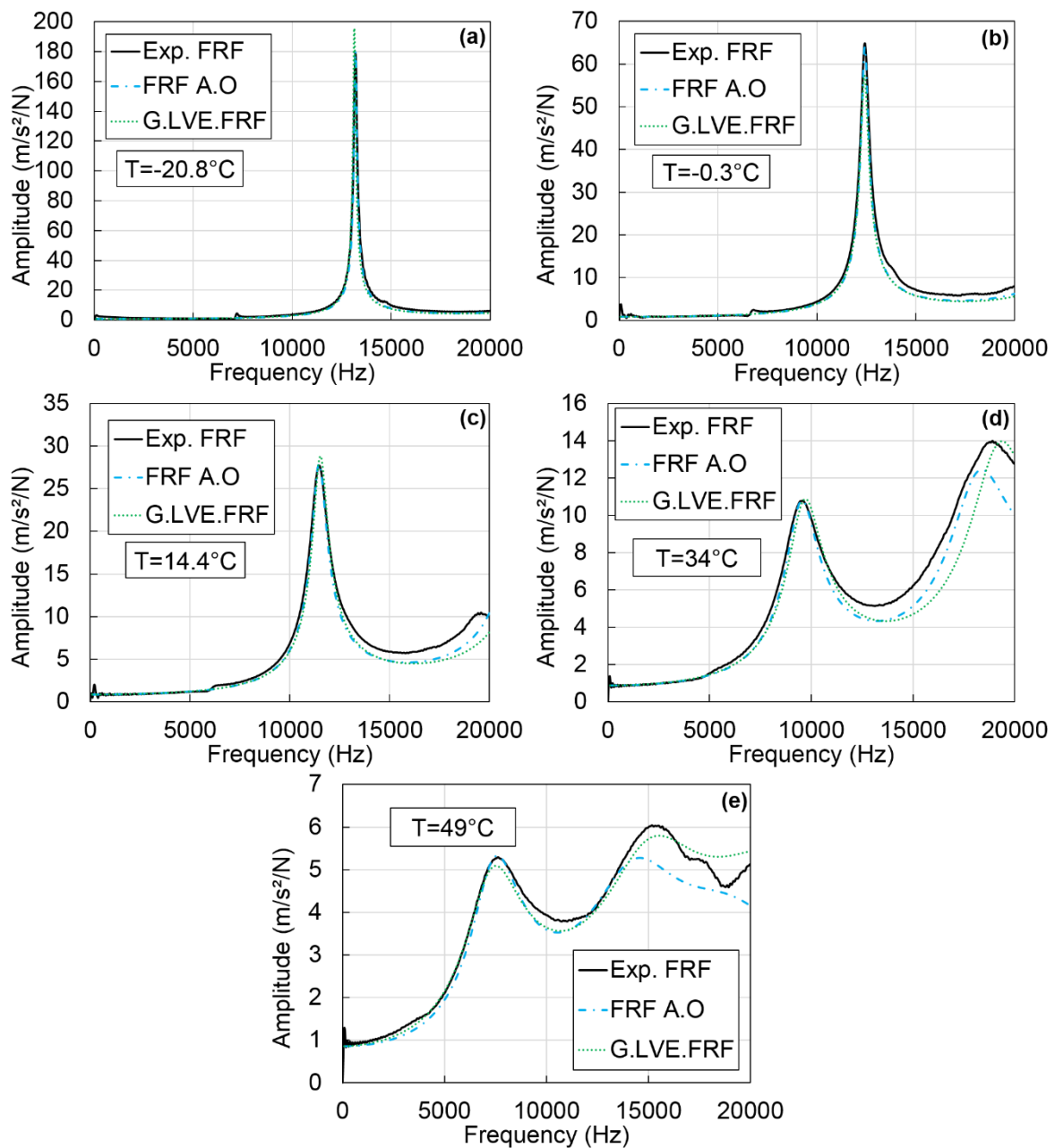


Figure L.3 Comparison of the experimental FRFs (noted Exp. FRF) with the FRFs after optimization (noted FRF A.O) and the global LVE FRFs (noted G.LVE FRF) obtained with method IV for specimen GB5-C4. (a) $T=-20.8^{\circ}\text{C}$; (b) -0.3°C ; (c) 14.4°C ; (d) 34°C ; (e) 49°C .

Table L.4. Values of the four constants E_0 , $\tau_{E15^\circ\text{C}}$, k and δ of the 2S2P1D model determined from dynamic tests at each temperature in the first step of method III for specimen GB5-C4.

Temperature ($^\circ\text{C}$)	E_0 (MPa)	$\tau_{E15^\circ\text{C}}$ (s)	k	δ
-20.8	40 049	1.4E+00	0.152	2.00
-0.3	38 781	2.5E+00	0.140	1.56
14.4	37 481	9.7E-01	0.171	2.02
34	42 749	3.5E-01	0.157	2.07
49	42 778	5.2E-01	0.187	2.01

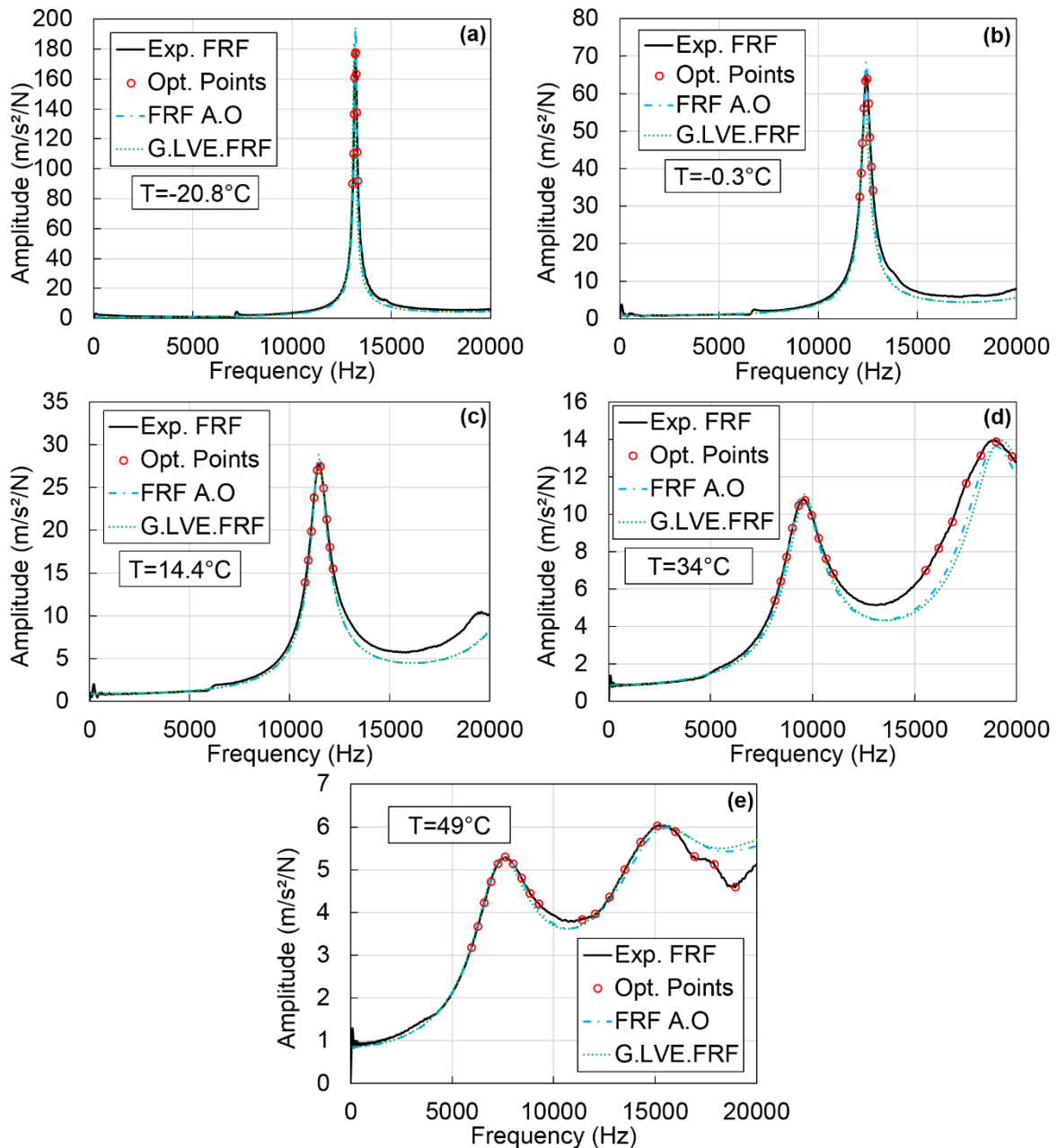


Figure L.4 Comparison of the experimental FRFs (noted *Exp. FRF*) with the FRFs after optimization (noted *FRF A.O.*) and the global LVE FRFs (noted *G.LVE FRF*) obtained with method III for specimen GB5-C4. Values of the experimental FRFs at the frequencies where the optimization is performed (noted *Opt. Points*) are also plotted. (a) $T = -20.8^\circ\text{C}$; (b) -0.3°C ; (c) 14.4°C ; (d) 34°C ; (e) 49°C .

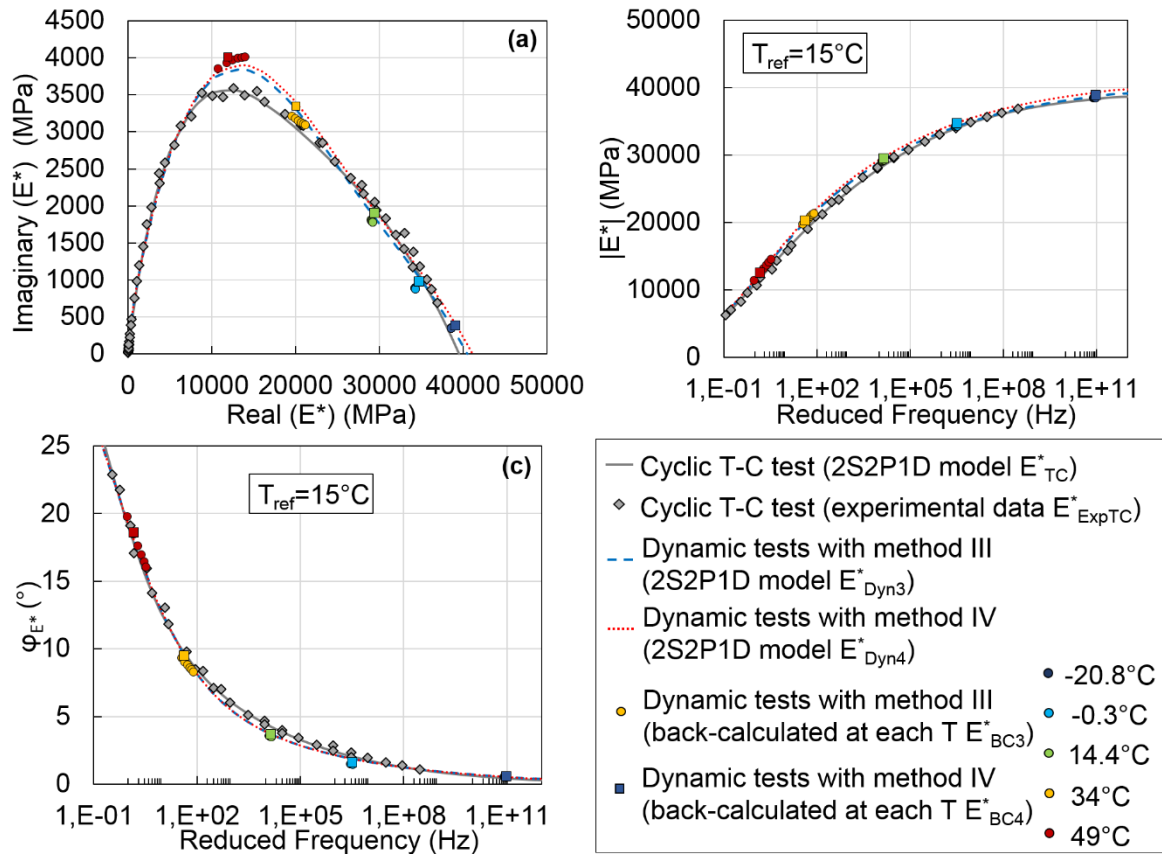


Figure L.5 Comparison of the values of the complex modulus determined from dynamic tests with method III (E^*_{BC3} and E^*_{Dyn3}) and method IV (E^*_{BC4} and E^*_{Dyn4}) with the values of the complex modulus determined from cyclic tests (E^*_{ExpTC} and E^*_{TC}). (a) Cole-Cole plot; (b) and (c) master curves of the norm and of the phase angle of the complex modulus at 15°C. Results for specimen GB5-C4.

**APPENDIX M - RESULTS OF THE MHRAPC
EXPERIMENTAL CAMPAIGN**

SPECIMEN WF-4

Table M.1. First resonance frequency and values of $|E^*_{BC4}|$ and $\varphi_{E^*_{BC4}}$ determined from dynamic tests at each temperature in the first step of method IV for specimen WF-4.

Temperature (°C)	1 st resonance frequency (Hz)	$ E^*_{BC4} $ (MPa)	$\varphi_{E^*_{BC4}}$ (°)
-20.7	15 193	34 878	0.62
-0.1	14 239	30 637	1.8
15.3	12 804	24 763	4.7
34.2	10 342	15 955	11.7
48.5	7 888	8 991	22.5

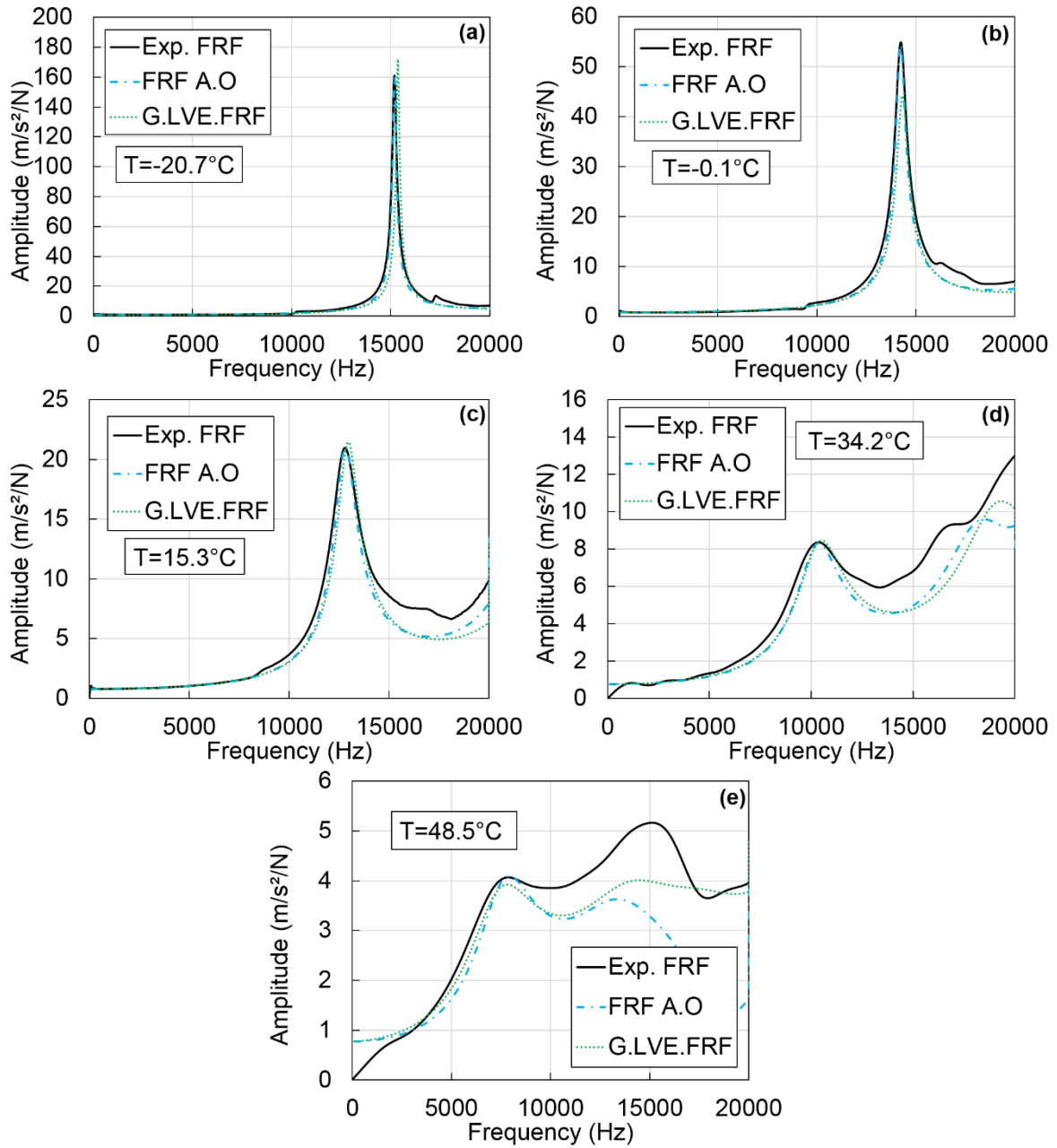


Figure M.1 Comparison of the experimental FRFs (noted Exp. FRF) with the FRFs after optimization (noted FRF A.O) and the global LVE FRFs (noted G.LVE.FRF) obtained with method IV for specimen WF-4. (a) $T=-20.7^{\circ}\text{C}$; (b) -0.1°C ; (c) 15.3°C ; (d) 34.2°C ; (e) 48.5°C .

Table M.2. Values of the four constants E_0 , $\tau_{E15^\circ\text{C}}$, k and δ of the 2S2PID model and of the Poisson's ratio ν determined from the 2nd round of dynamic tests at each temperature in the first step of method V for specimen WF-4.

Temperature (°C)	E_0 (MPa)	$\tau_{E15^\circ\text{C}}$ (s)	k	δ	ν
-20.7	34 741	1.2E-01	0.171	2.17	0.111
-0.1	32 752	1.4E+00	0.170	2.37	0.091
15.3	33 800	1.2E-01	0.172	1.90	0.198
34.2	33 400	1.5E-01	0.192	2.00	0.280
48.5	37 300	1.5E-01	0.192	2.00	0.280

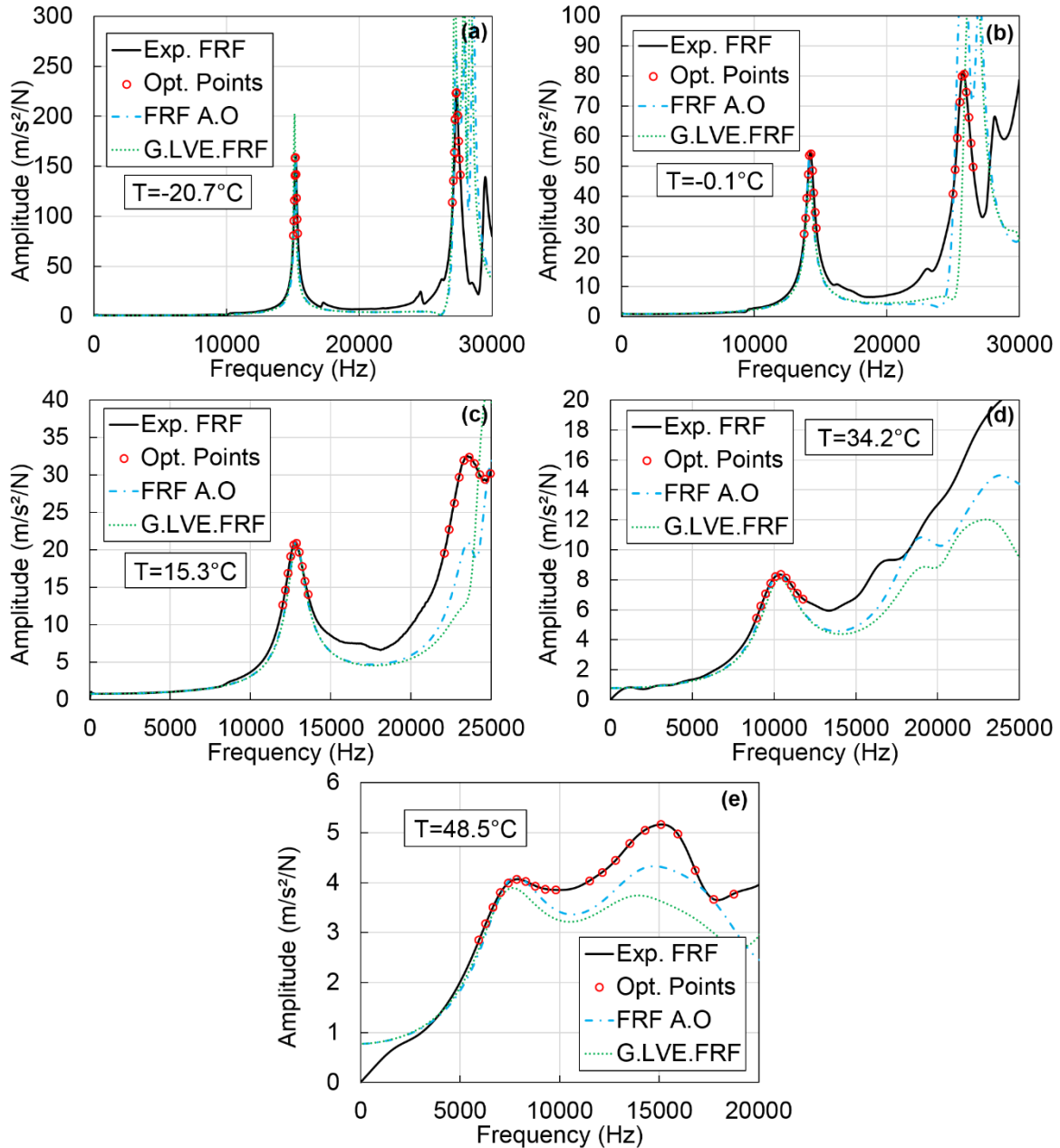


Figure M.2 Comparison of the experimental FRFs (noted Exp. FRF) with the FRFs after optimization (noted FRF A.O.) and the global LVE FRFs (noted G.LVE FRF) obtained with method V for specimen WF-4. Values of the experimental FRFs at the frequencies where the optimization is performed (noted Opt. Points) are also plotted. (a) T=-20.7°C; (b) -0.1°C; (c) 15.3°C; (d) 34.2°C; (e) 48.5°C.

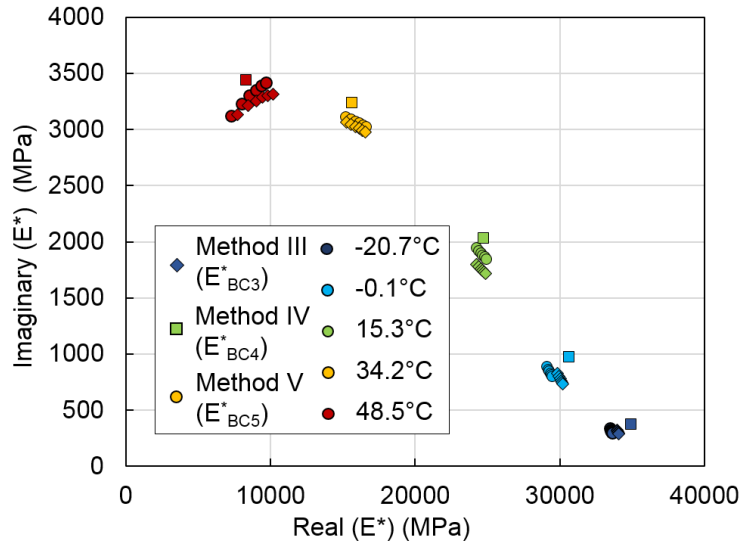


Figure M.3 Comparison of the values of the complex modulus back-calculated from dynamic tests at each temperature with methods III (E^*_{BC3}), IV (E^*_{BC4}) and V (E^*_{BC5}). Results for specimen WF-4.

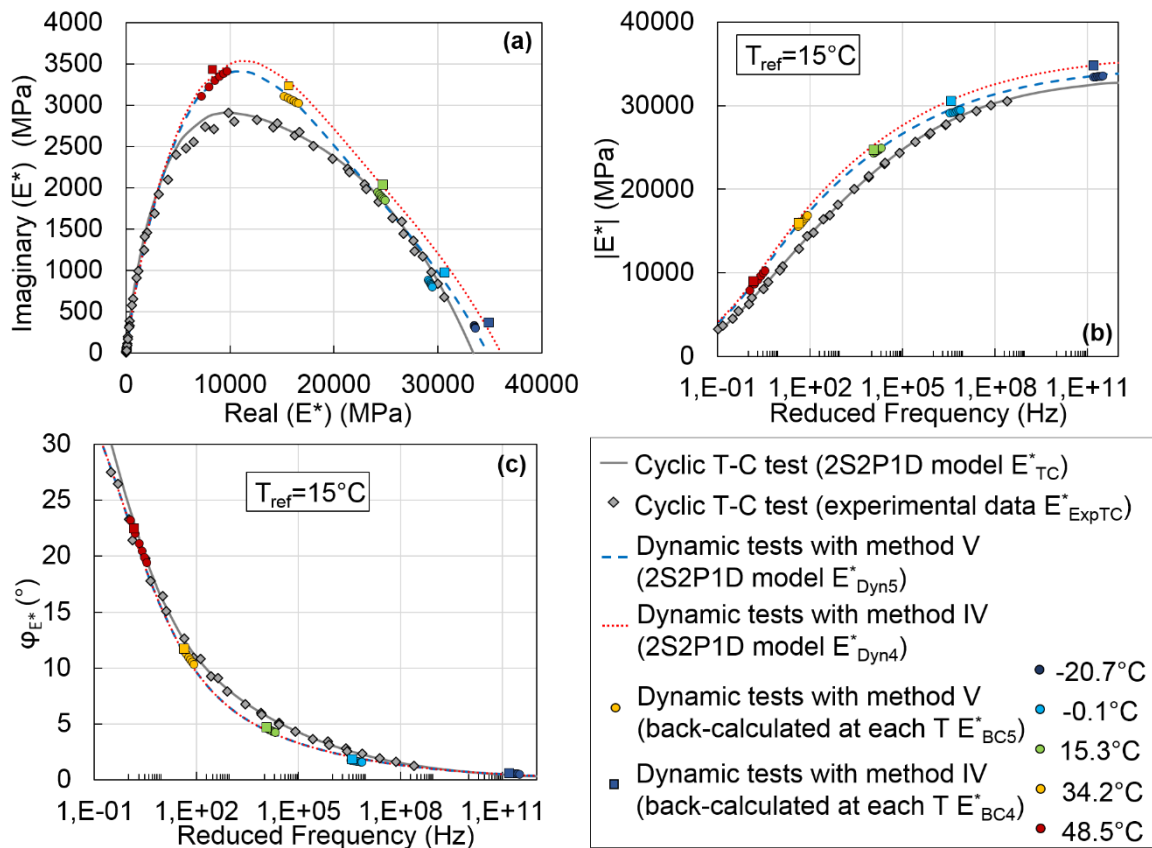


Figure M.4 Comparison of the values of the complex modulus determined from dynamic tests with method IV (E^*_{BC4} and E^*_{Dyn4}) and method V (E^*_{BC5} and E^*_{Dyn5}) with the values of the complex modulus determined from cyclic tests (E^*_{ExpTC} and E^*_{TC}). (a) Cole-Cole plot; (b) and (c) master curves of the norm and of the phase angle of the complex modulus at 15°C. Results for specimen WF-4.

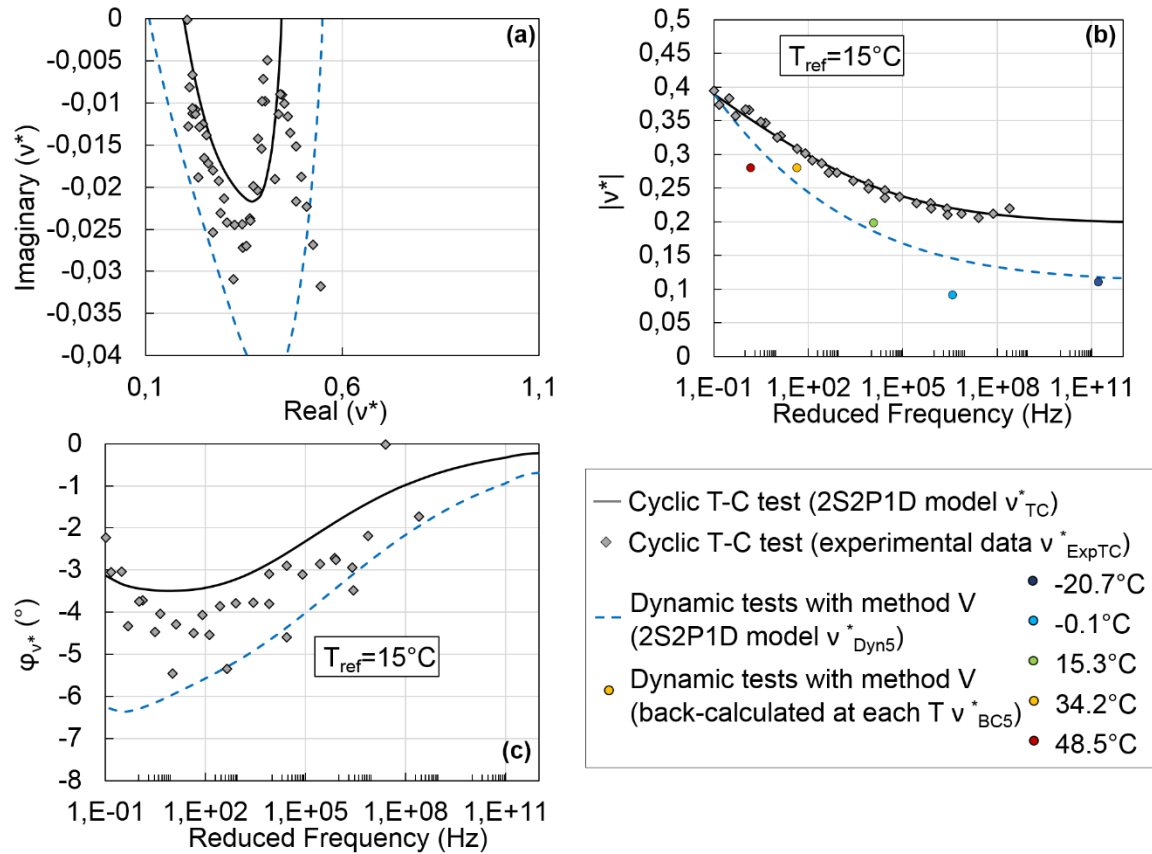


Figure M.5 Comparison of the values of the complex Poisson's ratio determined from dynamic tests with method V (real values v_{BC5} and v^*_{Dyn5}) with the values of the complex Poisson's ratio determined from cyclic test (v^*_{ExpTC} and v^*_{TC}). (a) Cole-Cole plot; (b) and (c) master curves of the norm and of the phase angle of the complex Poisson's ratio at 15°C. Results for specimen WF-4.

SPECIMEN WF-6

Table M.3. First resonance frequency and values of $|E^*_{BC4}|$ and $\varphi_{E^*_{BC4}}$ determined from dynamic tests at each temperature in the first step of method IV for specimen WF-6.

Temperature (°C)	1 st resonance frequency (Hz)	$ E^*_{BC4} $ (MPa)	$\varphi_{E^*_{BC4}}$ (°)
-21.1	15 696	38 037	0.61
-0.3	14 739	33 545	1.8
14.9	13 326	27 412	4.6
34.3	10 688	17 590	11.8
48.8	8 180	10 051	22.2

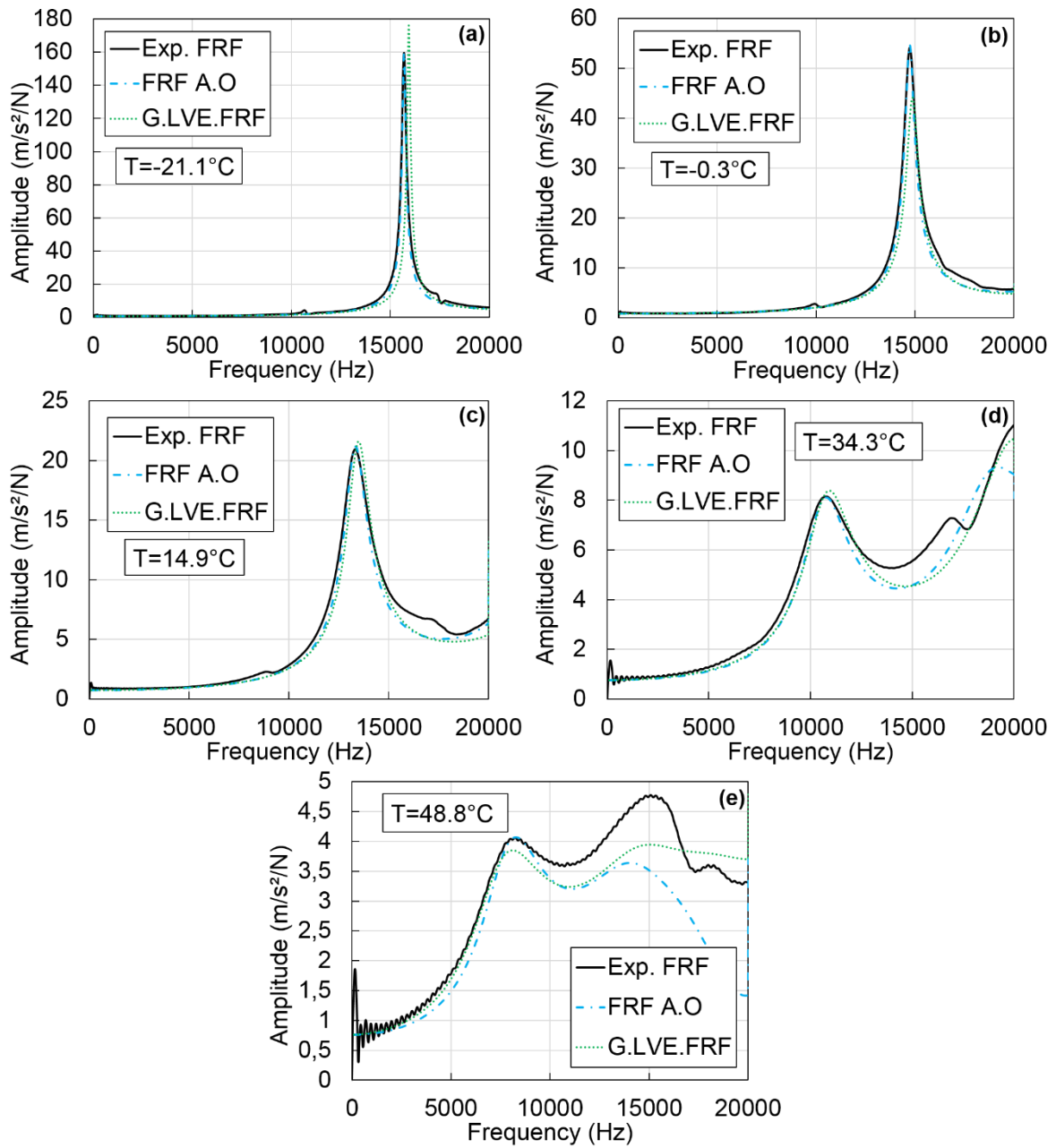


Figure M.6 Comparison of the experimental FRFs (noted Exp. FRF) with the FRFs after optimization (noted FRF A.O) and the global LVE FRFs (noted G.LVE.FRF) obtained with method IV for specimen WF-6. (a) $T=-21.1^{\circ}\text{C}$; (b) -0.3°C ; (c) 14.9°C ; (d) 34.3°C ; (e) 48.8°C .

Table M.4. Values of the four constants E_0 , $\tau_{E15^\circ\text{C}}$, k and δ of the 2S2PID model and of the Poisson's ratio ν determined from the 2nd round of dynamic tests at each temperature in the first step of method V for specimen WF-6.

Temperature (°C)	E_0 (MPa)	$\tau_{E15^\circ\text{C}}$ (s)	k	δ	ν
-21.1	38 995	1.2E-01	0.168	2.37	0.238
-0.3	37 850	7.5E-01	0.149	1.81	0.237
14.9	41 200	3.2E-01	0.143	2.31	0.243
34.3	40 000	1.3E-01	0.185	2.15	0.280
48.8	40 000	1.6E-01	0.184	1.78	0.360

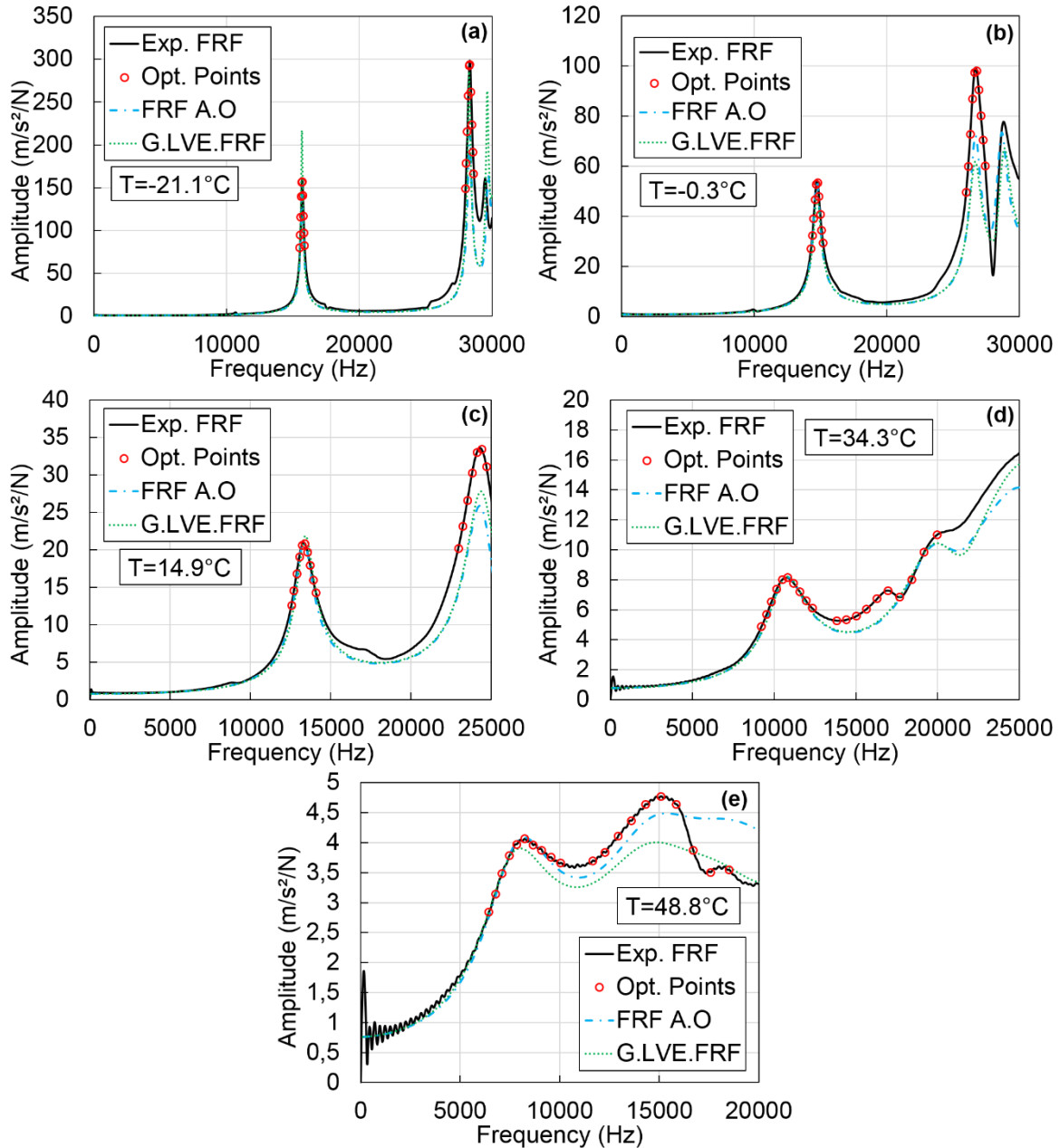


Figure M.7 Comparison of the experimental FRFs (noted Exp. FRF) with the FRFs after optimization (noted FRF A.O) and the global LVE FRFs (noted G.LVE FRF) obtained with method V for specimen WF-6. Values of the experimental FRFs at the frequencies where the optimization is performed (noted Opt. Points) are also plotted. (a) $T=-21.1^\circ\text{C}$; (b) -0.3°C ; (c) 14.9°C ; (d) 34.3°C ; (e) 48.8°C .

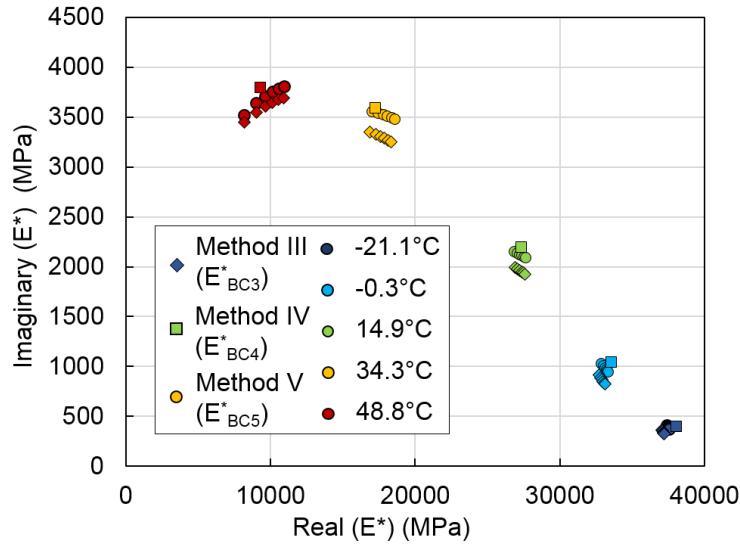


Figure M.8 Comparison of the values of the complex modulus back-calculated from dynamic tests at each temperature with methods III (E^*_{BC3}), IV (E^*_{BC4}) and V (E^*_{BC5}). Results for specimen WF-6.

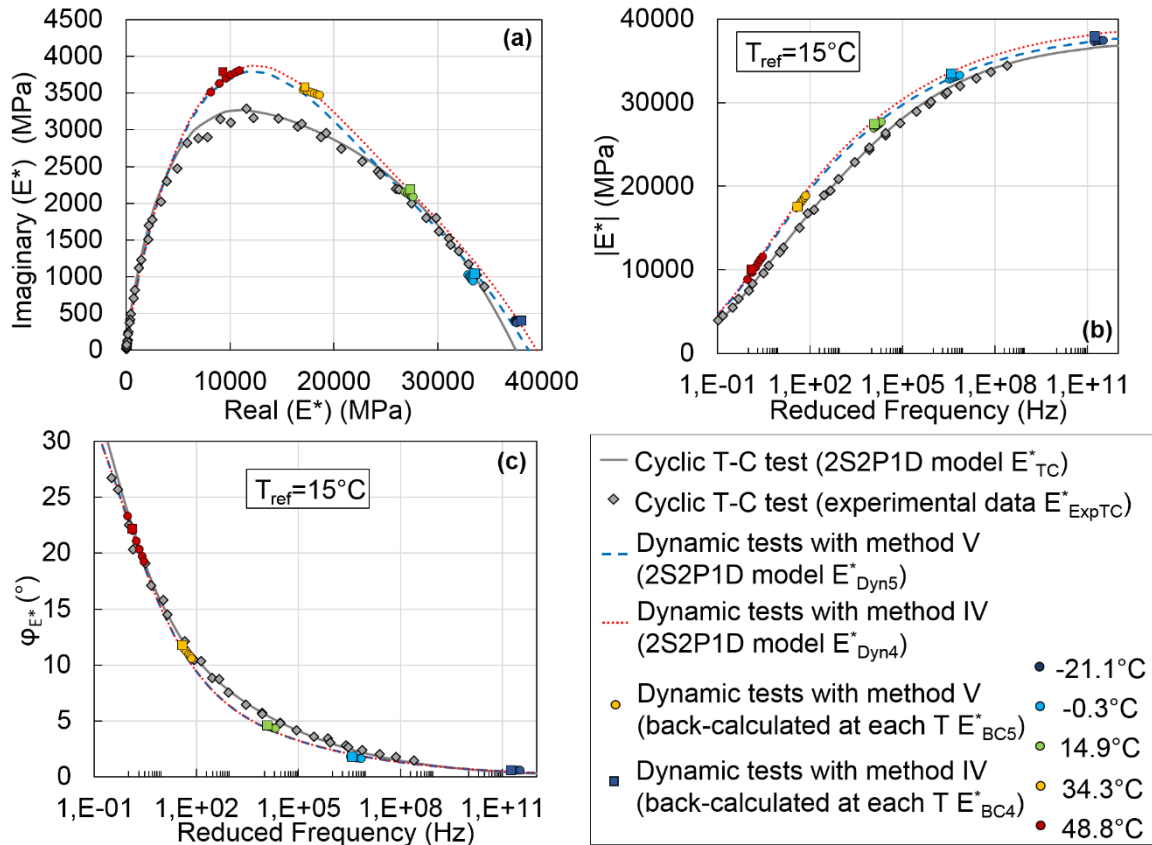


Figure M.9 Comparison of the values of the complex modulus determined from dynamic tests with method IV (E^*_{BC4} and E^*_{Dyn4}) and method V (E^*_{BC5} and E^*_{Dyn5}) with the values of the complex modulus determined from cyclic tests (E^*_{ExpTC} and E^*_{TC}). (a) Cole-Cole plot; (b) and (c) master curves of the norm and of the phase angle of the complex modulus at 15°C. Results for specimen WF-6.

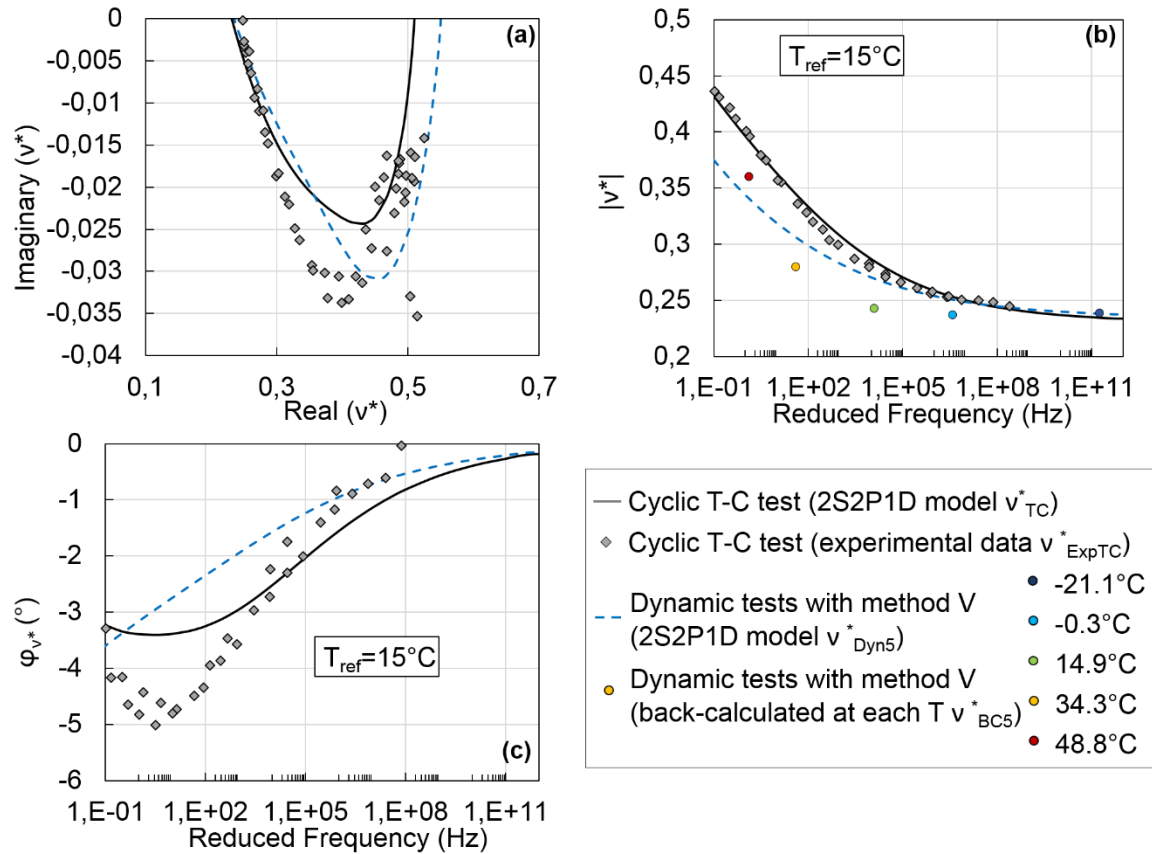


Figure M.10 Comparison of the values of the complex Poisson's ratio determined from dynamic tests with method V (real values v_{BC5} and v_{Dyn5}^*) with the values of the complex Poisson's ratio determined from cyclic test (v_{ExpTC}^* and v_{TC}^*). (a) Cole-Cole plot; (b) and (c) master curves of the norm and of the phase angle of the complex Poisson's ratio at 15°C. Results for specimen WF-6.

SPECIMEN WF-8

Table M.5. First resonance frequency and values of $|E^*_{BC4}|$ and $\varphi_{E^*_{BC4}}$ determined from dynamic tests at each temperature in the first step of method IV for specimen WF-8.

Temperature (°C)	1 st resonance frequency (Hz)	$ E^*_{BC4} $ (MPa)	$\varphi_{E^*_{BC4}}$ (°)
-21	15 468	37 217	0.61
-0.3	14 519	32 793	1.8
15	13 071	26 567	4.8
34.2	10 517	17 153	11.8
48.7	7 990	9 498	22.5

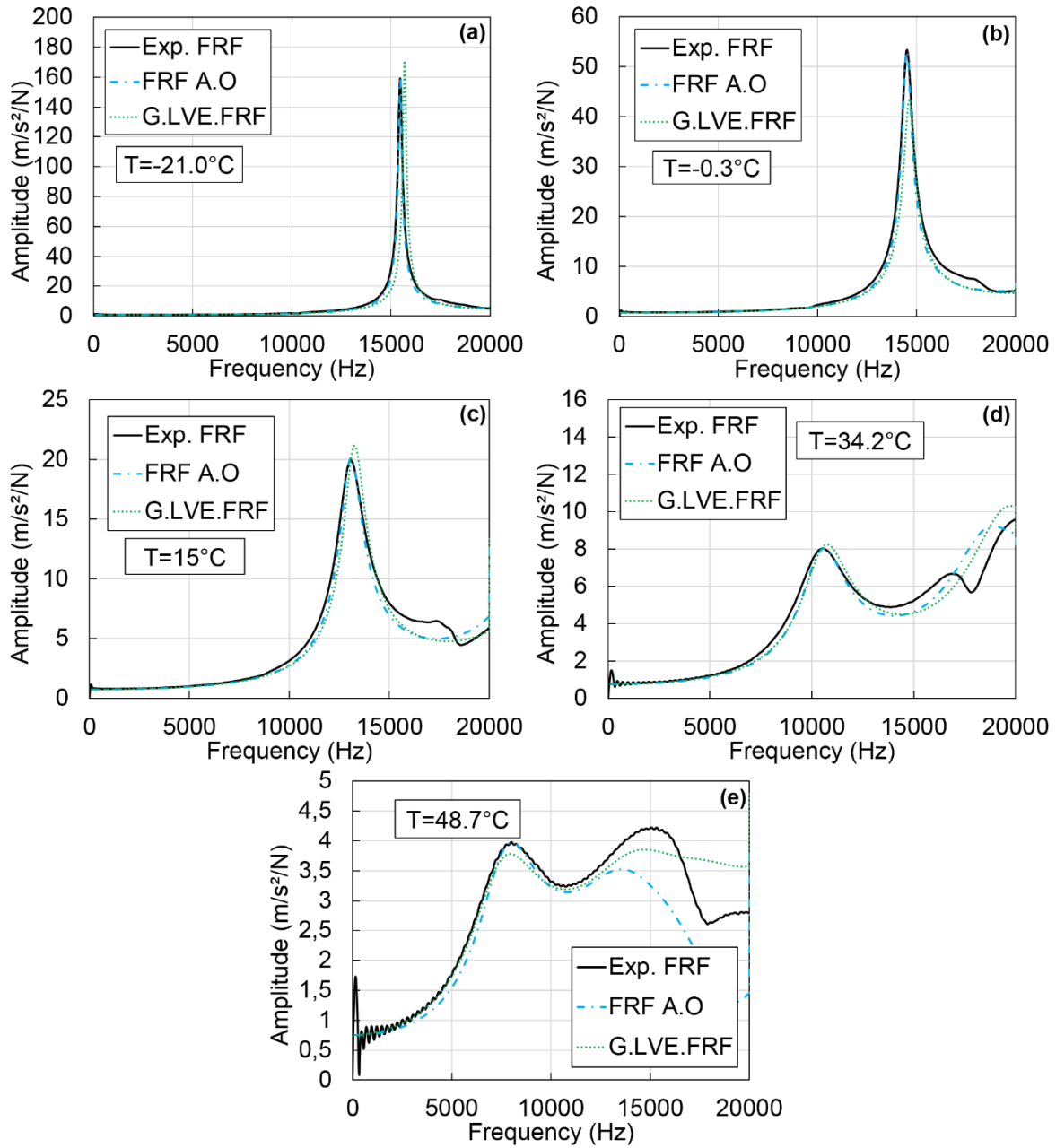


Figure M.11 Comparison of the experimental FRFs (noted Exp. FRF) with the FRFs after optimization (noted FRF A.O) and the global LVE FRFs (noted G.LVE.FRF) obtained with method IV for specimen WF-8. (a) $T=-21^{\circ}\text{C}$; (b) -0.3°C ; (c) 15°C ; (d) 34.2°C ; (e) 48.7°C .

Table M.6. Values of the four constants E_0 , $\tau_{E15^\circ\text{C}}$, k and δ of the 2S2PID model and of the Poisson's ratio ν determined from the 2nd round of dynamic tests at each temperature in the first step of method V for specimen WF-8.

Temperature (°C)	E_0 (MPa)	$\tau_{E15^\circ\text{C}}$ (s)	k	δ	ν
-21	37 344	4.5E-02	0.188	2.40	0.205
-0.3	35 613	4.5E-01	0.188	2.39	0.184
15	36 558	2.5E-01	0.174	2.31	0.210
34.2	37 158	1.1E-01	0.183	1.94	0.240
48.7	37 762	1.7E-01	0.199	1.84	0.300

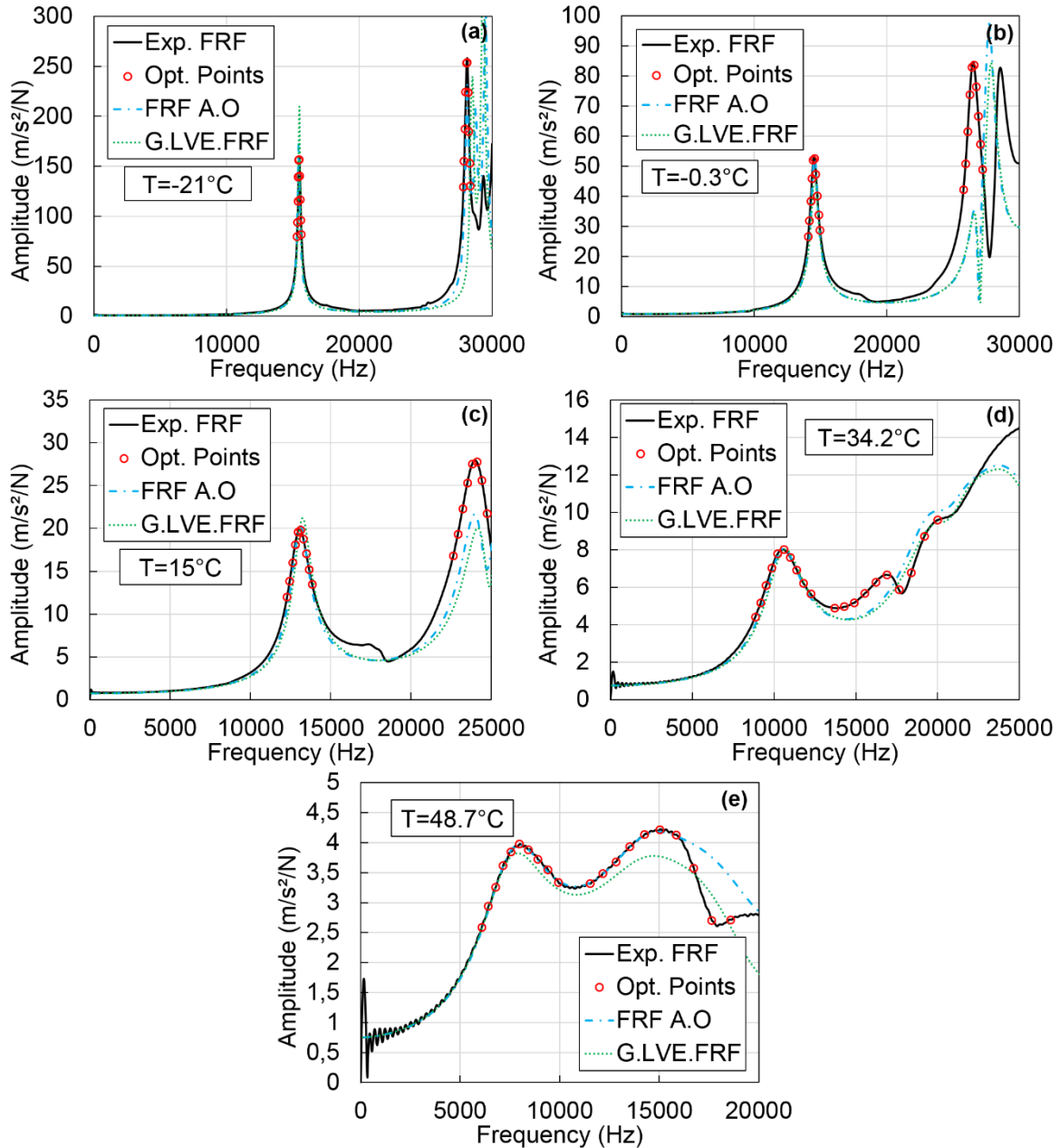


Figure M.12 Comparison of the experimental FRFs (noted Exp. FRF) with the FRFs after optimization (noted FRF A.O) and the global LVE FRFs (noted G.LVE FRF) obtained with method V for specimen WF-8. Values of the experimental FRFs at the frequencies where the optimization is performed (noted Opt. Points) are also plotted. (a) $T=-21^\circ\text{C}$; (b) -0.3°C ; (c) 15°C ; (d) 34.2°C ; (e) 48.7°C .

**APPENDIX N - RESULTS OF THE MAP
EXPERIMENTAL CAMPAIGN**

SPECIMEN GB-L-1

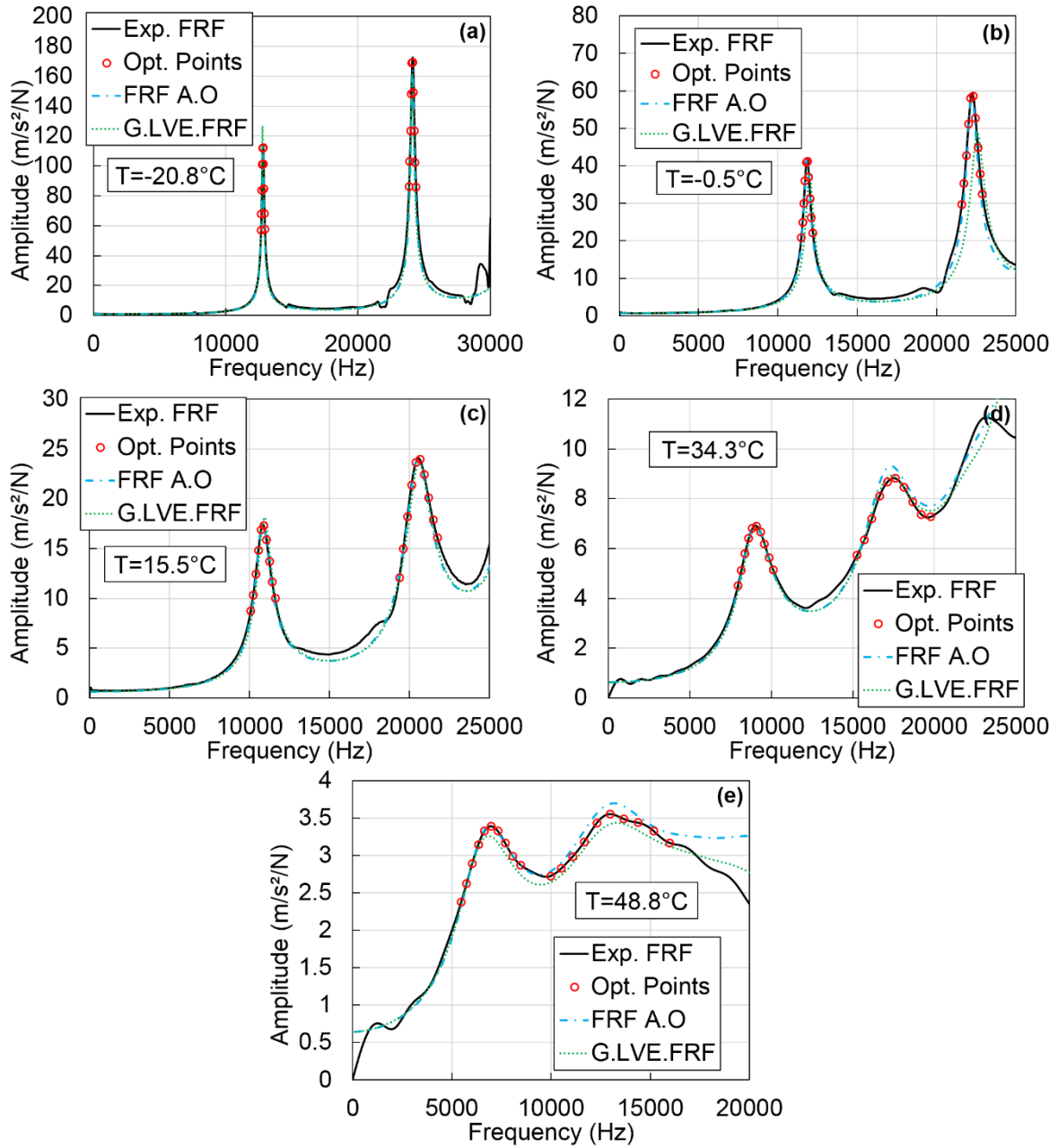


Figure N.1 Comparison of the experimental FRFs measured at the end of the project (noted *Exp. FRF*) with the FRFs after optimization (noted *FRF A.O*) and the global LVE FRFs (noted *G.LVE FRF*) for specimen GB-L-1. Values of the experimental FRFs at the frequencies where the optimization is performed (noted *Opt. Points*) are also plotted. (a) $T = -20.8^{\circ}\text{C}$; (b) -0.5°C ; (c) 15.5°C ; (d) 34.3°C ; (e) 48.8°C .

Table N.1. Values of the four constants E_0 , $\tau_{E15^\circ\text{C}}$, k and δ of the 2S2P1D model and of the Poisson's ratio ν determined from dynamic tests at each temperature in the first step of method V for specimen GB-L-1.

Temperature ($^\circ\text{C}$)	E_0 (MPa)	$\tau_{E15^\circ\text{C}}$ (s)	k	δ	ν
-20.8	39 259	3.8E-03	0.191	1.92	0.301
-0.5	37 840	2.9E+00	0.142	2.18	0.327
15.5	41 459	9.0E-02	0.137	1.71	0.333
34.3	41 650	1.7E-01	0.178	2.04	0.385
48.8	41 549	2.6E-01	0.207	1.87	0.497

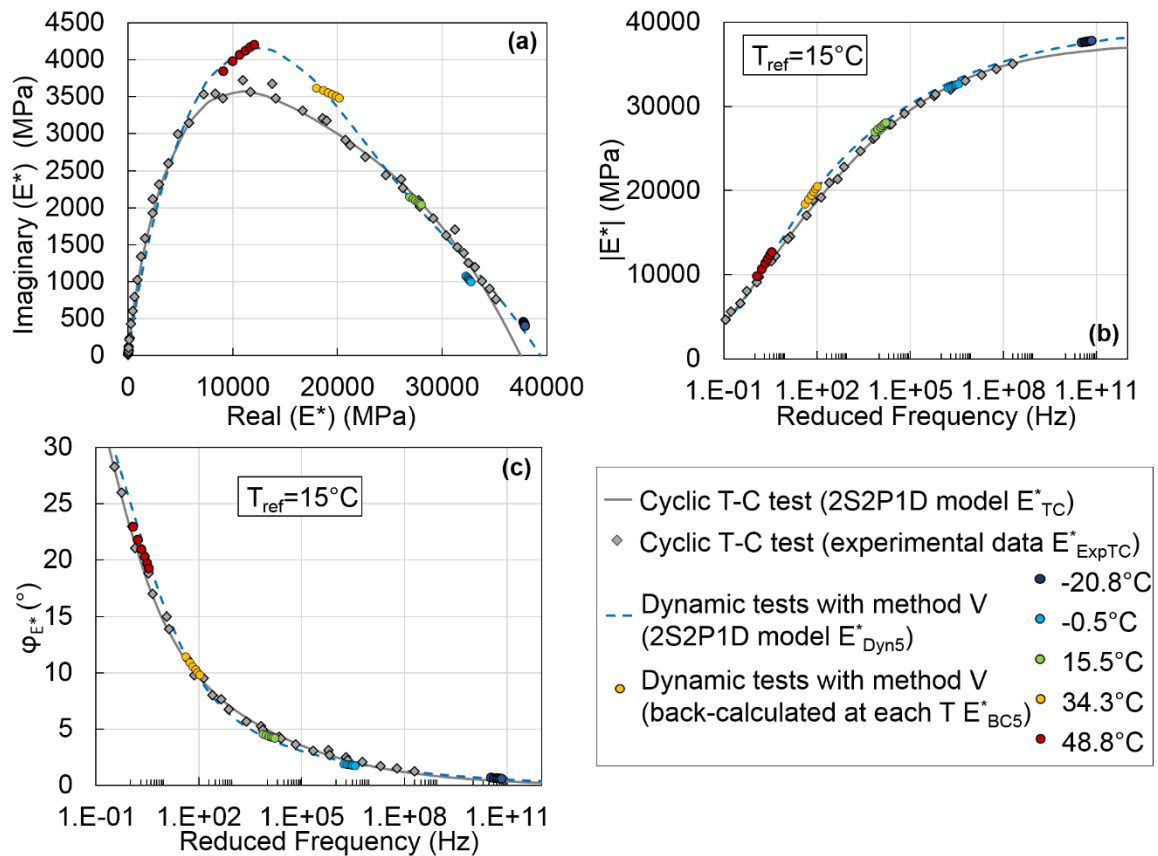


Figure N.2 Comparison of the values of the complex modulus determined from dynamic tests with method V (E_{BC5}^* and E_{Dyn5}^*) with the values of the complex modulus determined from cyclic tests (E_{ExpTC}^* and E_{TC}^*). (a) Cole-Cole plot; (b) and (c) master curves of the norm and of the phase angle of the complex modulus at 15°C . Results for specimen GB-L-1.

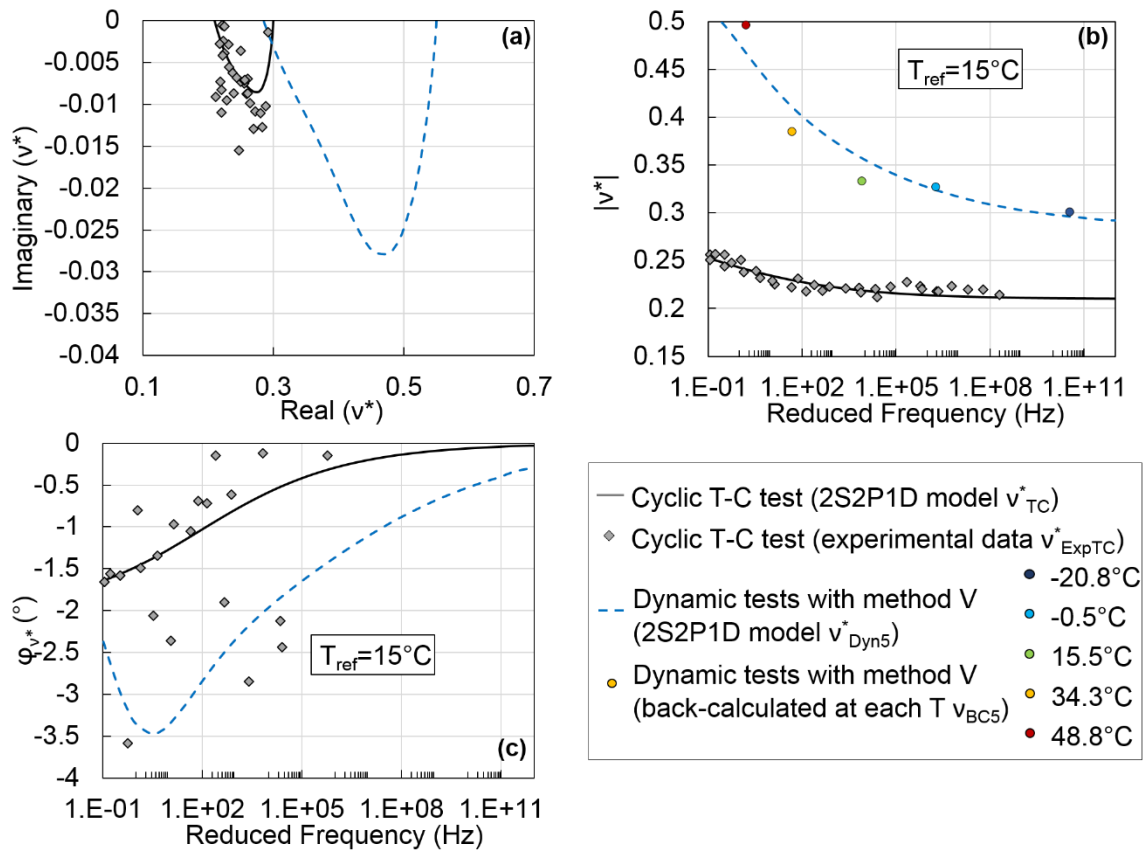


Figure N.3 Comparison of the values of the complex Poisson's ratio determined from dynamic tests with method V (real values v_{BC5} and v^*_{Dyn5}) with the values of the complex Poisson's ratio determined from cyclic test (v^*_{ExpTC} and v^*_{TC}). (a) Cole-Cole plot; (b) and (c) master curves of the norm and of the phase angle of the complex Poisson's ratio at 15°C . Results for specimen GB-L-1.

SPECIMEN GB-L-2

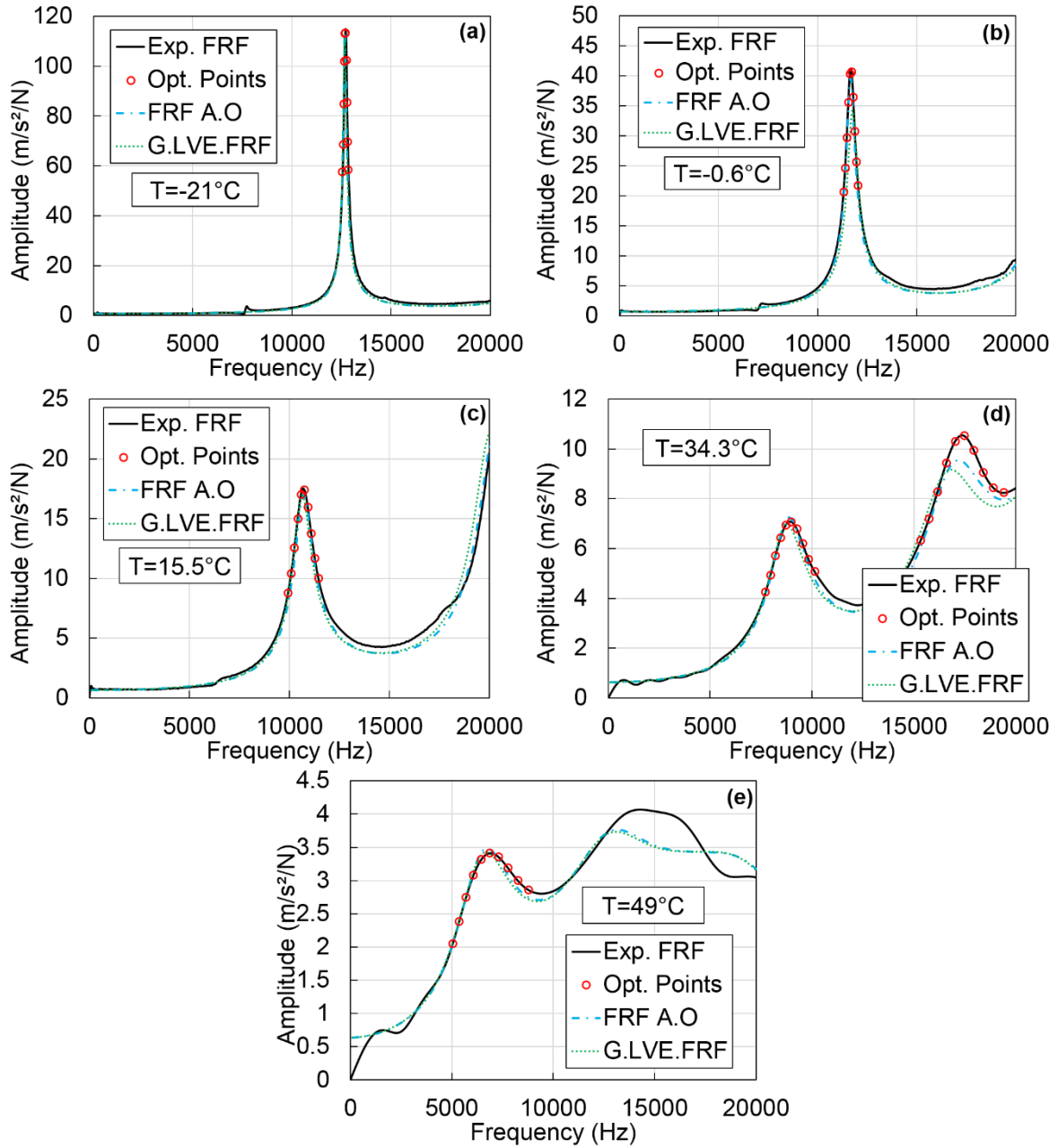


Figure N.4 Comparison of the experimental FRFs (noted Exp. FRF) with the FRFs after optimization (noted FRF A.O) and the global LVE FRFs (noted G.LVE FRF) for specimen GB-L-2. Values of the experimental FRFs at the frequencies where the optimization is performed (noted Opt. Points) are also plotted. (a) $T=-21^{\circ}\text{C}$; (b) -0.6°C ; (c) 15.5°C ; (d) 34.3°C ; (e) 49°C .

Table N.2. Values of the four constants E_0 , $\tau_{E15^\circ\text{C}}$, k and δ of the 2S2P1D model determined from dynamic tests at each temperature in the first step of method III for specimen GB-L-2.

Temperature ($^\circ\text{C}$)	E_0 (MPa)	$\tau_{E15^\circ\text{C}}$ (s)	k	δ
-21	37 874	4.5E-02	0.172	2.16
-0.6	34 940	5.1E-01	0.181	2.49
15.5	34 647	6.7E-02	0.187	1.56
34.3	30 408	4.5E-01	0.234	1.83
49	40 886	2.4E-01	0.177	1.97

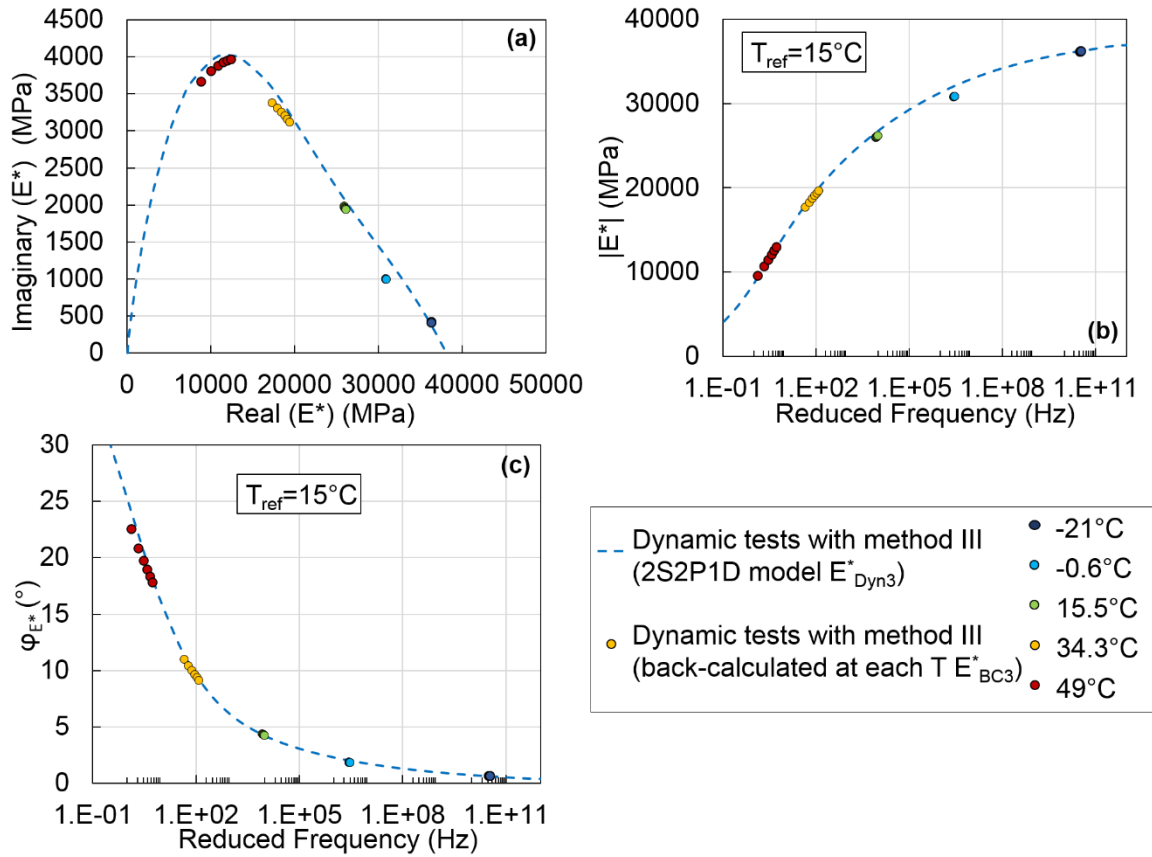


Figure N.5 Values of the complex modulus determined from dynamic tests with method III (E^*_{BC3} and E^*_{Dyn3}). (a) Cole-Cole plot; (b) and (c) master curves of the norm and of the phase angle of the complex modulus at 15°C . Results for specimen GB-L-2.

SPECIMEN GB-L-3

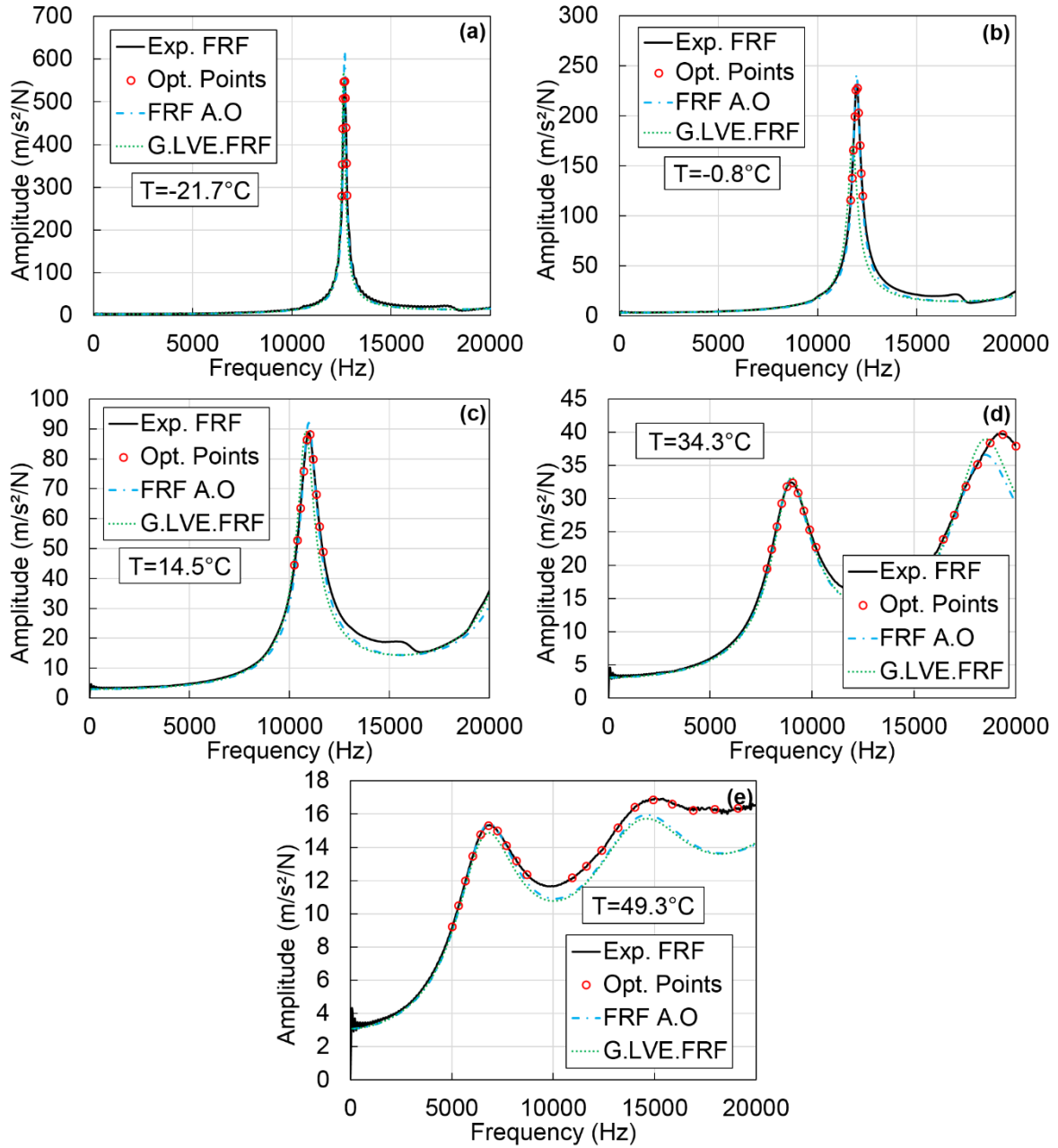


Figure N.6 Comparison of the experimental FRFs (noted Exp. FRF) with the FRFs after optimization (noted FRF A.O) and the global LVE FRFs (noted G.LVE FRF) for specimen GB-L-3. Values of the experimental FRFs at the frequencies where the optimization is performed (noted Opt. Points) are also plotted. (a) $T=-21.7^{\circ}\text{C}$; (b) -0.8°C ; (c) 14.5°C ; (d) 34.3°C ; (e) 49.3°C .

Table N.3. Values of the four constants E_0 , $\tau_{E15^\circ\text{C}}$, k and δ of the 2S2P1D model determined from dynamic tests at each temperature in the first step of method III for specimen GB-L-3.

Temperature ($^\circ\text{C}$)	E_0 (MPa)	$\tau_{E15^\circ\text{C}}$ (s)	k	δ
-21.7	36 206	9.4E-02	0.172	2.22
-0.8	34 085	5.2E-01	0.193	2.13
14.5	34 691	4.8E-01	0.168	1.96
34.3	39 010	2.1E-01	0.172	2.12
49.3	40 219	2.2E-01	0.179	1.83

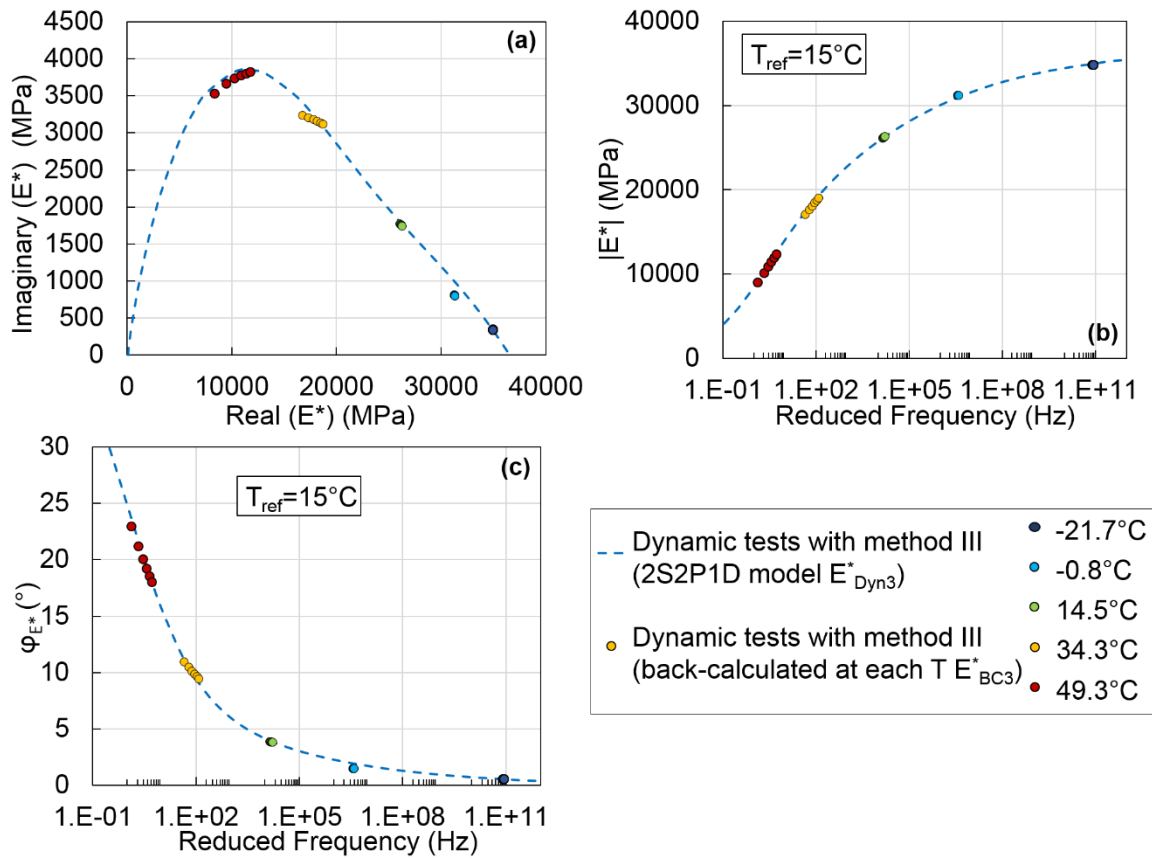


Figure N.7 Values of the complex modulus determined from dynamic tests with method III (E^*_{BC3} and E^*_{Dyn3}). (a) Cole-Cole plot; (b) and (c) master curves of the norm and of the phase angle of the complex modulus at 15°C . Results for specimen GB-L-3.

SPECIMEN GB-L-4

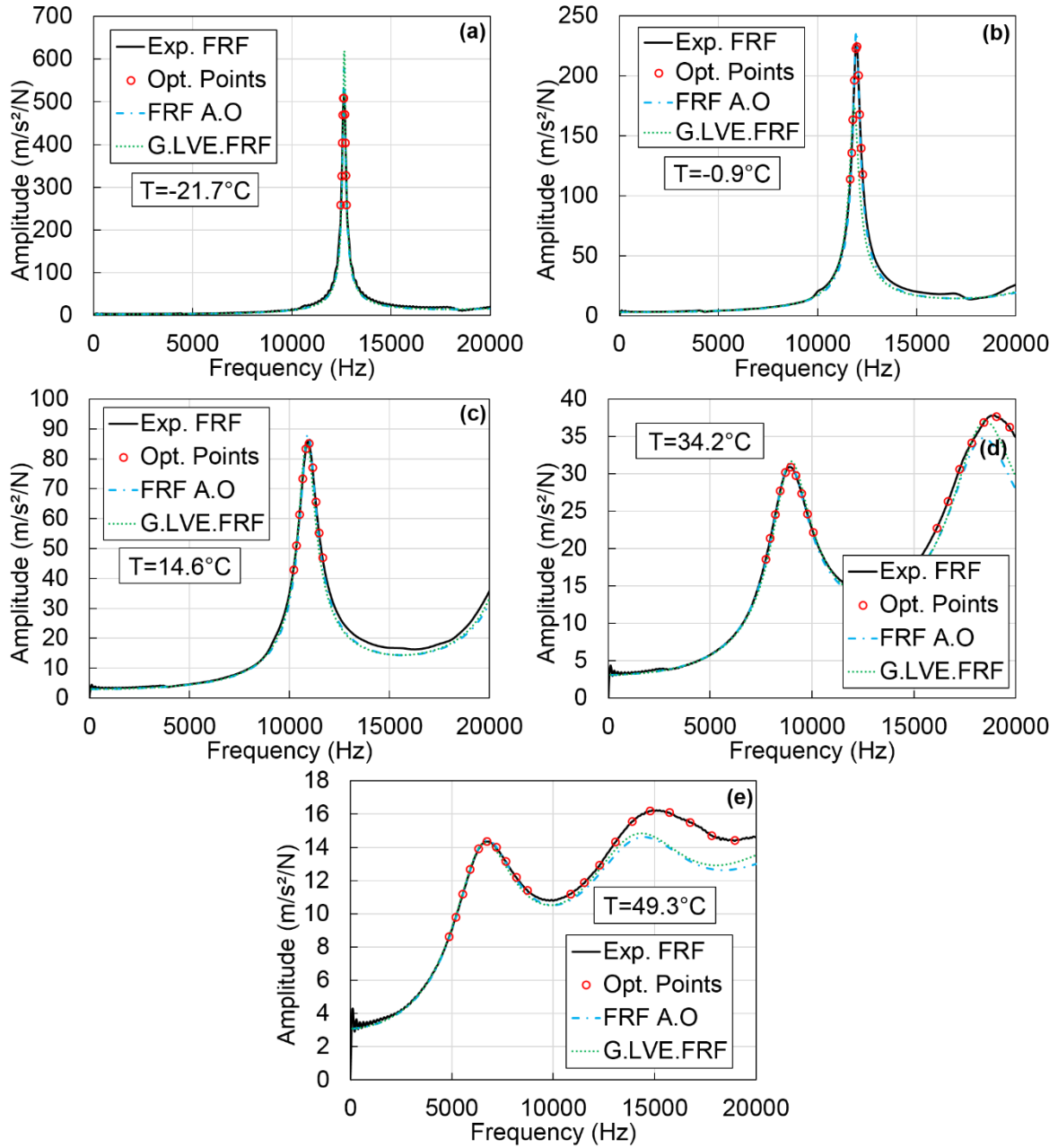


Figure N.8 Comparison of the experimental FRFs (noted Exp. FRF) with the FRFs after optimization (noted FRF A.O) and the global LVE FRFs (noted G.LVE FRF) for specimen GB-L-4. Values of the experimental FRFs at the frequencies where the optimization is performed (noted Opt. Points) are also plotted. (a) $T=-21.7^{\circ}\text{C}$; (b) -0.9°C ; (c) 14.6°C ; (d) 34.2°C ; (e) 49.3°C .

Table N.4. Values of the four constants E_0 , $\tau_{E15^\circ\text{C}}$, k and δ of the 2S2P1D model determined from dynamic tests at each temperature in the first step of method III for specimen GB-L-4.

Temperature ($^\circ\text{C}$)	E_0 (MPa)	$\tau_{E15^\circ\text{C}}$ (s)	k	δ
-21.7	36 272	2.0E-02	0.174	1.89
-0.9	34 331	8.7E-01	0.186	2.23
14.6	33 727	2.9E-01	0.188	1.98
34.2	37 766	1.8E-01	0.183	2.04
49.3	38 586	2.0E-01	0.195	1.66

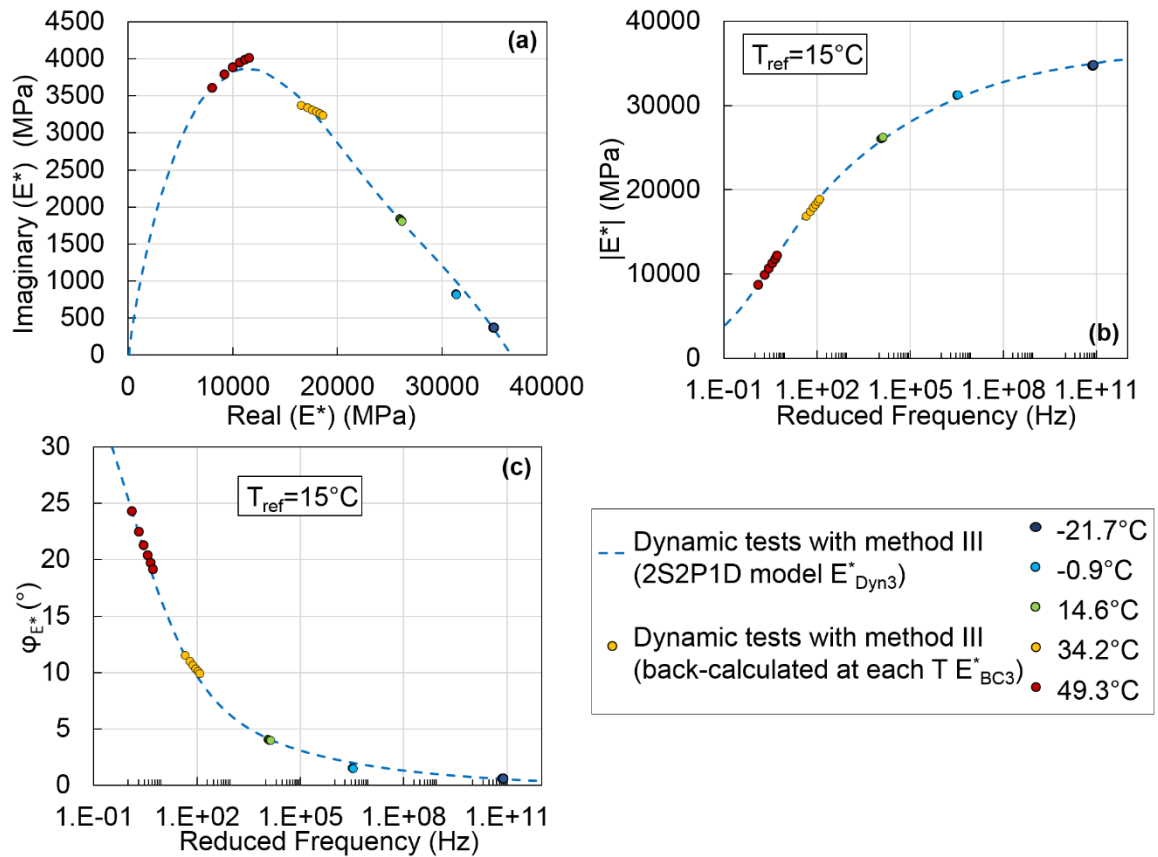


Figure N.9 Values of the complex modulus determined from dynamic tests with method III (E^*_{BC3} and E^*_{Dyn3}). (a) Cole-Cole plot; (b) and (c) master curves of the norm and of the phase angle of the complex modulus at 15°C . Results for specimen GB-L-4.

SPECIMEN GB-L-5

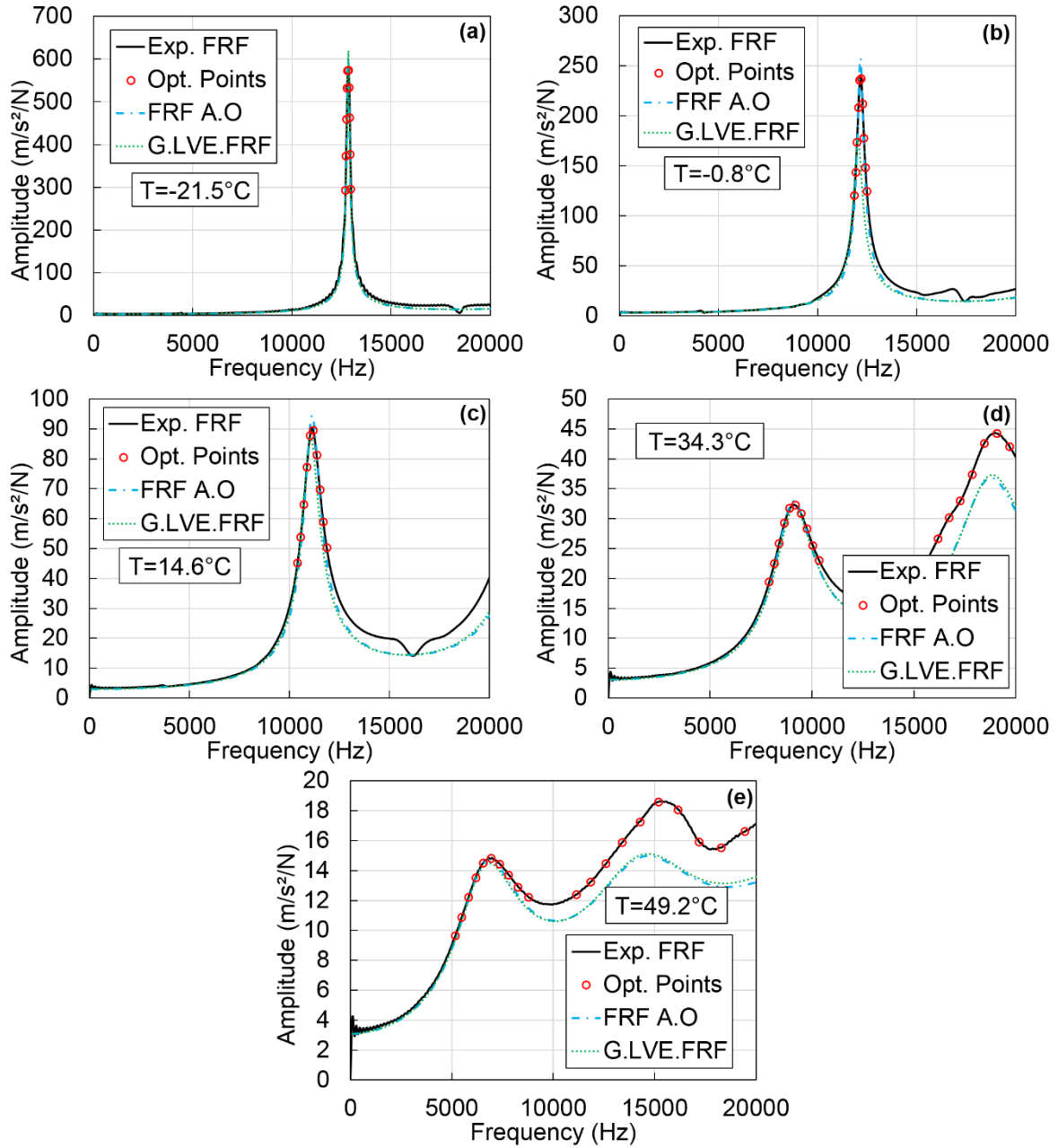


Figure N.10 Comparison of the experimental FRFs (noted Exp. FRF) with the FRFs after optimization (noted FRF A.O) and the global LVE FRFs (noted G.LVE FRF) for specimen GB-L-5. Values of the experimental FRFs at the frequencies where the optimization is performed (noted Opt. Points) are also plotted. (a) $T=-21.5^{\circ}\text{C}$; (b) -0.8°C ; (c) 14.6°C ; (d) 34.3°C ; (e) 49.3°C .

Table N.5. Values of the four constants E_0 , $\tau_{E15^\circ\text{C}}$, k and δ of the 2S2P1D model determined from dynamic tests at each temperature in the first step of method III for specimen GB-L-5.

Temperature ($^\circ\text{C}$)	E_0 (MPa)	$\tau_{E15^\circ\text{C}}$ (s)	k	δ
-21.5	36 921	1.1E-01	0.170	2.21
-0.8	34 716	1.1E+00	0.190	2.23
14.6	33 559	3.8E-01	0.196	1.99
34.3	37 485	2.4E-01	0.183	2.03
49.3	41 347	1.9E-01	0.186	1.80

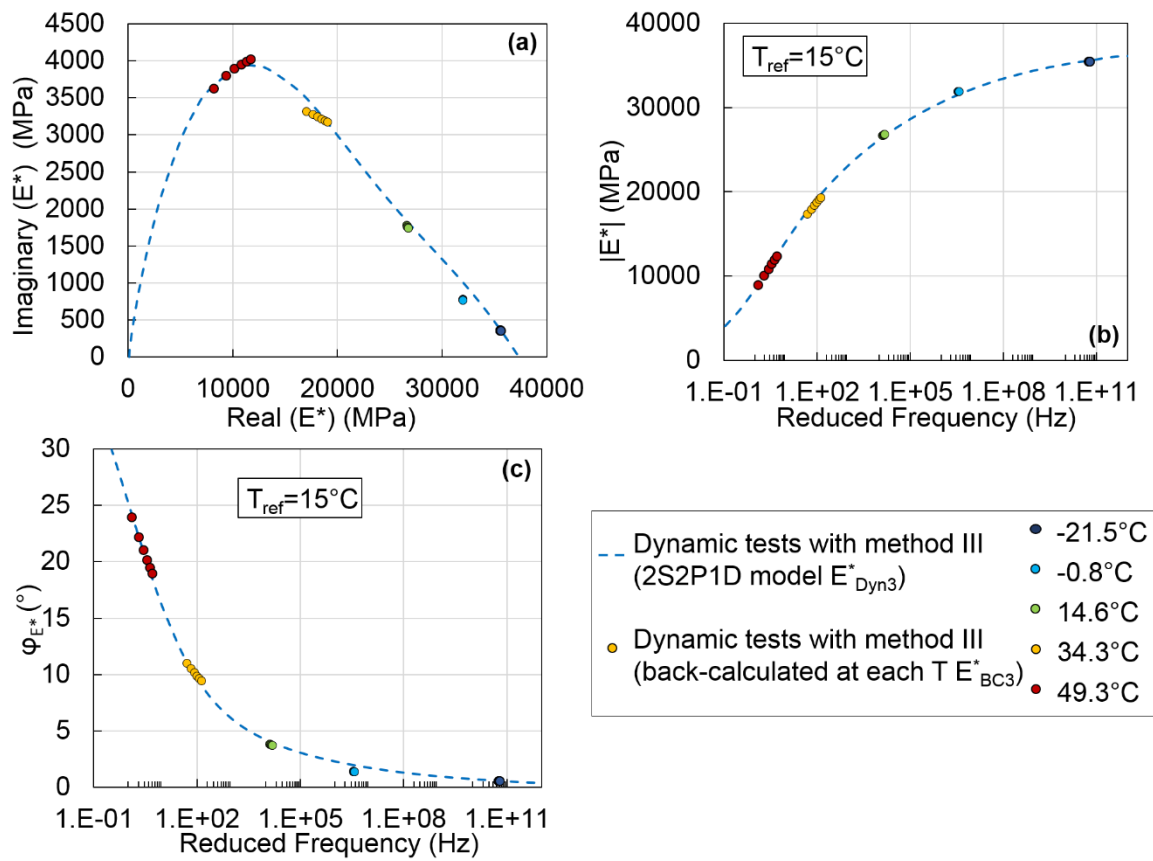


Figure N.11 Values of the complex modulus determined from dynamic tests with method III (E^*_{BC3} and E^*_{Dyn3}). (a) Cole-Cole plot; (b) and (c) master curves of the norm and of the phase angle of the complex modulus at 15°C . Results for specimen GB-L-5.

SPECIMEN GB'-L-1

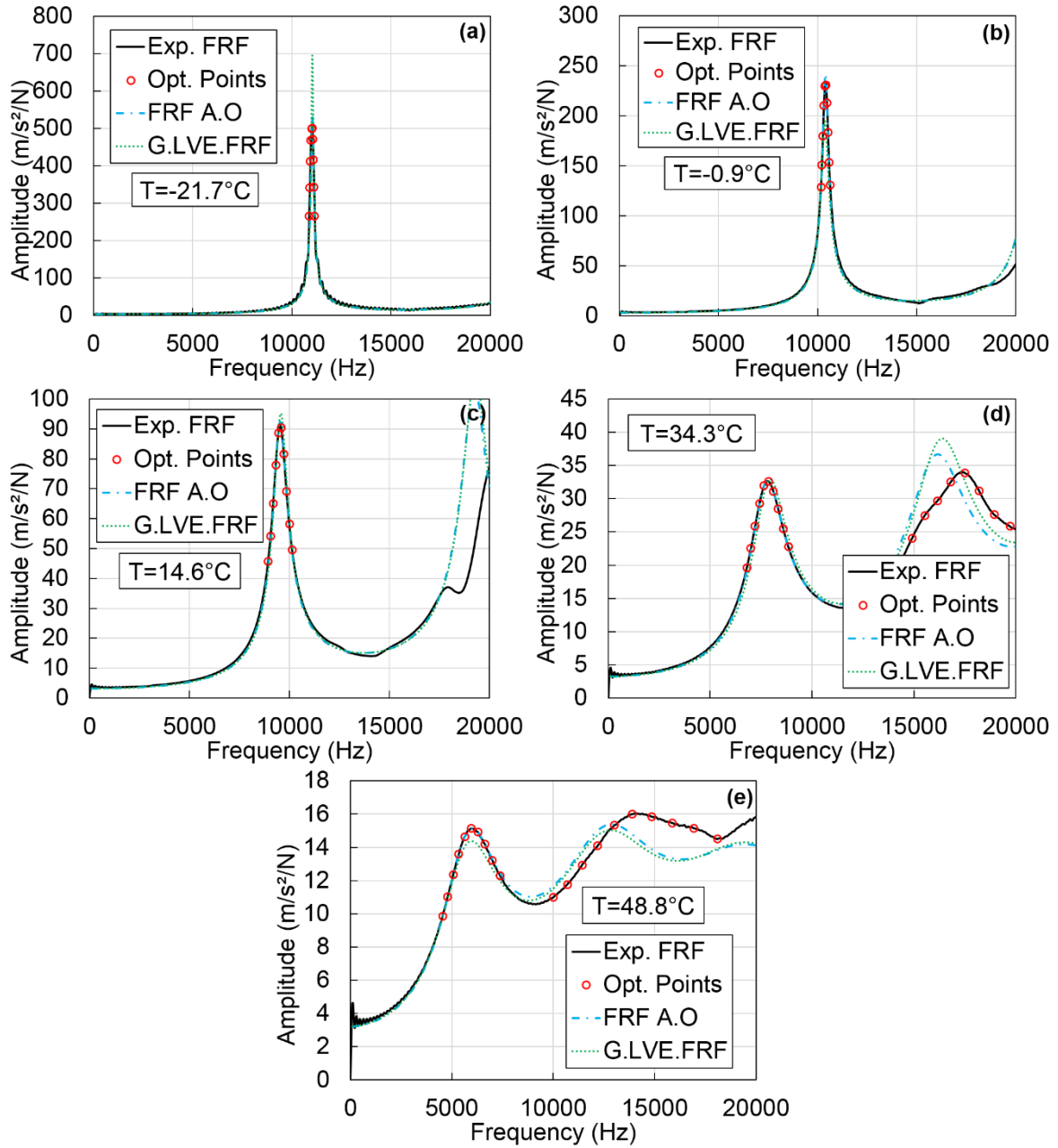


Figure N.12 Comparison of the experimental FRFs (noted Exp. FRF) with the FRFs after optimization (noted FRF A.O.) and the global LVE FRFs (noted G.LVE FRF) for specimen GB'-L-1. Values of the experimental FRFs at the frequencies where the optimization is performed (noted Opt. Points) are also plotted. (a) $T = -21.7^{\circ}\text{C}$; (b) -0.9°C ; (c) 14.6°C ; (d) 34.3°C ; (e) 48.8°C .

Table N.6. Values of the four constants E_0 , $\tau_{E15^\circ C}$, k and δ of the 2S2P1D model determined from dynamic tests at each temperature in the first step of method III for specimen GB'-L-1.

Temperature ($^\circ\text{C}$)	E_0 (MPa)	$\tau_{E15^\circ C}$ (s)	k	δ
-21.7	26 537	5.1E-02	0.169	2.29
-0.9	25 002	3.9E+00	0.174	2.58
14.6	25 582	1.3E+00	0.168	2.45
34.3	27 654	1.7E-01	0.178	1.91
48.8	28 732	2.0E-01	0.192	1.61

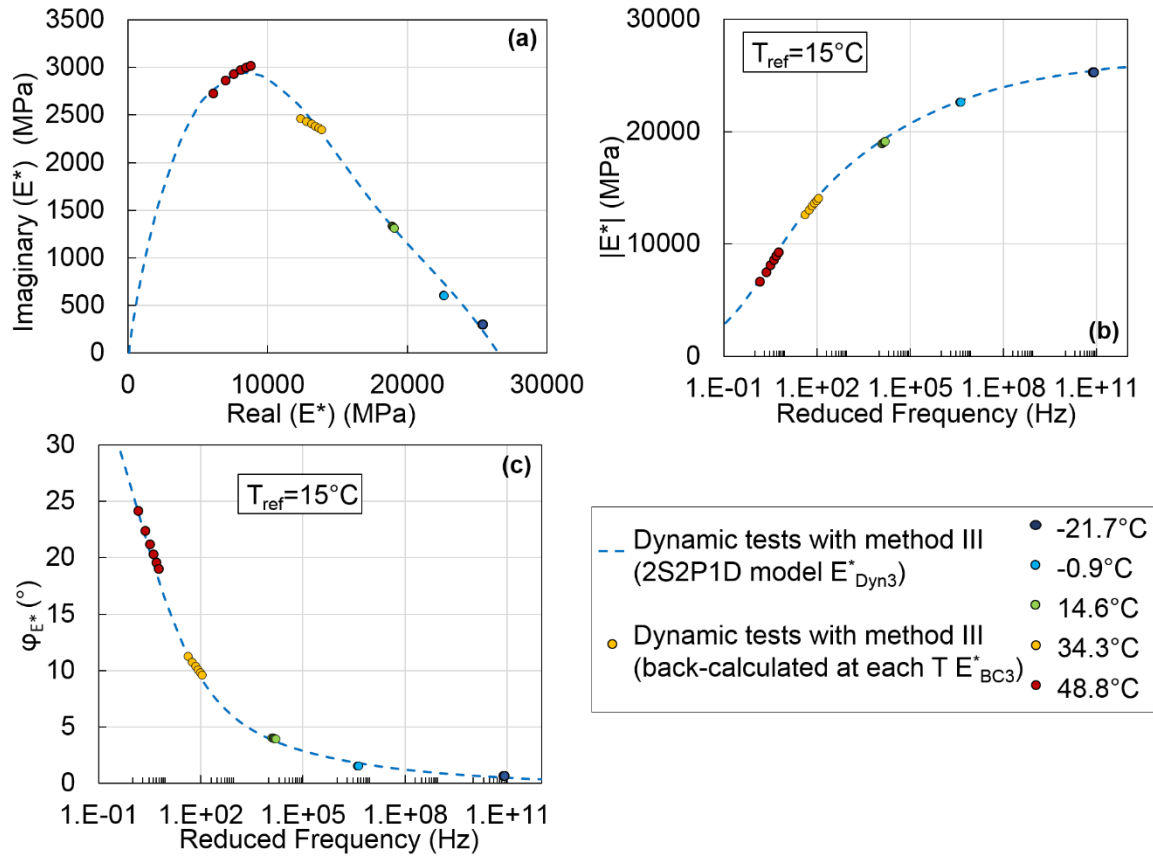


Figure N.13 Values of the complex modulus determined from dynamic tests with method III (E_{BC3}^* and E_{Dyn3}^*). (a) Cole-Cole plot; (b) and (c) master curves of the norm and of the phase angle of the complex modulus at 15°C . Results for specimen GB'-L-1.

SPECIMEN GB'-L-2

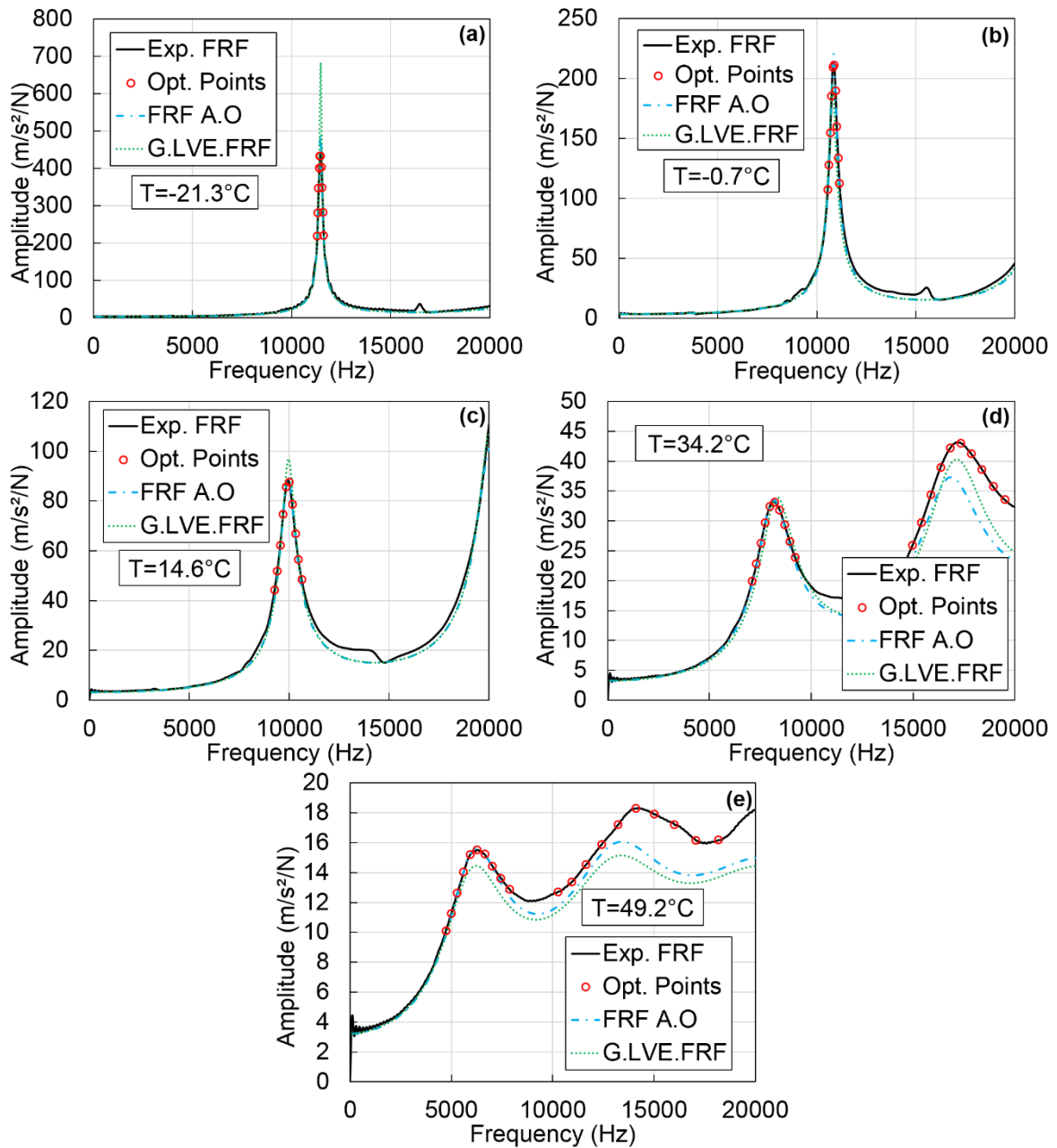


Figure N.14 Comparison of the experimental FRFs (noted Exp. FRF) with the FRFs after optimization (noted FRF A.O) and the global LVE FRFs (noted G.LVE FRF) for specimen GB'-L-2. Values of the experimental FRFs at the frequencies where the optimization is performed (noted Opt. Points) are also plotted. (a) $T=-21.3^{\circ}\text{C}$; (b) -0.7°C ; (c) 14.6°C ; (d) 34.2°C ; (e) 49.2°C .

Table N.7. Values of the four constants E_0 , $\tau_{E15^\circ\text{C}}$, k and δ of the 2S2P1D model determined from dynamic tests at each temperature in the first step of method III for specimen GB'-L-2.

Temperature ($^\circ\text{C}$)	E_0 (MPa)	$\tau_{E15^\circ\text{C}}$ (s)	k	δ
-21.3	28 533	1.9E-02	0.168	2.00
-0.7	26 873	2.6E-01	0.195	2.15
14.6	27 249	4.6E-01	0.177	2.14
34.2	29 993	1.9E-01	0.178	2.01
49.2	31 244	2.2E-01	0.184	1.68

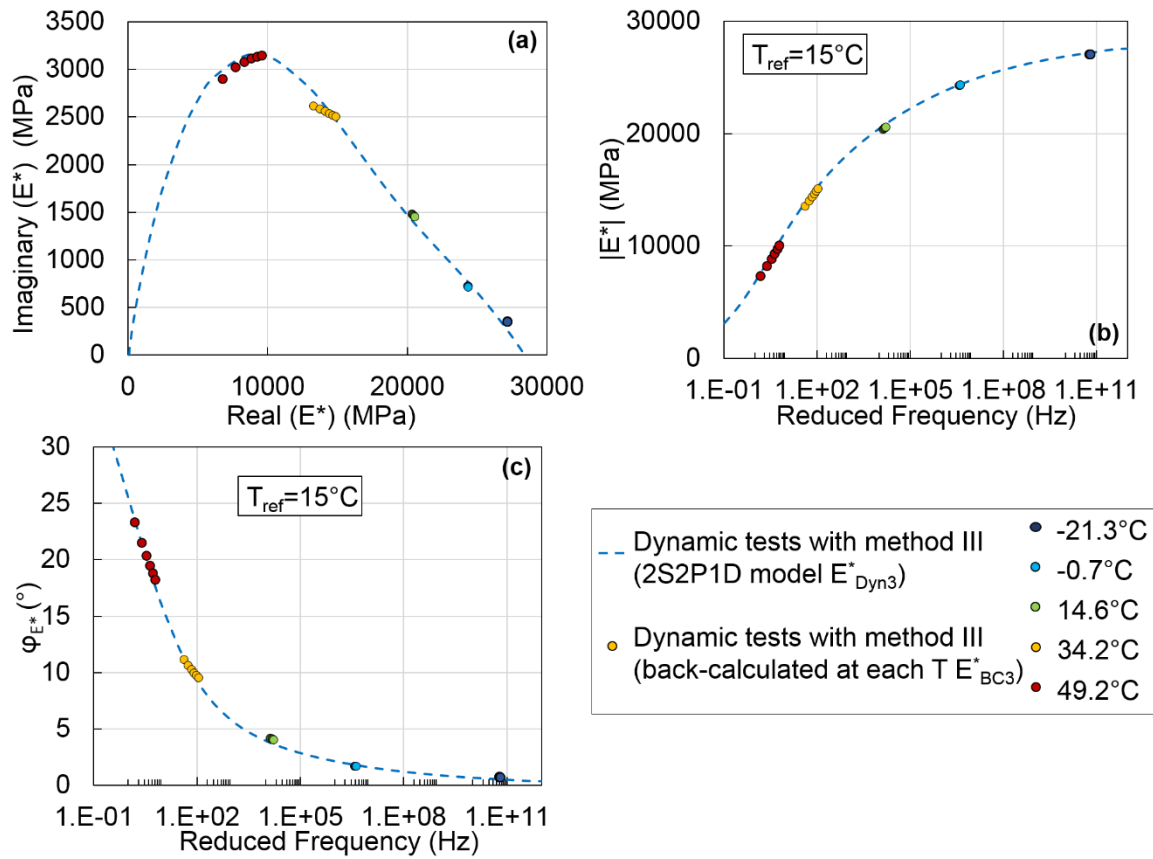


Figure N.15 Values of the complex modulus determined from dynamic tests with method III (E^*_{BC3} and E^*_{Dyn3}). (a) Cole-Cole plot; (b) and (c) master curves of the norm and of the phase angle of the complex modulus at 15°C . Results for specimen GB'-L-2.

SPECIMEN GB'-L-3

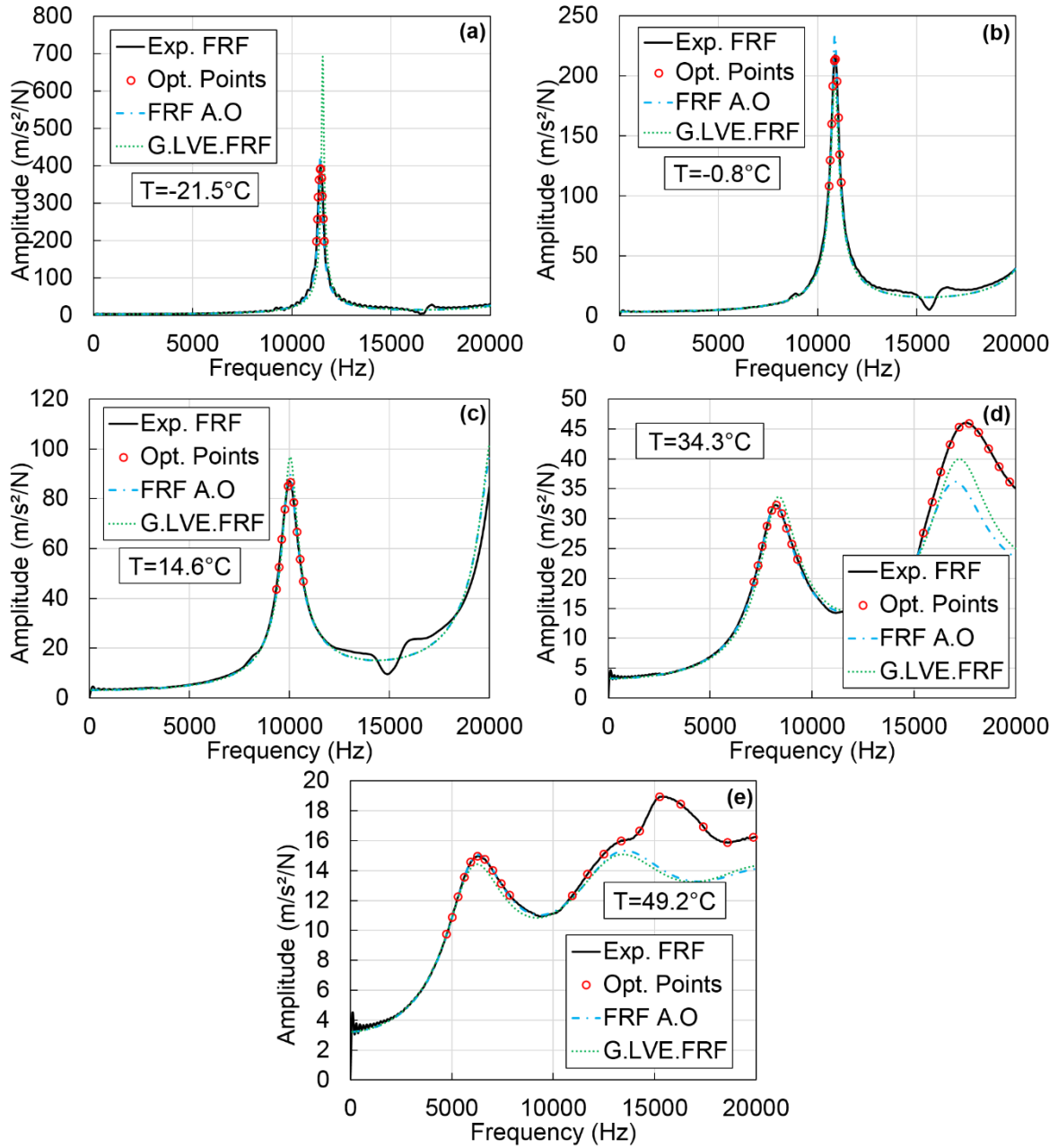


Figure N.16 Comparison of the experimental FRFs (noted Exp. FRF) with the FRFs after optimization (noted FRF A.O) and the global LVE FRFs (noted G.LVE FRF) for specimen GB'-L-3. Values of the experimental FRFs at the frequencies where the optimization is performed (noted Opt. Points) are also plotted. (a) $T=-21.5^{\circ}\text{C}$; (b) -0.8°C ; (c) 14.6°C ; (d) 34.3°C ; (e) 49.2°C .

Table N.8. Values of the four constants E_0 , $\tau_{E15^\circ\text{C}}$, k and δ of the 2S2P1D model determined from dynamic tests at each temperature in the first step of method III for specimen GB'-L-3.

Temperature ($^\circ\text{C}$)	E_0 (MPa)	$\tau_{E15^\circ\text{C}}$ (s)	k	δ
-21.5	28 553	1.4E-02	0.166	2.21
-0.8	26 836	3.5E-01	0.190	2.05
14.6	27 596	3.3E-01	0.174	2.00
34.3	30 322	1.7E-01	0.182	1.95
49.2	31 851	1.9E-01	0.185	1.58

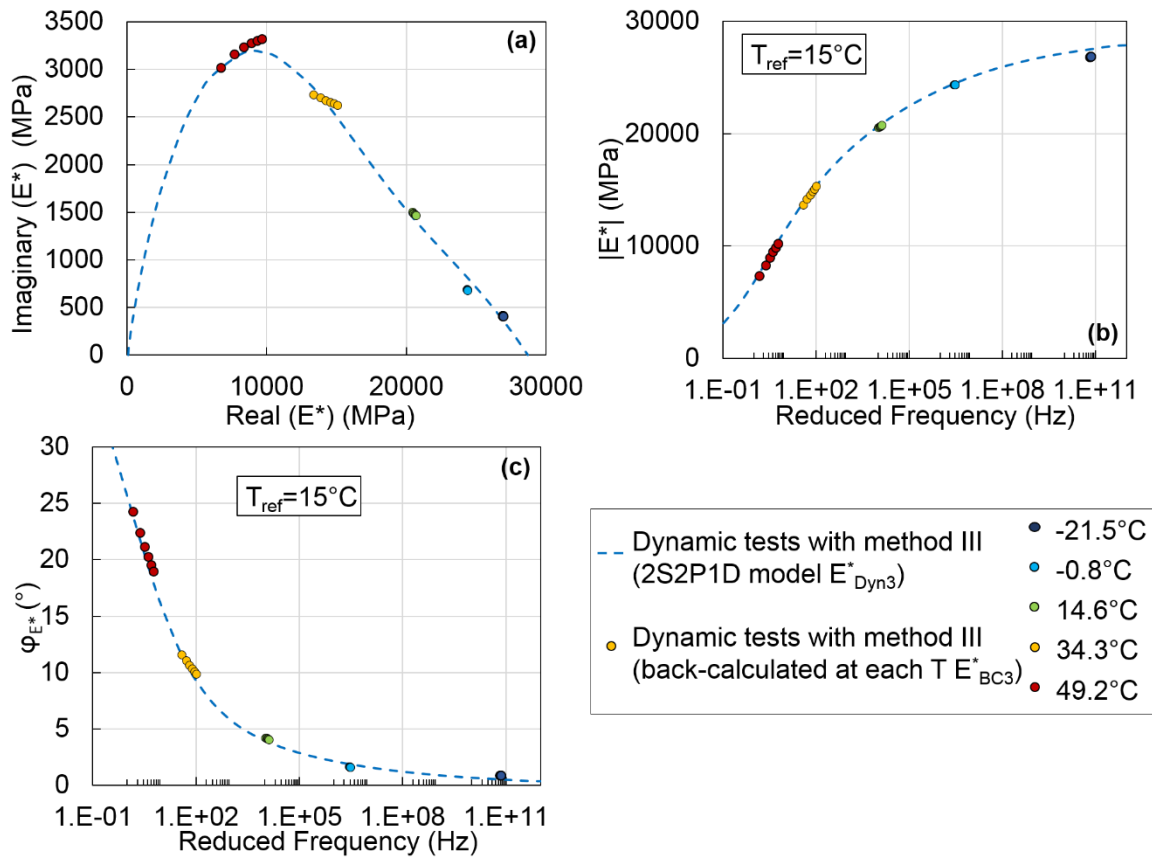


Figure N.17 Values of the complex modulus determined from dynamic tests with method III (E^*_{BC3} and E^*_{Dyn3}). (a) Cole-Cole plot; (b) and (c) master curves of the norm and of the phase angle of the complex modulus at 15°C . Results for specimen GB'-L-3.

SPECIMEN GB-T-1

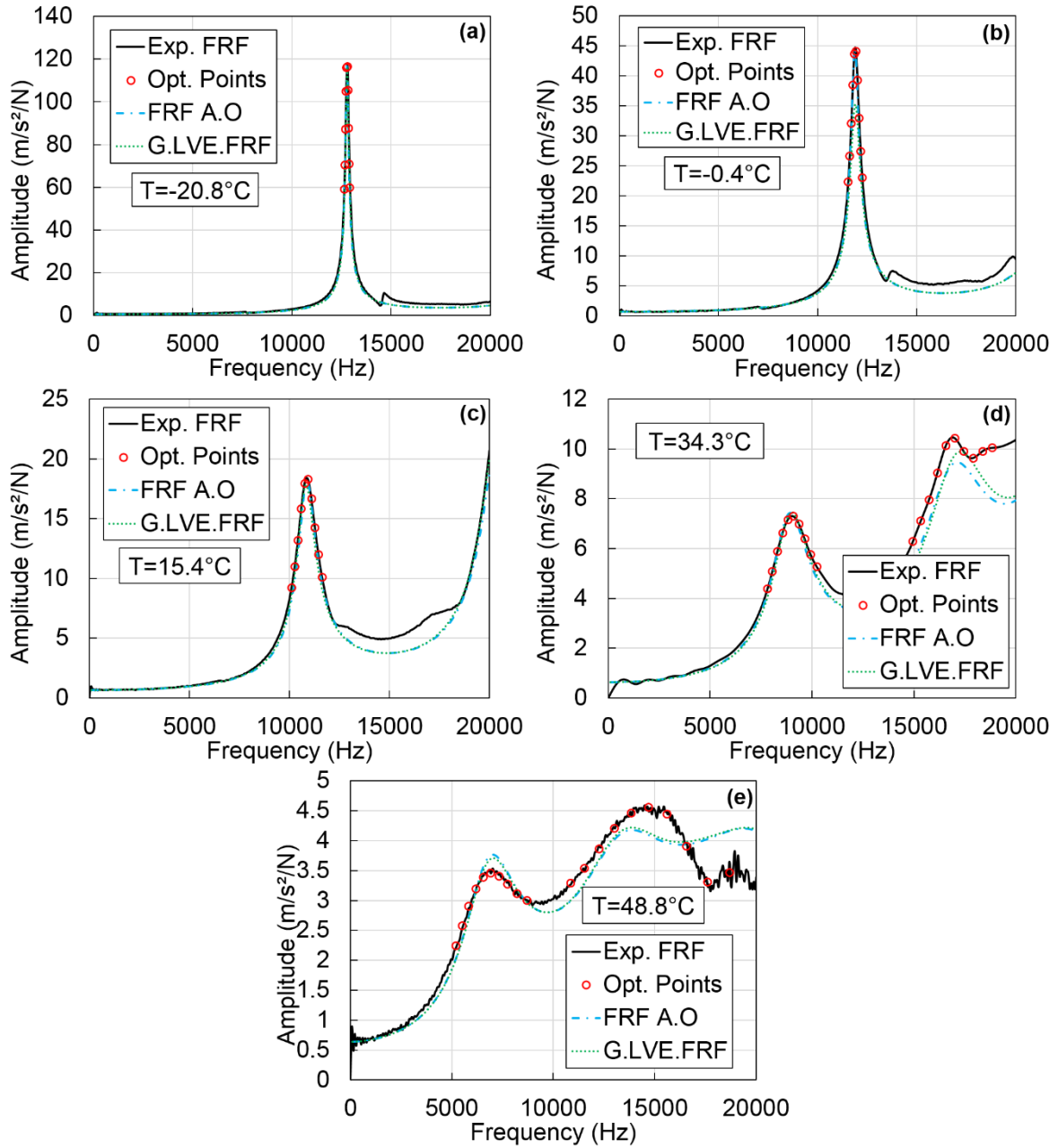


Figure N.18 Comparison of the experimental FRFs (noted Exp. FRF) with the FRFs after optimization (noted FRF A.O.) and the global LVE FRFs (noted G.LVE FRF) for specimen GB-T-1. Values of the experimental FRFs at the frequencies where the optimization is performed (noted Opt. Points) are also plotted. (a) $T = -20.8^{\circ}\text{C}$; (b) -0.4°C ; (c) 15.4°C ; (d) 34.3°C ; (e) 48.8°C .

Table N.9. Values of the four constants E_0 , $\tau_{E15^\circ\text{C}}$, k and δ of the 2S2P1D model determined from dynamic tests at each temperature in the first step of method III for specimen GB-T-1.

Temperature ($^\circ\text{C}$)	E_0 (MPa)	$\tau_{E15^\circ\text{C}}$ (s)	k	δ
-20.8	38 724	1.8E-01	0.159	2.10
-0.4	36 596	1.7E+00	0.155	2.05
15.4	38 898	4.7E-01	0.150	2.06
34.3	40 423	2.2E-01	0.165	2.05
48.8	32 973	6.5E-01	0.222	1.74

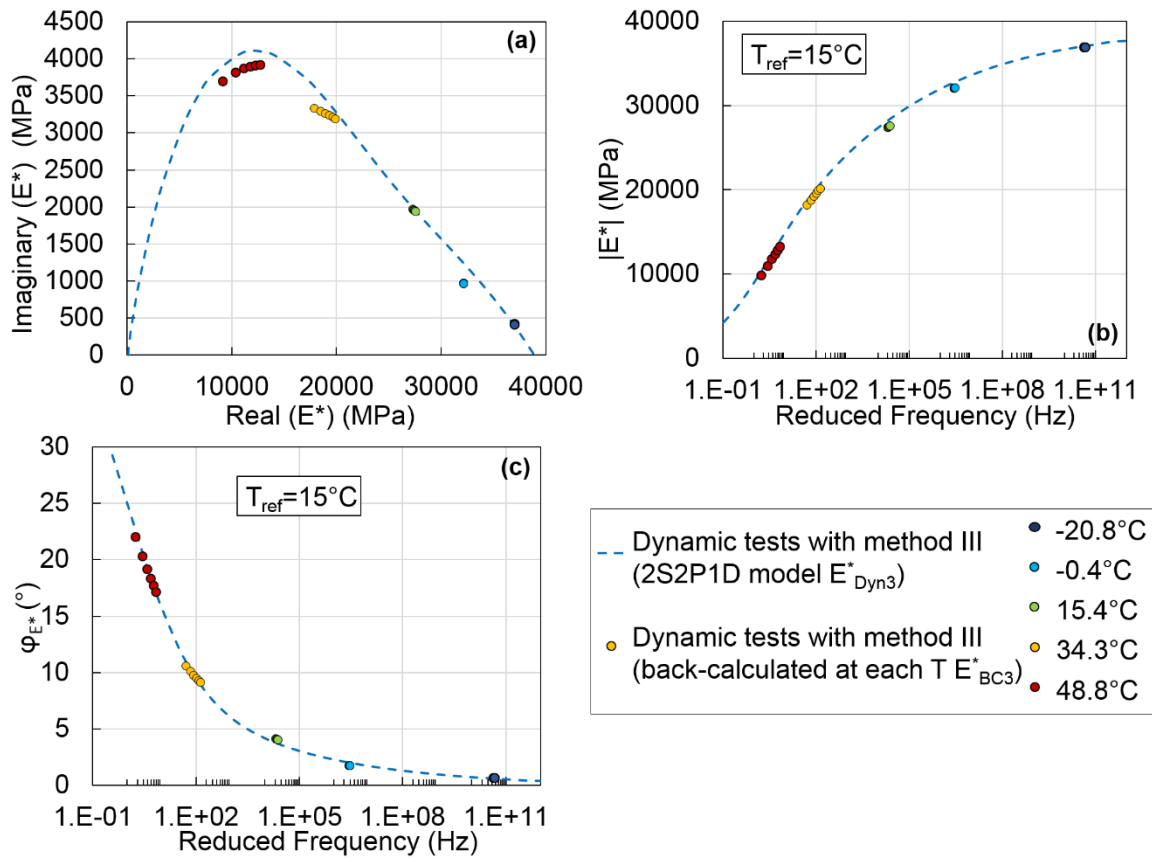


Figure N.19 Values of the complex modulus determined from dynamic tests with method III (E^*_{BC3} and E^*_{Dyn3}). (a) Cole-Cole plot; (b) and (c) master curves of the norm and of the phase angle of the complex modulus at 15°C. Results for specimen GB-T-1.

SPECIMEN GB-T-2

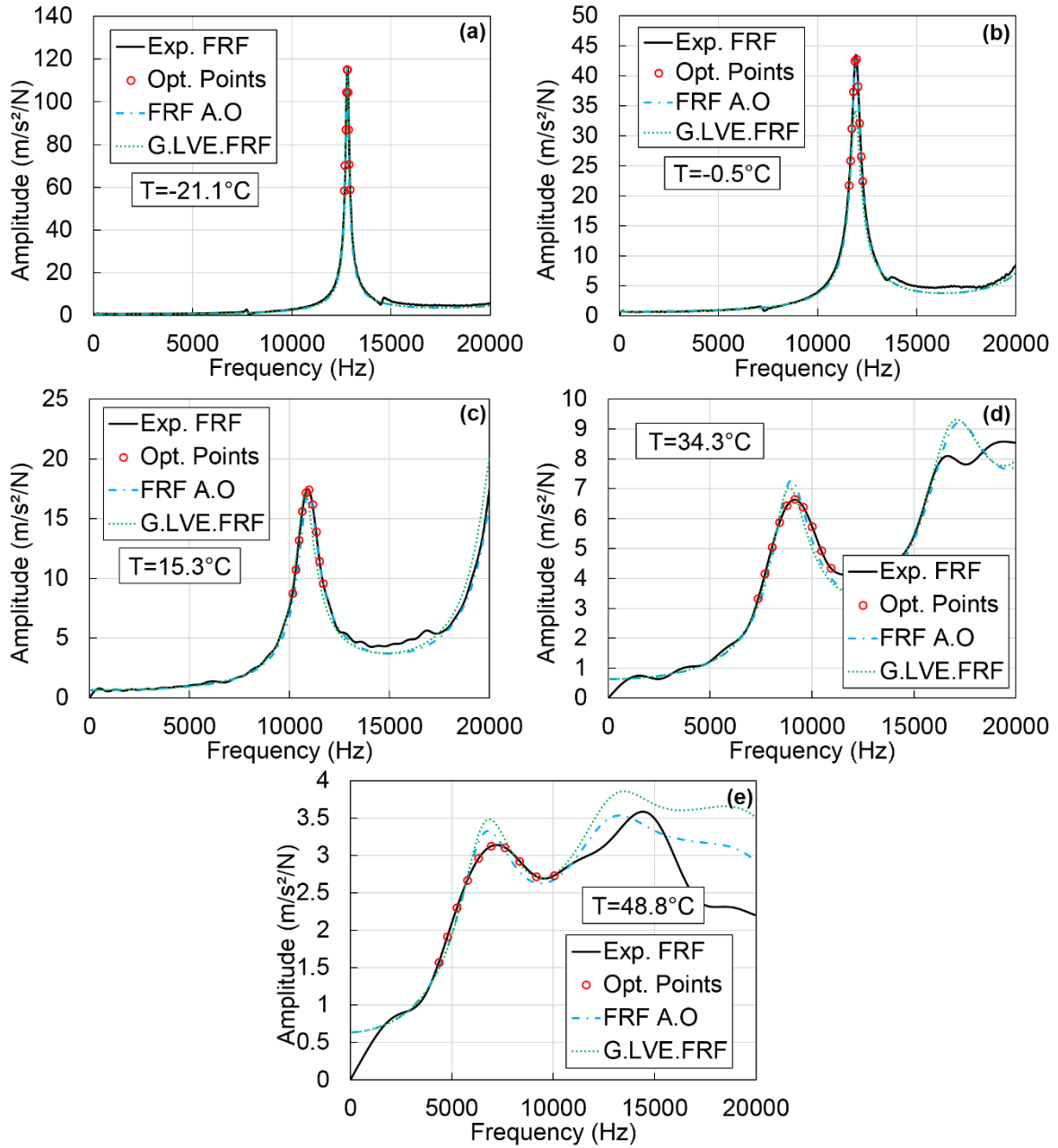


Figure N.20 Comparison of the experimental FRFs (noted Exp. FRF) with the FRFs after optimization (noted FRF A.O) and the global LVE FRFs (noted G.LVE FRF) for specimen GB-T-2. Values of the experimental FRFs at the frequencies where the optimization is performed (noted Opt. Points) are also plotted. (a) $T=-21.1^{\circ}\text{C}$; (b) -0.5°C ; (c) 15.3°C ; (d) 34.3°C ; (e) 48.8°C .

Table N.10. Values of the four constants E_0 , $\tau_{E15^\circ C}$, k and δ of the 2S2P1D model determined from dynamic tests at each temperature in the first step of method III for specimen GB-T-2.

Temperature ($^\circ C$)	E_0 (MPa)	$\tau_{E15^\circ C}$ (s)	k	δ
-21.1	39 008	6.1E-02	0.151	1.60
-0.5	37 119	2.7E-01	0.157	1.65
15.3	36 032	2.5E-01	0.194	2.12
34.3	41 137	2.3E-01	0.170	2.13
48.8	40 567	2.1E-01	0.183	1.80

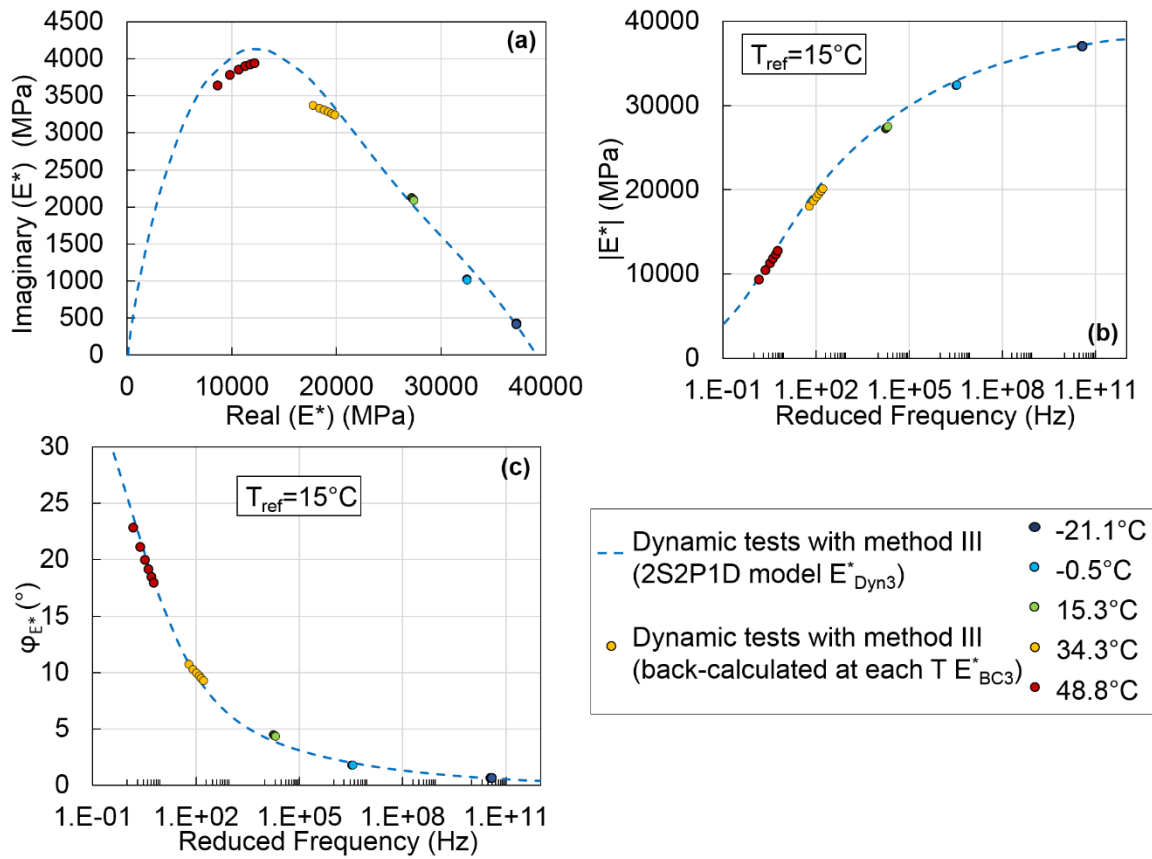


Figure N.21 Values of the complex modulus determined from dynamic tests with method III (E^*_{BC3} and E^*_{Dyn3}). (a) Cole-Cole plot; (b) and (c) master curves of the norm and of the phase angle of the complex modulus at $15^\circ C$. Results for specimen GB-T-2.

SPECIMEN BB-L-1

Table N.11. Values of the four constants E_0 , $\tau_{E15^\circ C}$, k and δ of the 2S2PID model and of the Poisson's ratio ν determined from dynamic tests at each temperature in the first step of method V for specimen BB-L-1.

Temperature ($^\circ C$)	E_0 (MPa)	$\tau_{E15^\circ C}$ (s)	k	δ	ν
-20.9	41866	1.3E-01	0.160	2.11	0.265
-0.4	40213	1.4E+00	0.162	2.26	0.273
15.1	40736	8.4E-02	0.181	2.18	0.283
29.4	45392	3.1E-02	0.186	2.08	0.375
43.9	41716	3.9E-02	0.229	1.47	0.347

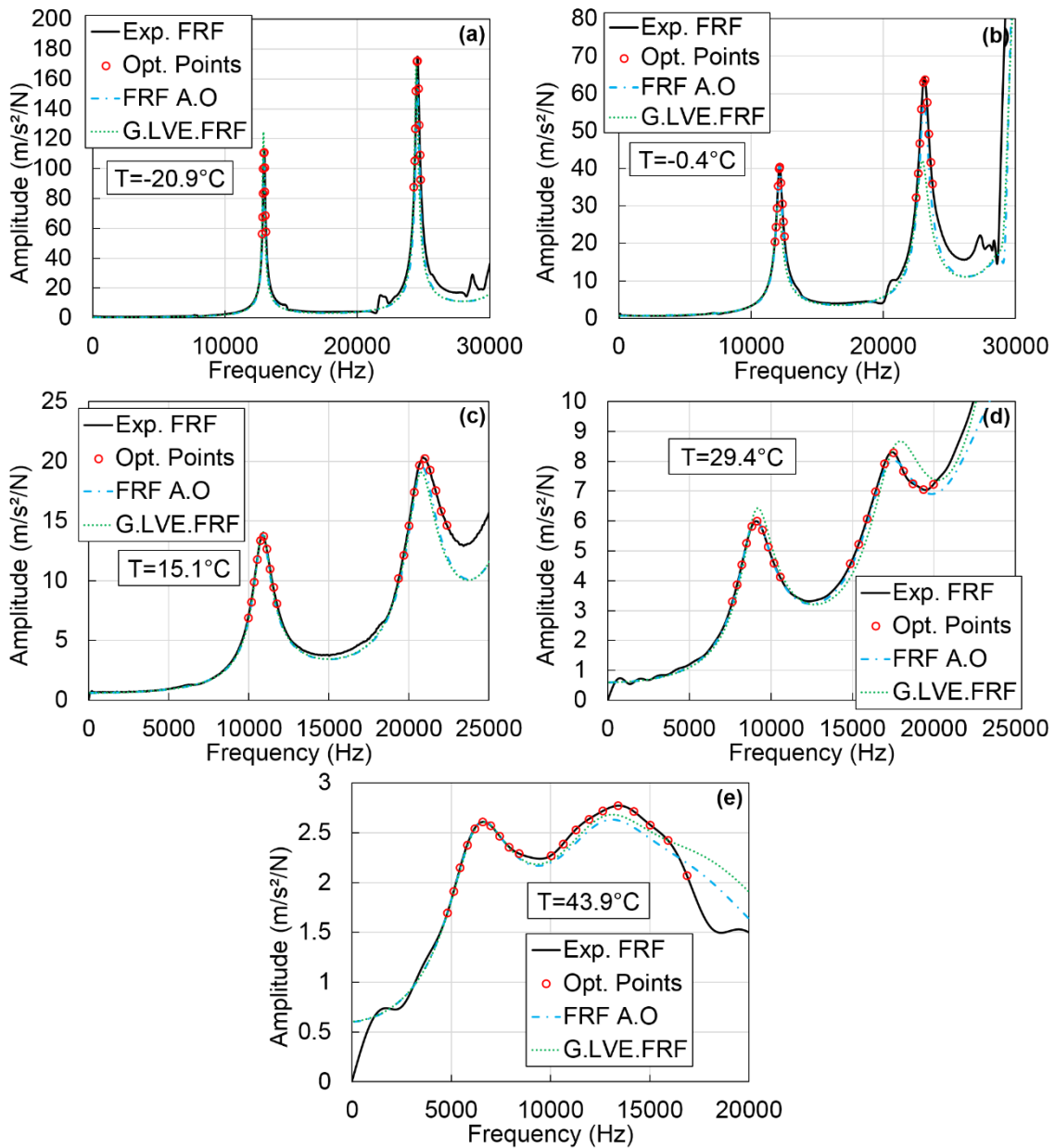


Figure N.22 Comparison of the experimental FRFs (noted Exp. FRF) with the FRFs after optimization (noted FRF A.O) and the global LVE FRFs (noted G.LVE FRF) for specimen BB-L-1. Values of the experimental FRFs at the frequencies where the optimization is performed (noted Opt. Points) are also plotted. (a) $T = -20.9^\circ C$; (b) $-0.4^\circ C$; (c) $15.1^\circ C$; (d) $29.4^\circ C$; (e) $43.9^\circ C$.

SPECIMEN BB-L-2

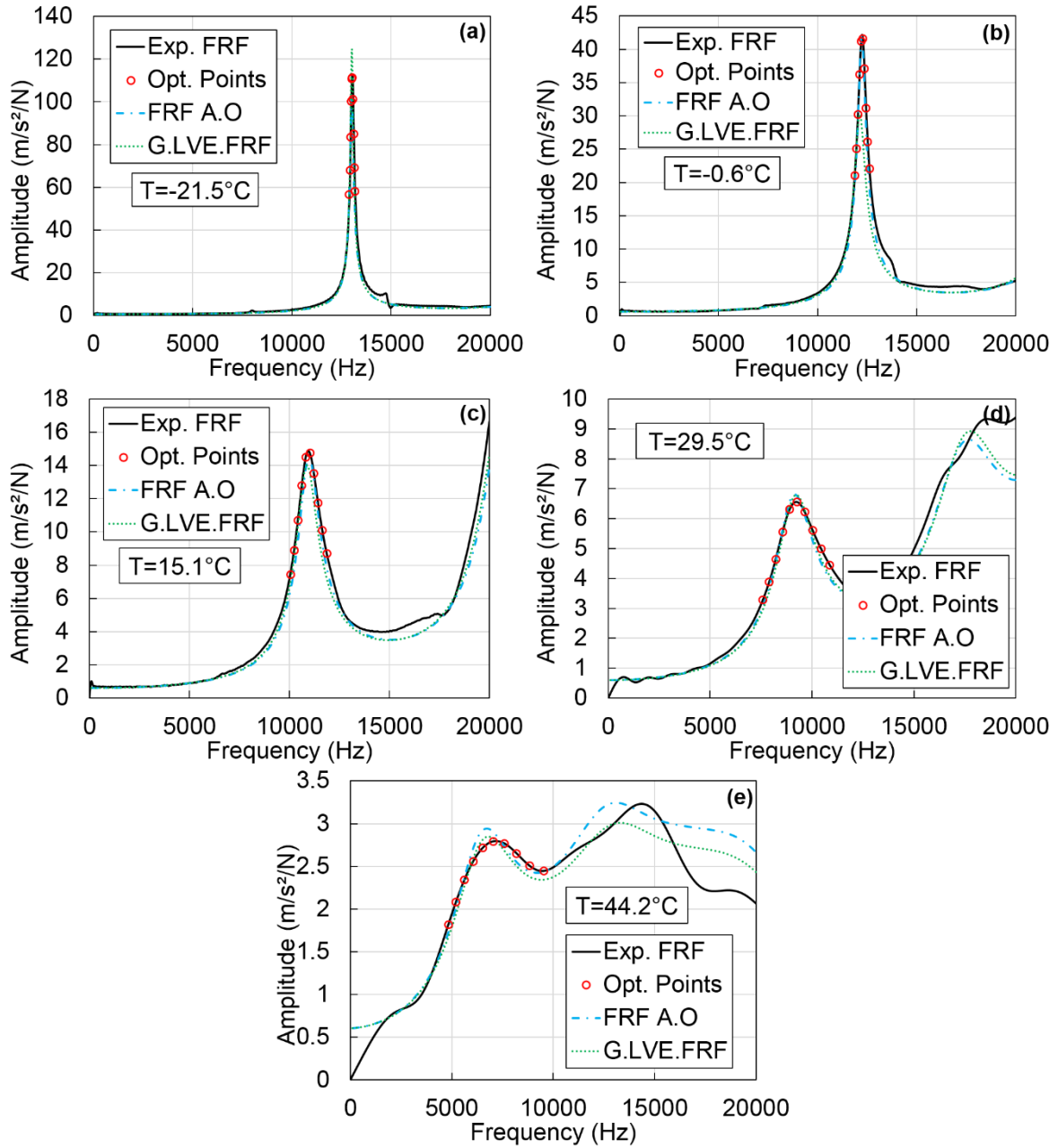


Figure N.23 Comparison of the experimental FRFs (noted *Exp. FRF*) with the FRFs after optimization (noted *FRF A.O.*) and the global LVE FRFs (noted *G.LVE FRF*) for specimen BB-L-2. Values of the experimental FRFs at the frequencies where the optimization is performed (noted *Opt. Points*) are also plotted. (a) $T=-21.5^{\circ}\text{C}$; (b) -0.6°C ; (c) 15.1°C ; (d) 29.5°C ; (e) 44.2°C .

Table N.12. Values of the four constants E_0 , $\tau_{E15^\circ\text{C}}$, k and δ of the 2S2P1D model determined from dynamic tests at each temperature in the first step of method III for specimen BB-L-2.

Temperature ($^\circ\text{C}$)	E_0 (MPa)	$\tau_{E15^\circ\text{C}}$ (s)	k	δ
-21.5	42285	2.6E-01	0.152	2.25
-0.6	40206	3.6E-01	0.163	1.74
15.1	46102	1.1E-01	0.142	2.11
29.5	41101	7.7E-02	0.188	2.08
44.2	49719	2.6E-02	0.101	1.76

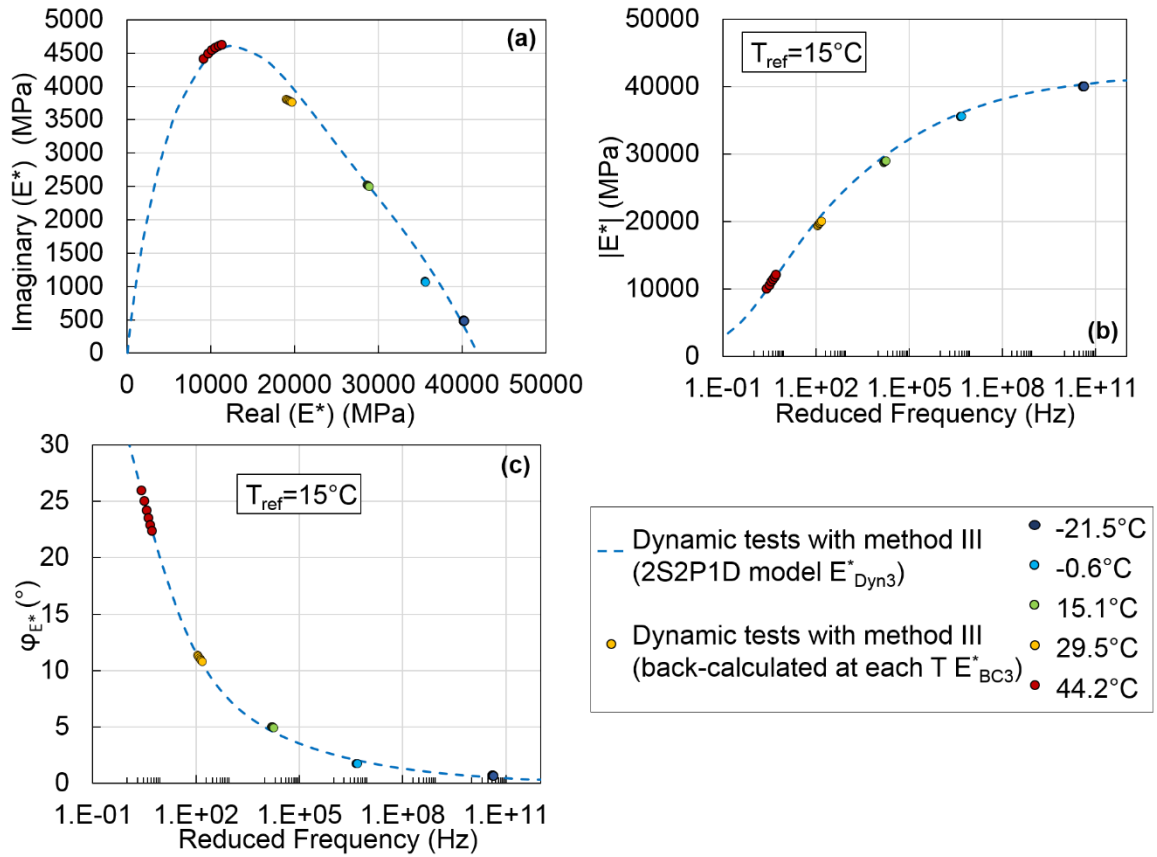


Figure N.24 Values of the complex modulus determined from dynamic tests with method III (E^*_{BC3} and E^*_{Dyn3}). (a) Cole-Cole plot; (b) and (c) master curves of the norm and of the phase angle of the complex modulus at 15°C . Results for specimen BB-L-2.

SPECIMEN BB-T-1

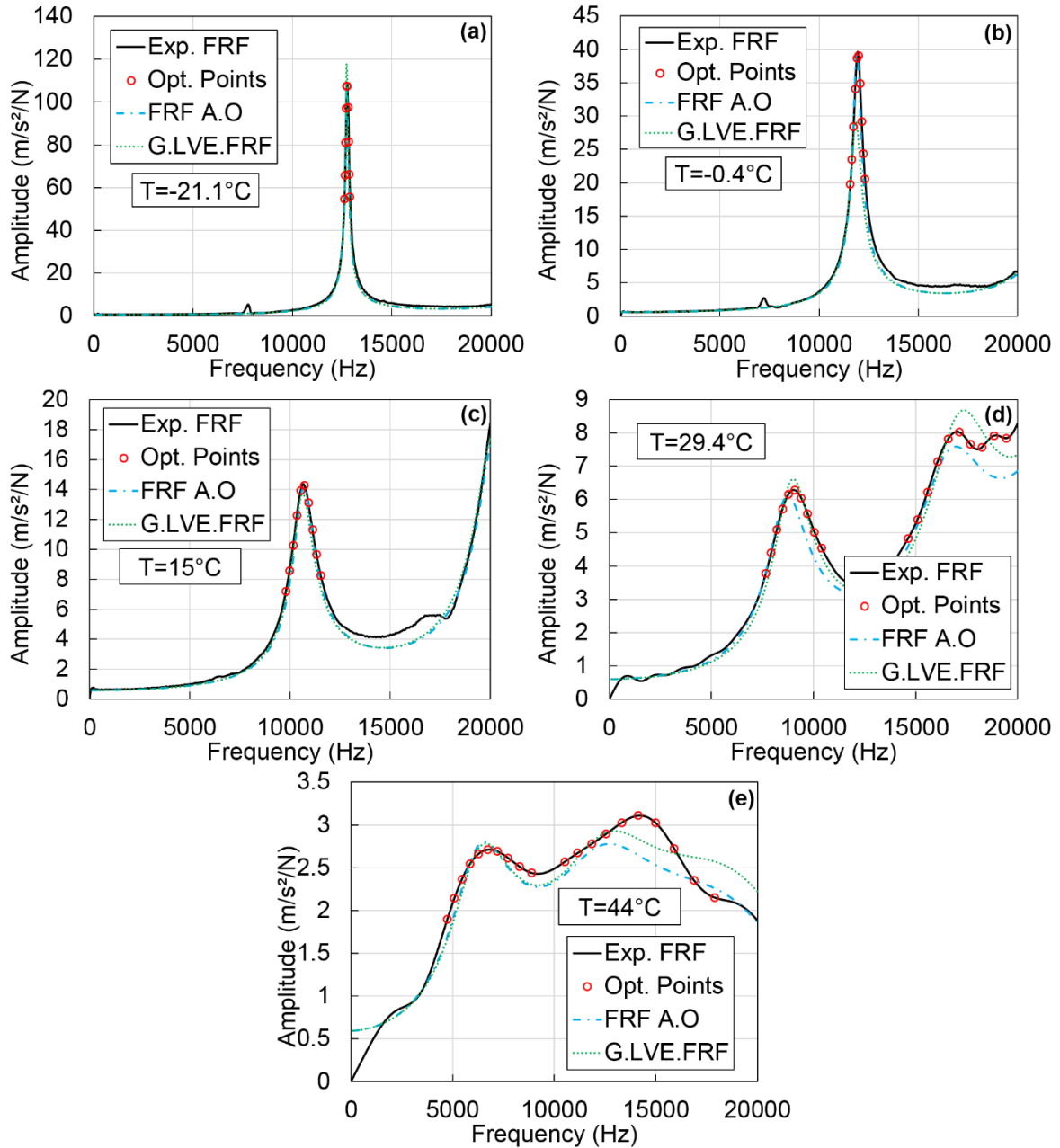


Figure N.25 Comparison of the experimental FRFs (noted *Exp. FRF*) with the FRFs after optimization (noted *FRF A.O.*) and the global LVE FRFs (noted *G.LVE FRF*) for specimen *BB-T-1*. Values of the experimental FRFs at the frequencies where the optimization is performed (noted *Opt. Points*) are also plotted. (a) $T=-21.1^{\circ}\text{C}$; (b) -0.4°C ; (c) 15°C ; (d) 29.4°C ; (e) 44°C .

Table N.13. Values of the four constants E_0 , $\tau_{E15^\circ\text{C}}$, k and δ of the 2S2P1D model determined from dynamic tests at each temperature in the first step of method III for specimen BB-T-1.

Temperature ($^\circ\text{C}$)	E_0 (MPa)	$\tau_{E15^\circ\text{C}}$ (s)	k	δ
-21.1	40511	6.7E-02	0.168	2.15
-0.4	38399	4.2E-01	0.171	1.97
15	38176	9.4E-02	0.188	2.04
29.4	41130	7.3E-02	0.197	2.51
44	44547	4.5E-02	0.199	1.85

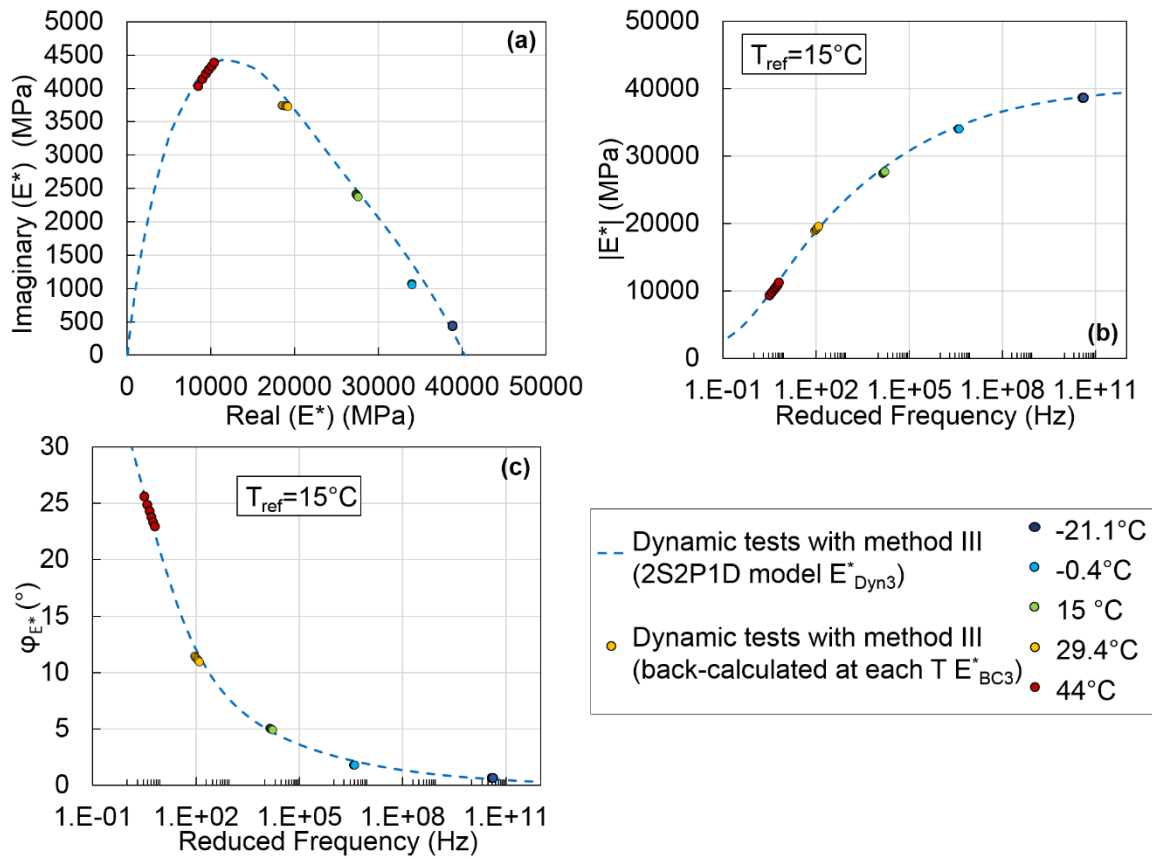


Figure N.26 Values of the complex modulus determined from dynamic tests with method III (E^*_{BC3} and E^*_{Dyn3}). (a) Cole-Cole plot; (b) and (c) master curves of the norm and of the phase angle of the complex modulus at 15°C . Results for specimen BB-T-1.

SPECIMEN BB-T-2

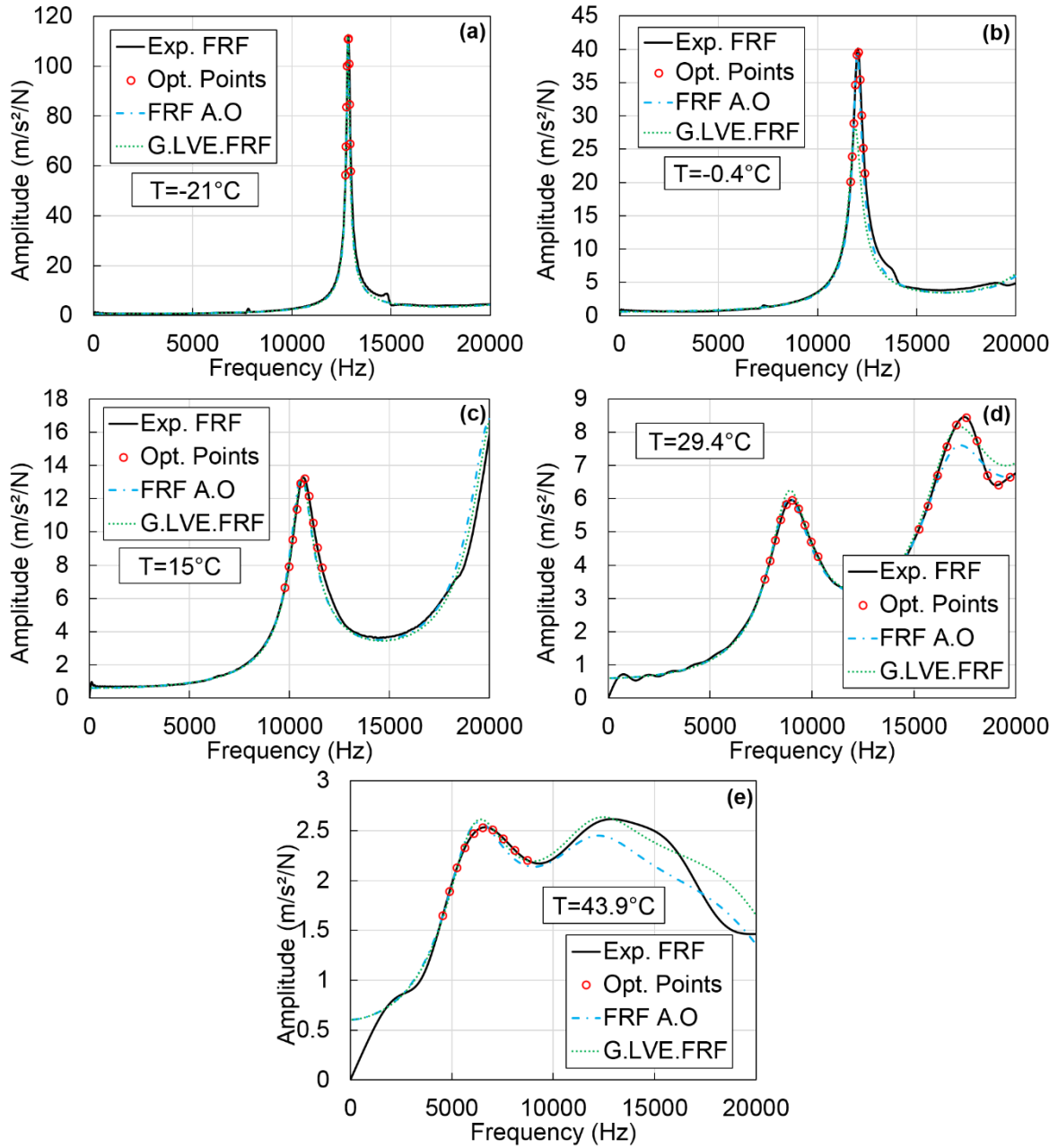


Figure N.27 Comparison of the experimental FRFs (noted *Exp. FRF*) with the FRFs after optimization (noted *FRF A.O.*) and the global LVE FRFs (noted *G.LVE FRF*) for specimen BB-T-2. Values of the experimental FRFs at the frequencies where the optimization is performed (noted *Opt. Points*) are also plotted. (a) $T=-21^{\circ}\text{C}$; (b) -0.4°C ; (c) 15°C ; (d) 29.4°C ; (e) 43.9°C .

Table N.14. Values of the four constants E_0 , $\tau_{E15^\circ\text{C}}$, k and δ of the 2S2P1D model determined from dynamic tests at each temperature in the first step of method III for specimen BB-T-2.

Temperature ($^\circ\text{C}$)	E_0 (MPa)	$\tau_{E15^\circ\text{C}}$ (s)	k	δ
-21	41202	1.9E-02	0.177	2.00
-0.4	39344	3.3E-01	0.169	1.89
15	47529	1.4E-01	0.136	2.57
29.4	41915	3.1E-02	0.185	1.87
43.9	40868	3.7E-02	0.214	1.56

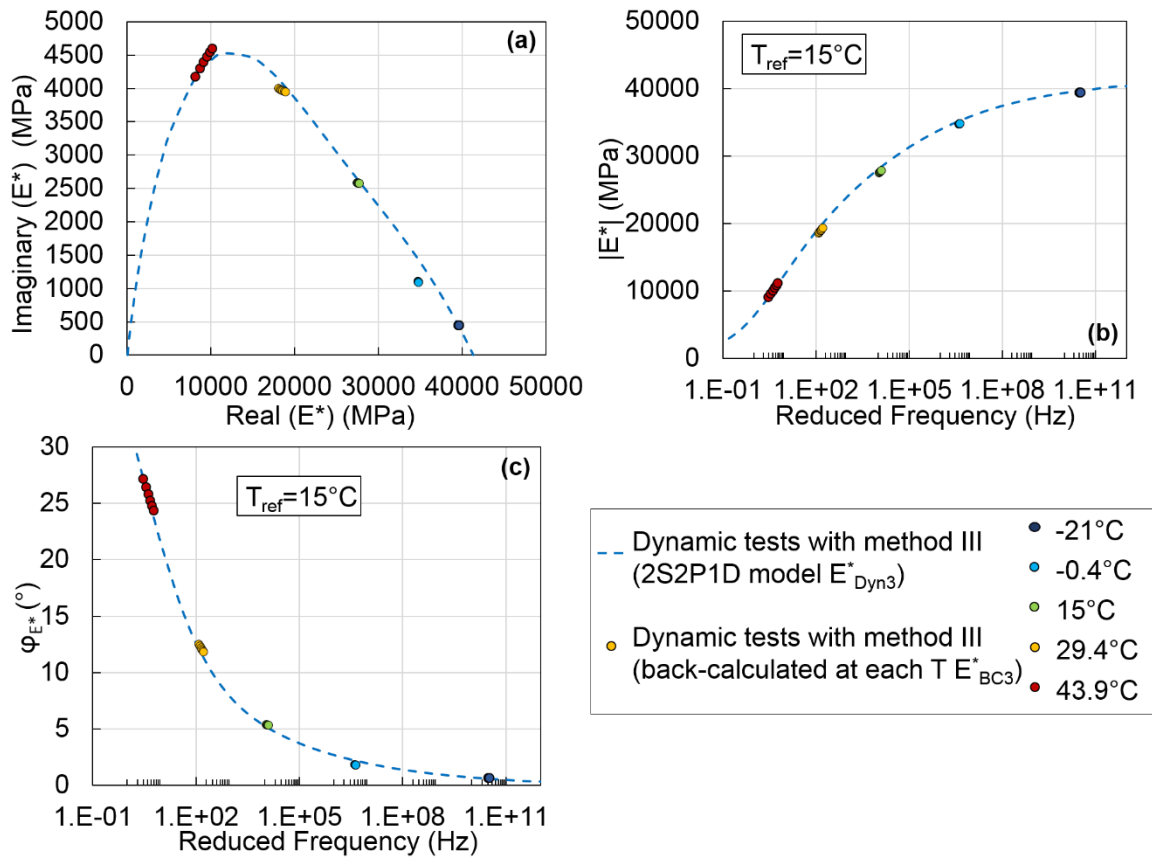


Figure N.28 Values of the complex modulus determined from dynamic tests with method III (E_{BC3}^* and E_{Dyn3}^*). (a) Cole-Cole plot; (b) and (c) master curves of the norm and of the phase angle of the complex modulus at 15°C . Results for specimen BB-T-2.